

UNIVERSITY OF BELGRADE  
SCHOOL OF ELECTRICAL ENGINEERING

Kosta M. Jovanović

**MODELING AND CONTROL OF THE  
ANTHROPOMIMETIC ROBOT WITH  
ANTAGONISTIC JOINTS IN CONTACT  
AND NON-CONTACT TASKS**

Doctoral Dissertation

Belgrade, 2015

УНИВЕРЗИТЕТ У БЕОГРАДУ  
ЕЛЕКТРОТЕХНИЧКИ ФАКУЛТЕТ

Коста М. Јовановић

**МОДЕЛИРАЊЕ И УПРАВЉАЊЕ  
АНТРОПОМИМЕТИЧКОГ РОБОТА СА  
АНТАГОНИСТИЧКИМ ПОГОНИМА У  
КОНТАКТНИМ И БЕСКОНТАКТНИМ  
ЗАДАЦИМА**

докторска дисертација

Београд, 2015

# Thesis Committee

Dr. **Veljko Potkonjak**, Thesis Supervisor

Full Professor

School of Electrical Engineering, University of Belgrade, Serbia

Dr. **Mirjana Popović**

Full Professor

School of Electrical Engineering, University of Belgrade, Serbia

Dr. **Aleksandar Rodić**

Scientific Advisor

Mihailo Pupin Institute, University of Belgrade, Serbia

Dr. **Alin Albu-Schäffer**

Full Professor

Technical University Munich, Germany; and

Director of the Institute of Robotics and Mechatronics, German Aerospace Center-DLR

**Željko Đurović**, PhD

Full Professor

School of Electrical Engineering, University of Belgrade, Serbia

# Acknowledgments

*A number of people have helped pave the way to my PhD. My special gratitude goes to:*

*My wife **Marija**, for all the love and support, and because she learned what ZMP was when that was really important;*

*My parents **Dušica** and **Miloš**, for their unconditional support and for making it possible for me to become professionally involved in what I love;*

*My mentor Prof. **Veljko Potkonjak**, for all the opportunities he has given me, for his enormous support, and for teaching me how to become a better person and a better professional;*

*My colleagues **Bratislav**, **Predrag** and **Nenad**, because our team work was extremely enjoyable;*

*Prof. **Alin Albu-Schäffer**, for giving me a chance and for being my supervisor during my research stay at the DLR Institute of Robotics and Mechatronics;*

*Prof. **Owen Holland**, for a number of ideas, discussions, and consultations; and*

*My colleagues from the Signals & Systems Department and my office mates **Branko**, **Zaviša** and **Vladimir**, for making my job personally rewarding;*

*The research leading to this PhD thesis has received funding from the European Community's Seventh Framework Programme FP7/2007-2013, Challenge 2 (Cognitive Systems, Interaction, Robotics), under Grant Agreement no. 231864-ECCEROBOT, and from the Serbian Ministry of Education, Science and Technological Development under Agreement no. TR35003.*

**Kosta M. Jovanović**

*Belgrade, December 28<sup>th</sup>, 2015.*

**Dissertation title:** Modeling and control of the anthropomimetic robot with antagonistic joints in contact and non-contact tasks

**Abstract.** The thesis considers a very popular and rapidly growing topic in robotics – modeling and control of anthropomimetic robots, in particular robots that feature compliant antagonistic actuation. The term ‘anthropomimetic’ refers to a robot of fully human-like appearance, but also human-like inner structure and functionality. The motivation for the thesis came from the involvement of the author and the School of Electrical Engineering, University of Belgrade in the project Eccerobot (*Embodied Cognition in a Compliantly Engineered Robot*), funded by European 7<sup>th</sup> Framework Programme, and the project *Ambient Intelligent Service Robots of Anthropomorphic Characteristics* funded by Serbian Ministry of Education, Science and Technological Development.

Since conventional rigid actuators have become obsolete for inherently-safe future robotic applications, the design and control of novel compliant actuators have recently been under intensive investigation. In particular, variable stiffness (impedance) actuators (VSAs), which can trade-off between robot trajectory tracking and overall safety, are the focus of robotics research. We focus on antagonistically-driven joints, as a subgroup of bio-inspired VSAs.

The thesis is organized in six sections and bibliography.

The first section outlines the main ideas and motivation for the work. It presents research directions, points of view and initiatives in the design and control of compliant robots, with special emphasis on antagonistic drives. It also addresses safety issues of future service robots, and lists technologies, trends, and approaches towards achieving that goal: moving from stiff to compliant actuators, the benefits introduced by passive and active compliance, VSA, etc. As a special group of bio-inspired VSAs in robotics, antagonistic actuators are reviewed comprehensively. Such a detailed review of antagonistic actuator design aims to highlight the importance of the subject, on the one hand, while on the other hand it presents the technology that will be intensively exploited in future anthropomimetic robots.

The second section presents a development of the simulation-based model of the robot driven by antagonistically-actuated compliant drives. To that end, Stepanjenko's method to robot modeling is exploited since it has demonstrated superior performance in simulating robot dynamics. To begin with, basic models of antagonistically-actuated joints that resemble typical human-like antagonistic structures are introduced. These models are incorporated into the upper-body anthropomorphic robot model, which is a close approximation of the Eccerobot prototype. Since such a robot is intended to work in proximity to humans and directly interact with its surroundings, modeling of contacts is introduced. This section as a whole represents an efficient and accurate tool for simulating the anthropomorphic robot dynamic, which is then implemented in Matlab and C++. Two simulation case studies are presented. The first emulates an anthropomorphic robot on a wheeled-base, working in an unstructured environment and therefore exposed to impulse and long-term external disturbances. Here the model is used to observe the robot's zero-moment-point and thus its balance. The second case study emulates intentional contact – grasping of an object. Models of all contact stages are demonstrated: approach, impact and in-contact-motion phases. Although some applications to the physical robot Cassius [1] and the simulation-base study [2] have already been implemented, there are numerous possibilities for prospective model utilization: simulation and analysis of biomechanical systems/subsystems, study of potential transfer from biological concepts to bio-inspired robotics, anthropomorphic robot system design and analysis, simulation of anthropomorphic robots in interaction tasks, development of model-based advanced control techniques for anthropomorphic robots, testing of anthropomorphic control approaches with additional possibilities of control in interaction tasks, etc.

The main outcomes of this section, relating to anthropomorphic model development and extension to include analysis of contact dynamics, have already been published in [3]. At the same time, the simulation model served as a platform for the development of control algorithms elaborated in the following sections.

The third section presents the contribution of this thesis to the control of antagonistically actuated, linear/non-linear, cable driven, compliant robot joints, using

control methods that rely on the conventional control theory. After an overview of the background work on antagonistic actuator control and feedback linearization in robot control, an upgraded puller-follower approach, outlined in the Master's thesis of Svetozarevic [4], is presented. This biologically-inspired and energy efficient approach simultaneously controls joint position and force in one of the antagonistic tendons. In the present thesis, the puller-follower approach extends to control joint position and joint stiffness. An initially demonstrated single-joint control algorithm, based on feedback linearization, is optimized to compensate for gravity load, changeable effective joint inertia and dynamic coupling in multi-joint systems, by introducing the robust control theory. In addition to  $H_\infty$  loop-shaping robust control, methods based on the non-linear and multivariable control theories were exploited in the puller-follower control scheme. This section ends with limitations and issues that remain open and will be the topic of future research.

In addition to control methods that rely on conventional engineering techniques, several cognitive approaches to the control of antagonistically coupled compliant drives in robotics were developed. In accordance with a bio-inspired background and fully human-like design of the anthropomorphic robot, the focus was on human-like control as well – control based on experience, learning and heuristics. To that end, nearest-neighbor algorithms for feedforward and feedback control of the anthropomorphic robot, an algorithm for neural network feedforward control using radial-basis networks, and an algorithm for feedback control based on on-line estimation of kinematic coefficients and fuzzy rules were developed. Although cognitive algorithms were not of primary importance in this thesis, they present a step forward in the control of a fully anthropomorphic robot since engineering-based control algorithms reach their limits if multi-articular muscles or multi-axes joints are considered. On the other hand, cognitive methods outlined in the thesis can be applied to such systems without restrictions. Finally, a comparative simulation study in Matlab was carried out to highlight the main features of the developed cognitive-based control schemes. The scientific contributions regarding cognitive-based control algorithms are presented in the fourth section of the thesis, while all contributions to control anthropomorphic robots are outlined in a paper [5].

The fifth section provides the point of view and initial research on antagonistically-driven compliant joint control in contact tasks. The proposed control approach is a mixture of state-of-the-art conventional and widely adopted impedance control techniques and bio-inspired patterns of biological antagonistic structures. The main observations, findings, and contributions of the thesis are summarized once again in the final section.

Ultimately, we could say that future service robots will not be controlled using exclusively analytical models, conventional control methods or experience-based learning. A combination of all these approaches needs to be elaborated to deal with numerous and diverse tasks, which will be required from robots. Therefore, this thesis is expected to contribute to modeling and control of future human-like service robots. Furthermore, there are areas that could benefit from exact analytical models of human dynamics or the developed control algorithms: gaming industry, biomechanics, motor control, etc.

In summary, the author's contributions presented in detail in this thesis have resulted in a total of 25 publications (one book chapter, four papers in international journals with an impact factor, three papers in domestic journals, eight international conference papers, and nine domestic conference papers).

**Keywords:** anthropomorphic robot, analytical model of robot dynamics, contact dynamics, antagonistic drive, feedback linearization, puller-follower method, the nearest-neighbor method, impedance control.

**Scientific field:** Electrical and Computer Engineering

**Research area:** Robotics and Control Systems

**UDC number:** 621.3

**Наслов тезе:** Моделирање и управљање антропомиметичког робота са антагонистичким погонима у контактним и бесконтактним задацима

**Резиме.** У тези је обрађена врло актуелна тема у области роботике - моделирање и управљање антропомиметичким роботима, посебно оним са еластичним антагонистичким погонима. Појам антропомиметички се односи на робота који подсећа на човека не само својим изгледом, већ и унутрашњом структуром и функционалношћу. Мотивација за израду ове дисертације је произишла из активности аутора на Електротехничком факултету у Београду, а у оквиру пројекта *Eccerobot - Embodied Cognition in a Compliantly Engineered Robot*, финансираног од стране седмог оквирног програма Европске уније и пројекта „Амбијентално интелигентни сервисни робота антропоморфних карактеристика“, финансираног од стране Министарства за просвету, науку и технолошки развој Републике Србије.

С обзиром на недостатке конвенционалних крутих актуатора у будућим роботским апликацијама које захтевају висок степен безбедности, развој и управљање нових актуатора који укључују еластичност је од великог значаја. Посебно је значајан развој актуатора са променљивом крутошћу VSA (од енглеског назива “*variable stiffness actuator*”) који омогућавају подешавање крутости током рада и самим тим дају компромис између прецизности рада робота и безбедности његовог окружења. Фокус нашег истраживања су работи са антагонистичким погонима као посебна група билошки инспирисаних VSA.

Дисертација је организована у шест поглавља уз преглед литературе.

У првом поглављу су истакнуте главне идеје и мотивација за рад на овој теми, као и правци истраживања у развоју и управљању зглобова са еластичношћу, са нагласком на антагонистичке погоне. У овом поглављу се истичу безбедносни изазови будућих сервисних робота, наводе се одговарајуће технологије и трендови: еластични актуатори, појмови активне и пасивне попустљивости и VSA. Као група од посебног интереса међу VSA, приказан је детаљан пресек стања на тему антагонистичких актуатора у роботизици.

Развој симулационог модела динамике робота погоњеног антагонистички упареним еластичним актуаторима је детаљно приказан у другом поглављу дисертације. У том циљу, искоришћен је Степањенков метод за моделирање

робота у складу са његовим супериорним карактеристикама када се ради о симулацији динамике робота. Приказани су модели два основна антагонистички погоњена зглоба робота који представљају типичне структуре човекових зглобова погоњених антагонистички упареним мишићима. Ови модели појединих зглобова су интегрисани у модел горњег дела антропомиметичког робота (од струка на више) по узору на прототип *Eccerobot*-а. Узимајући у обзир да је такав робот превасходно намењен за рад у непосредном људском окружењу, посебна пажња је посвећена моделирању контаката. Ово поглавље даје ефикасан алат за симуирање динамике антропомиметичког робота који је и примењен у *Matlab*-у са реализацијом појединих делова у C++. У том циљу су приказана и два примера заснована на симулацијама. Први пример представља антропомиметичког робота на покретној основи који ради у неструктурираном окружењу које га као такво излаже кратким (импулсним) и дугорочним поремећајима. Овде је развијени модел искоришћен за анализу динамичког баланса посматрањем тачке нултог момента. Други пример преставља робота који наменски хвата објекат у простору. На овај начин су демонстриране све три фазе моделирања контактних задатака између робота и објекта: приближавање, нееластични судар и кретање у контакту. Иако је развијени модел већ нашао примену и на реалном роботу *Cassius* [1] и студији базираној на симулацији на основу модела [2], постоји још много могућности за употребу модела: симуирање и анализа биомеханичких система или делова система, испитивање могућности коришћења биолошких коцепата у био-инспирисаној роботици, симуирање робота у контактним задацима, анализа и развој структуре антропомиметичких робота, развој напредних метода управљања антропомиметичким роботима на бази модела, тестирање алгоритама управљања антропомиметичким роботима у контактним и бескотактним задацима, итд. Главни резултати који обухватају развој модела антропомиметичког робота и његову надградњу у правцу анализе динамике контактних задатака су обухваћени у публикацијама закључно са радом у међународном часопису са импакт фактором [3]. У исто време, развијени симулациони модел је служио као платформа за даљи рад и развој алгоритама управљања приказаних у дисертацији.

У трећем поглављу су приказани доприноси у области управљања антагонистички погоњеним, линеарним/нелинеарним, еластичним зглобом робота

са жичаним преносом. Приказане управљачке методе се ослањају на конвенционалну теорију управљања. Након пресека стања у области управљања антагонистичким актуаторима и употребе повратне спреге за линеаризацију (енг. *feedback linearization*) у управљању роботима, унапређује се тзв. „пулер-фоловер“ приступ иницијално уведен у раду [4]. Овај биолошки инспирисан приступ се заснива на енергетски ефикасном истовременом управљању позиције зглоба робота и затезне силе у једном од антагонистички упарених тендона. У овој тези, пулер-фоловер (енг. *puller-follower*) приступ је проширен за потребе истовременог управљања позицијом зглоба и његове крутости. Затим, иницијално уведени приступ за контролу једног зглоба робота који се заснива на фидбек линеаризацији је прилагођен за компензацију гравитационог оптерећења, ефективног момента инерције у сваком зглобу, као и динамичког спрезања у системима са више повезаних тела. Поред  $H_\infty$  робусне методе за подешавање функције преноса у отвореној спрези (енг.  $H_\infty$  *loop shaping*), методе нелинеарне и мултиваријабилне терорије управљања су примењене на коначну управљачку шему пулер-фоловер методе. Овај део дисертације се завршава навођењем ограничења у примени поменутог метода и отворених питања као могућих праваца даљег рада.

Поред метода управљања које се заснивају на конвенционалним инжењерским принципима, у дисертацији је приказан развој неколико когнитивних метода управљања антагонистичким еластичним актуаторима у роботици. У складу са дизајном антропомиметичких робота, развијене су и методе које се у складу са људским понашањем заснивају на искуству, учењу и хеуристици. Развијен је метод најближег суседа (енг. *the nearest-neighbor*) за управљање у повратној спрези (енг. *feedback*) и директној грани (енг. *feedforward*). Такође, управљање у директној грани је реализовано употребом неуралних мрежа тзв. радијалне основе (енг. *radial-basis neural networks*), а управљање у повратној спрези пројектовано на бази тренутне процене кинематичких коефицијената и фази правила (енг. *fuzzy rules*). Ове когнитивне методе представљају значајан корак ка коначној шеми управљања антропомиметичким роботом имајући у виду да конвенционалне инжењерске управљачке методе не дају решења за контролу вишеосних роботских зглобова или тендона који истовременом делују на више оса робота, где се когнитивне методе управљања могу применити без додатних ограничења.

Демонстрација пројектованих метода управљања је урађена кроз симулационе примере у програмском језику *Matlab*. Научни доприноси који се односе на ове методе су приказани у четвртом одељку дисертације, док се збирни резултати на тему управљања антропомиметичким роботима дати у раду [5].

У петом одељку дисертације приказана су иницијална истраживања и ставови на тему управљања антагонистички погоњеним еластичним зглобовима у контактним задацима. У том циљу, предложена је управљачка шема која представља модификацију опште прихваћене методе импедансног управљања на бази биолошки инспирисаних образаца за поделу оптерећења између два антагонистички упарена тендона. Главна запажања, закључци и доприноси дисертације су сумирани у завршном одељку.

Можемо наслутити да ће коначна управљачка шема антропомиметичких робота користити комбинацију различитих метода управљања: управљање на бази аналитичких модела динамике, конвенционалних метода или техника на бази учења и искуства. У складу са тим очекујемо да ће ова теза допринети ефикасном моделирању и управљању будућих хуманоидних и сервисних робота уопште. Такође, резултати тезе могу бити искоришћени у областима: индустрије видео игара, биомеханике, моторне контроле, итд.

Доприноси аутора који се директно тичу тематике ове дисертације сумирани су у укупно 25 публикација (1 поглавље у књизи, 4 рада у међународним часописима са импакт фактором, 3 рада у домаћим часописима, 8 радова на међународним конференцијама и 9 радова на међународним и домаћим конференцијама одржаним у Србији).

**Кључне речи:** антропомиметички робот, аналитички модел динамике робота, динамика контакта, антагонистички погон, фидбек линеаризација, пулер-фоловер метода, метода најближег суседа, импедансно управљање.

**Научна област:** Електротехника и рачунарство

**Ужа научна област:** Роботика и управљање системима

**УДК број:** 621.3

# Contents

1	Introduction.....	1
1.1	Idea and motivation.....	3
1.2	Towards inherently safe future service robots .....	6
1.2.1	Stiff vs compliant actuation.....	8
1.2.2	Active vs passive compliance.....	13
1.2.3	Variable stiffness actuation (VSA).....	16
1.3	Anthropomimetic robots .....	21
1.4	Review of antagonistic actuator designs .....	27
1.4.1	Antagonistic actuators based on electrical drives.....	32
1.4.2	Antagonistic actuators based on hydraulic/pneumatic drives.....	41
1.5	Thesis overview .....	47
1.6	Thesis contributions and related publications .....	49
2	Dynamics model of a robot with antagonistic joints in non-contact and contact tasks .....	57
2.1	Background work.....	58
2.2	Structure of the anthropomimetic robot – Eccerobot .....	66
2.3	Analytical approach to modeling in non-contact tasks .....	68
2.3.1	Models of antagonistically-driven compliant joints .....	69
2.3.1.1	Circular (linear) joint model .....	71
2.3.1.2	Triangular (non-linear) joint model .....	74
2.3.2	Multi-joint robot model.....	76
2.4	Analytical approach to modeling in contact tasks.....	80
2.4.1	Models of in-contact motions.....	86
2.4.1.1	Rigid contact.....	87
2.4.1.2	Soft contact .....	88
2.4.1.3	Elastodynamic contact .....	90

2.4.2	Models of impact phenomena .....	91
2.5	Verification of developed analytical models through simulations .....	93
2.5.1	Case study 1: Analysis of robot's dynamic balance in non-contact and contact tasks .....	94
2.5.2	Case study 2: Analysis of grasping an object in the vertical plane, demonstrating the phases of contact: approach, impact, and in-contact motion .....	105
2.6	Conclusion .....	110
3	Engineering control approaches .....	113
3.1	Background work .....	116
3.1.1	Control of antagonistically-coupled electric drives .....	118
3.1.2	Control of antagonistically-coupled pneumatic/hydraulic drives .....	122
3.2	Feedback linearization for compliant robot joint control .....	126
3.3	Puller-follower control concept .....	128
3.3.1	Antagonistic joints with linear tendon characteristics .....	137
3.3.2	Antagonistic joints with quadratic tendon characteristics .....	141
3.3.3	Antagonistic joints with exponential tendon characteristics .....	143
3.3.4	Simulation results .....	145
3.4	Puller-follower control concept for decoupled position and stiffness control .....	151
3.4.1	Antagonistic joints with quadratic tendon characteristics .....	157
3.4.2	Antagonistic joints with exponential tendon characteristics .....	158
3.4.3	Simulation results .....	159
3.5	Enhancement of the puller-follower approach .....	167
3.5.1	Gravity compensation .....	168
3.5.2	Estimation of effective joint inertia .....	169
3.5.3	$H^\infty$ loop shaping robust control .....	170
3.5.4	Simulation results .....	180
3.6	Final comments on the puller-follower control concept for musculoskeletal system control .....	184
4	Cognition-based control approaches .....	188
4.1	Background work .....	189
4.2	Introduction to cognitive approaches .....	195

4.3	Feedforward control .....	197
4.3.1	Experience base .....	197
4.3.2	Nearest-neighbor feedforward approach .....	200
4.3.3	Neural network approach .....	205
4.4	Feedback control .....	208
4.4.1	Nearest-neighbor feedback approach .....	209
4.4.2	Approach based on online estimation of kinematic coefficients and fuzzy logic .....	213
4.4.2.1	Kinematic coefficient estimation algorithm .....	214
4.4.2.2	An example of kinematic coefficient evaluation for a two-DoF planar robot .....	218
4.4.2.3	Fuzzy logic algorithm .....	220
4.5	Simulation results .....	223
4.6	Conclusions .....	229
5	Control of a robot with antagonistically coupled compliant drives in contact tasks .....	232
5.1	Impedance robot control .....	234
5.2	Bio-inspired force distribution between antagonistic drives .....	238
5.3	Impedance control of robots with antagonistically-coupled compliant joints .....	244
6	Findings, conclusions & directions of ongoing research .....	251
7	Bibliography .....	257

# 1 Introduction

Since conventional stiff robot drives have obviously come close to the limits of their applicability, many new areas in contemporary robotics have appeared. This thesis could partly be classified among many of them:

**Passively compliant robots** - robots whose design contains elastic elements. They inevitably constitute a more complex mechanism, but the complexity could be justified by inherent robot safety, impact absorption, increased energy efficiency (energy storage and recovery in elastic elements), etc.

**Actively compliant robots** – robots that achieve compliant behavior using control schemes. They include control of conventional stiff robotic actuators mimicking the behavior of an elastic element. Although no energy can be stored in the actuation system of this kind, and no shocks can be absorbed due to the limited bandwidth of the controller, active compliance is attractive since the controller can make compliance online adaptable.

**Variable impedance actuators (VIA)** – new-generation robotic actuators that can compromise between rigid (more accurate) mechanisms and compliant (safer) mechanisms. Due to their mechanical construction and control, these actuators control in real-time both the reference position and the mechanical impedance of the moving parts in such a way as to optimize performance while intrinsically guaranteeing safety. Their impedance behavior is often reduced to the static implied force-equilibrium deflection relation, so the term ‘variable stiffness actuator’ (VSA) is frequently used.

**Soft robots** – a concept interpreted in different ways. Soft robotics combines advances in biomechanics, biomedical engineering, mathematical modeling, computer science, chemistry, and biology to provide new robotic mechanisms and devices that can undergo dramatic changes in morphology, size, and control in order to adapt to various

environments. It integrates the examination, fabrication, utilization, modeling and control of novel soft and flexible materials, electronics, actuators and sensors.

**Bio-inspired robots** – robots and robot parts derived from their biological paragon. Typically, such a bio-actuator is an artificial muscle or a set of bio-sensors that resembles an insect eye. Although at first sight one can expect robots that faithfully copy humans, there are numerous projects aimed at creating animal robots that emulate their desired features: robot fish [6], octopus [7], etc.

**Biomimetics** – a science that handles issues and solves complex problems in advanced technology by mimicking elements, models, patterns and systems from nature, as products of evolution.

**Biomechatronics** – a science that exploits biology in addition to concurrent planning of mechanics and electronics. It assumes fabrication of new and customization of existing solutions in the design and control of mechatronic systems, through the implementation and adaptation of bio-inspired construction principles and control patterns found in biological counterparts.

Working on an international project among numerous attempts to achieve the oldest goal in robotics and science in general – the creation of an artificial human, we access analysis of the problem by extracting analytics. While the Eccerobot project [8] emerged from an idealized vision of combining all the above-mentioned novel robotics branches, our conventional engineering approach led us to extract analytics. Consequently, we turned to analysis and the development of conventional tools – modeling using exact analytics and control considering non-linear, multi-variable, robust control techniques complemented by experience and heuristics.

Exact mathematical modeling of humans, as well as humanoid robot dynamics, is of great importance since we first need to understand biomechanics in order to exploit principles that originate in nature. Such principles have been developing through evolution. Force and torque distribution of human or robot manipulators driven by mono-articular and bi-articular muscles, or drives in the case of robots, is an issue

addressed by many research groups in different fields: biomechanics, physiology, engineering, etc. Accurate modeling of dynamics is needed to contribute to any of these perspectives: for a biomechanical specialist to understand biological patterns and muscle pairing, and calculate parameters that are impossible or extremely difficult to measure, as muscle and tendon forces; and for an engineer to control a robotic device by solving optimization criteria for model-based estimated parameters, etc. Only one of numerous papers that emphasize the importance of dynamic parameter estimation in real time is [9]. There Dong and Mavridis first calculated the desired torque in each joint, which is a typical intermediate result of many robot control algorithms, and then estimated the force in poly-articular drives using Jacobian mapping between joint torque space and muscle force space. As expected, an optimization criterion was then proposed to keep forces within assumed boundaries and even retain the forces in the region assumed to be the best in terms of muscle dynamics. However, a lack of knowledge of accurate parameters of the system (human or robot) dynamics could deteriorate optimization process significantly.

The second scientific challenge addressed in this thesis is control of desired future safe robots of distinguished human-like characteristics. It is intuitively expected that as the complexity of robots grows, control of such a system will become an increasingly demanding and questionable task. Furthermore, as the robot structure moves away from conventional engineering solutions towards bio-inspiration, its control schemes become troublesome and require new perspectives.

This thesis tries to analyze the horizons of such research directions, establish limits imposed by technology, and provide some answers, but also open questions that will lead to new advances in the field.

## **1.1 Idea and motivation**

Humans perform everyday manipulation tasks efficiently and routinely, while effortlessly taking into account all the practical issues and limitations of the tasks.

Moreover, humans shape the environment to ensure full comfort for themselves, so it is more likely that future service robots will be adapted to such an environment, rather than the environment to the robots. In brief, we need to not only focus on the human-like appearance of the robot, but come up with an inner structure and functioning of the robot that are as close as possible to those of humans. Thus, acquiring models by observing human behavior patterns that have been evolving for centuries, in combination with complex analytic models and their exploitation through conventional engineering, is a good way to go. The imitation approach could dramatically reduce the need for exploration and reduce time, while already developed engineering principles in design and control of complex systems should be exploited as far as possible. Of course, the robots' morphology is assumed to be similar enough to that of humans, in order to make such models and patterns portable between humans and robots. To that end, we need robots that are not only shaped according to a human body but that also faithfully resemble human anatomy. Thus, we need anthropomimetic robots. Furthermore, once such a robot is built, we need to control it in an inherently safe and reliable manner. To that end, we need to learn from humans, to study their behavior patterns, to adapt human design and behavior patterns to the current level of technology, and, finally, to trade-off between achievable robot design and performance. Accordingly, the European funded project Eccerobot [10], [11] was launched to explore the current level of anthropomimetic robot technology (see Figure 1.1). The directions for the work on this thesis were set by the involvement of the School of Electrical Engineering, University of Belgrade in the project and the previous results of that institution in the fields of robot dynamics, biomechanics, and robot modeling and control.

Based on our interests and the role of the project, we have been dealing with a very interesting, promising and popular scientific topic of anthropomimetic robot modeling and control. Since novel advanced control techniques in robotics strongly rely on analytical models to compensate for their dynamics, modeling and control have become very close and inseparable topics.



*Figure 1.1. Eccerobot - the pioneer among anthropomorphic robots, and a motivation for the work on the thesis.*

The main characteristics of robots that resemble humans as closely as possible are at the same time properties which characterize the human musculoskeletal actuation system: antagonism, compliance, nonlinearity, and tendon coupling. Even though each of these features makes the modeling and control task more demanding, it offers distinct benefits:

- **Antagonism** introduces drive redundancy from a certain point of view, but enables control of both position and stiffness, if exploited in an appropriate way. It also enables the transfer of bio-inspired actuation design and control from biology to the engineering world;
- **Compliance** increases the overall safety for both the robot and its environment, while acting as a mechanical low-pass filter to external forces and thereby absorbing an impact. It can also increase energy efficiency of the whole system by transferring kinetic energy to elastic energy of elastic elements, and vice versa;

- **Non-linearities** enable variable stiffness tuning and allow one to take advantage of this and balance between accuracy and safety; and
- **Tendon coupling** enables drive relocation, and generally reduces inertia, friction, backlash and static load, thus enabling faster motion.

Therefore, the present thesis considers all the main characteristics of future safe robot actuation systems. This work will hopefully contribute to the modeling and control of a future anthropomorphic robot or at least facilitate and enhance its design, control and utilization.

## **1.2 Towards inherently safe future service robots**

Traditionally, engineers prefer to design and work with conventional stiff actuators, which make robots very fast and accurate. Although the well-known premise “the stiffer the better” [12] works excellently in a perfectly known environment, this is not a robot design that one would prefer for areas where interaction with the environment is possible. The common everyday environment is generally not specified, not known, stochastic and unpredictable. Moreover, contemporary robotics involves close collaboration between robots and humans, including even the realistic possibility of direct human-robot contact (interaction).

Although the overall safety of a robot depends on its mechanics, electronics and control, high interaction forces during impact are predominantly caused by high effective inertia. Although the safety of robots and their working environment is an extremely important issue, generally accepted quantifiers to describe these phenomena are still missing. The level of potential for serious injury due to impact is usually rated using head injury criteria (HIC), known from the automotive industry. However, a lot of effort has been expended to point out the effect of the mechanical robot structure on safety in interaction. Some notable results regarding safety issues and overall safety evaluation have been reported by Zinn from Stanford University [13] and particularly Haddadin

from the University of Hanover and DLR in [14], [15]. One of the solutions suggested to reduce impact is a soft covering, but it does not address the root cause of the problem. Sensors and related electronics that monitor and prevent a potential hazard (“active compliance”) constitute another approach to impact effect mitigation. However, limited bandwidth and unpredictable behavior as a result of faults may still occur even if most advanced electronics are employed. Therefore, the way to implement injury knowledge into robot control needs to be as suggested in [15].

Unfortunately, the majority of advanced robotic manipulators still have high effective inertia stemming from their requirements for high performance: a high payload and high composite speed. If only serial elasticity is introduced, link effective inertia for high frequency impacts will be equal to only link inertia, thus reducing overall effective inertia by actuator inertia multiplied by the squared gearbox ratio. On the other hand, the introduction of serial compliance results in the deterioration of certain desirable robot features. Therefore, the design and control of novel compliant robotic actuators and overall robot mechanics are the subject of research at a large number of research centers, and a lot of funds and effort have been invested to raise service robotics to a new level in this way. Some of the leading projects in the field have been: Phriends (funded by the EU FP6 Framework Programme) [16], and Saphari (funded by the EU FP7 Framework Programme) [17], both led by DLR Institute of Robotics and Mechatronics, KUKA, Italian Institute of Technology, La Sapienza University of Rome, etc.

Specifically, an elaboration of robot safety targeting a redundant compliant antagonistic joint configuration (pneumatic antagonistic actuators enriched by a small electric drive) is shown in [18]. Robot *S2ρ* was designed in collaboration between Stanford University and the Italian Institute of Technology, as a successor of the better known *DM<sup>2</sup>* manipulator. Besides redundancy, the robot uses KcKibben pneumatic actuators in an antagonistic configuration and consequently trades off some performance for safety, as shown in Subsection 1.4, which reviews antagonistic joint configurations.

Previously, the safety of robots and their environment has been increased by utilizing

numerous sensors of advanced features and real-time collision avoidance [19]. Such an approach led to very expensive systems due to both high sensor cost and computational cost of trajectory planning and control design. There are also numerous examples of robotic systems whose mechanical construction was covered by soft materials to reduce impact and increase safety to a certain extent [20]. An advanced version of robotic skin could be equipped with advanced electronics to detect and measure collisions [21].

One more proof of the current importance given to the topic of safe human-robots is the Georges Giralt PhD Award, which is an annual recognition by EURON (European Robotics Research Network) of the best PhD thesis in Europe. Namely, most of the nominees and laureates have come from the field; furthermore, for the title “Towards Safe Robots: Approaching Asimov's 1<sup>st</sup> Law” Sami Haddadin received the best PhD thesis award in 2012 [22].

In order to introduce the reader to robotic trends towards inherently safe robots, following is a brief description of the benefits and issues of compliant actuators, active and passive actuators, and finally variable impedance (stiffness/compliance/admittance) actuators that combine active and passive actuator advantages.

### **1.2.1 Stiff vs compliant actuation**

Brief definitions are needed before we start with a comparison between stiff (or rigid) and compliant actuators. An actuator is characterized as stiff if once it reaches the desired position, it stays there even though external forces/torques are applied to it (assuming that the intensity of external influences will not break the actuator and the actuator is of infinite power). An actuator is described as compliant if it allows deviations from its equilibrium position, depending on the applied external forces/torques. Actuator compliance is often achieved by placing arrangements of elastic elements between the drive and the link (Figure 1.2).

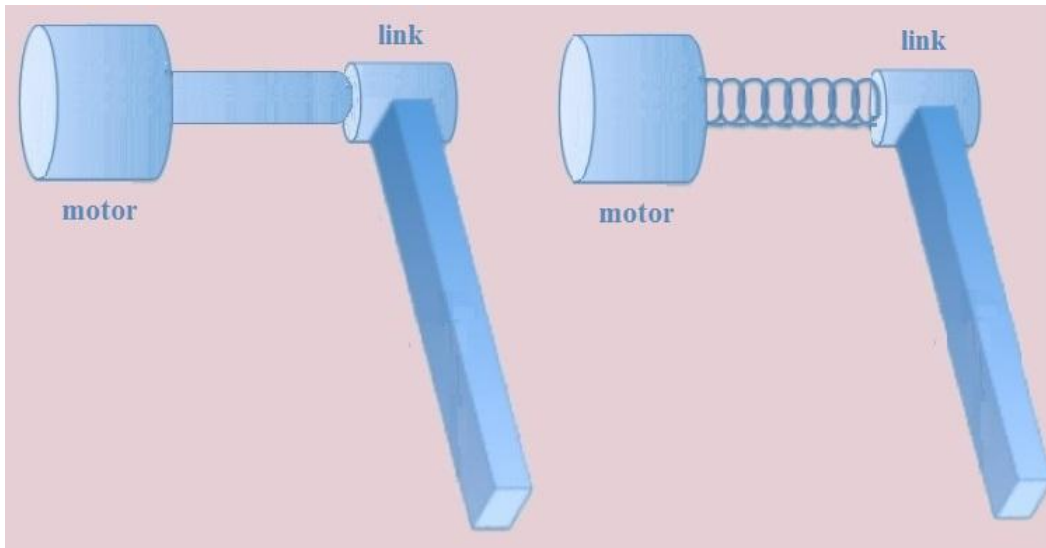


Figure 1.2. Stiff/rigid joint (left) and compliant joint (right). The compliance is introduced by placing the elastic element in the transmission between the drive and the link.

Although stiff robots are still superior in a fully deterministic environment and areas restricted to humans, while robots are increasingly used in non-deterministic areas. In areas where collision with a human is likely to occur, the good precision, stability, repeatability, high payload, force and torque capability, high bandwidth control, and high composite speed of stiff robots would most probably be traded off for safety. Thus, Hollerbach et al. in [23] list several general drawbacks, which are a limitation of sorts that can hardly be bridged with conventional stiff electric actuators:

- electric motors have poor torque density and, therefore, gear reduction is necessary for acceleration or dealing with heavy loads;
- gear boxes introduce additional friction, backlash, torque ripple and noise;
- effective (reflected) inertia is multiplied by squared  $N$  – where  $N$  is the gearbox ratio, so shock loads increase damage on both the actuator side and the environment side;
- a robot that interacts with its surroundings in order to complete the desired task or handle external disturbances must have an accurate model of the environment (for trajectory planning and control design), and such information is rather difficult to obtain.

Consequently, the use of rigid robots is questionable in numerous realistic scenarios, where robots are subjected to disturbances or even planned interaction, which is an inevitable component in the majority of contemporary robot applications. Despite the tradition to employ actuators that are as stiff as possible, reducing interface stiffness and including elasticity offer a number of advantages required in novel robotic applications:

- lower reflected inertia (link and drive inertia are decoupled via elasticity);
- less damage to the environment (since reflected inertia is reduced and position deviations compensate for contact forces);
- reduced impact shocks (elasticity in robotic joint low-passes filter shocks and therefore reduces peak forces);
- more accurate and stable force control (the force control problem is transferred to position control since the output force is proportional to the desired and achieved position difference multiplied by effective stiffness);
- possibility of energy storage (if properly controlled, elastic elements could serve as energy accumulators, allowing outperformance of elastic drives over stiff actuators).

Conventional hydraulic, pneumatic or electric drives cannot match these requirements without additional elements to achieve the desired compliance. Hydraulic actuators have the highest torque and power density and are capable of performing tasks that require huge forces or torques. However, their output impedance is virtually infinite and generates very high impact loads during collisions. Thus, hydraulic actuators could almost exclusively be used for position control applications and have very poor inherent safety characteristics. Pneumatic actuators, on the other hand, can be made very compliant in a wide frequency range due to the compressibility of gas as the working fluid. However, pneumatic actuators have very low bandwidth capabilities: control bandwidths are limited to several tens of Hz. Thus, while the natural compliance of pneumatic actuation reduces its effective inertia and increases overall safety, its low-bandwidth characteristic limits the performance of pneumatic robots. Due to limited safety features of pneumatic and hydraulic actuators, electric drives are widely used for actuation of novel robotic systems. The primary constraint of electric motors is their

relatively low torque and power density. Although direct drive systems are under development, they are still heavy, inefficient, and require high DC voltages to produce sufficient torque. To increase the torque output of electric drives, gearboxes are generally unavoidable. Unfortunately, the increase in torque and power density of geared electrical drives results in an increase in effective (reflected) output inertia, which is consequently multiplied by the squared gearbox ratio. In summary, in order to increase the overall safety of robot actuation, additional compliance needs to be introduced into conventional drives. Although here we mostly refer to compliance on a joint level, end-point compliance is of primary concern from application and safety points of view.

However, safety is not the only aspect that benefits from compliance. In robotic assembly systems, a problem may arise when the total positioning tolerance between the assembling part and the assembly machine is larger than the assembling clearance. Here end-effector compliance could be of key importance.

In this regard, the names of Pratt and Williamson are frequently mentioned because they have raised awareness about series elastic actuation (SEA) and its capabilities [12]. The SEA approach aims to overcome the limitations of high-impedance conventional actuators, by placing an elastic element between the output of the actuator and the robotic link. With the elastic element, high-frequency impedance is reduced and high interaction forces due to impact are lowered. At the same time, low-frequency impedance can be an object of control. The main imperfection of SEA is the saturation of torque and velocity, which are mutually dependent. Maximum output torque decreases with joint velocity and since it is a fundamental physical limitation of the actuator, no control loop can compensate for it. As such, the choice of serial elastic stiffness, in addition to the robot and motor inertial characteristics, determines the open-loop mode frequency. A stiffer coupling improves high-frequency torque performance but adversely affects the desirable closed-loop and open-loop impedance characteristics. Contrarily, a more compliant elastic element reduces torque capabilities, while preserving the desired impedance over a broader range. Consequently, as Pratt and Williams conclude in their famous work, SEA could be used to efficiently exploit lower-

frequency interaction tasks, such as walking using SEA as artificial tendons. However, in high-speed trajectory tracking or high-frequency disturbance rejection SEA limitations prevail.

Another benefit of elasticity in actuators is energy saving. If properly controlled, elastic elements could be used to store or release energy, and consequently improve energy efficiency. The use of elastic elements that can store and release energy in a robot thus becomes an important research topic as energy efficiency in robots has been underlined as one of the key issues for future service robots. The work of De Michieli et al. [24] highlights all aspects of robot energy efficiency that should be considered. The authors developed a simulation platform suitable for modeling the energy balances of a real humanoid robotic arm and their approach was validated thorough comparison with a real robot – robot James developed at LIRA-Lab, University of Genoa. Although the authors present comprehensive work on energy flow in a robotic system and show the energy balance influenced by the kinematics and dynamics of a robot, as well as actuators as energy converters, the robot is considered as an isolated energy system. Also, they conducted a preliminary investigation of the possibilities of saving and recovering energy during robot motion but they did not consider elastic elements as temporary energy accumulators and therefore did not think about robot control based on energy efficiency exploiting these energy saving devices. Obviously, the development of robots with elastic elements opens a completely new and wide research topic on energy efficiency of future service robots, their exploitation, and control which will definitely and strongly rely on energy optimization criteria. Often, in the case of compliant actuators, energy saving is not considered a high priority issue; instead, it is sidelined by safety, performance, design, control, etc. However, in the case of autonomous robots, energy efficiency is one of the most important features and the present thesis, therefore, considers energy efficient control. Laffranchi et al. at the Italian Institute of Technology explored energy consumption of two typical compliant actuator designs: serial elastic actuators and actuators based on antagonism [25]. The reported study focused on energy consumption in the elbow joint during a fast baseball throw. However, the study did not consider actuator design and introduced many assumptions that do not stand in general: no friction, no damping, massless actuators, massless transmission, etc. Simulation-

based results, which are founded upon approximate mathematical models, showed inferior energy performance of the antagonistic joint. Yet, the question arose: even if the same analysis had been performed for a repetitive task (hopping, walking, etc.), would the results have led to a different conclusion!?

Furthermore, energy storage in compliant robots allows outperforming of stiff robot dynamics. However, to achieve energy efficiency, compliance in actuators has to be exploited to match the natural dynamics of the system. Vanderborght et al. demonstrated that highly dynamic motions that outperform motions of rigid joints can be achieved by exploiting elasticity [26]. They used a single degree of freedom (DoF) driven by antagonistically coupled pneumatic drives to demonstrate energy saving in both simulations and real experiments.

A study about replacing a conventional stiff actuator with a compliant actuator of the same mass, with at least equal performance, is presented by Haddadin et al. in [27]. The authors explore under which conditions the elastic element and associated small motor could provide maximum link speed, superior to that of the original rigid link design, with a motor whose mass is equal to the mass of the entire corresponding SEA drive. Although they show superior behavior of the compliant joint, the requirements are satisfied under the assumptions of bang-bang control and short explosive motions, while their claims do not stand for longer time intervals of motions.

### **1.2.2 Active vs passive compliance**

Considering the above-mentioned trends in robotics, aimed at safety of robots and their environments, compliant actuation is needed. The previous subsection pointed out the benefits, but also the limitations introduced by compliant actuation. However, we did not discuss where compliance came from. Namely, one can distinguish between compliance introduced by mechanical design only, which is called “passive compliance” (intrinsic compliance), and software-based compliance, where the desired compliant robot behavior is introduced solely by a controller – “active compliance” [28], [29] (see Figure 1.3).

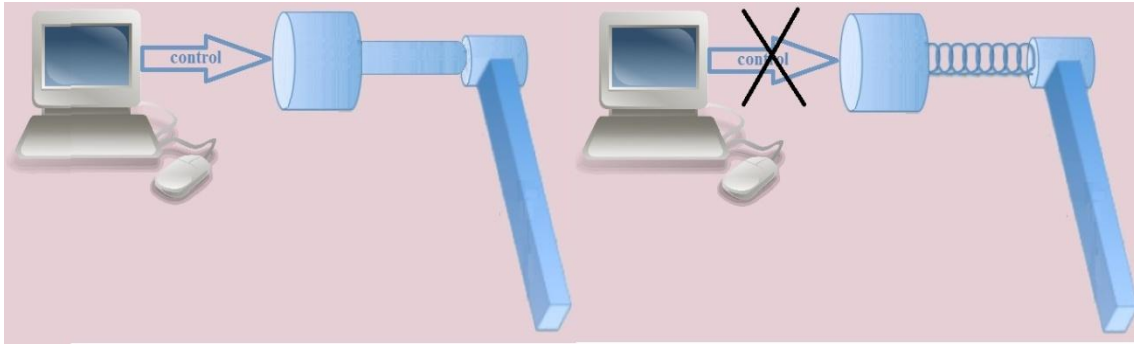


*Figure 1.3. Basic principle of active compliance – compliant joint behavior is purely a result of software action (left) and passive compliance – compliant joint behavior is a result of mechanical design (right).*

Many contemporary robotic applications include controlled interaction with the environment; however, undesirable interactions have to be handled as well. In that sense, active control represents immediate control of the active force between a robot and an environment. Naturally, active compliance has arisen from well-elaborated stiff robots, by the introduction of dedicating control. The greatest advantage of the active control approach lies in the fact that the active force can be controlled in an almost arbitrary manner. This means that collision-free motion can be performed in a rigid-like manner, whereas compliant behavior can be set when interaction is likely to occur. On the other hand, since compliant behavior of the robot is achieved by control; the control bandwidth is often not fast enough to detect impacts and reduce impact shock. The primary limitations of active compliance are feedback control constraints and stabilization problems [30]. Such sophisticated control also introduces expensive sensors and control units – fast and accurate enough to handle collisions. A failure in the electronics, noisy sensor data or even a bug in the software can have serious consequences for the robot and its environment. Furthermore, actuator saturation could hinder the desired impedance behavior.

Probably the greatest challenge in active control is estimation of the contact force. Sensors that measure six-component interaction force/torque directly are rarely used, while the identification of the contacted object – shape or mass, the detection of slip or surface friction, etc., are demanding [31]. A more common approach for estimating the contact force is to measure/estimate joint torques and then use an appropriate Jacobian

to relate joint torques to the contact force. However, estimating joint torques is also a challenge and is mostly undertaken by measuring the current and exploiting its direct proportional relation to the joint torque in the case of DC motor drives (see the application of Zollo et al. on the cable-driven anthropomorphic robot Dexter manufactured at Pisa, Italy) [32]. Note that by measuring the motor currents one can estimate the corresponding motor torque. Although the motor torque determines the joint torque, a deviation could appear due to non-linear gearbox characteristics.

With the development of integrated joint torque sensors [33], it became possible to implement joint torque control. The torque sensor integrated between the gearbox and the load enables accurate torque estimation and a higher control bandwidth. Therefore, some demanding control techniques using torque-feedback can be implemented, as well as feedback linearization techniques especially important for this thesis. The main idea of joint torque control is to compensate for inevitable friction and nonlinearities in actuators and transmission systems. Consequently, the Institute of Robotics and Mechatronics at the German Aerospace Center (DLR) stands out as the leading institution that exploits joint torque control in the design and control of DLR lightweight arms [29], while their DLR LWR-III robot is considered to be one of the most advanced among active compliant robots. Although the implementation of joint torque control allows excellent force control and, therefore, very low impedance at low frequencies, joint torque control is ineffective in reducing the impedance of the manipulator above the control bandwidth. The actuator inertia is still dominant in effective inertia at high frequencies, and therefore does not make robots inherently safe.

If mechanical elasticity is included in actuator construction, then such compliance is called passive or intrinsic. In general, passive compliance can partly overcome the limitations of achievable compliance by active control, especially when considering the protection from impact shocks and damage that could occur due to high-frequency disturbances. Thus, many of the benefits listed in Subsection 1.2.1 refer mostly to passive compliance and elastic elements, rather than active robot control: lower reflected inertia, reduced impact shocks, possibility of energy storage, etc. In contrast to active compliance, the robot remains compliant even in the case of deactivation or drive

malfunction, thus potentially increasing the safety of both humans and the environment interacting with the robot, and protecting the robot itself from external impacts. On the other hand, pure passive compliance in robotic actuators does not make the overall effective impedance variable; instead, it is determined by the elasticity of the elastic elements and the robot's pose. Passive compliance is always designed as static or quasi-static compliance, whereas active compliance can include dynamics (admittance/impedance control). Therefore, an initially designed and manufactured passively-compliant robotic system might be intended for a particular robot application, but it is hardly adaptable to any new scenarios. The most famous result in robotic assembly that relies on purely passive compliance (end-effector passive compliance) is "remote center compliance – RCC", which introduces an additional compliant element at the end-effector to facilitate assembly tasks [34]. Finally, passive elasticity inevitably causes a significant loss of link motion bandwidth and trajectory tracking accuracy.

In order to overcome the limitations of both passive and active compliance, and at the same time exploit the advantages of both, a new generation of robotic actuators – variable impedance actuators – is being developed.

### **1.2.3 Variable stiffness actuation (VSA)**

To avoid any misunderstanding, some remarks concerning the terminology are required. The term 'stiffness' refers to a purely static relation, whereas impedance stands for a general dynamic relation between the imposed force and actuator deflection. Therefore, the terms 'variable stiffness actuators' (VSA) and, more generally, 'variable impedance actuators' (VIA) are common. Since compliance is the opposite of stiffness, and admittance is the opposite of impedance, the terms 'variable compliance actuators' (VCA) and 'variable admittance actuators' (VAA) are sometimes used.

VSAs or, more generally, VIAs combine beneficial properties of both passive and active compliance. Namely, a VSA comprises elastic elements of changeable stiffness or elastic elements of constant stiffness, which can change the overall actuator stiffness due to mechanical arrangements within the actuator.

Many rules-of-thumb exist in stiffness control/planning: when accurate motion is desired, use high stiffness; while moving slowly, high stiffness is acceptable; when moving fast, use low stiffness; when impact is likely to occur, use low stiffness, etc. Thus, a detailed analysis of stiffness planning is needed. As such, variable stiffness in actuators is deemed to be the ideal solution, integrating both intrinsic (passive) compliance and control (active) compliance. The way in which mechanical impedance (including stiffness and damping) could optimally vary during motion, trading performance for safety during task execution can be a solution to the Safe Brachistochrone optimal control problem introduced by Bicchi and Tonietti in [35]. There the authors show that optimal behavior (safe and good tracking) of variable impedance mechanisms imposes high stiffness at low link velocities, while low stiffness should be commanded at high velocities, to decouple the actuator's inertia from the link's inertia. Also, they show that an important parameter for achieving high-performance motion with such mechanisms is the ratio of the maximum to minimum achievable actuator stiffness.

However, this benefit comes at a certain cost. First of all, the number of actuators increases. Consequently, a more complex mechanical design is required. Non-linear elastic elements need to be used to provide variable stiffness. Moreover, non-linearity and dynamic coupling of the complex design complicates VSA control.

Since VSA can be achieved in different implementations, there are only general criteria for good VSA design. First, stiffness control should be decoupled from position control. Then, stiffness should be independent from the external load and the available stiffness range should be as wide as possible (theoretically unlimited). The mechanism added to VSA to change the stiffness should require as little energy as possible and should not add inertia to the output link. Furthermore, no energy should be supplied to maintain a certain stiffness level. Finally, to fully exploit elastic energy storage and release, the variable stiffness mechanism should not reduce the maximum elastic energy storage capacity.

In order to comply with the general VSA design criteria and, in addition, consider their implementation in robotics, many design, manufacturing, and control issues need to be addressed. Initially, the practical realization (mechanical implementation) of the VSA concept is complex. The physical realization comprises the achievability of the desired stiffness range, desired displacement range, and complex torque/stiffness/deflection characteristics. Even if such requirements could be fully met, the size and ability of integration of such actuators in robotic joints would be questionable and troublesome.

The initial comprehensive review of VSA was presented by Van Ham et al. in [36]. They divide existing VSA conceptual designs into four groups (according to the source of variable stiffness):

**Equilibrium-controlled stiffness** uses a spring of constant stiffness in series with a traditional method of actuation, and variable stiffness is achieved by dynamically adjusting the equilibrium position of the spring using an additional actuator. In this way, stiffness-control or force-control, is converted into position control. Examples are actuators in the prosthesis industry [37], [38].

**Structure-controlled stiffness** modulates the effective physical properties of the elastic element, causing variations in the elastic element stiffness and therefore actuator stiffness. Examples include the mechanical impedance adjuster [39] and jack spring actuator [40].

**Mechanically-controlled stiffness** modulates effective stiffness of the actuator similarly to structure-controlled stiffness, but the full length of the elastic spring is always used, while variation occurs due to changed points where the elastic element is attached to the structure. Examples are MACCEPA [41] and DLR VS Joint [42].

**Antagonistically-controlled stiffness** often relies on two identical actuators with non-linear elastic elements, which are coupled antagonistically, working against each other. A detailed review of antagonism-based VSA is provided in Subsection 1.4, since antagonistically-controlled stiffness actuators are the main focus of the thesis.

Each design concept introduces some advances and drawbacks. There are differences even within a group and the presented concept might be optimized for a specific application. A detailed comparative analysis of these concepts can be found in [36], while a recent review of variable impedance actuators, as a guide for VIA design for different applications, is given in [43]. Besides providing insight into VSA mechanical designs, Vanderborght et al. in [44] discuss energy consumption as one of the key benefits of variable stiffness in robotic applications.

The biological paragon of variable stiffness actuators is a muscle, whose performance is superior to existing VSAs. Moreover, the human motor-control system is far more advanced in planning and control of muscle parameters. The power of the force-to-weight ratio, impedance range and control capabilities of existing VSAs are still not comparable of those of human skeletal muscles. Therefore, motion control, handling safety, and energy efficient behavior of humans are still superior to their technical counterparts in robots. An overview of human muscle performance is provided in [45]. The following muscle characteristics could be deemed desirable in novel robotic VSAs:

- force-to-weight ratio up to 1000:1,
- maximal force exceeding  $10kN$ ,
- shortening velocity up to  $5\text{ m/s}$ ,
- response time from  $3ms$ ,
- efficiency about 95%.

However, all the listed muscle characteristics are mutually dependent, so the maximal force is achieved only at the optimal muscle length and velocity, at high velocities, or when the muscle is shortened the available muscle force is in a very restricted range. The basic properties of the muscle force-length-shortening velocity are shown in Figure 1.4 (left). However, due to the restriction of skeletal muscles to produce solely an uni-directional force, muscles can only pull and not push, so most of their arrangement requires antagonistic coupling. Consequently, variable stiffness of such an actuated human joint is achieved.

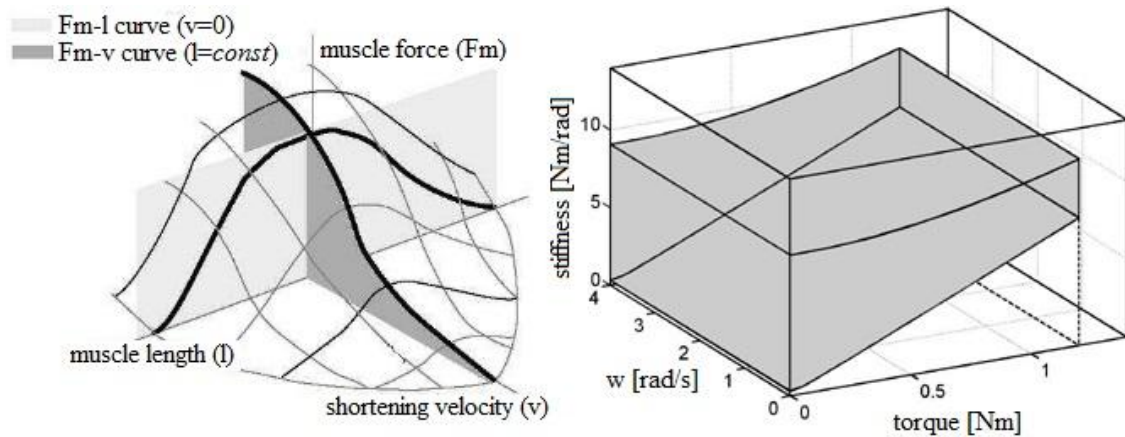


Figure 1.4. Force-length-velocity 3D plot of a human muscle as a biological paragon of variable stiffness actuators – VSAs (left); Torque-stiffness-velocity 3D plot of achievable characteristics of a qbmove actuator as a VSA representative (right).

On the other hand, conventional rigid drives are chosen so that the range of torque and velocity fits within the working area (continuous work region below the torque-speed characteristic). However, this is not sufficient for drives with variable stiffness actuation. Namely, not all combinations of torque-velocity-stiffness values are possible. A cross-analysis of actuator characteristics (torque, stiffness, and velocity) led to achievable triplets presented in a 3D graph. Similar to that of a muscle, but with differently appointed parameters (stiffness is given instead of length), the features of qbmove [46], representative of VSA actuators, are depicted in Figure 1.4 (right). Detailed insight, from a user's standpoint, into variable stiffness actuators is provided in [47].

Based on the scope of the present thesis, which analyzes the musculoskeletal robot structure and therefore the actuation system which resembles that of a human, the focus is on antagonistic drives as prime movers in a human body. Following the anthropomorphic principle, which is introduced in the following subsection, it is most likely that future service robots will be actuated exactly in this manner.

### 1.3 Anthropomimetic robots

A long time ago, the very famous work of Fukuda, Michelini, Potkonjak, Tzafestas, Valavanis, and Vukobratovic [48], claimed that humanoid robots would inevitably become more and more humanlike in their shape and behavior and that to that end humanoid robots should feature humanlike motion, humanlike intelligence and humanlike communication.

The majority of current humanoid robots, regardless of their human-like appearance, are actually designed as conventional machines. This is the case even with the most advanced humanoids such as Honda's ASIMO [49], which is capable of walking, running, hopping, climbing stairs, unscrewing lids, pouring liquid between two bottles, etc., or the winner of the human-size robot soccer league - Virginia Tech RoMeLa Lab's robot Charli [50], famous for performing a demanding Gangnam-style robot dance [51].

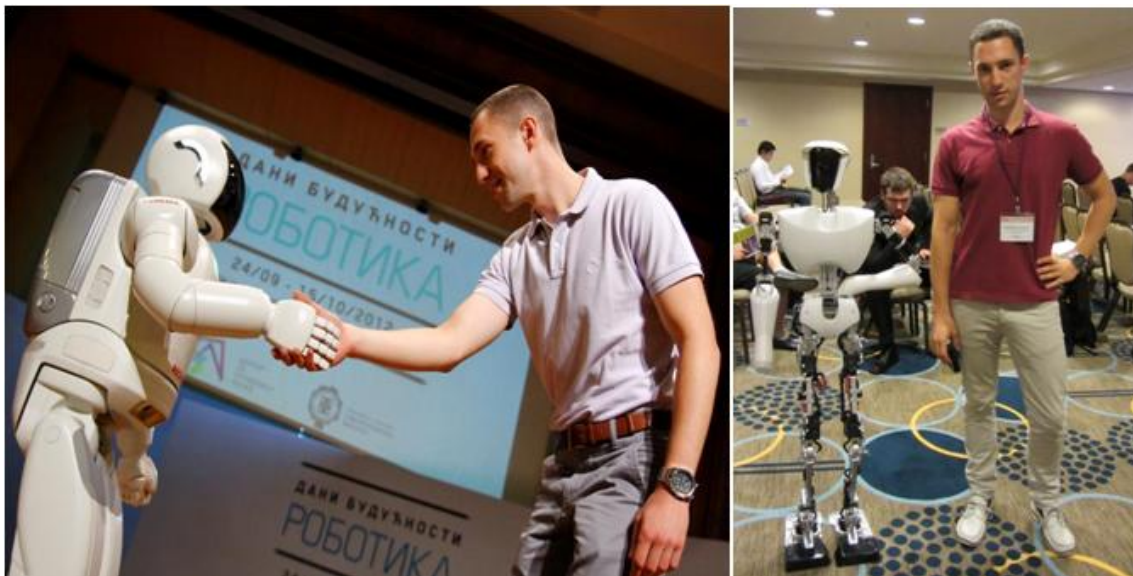


*Figure 1.5. Examples of mechanically most advanced humanoid robots: Honda's ASIMO performing at Days of the Future: Robotics in Belgrade, Serbia, 2012 (left); and RoMeLa Lab's CHARLI presentation at the 35<sup>th</sup> ASME conference on mechanisms and robotics, Washington, D.C., USA, 2011 (right).*

However, the mechanisms of these robots are very different from those of humans. In addition to a very large number of DoFs in a highly articulated multi-element skeleton,

the human body features tendon-driven redundant actuation (joints moved by more than one muscle), multi-articular joint actuators (tendons often cross more than one joint), compliance (in both muscles and tendons), and complex joints (with no clearly defined axes of rotation, as in the spine and the shoulder girdle). In addition, human muscles have power-to-weight actuation ratios far above those of current robot actuators. In conjunction with the human control system, these factors enable a degree of maneuverability unmatched by current robots. To approach the performance levels of the human system, an effective strategy might therefore be to design robot actuators to imitate the muscle system. Such biologically-inspired robotic solutions open up a new and promising direction of research – anthropomimetic robots. The new term – anthropomimetics – is proposed by Holland in [52]. It concerns a new principle in robot design and manufacturing – mimicking of the human body, skeleton, and muscle system as closely as possible. The goal is to not just replicate the human structure, but to attain a high level of performance, analogous to the human paragon. Holland and Knight argue that restrictions in the application of robots in our daily life can be overcome only if we construct a robot with a fully human morphology, maneuverability, functionality, and, finally, intelligence. Such a robot would fit an environment completely adapted to humans, without restriction, would be capable of performing common household tasks, and would interact with humans in an inherently safe manner. To that end, the robot should not only be constructed targeting human anatomy, including significant passive compliance for safety and smooth motion, but should also be self-conscious, to use its natural dynamics and achieve a high level of energy efficiency. Moreover, a high level of robot intelligence, acquired from experience, is needed.

The ambitious idea of an anthropomimetic robot at the present level of technology is challenging from many perspectives, where robots still cannot compete with humans and biology: construction comparable to the skeleton, actuators comparable to muscles, sensors comparable to human sensing, control comparable to the human neural system, etc.

An adult skeleton comprises about 206 bones, many of which are replicated in the robot and hand-crafted with caprolactone polymer. This material is used to replicate bones,

since it has pronounced bone-like features (tough and springy) when cold, but is easy to hand-mold when heated to only 60 °C. Its characteristics could be further improved by adding other materials. Due to specific shapes (e.g. pelvis or vertebrae) and materials, a skeleton replica could hardly be produced by machines or even applying advanced techniques such as the 3D printer.

The realization of artificial muscles is particularly demanding since there is no actuator as perfect as the human muscle. Therefore, there is still a huge demand for further development and control of novel human-like actuators as a potential breakthrough in robotic applications. This topic is also addressed later in the thesis. So far, most of the tendon driven and compliant drives that mimic human muscles are electric drives equipped with gearboxes as active elements (corresponding to muscles). The geared drives are then connected with inelastic thread in series, with an optional elastic element that functions as a muscle tendon. Such a complex structure is inevitable, to achieve grace, smoothness, speed, efficiency, and robustness comparable to human movement dynamics. The properties of these components can be changed to mirror the characteristics of a particular muscle. In order to match the maneuverability of humans and human-like movement dynamics, the attachment points of these “artificial muscles” need to also be replicated from humans.

At first sight, the human sensing system is the easiest to replicate at the current level of technology. Strain gauges for tendon force estimation, or encoders and current sensors in electric drives, in combination with cameras, could faithfully resemble human proprioceptive sensors (muscle spindles for muscle stretching and the Golgi tendon organ for force estimation) and human vision. The main issue here is how to organize data from multiple sources. Even more so, the question is how to use these pieces of information. Thus, fusing sensory information is another challenge in anthropomorphic robotics.

Moreover, not only are the skeleton and sensory-actuation units of biological systems superior to those available in robot technology. The biological “control unit” comprises

a central high-level control unit - central nervous system (CNS), which carries out slower but very complex control tasks, and distributed control units for very fast decision-making and control (reflex arcs closed through the spinal cord). In order to cope with a large number of actuators and sensors, robot needs a complex and distributed control/software architecture. Under the Eccerobot project, Jäntsch et al. have already presented a distributed architecture that resembles neuronal circuits of the spinal cord, brain stem, and forebrain, which constitutes exceptional hierarchical control [53]. This hierarchy (see *Figure 1.6*) comprises distributed electrical control units (ECUs) for low-level actuator feedback loops, while the high-level central processor unit commands motion planning via a controller area network.

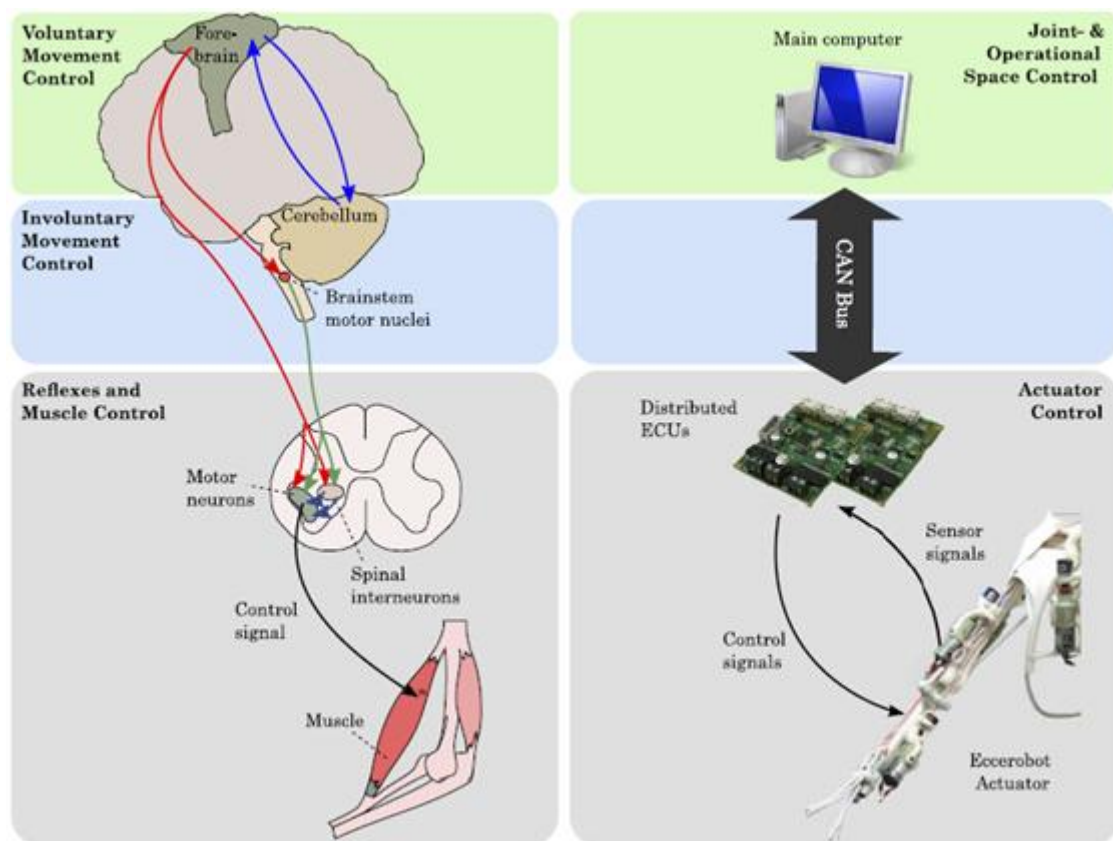


*Figure 1.6. Example of distributed control architecture that seeks to resemble its biological paragon in humans. Electrical control units (ECUs) are used for low-level actuator feedback loops, mimicking reflex arcs that are closed through the spinal cord, while a high-level central processor unit acquires all sensory data and commands motion planning via a controller area network that emulates the central nervous system.*

Working to meet these requirements brought about by the anthropomimetic concept, there are two research teams whose results stand out: a European consortium [8] led by Prof. Holland (University of Sussex, The Robot Studio – France, University of Zurich – UZ, Technical University of Munich – TUM, and School of Electrical Engineering, University of Belgrade) and the JSK Group [54] of Prof. Inaba at the University of Tokyo.

The achievements of the first team are an outcome of the work under the ECCEROBOT project (European 7<sup>th</sup> Framework Program, project “Embodied Cognition in a Compliantly Engineered Robot”). The results of more than three years of research in designing, manufacturing, simulating, and, probably most importantly, controlling anthropomimetic robots are presented in [11], [55], [10], [3], [56], [5]. Following the idea of anthropomimetic robot design, four anthropomimetic torsos have been fabricated so far. Each of them was constructed as an advanced prototype of its predecessor (Figure 1.7). The first among them, ECCE-1, was built in 2009; it is founded upon the Cronos robot but has an improved sensory-actuation system. Prototype ECCE-2 from 2010 was special for its convincing replica of the human neck and head, ECCE-3 manufactured in 2011 introduced a human-like spine, while the final prototype ECCE-4, completed in 2012, featured human-like shoulder blades and was mounted on a mobile base.



*Figure 1.7. Evolution of Eccerobot prototype, from left to right: ECCE-1 (2009), ECCE-2 (2010), ECCE-3 (2011), and ECCE-4 (2012).*

The work most similar to the Eccerobot project is a long-running series of

musculoskeletal robot projects at the Tokyo JSK Laboratory. In order to realize natural and diverse motions like in humans, as well as to uncover and understand human-like intelligence to manage these complicated musculoskeletal body structures, they have developed impressive engineered robots: Kenta [57], Kotaro [58] (and its power version Kojiro [59]), Kenzoh [60], and Kenshiro [61]. These projects have also analyzed the benefits of the radically novel anthropomorphic design, but took legs into consideration as well. A detailed review of the progress of JSK Lab's anthropomorphic robot can be found in [62].

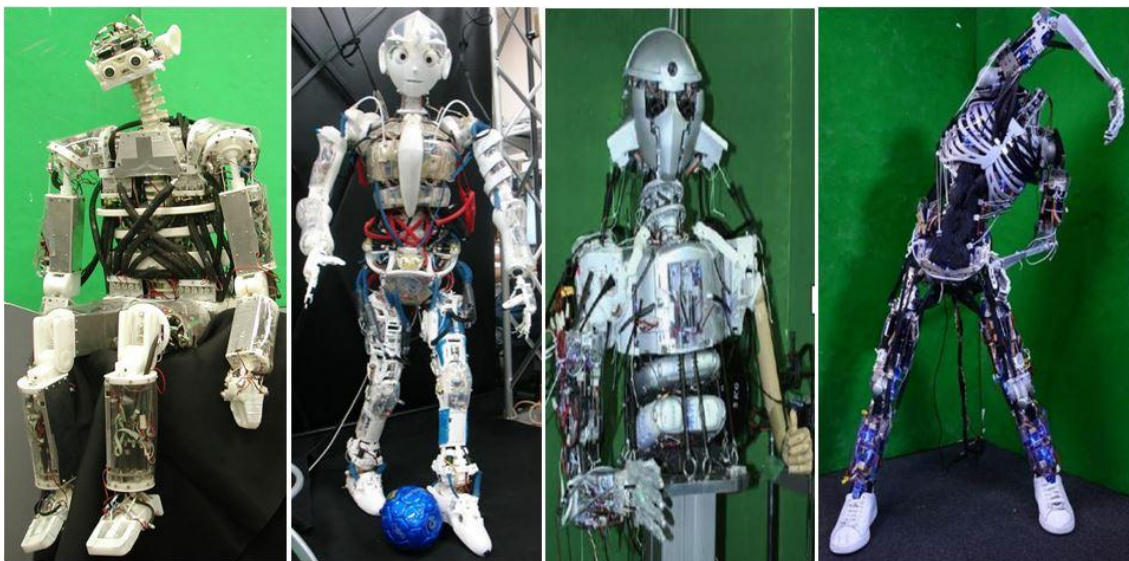


*Figure 1.8. Evolution of anthropomorphic legged robots at JSK Lab of the University of Tokyo. From left to right: Kenta (2003), Kotaro/Kojiro (2006), Kenzoh (2010), and Kenshiro (2013).*

Finally, the anthropomorphic principle in humanoid robotics lies not only in replicating the morphological appearance of humans, but also in capitalizing on those replicas of the human body, such as the equivalents of muscles, tendons, bones, and joints. From the very beginning, it was evident that an analytical approach would face numerous difficulties in anthropomorphic robot modeling, as an initial step towards further development. Obstacles arise in multi-DoF joint modeling (as well as actuating and sensing), bi-articular and poly-articular muscles influencing several DoFs simultaneously, and advanced human-shaped elements (e.g. shoulder blade, with a questionable number of DoFs). Considering control of such a system, the discussion

could become even more complicated, not only because of the above-mentioned challenges, which conventional engineering has not yet resolved, but also because of issues that are particularly demanding from a control point of view. A highly non-linear, multi-variable system is particularly complex due to input-output relations that are not fully defined. Moreover, high redundancy introduces an optimality problem. Finally, since the inherent safety of robots is ensured by their intrinsic stiffness, low intrinsic damping causes many oscillations that compromise the stability of the anthropomorphic system. Certain preliminary issues of anthropomorphic robot control are highlighted in [63].

Although some progress has been made in the design, simulation, and control of anthropomorphic robots, as often quoted in connection with the Eccerobot project, we have barely scratched the real potential of this novel approach. However, for deeper analytical insight into the topic, we have to make an approximation, simplify the original system and gradually make it truly complex. That is how the problem was eventually approached in the work presented here as the contribution of this thesis.

## **1.4 Review of antagonistic actuator designs**

According to the above-mentioned theory, antagonistically coupled drives stand out as a solution to variable stiffness actuation for future inherently safe robots. Among VSAs, antagonistic drives are characterized as a bio-inspired solution where both drives contribute equally to both joint position and stiffness. It is a well-known fact that human antagonistic muscles contract simultaneously, even though the use of one muscle is enough while bending a joint [64]. Although only one antagonistic actuator can be activated while bending a joint in robotic applications, that leads to invariable or even uncontrollable joint stiffness. This was demonstrated by Tsujiuchi et al. in [65], who developed a PID controlled system that features good trajectory tracking but with stiffness issues. Despite some disadvantages, such as difficult design of the non-linear elastic elements and the need to constantly control both actuation units to regulate the position/stiffness of the joint, many different engineering solutions based on the antagonistic principle have been explored. Before we focus on antagonistically coupled

drives, we will briefly recall some important works that do not represent antagonistically actuated joints but are deemed to be important related research. These research efforts suggest ideas and solutions that could possibly be transferred and adapted to antagonistic systems. Ultimately, they contribute to the development of bio-inspired, tendon driven, compliant and antagonistically coupled actuators.

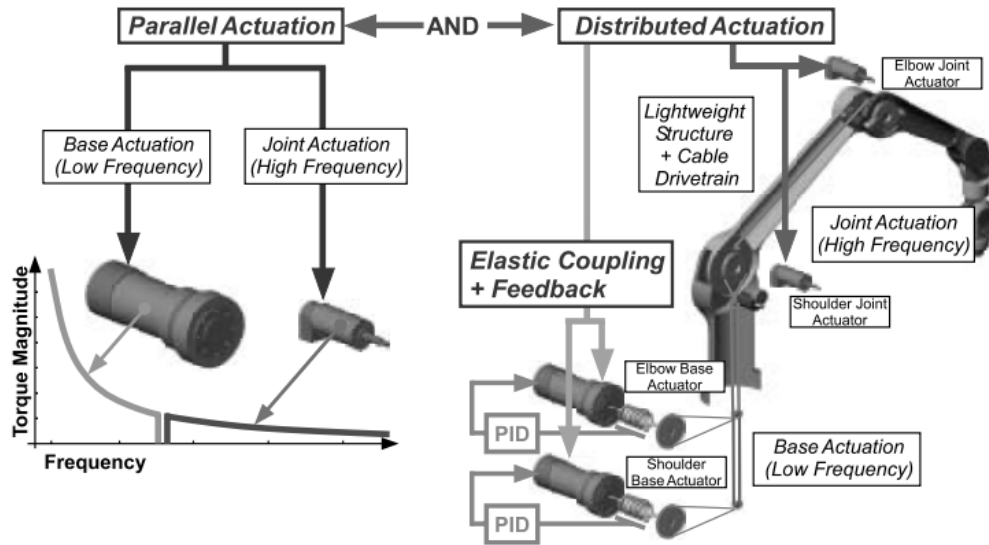


Figure 1.9.  $DM^2$  approach: torque partition among low-frequency high-torque and high-frequency low-torque actuators, contributing in parallel to overall joint torque (left); Actuator distribution: large, low-frequency actuators are tendon driven SEA located at the base to reduce effective inertia, whereas small, high-frequency actuators are located at the joints to enable high bandwidth control (right).

Not pioneering but surely one of the works that finally implemented the idea of role sharing among coupled actuators was presented by Zinn and Khatib [13]. Their teams from Stanford University proposed and designed a new actuation approach for human-friendly manipulator design – Distributed Macro-Mini Actuation Approach ( $DM^2$ ). The main characteristics of this approach, also featured in the bio-inspired antagonistic design, are tendon transmission, passive compliance, and drive redundancy. The approach partitions torque generation into a low-frequency component of high power, as the main drive, and a low power high-frequency component as the supporting drive (see Figure 1.9). The effectiveness of such distribution can clearly be seen, keeping in mind that most manipulation tasks involve position or force control, which is dominated by

low-frequency torques. The biomechanical inspiration for drive division into fast and slow parts is also pointed-out by Potkonjak et al. [66], [67]. In [13], high-frequency torque actuators are placed in the joints to achieve high-bandwidth control and they are almost exclusively used for disturbance rejection. Additionally, the DM<sup>2</sup> approach distributes torque generation between the main and the supporting drive, based on torque magnitude. The main drive is responsible for generating high torques, such that the safety of the manipulator primarily depends on the coupling of this motor with the manipulator (since the supporting motor can generate only low torques). The main drive is coupled to the manipulator using serial elasticity in order to reduce effective inertia.

There is one more justifiable reason why engineers tend to design technical solutions that originate from biological systems. Namely, if any obstacles appear in the design, control or implementation phase, we can turn to biology once again and find ideas for a solution. So, Xiong et al. [68] suggested a variable admittance robot controller based on a virtual antagonistic mechanism. “Virtual” here means that every joint physically actuated by a standard servo motor can produce variably compliant motions, as if driven by a pair of antagonistically paired muscles. The main idea of that paper relies on the assumption that the passive properties of muscles play a key role in animal joint stability, when confronted with external perturbations. In that way, they intended to build a rather simple mechanism but retain the performance of a more complex mechanism based on antagonistically coupled drives. Of course, since antagonism was only “virtual” and its functionality was achieved mainly by control, not all the features of a full antagonistic system, such as decoupled control of position and stiffness, could be accomplished. Regardless, the controller was successfully implemented on their hexapod robot, by reducing the contact force and preventing leg damage when imposed on either static or dynamic perturbations.

One more instance of a lightweight, tendon driven, compliant, bio-inspired robot design was produced under the BioRob project [69]. There a conventional rotary electric actuator (DC drive) is elastically coupled to the actuated joint by means of a pair of cables and springs, similar to an antagonistic configuration but with both cables attached to the same electrical drive. Additional reduction in inertia is achieved by

moving the electric drive to the beginning of the preceding link, while at the same time reducing the static load. Furthermore, lengthening of the elastic elements is measured by incremental encoders at the drive and the joint itself, and forces acting on the system are inexpensively and easily calculated from these elongations. This eliminates the need for costly and heavy torque sensors. Initial testing shows a weight to payload ratio of 1:2.5, which is quite good for this low cost bio-inspired solution. Nevertheless, severe constraints apply to this design: the range of possible payloads is limited by the characteristics of the elastic elements, oscillations caused by the elasticity in the actuation require a significant control design effort, etc. In fact, that was one of the first projects that highlighted control as a key challenge in robotic systems of this kind.

Finally, many roboticists have opted for antagonistic joints since they can control joint position and impedance, and at the same time, using tendons and cabling, relocate drives and achieve miniaturization of robotic hands, reduce inertia, and increase robustness. Furthermore, technical implementation of antagonism can extract solutions that mimic biological muscle-tendon units and their control patterns. Antagonism in the engineering world can be achieved using two conventional electric motor drives and even more biologically inspired forms, such as pneumatic (or hydraulic) muscle-like actuators. In the latter case, compliance is an inherent characteristic of the actuator, whereas for an electrical design compliant elements (mostly elastic springs) have to be added to the system. Typically, antagonistic mechanisms increase the construction and maintenance effort, and complicate system identification and controllability (due to non-linearity and friction properties), such that thorough planning and advanced design/production technologies are necessary for manufacturing and utilizing such mechanisms. Jacobsen et al. in [70] listed optimal goals for the design of antagonistically actuated joints and their control:

- minimum antagonism – not more than two opposing actuated drives per joint,
- low co-contraction (minimum tendon tension) in either passive or active performance,
- high stiffness in position control,
- low impedance in force control, and
- simple implementation.

Chou and Hannaford elaborated on the preferred design of antagonistic actuators in [71]. Their point of view relies on a bio-inspired design that resembles antagonistically coupled human muscles. Although at that time and that level of technology one could not expect an actuator to accurately mimic the overall static and dynamic behavior of a muscle, they set criteria that should have been followed as far as possible (complete quotation):

- strength to weight ratio ( $N/kg$ ) and tension intensity ( $N/cm^2$ ) equal to or greater than those of a skeletal muscle,
- contraction ratio ( $\Delta l/l$ ) and speed of contraction ( $\Delta \dot{l}/\dot{l}$ ) comparable to those of a skeletal muscle.
- variation in force with length comparable to that of a muscle (Gordon et al. in [72]),
- damping behavior comparable to a skeletal muscle – for example, nonlinear damping following Hill’s model [73] would be an excellent approximation. Although there are many known subtleties to the dynamics of muscle contraction, accurate reproduction of Hill’s force-velocity relation would be a huge step towards more biological actuation characteristics,
- flexibility to curve around bones and ligaments and rub against neighboring actuators (for example in the deltoid muscle), so that it can be integrated within the skeleton,
- ability to be easily manufactured in a range of physiologically relevant lengths at low cost,
- compatibility with widely available power sources and environmental conditions, and
- reliable performance of many cycles without failure. This will be especially valuable for future experiments in motor learning control.

Moreover, antagonistically paired muscles are indeed the prime movers of a human body. Accordingly, robotics would profit from analysis of antagonism in humans, while, on the other hand, once antagonistic actuators are mastered, they will be widely used in future musculoskeletal mechanisms. Typical antagonistic muscle pairs in humans are:

- biceps and triceps (elbow muscles),
- biceps femoris and rectus femoris (knee muscles),
- soleus and tibialis anterior (ankle muscles),
- rectus abdominis and erector spinae (lower-torso antagonistic muscles),
- pectoralis major and latissimus dorsi (upper-torso antagonistic muscles),
- maximus gluteus and iliacus/psoas major (hip muscles).

The following paragraphs provide comprehensive insight into the development of compliant robotic actuators based on antagonism. First, the most famous electrical drives are discussed in detail, as a technology that has prevailed in recent years and which is consistent with the focus of this thesis. Afterwards, the most important results that exploit hydraulic and pneumatic drives in antagonistic configurations are presented, as a technology that more faithfully resembles the human muscle (“human actuation units”), but suffers from a few technological limitations that limit their use in contemporary, safe and precise robotics applications.

#### **1.4.1 Antagonistic actuators based on electrical drives**

In order to achieve variable stiffness using antagonistically coupled drives, a non-linear characteristic of elastic elements is needed (see Section 3 for more details). To that end, researchers have proposed numerous solutions, including conical springs [74] such as linear springs with dedicated pulley system [75], rolamite springs [76], leaf springs [39], etc. However, regardless of the chosen approach, it was extremely difficult to accurately design them to meet a specific force-length relationship. It was, therefore, necessary to consider estimating the stiffness and closing the feedback accordingly. At the same time, while linear springs were commercially widespread and readily available, and had reliable force-length characteristics, none of the non-linear springs could be procured easily. This fact led to novel nonlinear spring mechanisms, which could shape the non-linear force length relationship from linear springs (Figure 1.10 - left). Migliore et al. in [77] exploited their mechanism to design an antagonistically-actuated robotic joint

(Figure 1.10 - right).

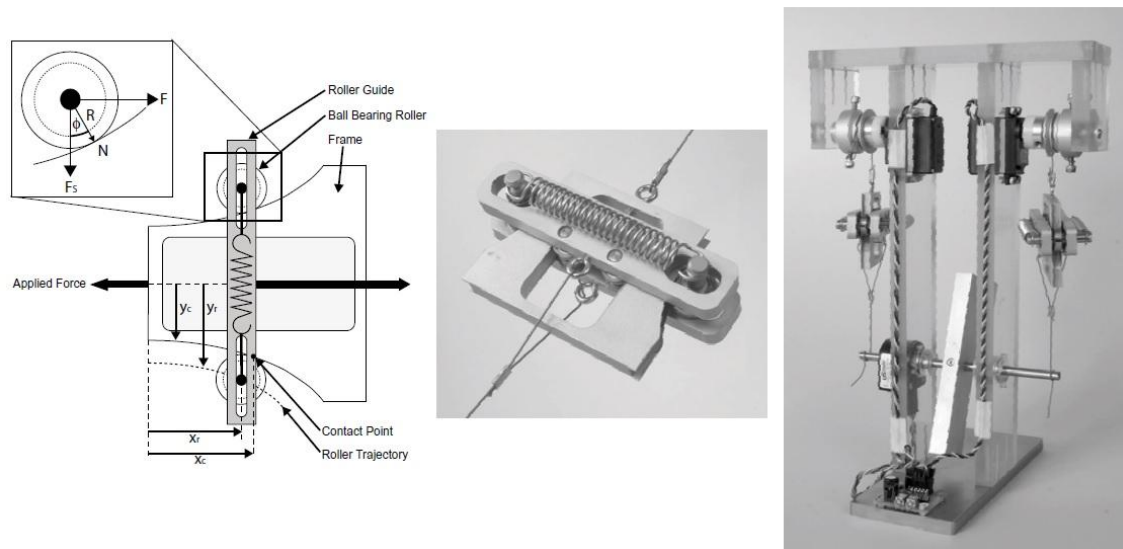


*Figure 1.10. Design of non-linear elasticity shaping device (Migliore et al. [77]). When force is applied to the device, the rollers are pushed along the expanding contour and stretch is applied to a pair of linear springs (one is not visible in the background) - (left); Physical realization of a device used to produce a quadratic force-length relationship (middle); Mechanism employed in an antagonistically actuated single DoF robotic joint with series-elastic actuation of user-shaped quadratic characteristics (right).*

One of the first integrations of antagonistic joints within a fully functional forearm prosthesis of the same size as an adult's forearm was undertaken by Koganezawa et al. in Japan almost two decades ago [74]. By imitating a skeleto-muscular articulation system, the authors developed an antagonistic muscle-like actuator (AMA). The main idea was to use all the benefits introduced by antagonistic tendon-driven actuators and at the same time deal with their main drawback – the number of actuators (which is double the number of joints). The AMA structure is schematically represented in Figure 1.11. A pair of ball-screw nuts, driven by the main drive – DC motor, rotate or co-contract the hinge joint depending on stepping motor activity and the corresponding gear coupling. Integration of one AMA actuator (one DC motor, one stepper motor and several ball-screw nut pairs) for driving several degrees of freedom is depicted in Figure 1.11 (right). The main drawback of this type of antagonistic actuation was that independent simultaneous movements of some DoFs were not possible. Simultaneous

control of stepping and DC motors could only partly compensate for this issue and even a very sophisticated controller could not surmount the physical limitation. Thus, elaboration of both the design and control of biologically-inspired antagonistic actuation was necessary.

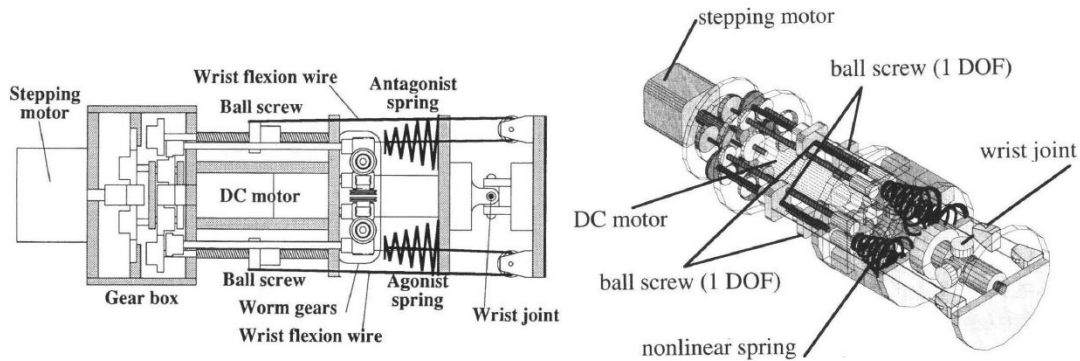


*Figure 1.11. AMA actuator structure: one DC motor drives a pair of ball-screw nuts, which rotate or co-contract the hinge joint via non-linear conical springs, depending on stepping motor activity and corresponding gear system (left); AMA part of human-size forearm prosthesis (right).*

Several years later, after they announced their first antagonistic setup (AMA), Koganezawa et al. [78], [79] presented a new actuator – ANLES (Actuator with Non-Linear ElaSticity). The idea was to create an actuator with a guide shaft of non-uniform radius and torsion springs coupled to a transmission cylinder. This provided user shaped non-linear elasticity, as a prerequisite for stiffness control. Mimicking the antagonistic skeleto-muscular system, the antagonistic coupling of two ANLESeS, coupled to joints via bevel gears and spur gears, was presented in [78] (Figure 1.12). However, this antagonistic structure suffered from several imperfections; the three most evident were high friction [79], gear backlash, and actuator volume. Another contribution of the authors was the proposed joint angle control based on initial torsion angle deflection estimation and on-line joint mass estimation using the Newton-Raphson numerical method. Despite substantial mechanical enhancements, two major actuator operation issues remained: reduced applicable volume of the actuator and reliable competitive control.

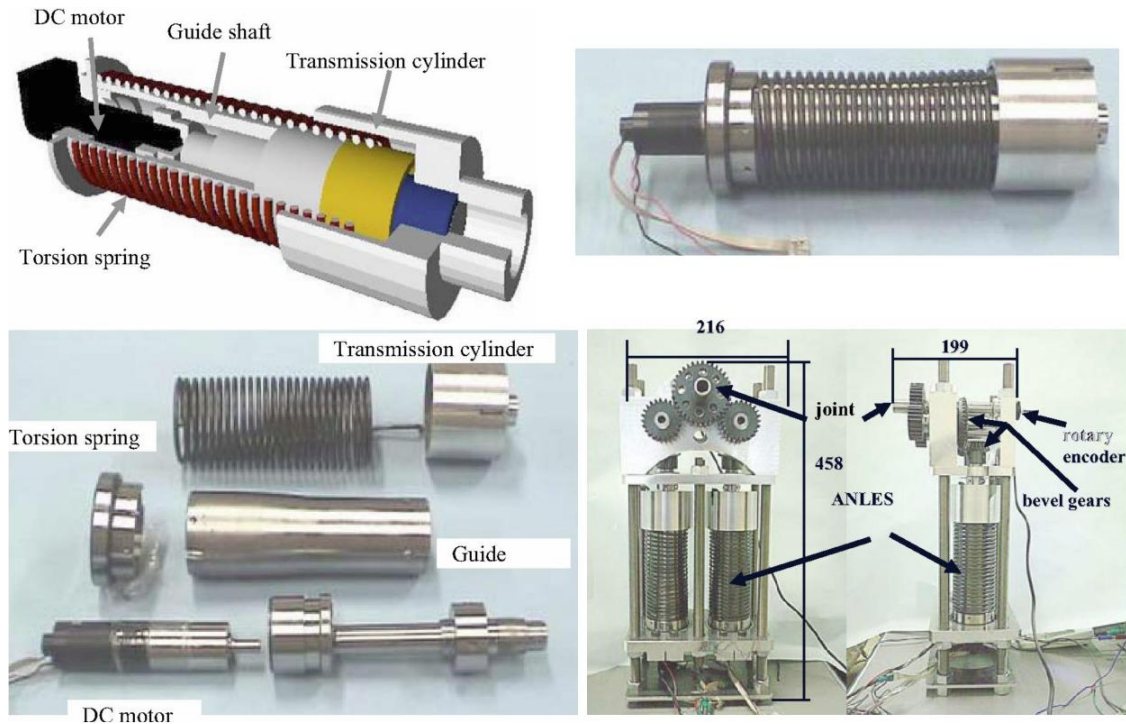


Figure 1.12. ANLES CAD model (top left); Fully assembled ANLES (top right); Building elements of ANLES (bottom left); Front and side views of assembled antagonistic joint driven by two ANLES (bottom right).

At that time, there were several research groups developing compliant mechanisms based on the same principle: building relatively complex mechanical structures to achieve a non-linear length-force characteristic using commercially available linear springs. Hurst et al. [80] at Carnegie Mellon University designed an actuator prototype for highly dynamic legged locomotion. They tried to combine software control with actuator intrinsic compliance to match the natural system dynamic and consequently realize energy-efficient periodical movements (hopping, running, etc.), as in the case of humans and animals. The force-length relationship could be changed by choosing different shapes of spiral pulleys (denoted by  $G(Z_A)$  and  $G(Z_B)$  in Figure 1.13 (top left), where  $Z_{A/B} = x_3 \pm \Delta x$ ). Besides motor position, one can control spring pre-tension via position  $x_3$ . Of course, if the spring was itself linear, this additional mechanism served to reshape the final force-length relationship. Given that the high-frequency behavior of the system is generally handled by the springs, low friction and inertia are the most important in this part of the actuator. The low-frequency behavior of the system is handled by the motor, and thus friction and inertia can be overcome by relatively low-

bandwidth software compensation. Some basic tests showed that a prototype based on this principle faced several problems, such as difficulties with the shape of spiral pulleys, to match exact force-length characteristics, as well as hysteresis caused by friction.

Tonietti et al. [81] at the Bioengineering and Research Center “E. Piaggio”, University of Pisa, developed another actuator that could simultaneously control position and mechanical impedance, while optimizing performance and guarantying safety. This work introduced the implementation of feedback for joint impedance and position control in spite of model parameter mismatches or unforeseeable disturbances. The authors also pointed out certain advances, such as rapid stiffness variation and a more compact design, compared to previous prototypes of compliant actuators based on the antagonistic principle. However, accurate overall stiffness estimation of the mechanism was questionable since it assumed ideal symmetry and required several approximations to avoid computational complexity.

The same group at the University of Pisa presented an enhanced version of their variable impedance actuator applying the antagonistic principle – VSA-II [82]. The new version featured extended torque capacities, a longer life cycle and several aspects that facilitated its easier integration into novel robotic mechanisms. The core of VSA-II was a transmission system based on 4-bar mechanisms (Figure 1.14). The role of the transmission system was to achieve the desired non-linear torque-displacement characteristic between the input torque applied by the motors and the angular deflection of the joint shaft. Note that commercially-available linear springs were still used as elastic elements, while non-linearity was achieved using the transmission system. One could shape this characteristic by suitably selecting link lengths (OA and OC of length  $R$  and BA and BC of length  $L$ ), in combination with linear spring stiffness  $k$ . Initial tests of VSA-II confirmed the listed improvements, but there were still some limitations that hindered its wider application, which included reduced range  $\theta \in (0, \theta_{max}]$ , where the limits were specified by mechanical construction:  $\theta_{min} = 0$  would lead to singularity and  $\theta_{max} = 2\arcsin(L/R)$  was a geometric constraint.

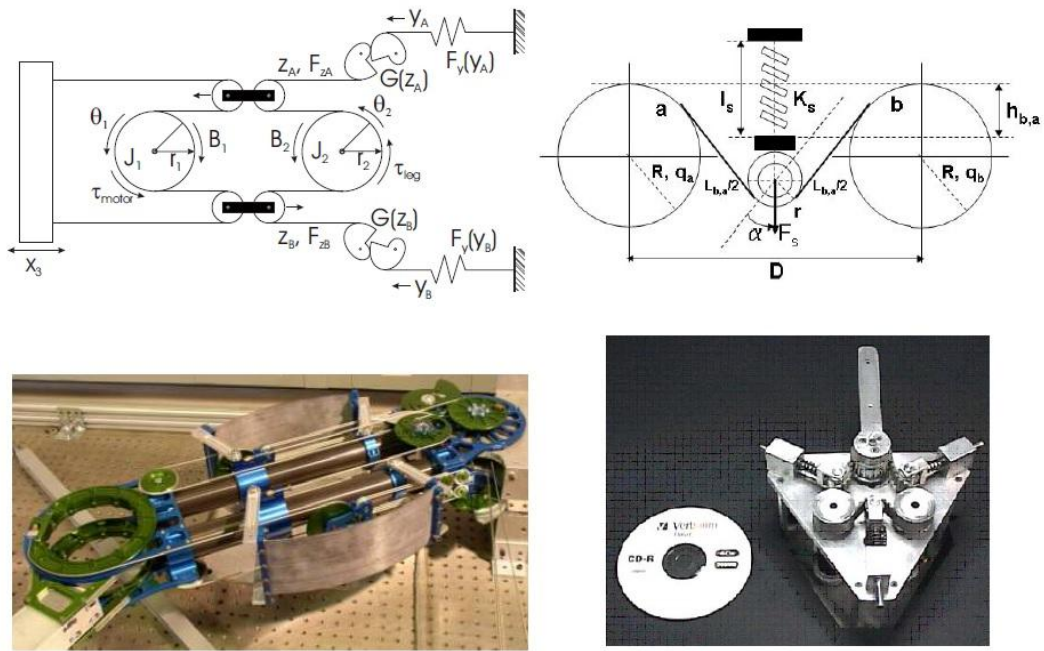
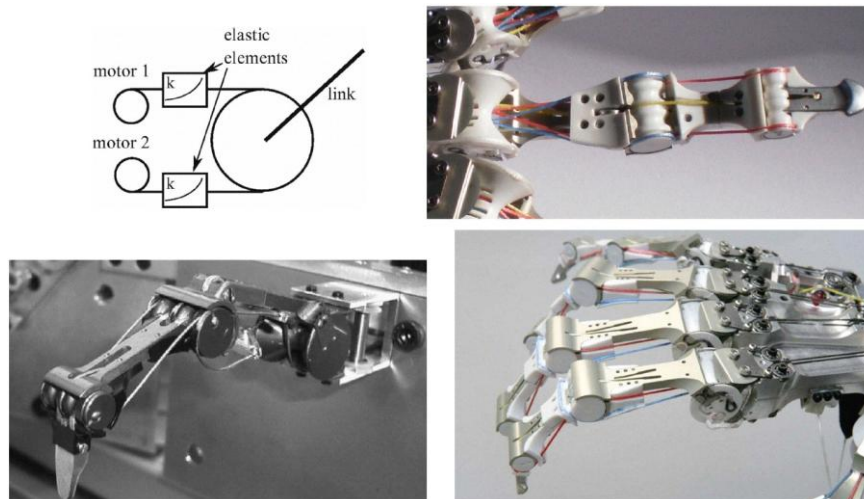


Figure 1.13. Functional scheme of actuator for highly dynamic legged locomotion designed by Hurst et al. [80] at Carnegie Mellon University. The original spring force-length relationship  $F_y(y_{A/B})$  could be shaped by choosing a different shape of spiral pulleys (denoted by  $G(Z_A)$  and  $G(Z_B)$ ). Overall joint stiffness and position are controlled by motor position  $\theta_1$  and spring pretensions  $x_3$  (top left); Prototype of highly dynamic legged locomotion designed at Carnegie Mellon University (bottom left); Functional scheme of one side of the variable impedance actuator designed by Tonietti [81] at the University of Pisa (top right); Prototype of the variable impedance actuator VSA at the University of Pisa. The transmission belt connects the DC motor pulleys to the main joint shaft, while the transmission belt is tensioned by passive elastic elements  $K_s$  to shape joint stiffness (bottom right).



Figure 1.14. Functional scheme of VSA-II (4-bar transmission mechanism). Link  $OA$  is driven by a motor at  $O$ . The torque spring  $k$  is linear, while stiffness seen at  $O$  attains non-linearity through geometry (left); VSA-II prototype (middle); Test-bed for evaluation of VSA-II integration into a robotic joint (right).

DLR Institute of Robotics and Mechatronics, one of the leading European institutions in the field of variable stiffness actuation (and general safe human-robot interaction), stands out with several novel robotic mechanism and solutions. One of the most interesting is the development of the DLR Hand Arm System (HASy) [83]. DLR's point of view consists of understanding the human hand in a functional way, rather than straightforward copying of its anatomy. HASy tends to reach the human archetype regarding size, weight and performance using variable stiffness actuators developed at DLR. Thus, several variable stiffness actuation principles are employed and one of them is also antagonistic. To comply with size, functionality and robustness requirements, Grebenstein et al. [84] designed an antagonistically driven finger (Figure 1.15). The design integrated all drives of the hand into the forearm. Tendon routing and antagonistic actuation were optimized to minimize friction and wear. In order to reduce control complexity, the authors tried to avoid non-linearities and the tendons were therefore fixed on a cylindrical pulley, providing a constant moment arm in contrast to the human hand. Preliminary experiments demonstrated promising performance with a maximal fingertip force of 30N in the stretched-out configuration, and good robustness against impact.



*Figure 1.15. Functional scheme of antagonistic actuation employed in fingers of DLR Hand Arm System [83] (top left); First prototype of DLR anthropomorphic finger (bottom left); Second prototype of DLR anthropomorphic finger (top right); Assembled hand using antagonistic actuation for finger control (bottom right). Tendon routing was optimized to minimize friction and wear, while all drives of the hand were moved to the forearm to fit human size.*

For an achievable stiffness range and successful control of both position and stiffness, the crucial element was the adjustment of non-linear force-deflection characteristics in each individual elastic element of an antagonistic setup. To that end, DLR devoted special attention to this issue and finally presented a flexible antagonistic spring element (FAS) in a paper by Friedl et al. [85]. They advocated antagonistically coupled tendon drives as the best and only choice if one wishes to integrate drives in a human-size arm and achieve the functionality of a human hand. Furthermore, they highlighted overall tendon characteristics for best performance, when employed for tendon transmission in a robotic hand (durability, minimal banding radius, attaching capabilities, minimal friction with sliding surfaces, minimal stretching force of  $350N$ , etc.). In addition, they experimentally proved dyneema (trademarked as the world's strongest fiber) ropes, which are superior to steel tendons. A very compact actuator design was followed by compact sensors, whose characteristics, such as non-linearity and self-calibration, should be further improved to enable reliable and accurate control of FAS-driven antagonistic joints.

If a classical uni-directional antagonistic scheme is used, the maximum joint torque is limited by the maximum of torques of each drive in an antagonistic configuration. To overcome this limitation and in accordance with their intention to build robotic manipulators/arms that copy human functionality while fitting human size, rather than simply copy human mechanisms, DLR Institute of Robotics and Mechatronics put forward a modified antagonistic principle – bidirectional antagonism. This design, presented by Petit et al. in [86], relies on the fact that unlike human muscles, electric motors are able to act in both directions. Bidirectionality means that each of two motors is connected bidirectionally to a link, to drive it in both directions. This was achieved by replacing a single tendon between one motor and the link with cables, forming a complete loop around them, which were rigidly connected to the link and the motor. Thus, both motors, in each joint direction, contribute to the overall joint torque (Figure 1.16). Still, elastic elements partially decouple the motors from the link. This design compensated several features. Probably the most important one was the prevention of tendon slackening, so that system controllability was ensured. Moreover, such coupled antagonistic motors can deliver more torque to the joint axis in the so-called “helping

mode”.

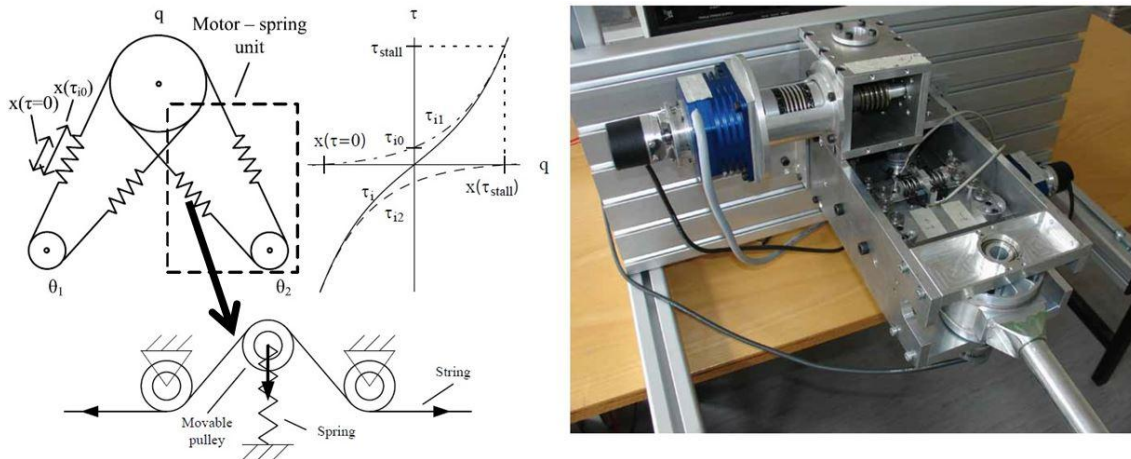
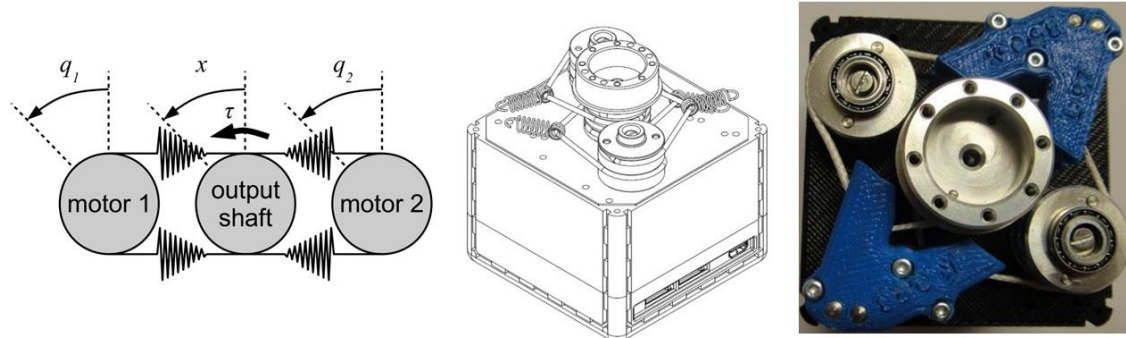


Figure 1.16. Functional scheme of DLR bidirectional antagonistic drive. Both motors contribute to overall joint torque in either joint direction, so torque range is expanded (top left); Pre-tension springs are added to achieve a non-linear relationship between spring length and pulley deflection (bottom left); Prototype of DLR bidirectional antagonistic drive (right).

Due to sophisticated technology, hardware platforms that enable work with robots driven by antagonistically coupled drives are generally not affordable to researchers worldwide. To bridge the gap, QB Robotics [87] designed a low-cost open source hardware platform – a series of qbmove actuators. Qbmove maker pro is a variable stiffness actuator with bidirectional springs in an antagonistic configuration [46]. Although very simple in design, the series of qbmove actuators raises the whole generation of compliant actuators to a new level – it is low-cost, affordable and based on the fully open-source principle. All mechanical and electrical drawings, building instructions, and manuals are available, so one can chose to build their own actuator or purchase it to save time. The inventor of QB move actuators is the Italian company QB Robotics, a spin-off of the University of Pisa and the Italian Institute of Technology located in Genoa. QB Robotics was established to build and promote robotic actuators that can move safely, smoothly, and efficiently, exploiting natural principles of motion control. In other words, they aim to follow patterns and principles that originate from skeleton/muscular systems of mammals. For insight, the qbmove maker pro actuator delivers a continuous output power  $P_{NOM} = 4.8 W$  (nominal torque  $\tau_{NOM} = 1.2 Nm$

and nominal angular velocity  $\omega_{NOM} = 4 \text{ rad/s}$ ). In order to be widely used and employed, besides the low cost, qbmove maker pro offers the possibility of using common electrical interfaces (USB type B and RS485) for communication. The actuator covers the full-circle range of  $\pm 180 \text{ deg}$ .



*Figure 1.17. Functional scheme of bidirectional antagonistic drive employed in qbmove maker pro actuator designed by QB Robotics; (middle) Schematic of qbmove maker pro actuator (left); Prototype of low-cost qb move maker pro actuator, most of whose parts could be built using a 3D printer (right).*

Although bidirectional antagonistic actuators introduce better performance capabilities and increase maximal net joint, they are more reliable solutions compared to classical antagonistic actuator arrangements. Fillipini et al. in [88] presented a simulation study on safety of different antagonistic arrangements: classical, cross-coupled and bidirectional. There, they used state-based methods for dependability assessments (Markov chains) to prove that a classical antagonistic arrangement is the most reliable due to the simplicity of its mechanical implementation. However, they showed that fault management actions could make bi-directional design predominant or at least equally well as the classical antagonistic design.

#### **1.4.2 Antagonistic actuators based on hydraulic/pneumatic drives**

Although of secondary importance in this thesis, the following paragraphs provide insight into hydraulically and pneumatically actuated antagonistic robotic joints. In spite of the fact that such actuators seem more human-like, there are some features which strongly limit their utilization. Furthermore, the servo control complexity of hydraulic

actuators makes them inappropriate for dexterous manipulation of contemporary robots. Thus, pneumatic actuators have been better choice for the design of artificial musculoskeletal units; however, electric drives complemented with elastic elements have been prevalent in recent years.

One of the first implementations of antagonistic drives (not only pneumatically driven, but in general) was the Utah/M.I.T. Dexterous Hand [89] co-developed by the Center for Engineering Design at the University of Utah and the Artificial Intelligence Laboratory of the Massachusetts Institute of Technology. It was a very complicated realization of a robotic joint actuated by two antagonistically-coupled pneumatic actuators controlled by two-stage jet valves. For that purpose, the authors developed a pneumatic valve with an integrated pressure control loop, so that the driven pneumatic cylinder would operate as a force source, thereby avoiding oscillation problems induced by gas compressibility. Although the use of such an actuator resulted in a very high bandwidth and low output impedance, the system was prone to instabilities.

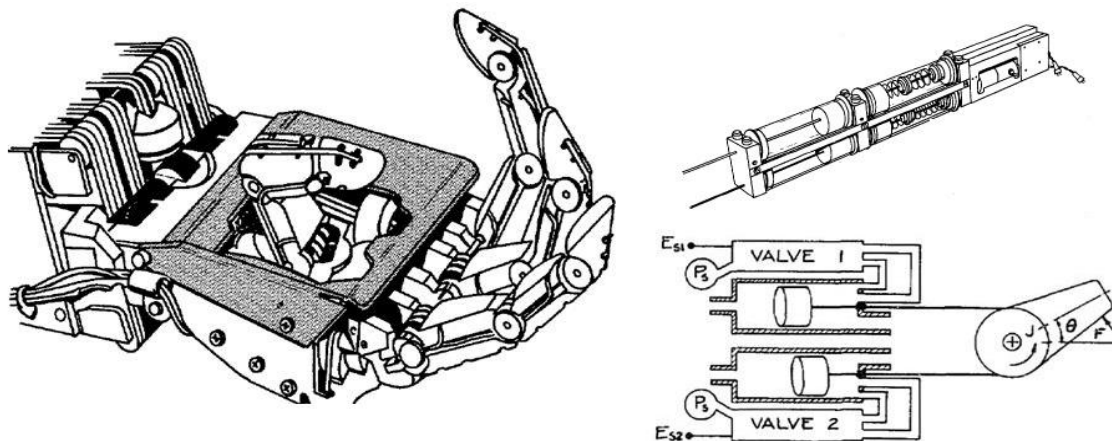


Figure 1.18. (left) Line drawing of Utah/M.I.T. Dexterous Hand; (right) Each joint is operated by two tendons, tensioned by actuators, consisting of low-stiction cylinders and pressure control valves.

The Advanced Robotics Technology and Systems Laboratory from Scuola Superiore Sant'Anna and the Control Systems Laboratory from the National Technical University of Athens presented their prototype of a robot manipulator with antagonistically driven joints – NEUROARM [90]. This project was one of few that used hydraulic drives, since if one opted to avoid electrical drives, pneumatic drives would be preferable due

to a higher control bandwidth, integration capabilities, etc. The manipulator was designed to be exploited in joint neuroscience and robotics experiments, and primarily for investigations in the field of human motion control. It proposes two different designs of revolute joints: the shoulder – simple pulley driven linear configuration; the elbow – involving a non-linear relation between the moment arm of the flexor unit and the joint angle.

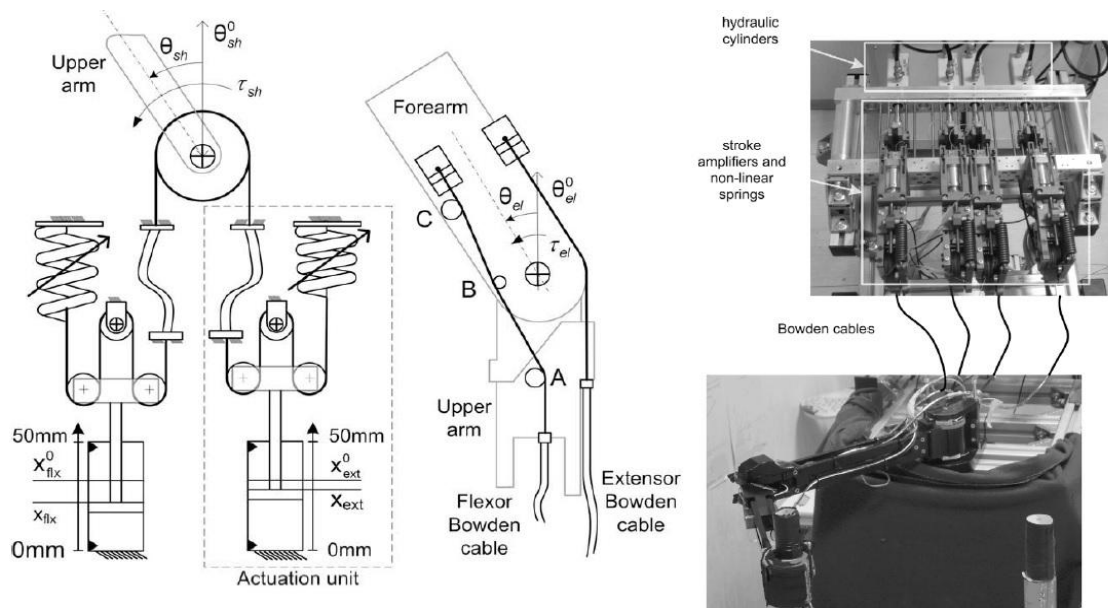


Figure 1.19. Functional scheme of NEUROARM shoulder – linear antagonistic joint driven by hydraulic actuators (left); Functional scheme of NEUROARM elbow – non-linear joint driven by hydraulic actuators (featuring a non-linear relation between the moment arm of the flexor unit and the joint angle) - (middle); NEUROARM platform actuated by antagonistically-coupled hydraulic drives dedicated to research on human motion control (right).

Contrary to hydraulic actuators, pneumatic actuators have been widely exploited as another approach that comprises series elasticity to mimic artificial muscles, which has been exhibited in various realizations [91], [92]. Among these realizations, the braided-type McKibben actuator, as a pneumatic artificial muscle (PAM), has been used most often for robotic applications [93]. Continuing the work of their distinguished Prof. Kato on bipeds in the early 1970s, Yamaguchi and Takanishi from Waseda University built the first anthropomorphic biped walking robot with antagonistically coupled PAMs as primary actuators [94]. Copying human stiffness variation during walking, they proposed a mechanism for non-linear elasticity in transmission. They experimentally

demonstrated a bipedal walking speed of about 8s per 0.1m step. In [95] Tondu et al. presented the design of a seven-DoF anthropomorphic robot arm, entirely actuated by antagonistic McKibben artificial muscle pairs. This manipulator (see *Figure 1.20 - 3*) was perceived as the first teleoperated robot driven by antagonistic joints. A German consortium designed an antagonistically actuated setup using PAMs as an actuation unit for their humanoid robot ZAR in [96] (*Figure 1.20 - 4*). Tsagarakis and Caldwell developed a pneumatically-actuated lightweight exoskeleton for upper arm training/rehabilitation in [97].

Probably the most popular projects in Europe on this topic have been Lucy, carried out by Lefeber and his team at Vrije University of Brussels [98], and Shadow Hand for dexterous manipulation led by Helger Ritter of the Neuroinformatics Group at Bielefeld University [99]. Lucy (see *Figure 1.21 - 2*) was a biped whose joints were actuated by pairs of antagonistically-coupled pleated pneumatic artificial muscles. These muscles were planned as lightweight pneumatic actuators working at low pressures and could be directly coupled without complex gearing mechanisms. The idea of the project was to create a robot for energy efficient walking, which led to on-line changeable passive stiffness of the actuators [100]. Therefore, a change in the natural frequency of the system was achieved while controlling angular joint positions, as humans do. Robustness of robot walk was facilitated since Lucy was restricted to moving only in the sagittal plane due to one-dimensional joints. Working towards their ultimate goal – to achieve dexterous human-like manipulation, the Shadow Hand research team created a hand comprised of 24 joints, 20 of which were actively controllable. Each joint was actuated by an antagonistic pair of McKibben-style pneumatic muscles, so the fingers were almost capable of performing human-like movements. However, in order to control air flow, 80 miniature solenoid on-off valves (one inlet and outlet valve per muscle) had to be integrated. Thus, although all PAMs were packed densely in the lower forearm and the joints were actuated by means of tendons routed through the wrist, and despite all the efforts to miniaturize the setup, it was still much larger than a human forearm (shown in *Figure 1.20 - 5*).

The next-generation pneumatically actuated human-like hand was designed at the Department of Mechanical Science and Bioengineering of Osaka University in Japan

and the company SQUSE Co. Ltd. In [101], Honda et al. presented this hand in the paper that revealed a five-fingered robot hand with low-pressure driven pneumatic actuators, where the robot faithfully mimicked the appearance of a human hand and musculoskeletal structure (see *Figure 1.20 - 6*). Thus, each joint had its own antagonistic McKibben pneumatic muscle pair. Advances in comparison to its predecessors were depicted in the construction, since the rubber inner tube was thinner and softer, resulting in low-pressurized actuation and consequently a smaller-size compressor, which reduced the size of the driving system. As such, the entire actuation unit could be arranged directly in the five-fingered robot hand.

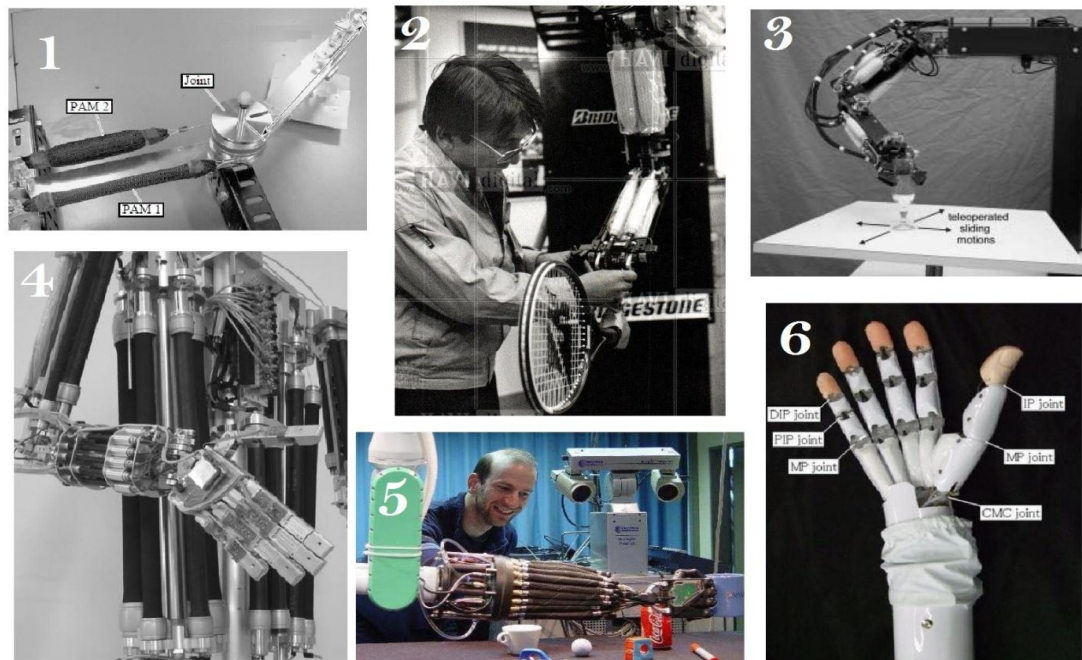


*Figure 1.20. Robot arms driven by pneumatically actuated muscles in an antagonistic configuration: 1 – typical configuration of single-degree-of-freedom robotic joint driven by antagonistic pneumatic artificial muscles; 2 – one of the first pneumatic robot arms constructed by Bridgestone, dedicated to corporate marketing activities; 3 – a seven-DoF robot arm constructed by Tondu et al. [95] at the Laboratory of Computer Systems and Automation, National Institute of Applied Sciences, Toulouse, France in 2005; 4 – ZAR4: humanoid muscle robot called “Zwei-Arm-Roboter V.4” [96], constructed by a German consortium – Technical University of Berlin and Technical University of Hamburg-Harburg, in 2005; 5 – Bielefeld 20-DOFs Shadow Hand constructed by Röhling et al. [99] at the Neuroinformatics Group, Faculty of Technology, Bielefeld University in 2007; 6 – five-fingered robot hand with integrated small-size low-pressurized antagonistic pneumatic actuators constructed by Nishikawa and his associates [101] from Osaka University and Shinshu University in 2010.*

Several robot arms driven by pneumatically actuated muscles in an antagonistic configuration are shown in *Figure 1.20*, while some of the results from publications on leg design using antagonistically coupled pneumatic units are presented in *Figure 1.21*.

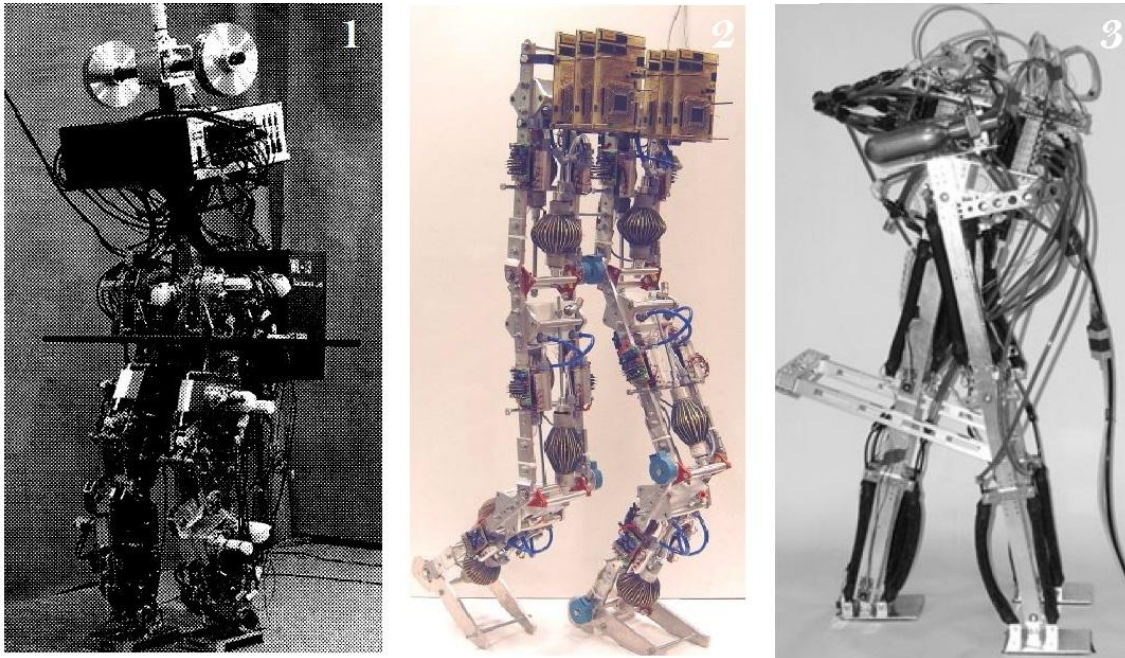


*Figure 1.21. Human-like bipeds driven by pneumatically actuated muscles in an antagonistic configuration: 1 – one of the first examples of a life-size biped walking robot with antagonistically driven joints constructed by Yamaguchi et al. [94] at Waseda University in 1986; 2 – Lucy biped, project carried out by Lefeber and his team at Vrije University of Brussels. The Lucy project team realized on-line changeable passive stiffness of the pneumatic actuators for energy efficient walking in 2005 [98]; 3 – biped robot powered by antagonistically-coupled pneumatic actuators capable of walking, jumping, and running, constructed at Osaka University in 2007 and presented by Hosoda et al. in [102].*

Although a widespread technology with satisfactory performance that has already been demonstrated in case studies, pneumatics actuators, as compliant actuators, inevitably have several drawbacks. Essentially, turbulent flow of compressed air jeopardizes system controllability and reduces robot motion accuracy. Also, the load-to-weight ratio is not favorable if one considers the weight and size of the needed compressors or compressed air bottles, which severely limit applications on a mobile platform, increase inertia of the manipulators, etc. In addition, the utilization of McKibben type actuators enables variable stiffness in a limited way since the range of achievable stiffness is

position-dependent [103]. The low control bandwidth of PAMs and low torque capacity are also issues that need to be addressed for PAM application to future service robots. Finally, the acoustic noise generated during operation make this kind of actuator inexpedient for many possible service robot applications in a human environment. Keeping in mind all the above-mentioned features, a future antagonistic actuator could combine pneumatic and electrical drives as suggested by Shin et al. in [18], who propose a hybrid actuation approach that consists of a pair of PAMs coupled to a low-inertia DC-motor in parallel. In their approach, PAMs were used to generate low frequency but a greater torque proportion, while high frequency actuation components were achieved using fast DC motors, therefore improving the overall bandwidth of the actuator.

## **1.5 Thesis overview**

The thesis is organized in six sections, followed by bibliography.

The first section outlines the main ideas and motivation for the work. It presents research directions, points of view and initiatives in the design and control of compliant robots, with special emphasis on antagonistically-actuated joints. It also addresses safety issues of future service robots, and lists technologies, trends, and approaches towards achieving that goal: moving from stiff to compliant actuators, the benefits introduced by passive and active compliance, variable stiffness actuators, etc. As a special group of bio-inspired variable stiffness actuators in robotics, antagonistic joints are reviewed comprehensively. Such a detailed review of antagonistic joint design aims to highlight the importance of the subject, on the one hand, while on the other hand it presents the technology that will be intensively exploited in future anthropomorphic robots.

The second section presents a detailed simulation-based model of the robot driven by antagonistically-actuated compliant drives. To begin with, basic models of antagonistic joints that resemble typical human-like antagonistic structures are introduced. These models are incorporated into the upper-body anthropomorphic robot model, which is a

close approximation of the Eccerobot prototype. Since such a robot is intended to work in collaboration with humans and directly interact with its surroundings, modeling of contacts is introduced. This section as a whole represents an efficient and accurate tool for simulating the anthropomimetic robot dynamic, which is implemented in Matlab for demonstration purposes. Two case studies are presented. The first emulates an anthropomimetic robot on a wheeled-base, working in an unstructured environment and therefore exposed to impulse and long term external disturbances. Here the model is used to observe the robot's zero-moment-point and thus its balance. The second case study emulates intentional contact – grasping of an object. Models of all contact stages are demonstrated: approach, impact and in-contact-motion phases. At the same time, the simulation model served as a platform for the development of control algorithms elaborated in the following sections.

The third section makes a contribution of this thesis to the control of an antagonistic, linear/non-linear, cable driven, compliant robot joint. After an overview of the background work on antagonistic joint control and feedback linearization in robot control, our puller-follower approach, initially introduced in the master's thesis of Svetozarevic [4], is presented. This biologically-inspired and energy efficient approach simultaneously controls joint position and force in one of the tendons. In the present thesis, the puller-follower approach extends to joint position and joint stiffness control. An initially demonstrated single-joint control algorithm based on feedback linearization is improved to compensate for gravity load, effective changeable joint inertia and dynamic coupling in multi-joint systems, by introducing the robust control theory. The third section ends with limitations and issues that remain open and will be the topic of future research.

Insight into real biological mechanisms and patterns of their behavior (control) intuitively leads us from an engineering control perspective through cognitive approaches to the control of antagonistically-coupled compliant drives in robotics. The research and scientific contributions of the present thesis to this topic are presented in the fourth section. Feedback and feedforward control is undertaken using heuristic control strategies based on optimization (depicted in the nearest-neighbor algorithm),

neural networks, and fuzzy logic. The fourth section ends with a comparative simulation study, which points out the main features of control schemes developed in that section.

Section 5 provides insight into the author's point of view and initial research on antagonistically-driven compliant joint control in interaction (contact) tasks. It presents a mixture of state-of-the-art conventional and widely adopted impedance control techniques and bio-inspired patterns of biological antagonistic structures.

The concluding Section 6 highlights the main findings and observations, summarizes the contribution of the thesis once again, and finally provides guidelines for further research on the topic.

## **1.6 Thesis contributions and related publications**

The work presented in the present thesis considers a very popular and rapidly growing topic in robotics – modeling and control of anthropomorphic robots, in particular robots with compliant antagonistic joints.

Since conventional rigid actuators have become obsolete for inherently-safe future robotic applications, the design and control of novel compliant actuators have recently been under intensive scrutiny. In particular, variable stiffness (impedance) actuators, which can trade-off between robot trajectory tracking and overall safety, are the focus of robotics research. Particular attention is paid to antagonistic actuators as a subgroup of bio-inspired variable stiffness actuators. Furthermore, future service robots of anthropomorphic design will strongly rely on the antagonism principle. Therefore, one of the first contributions of the thesis is a detailed review of the antagonistic joint design outlined in Section 1.

The main scientific contributions presented in the thesis relate to anthropomorphic robot modeling and control. Since the majority of advanced control techniques in robotics are model-based, in order to compensate for robot dynamics, modeling and control are very

closely-related research topics in advanced robotic systems. The author's contributions to this topic will be specified later in this subsection. At this point we list the relevant publications to allow the later discussion to directly relate contributions to publications.

Book chapter:

**(b1)** V. Potkonjak, K. Jovanovic, P. Milosavljevic, Chapter 20: “How to Control Anthropomorphic Robot: Engineering and Cognitive Approach”, *Springer Series on Mechanisms and Machine Science – New trends in Medical and Service Robotics*, Vol 20, pp. 299-314, (2014). (DOI:10.1007/978-3-319-05431-5)

Papers in international journals:

**(j1)** K. Jovanovic, V. Potkonjak, O. Holland, “Dynamic Modelling of an Anthropomorphic Robot in Contact Tasks”, *Advanced Robotics: The International Journal of the Robotics Society of Japan (Taylor & Francis)*, Vol 28(11), pp 793-806, (2014). (DOI:10.1080/01691864.2014.896748, IF=0.572, M23)

**(j2)** V. Antoska, K. Jovanovic, V. Petrovic, N. Bascarevic, M. Stankoviski, “Balance Analysis of the Mobile Anthropomorphic Robot Under Disturbances – ZMP Approach”, *International Journal of Advanced Robotic Systems (InTech)*, Vol 10(paper 206), pp 1-10, (2013). (DOI:10.5772/56238, IF=0.497, M23)

**(j3)** S. Wittmeier, C. Alessandro, N. Bascarevic, K. Dalamagkidis, A. Diamond, M. Jantsch, K. Jovanovic, R. Knight, H. G. Marques, P. Milosavljevic, B. Svetozarevic, V. Potkonjak, R. Pfeifer, A. Knoll, O. Holland, “Towards Anthropomorphic Robotics“, *Artificial Life*, (MIT press), Vol 19(1), pp 171-193, (2013). (DOI:10.1162/ARTL\_a\_00088, IF=1.386, M21)

**(j4)** V. Potkonjak, B. Svetozarevic, K. Jovanovic, O. Holland, “The puller-follower control of compliant and noncompliant antagonistic tendon drives in robotic system”, *International Journal of Advanced Robotic Systems (InTech)*, Vol 8, pp 143-155, (2012). (DOI: 10.5772/10690, IF=0.821, M23)

Papers in Serbian journals:

(sj1) K. Jovanović, J. Vranić, N. Miljković, “Hill’s and Huxley’s Muscle Models – Tools for Simulations in Biomechanics”, *Serbian Journal of Electrical Engineering*, Vol . 12(1), pp. 53-67, (2015). (DOI: 10.2298/SJEE1501053J)

(sj2) V. Petrovic, K. Jovanovic, V. Potkonjak. “Influence of External Disturbances to Dynamic Balance of the Semi-Anthropomorphic Robot”, *Serbian Journal of Electrical Engineering*, Vol 11(1), (2014) pp 145-158 (DOI: 10.2298/SJEE131014013P)

(sj3) B. Svetozarevic, K. Jovanovic, “Control of Compliant Anthropomorphic Robot Joint”, *Serbian Journal of Electrical Engineering*, Vol 8(1), (2011) pp 85-93 (DOI:10.2298/SJEE1101085S)

International conferences:

(c1) V. Potkonjak, N. Bascarevic, P. Milosavljevic, K. Jovanovic, O. Holland, “Experience-Based Fuzzy Control of an Anthropomorphic Robot“, *Proc. International Joint Conference on Computational Intelligence (CFP IJCCI 2012)*, Barcelona, Spain, pp 389-394, (2012). (DOI:10.5220/0004117503890394)

(c2) N. Bascarevic, K. Jovanovic, P. Milosavljevic, V. Potkonjak, O. Holland, “Tip-over Stability Examination of a Compliant Anthropomorphic Mobile Robot“, *Proc. 2012 IEEE International Conference on Control Applications (IEEE CCA 2012)*, Dubrovnik, Croatia, pp 1584-1589, (2012). (DOI:10.1109/CCA.2012.6402718)

(c3) P. Milosavljevic, K. Jovanovic, N. Bascarevic, V. Potkonjak, O. Holland, “Heuristic Machine-Learning Approach to the Control of an Anthropomorphic Robot Arm“, *Proc. 10th IFAC Symposium on Robot Control (IFAC SYROCO 2012)*, Dubrovnik, Croatia, pp 301-306, (2012). (DOI:10.3182/20120905-3-HR-2030.00098)

(c4) V. Potkonjak, K. Jovanovic, P. Milosavljevic, N. Bascarevic, O. Holland, “The Puller-Follower Control Concept For The Multi-Joint Robot With Antagonistically Coupled Compliant Drives”, *The 2nd IASTED International (Robo 2011)*, Pittsburgh, USA, pp 375-381, (2011). (DOI: 10.2316/P.2011.752-018)

(c5) V. Potkonjak, K. Jovanovic, B. Svetozarevic, O. Holland, D. Mikicic, “Modeling and Control of a Compliantly Engineered Anthropomorphic Robot in Contact Tasks”,

*The 35th ASME Mechanisms and Robotics Conference (ASME Mech 2011), Washington, DC, USA, pp 23-32, (2011). (DOI:10.1115/DETC2011-47256)*

*(c6) V. Potkonjak, B. Svetozarevic, K. Jovanovic, O. Holland, “Anthropomimetic Robot with Passive Compliance – Contact Dynamics and Control”, The 19th Mediterranean Conference on Control and Automation (IEEE MED 2011), Corfu, Greece, pp 1059 – 1064, (2011). (DOI:10.1109/MED.2011.5983000)*

*(c7) V. Potkonjak, B. Svetozarevic, K. Jovanovic, O. Holland, “Biologically-inspired control of a compliant anthropomimetic robot”, The 15th IASTED International Conference on Robotics and Applications, Cambridge, Massachusetts, USA, pp 182-189, (2010). (DOI:10.2316/P.2010.706-006)*

*(c8) V. Potkonjak, B. Svetozarevic, K. Jovanovic, O. Holland, “Control of Compliant Anthropomimetic Robot Joint”, International Conference of Numerical Analysis and Applied Mathematics, Rhodes, pp 1271-1274, (2010). (DOI:10.1063/1.3497932)*

International conferences held in Serbia and Serbian conferences:

*(sc1) K. Jovanovic, P. Milosavljevic, V. Potkonjak, “Control Design for Pick-and-Place Task Using Robot with Intrinsic Compliance - QB Robot”, The 2nd IcETRAN Conference, Srebrno jezero, Serbia, pp RO1.1- 1-6, (2015).*

*(sc2) B. Lukic, K. Jovanovic, “Influence of Mechanical Characteristics of a Compliant Robot on Cartesian Impedance Control Design”, The 2nd IcETRAN Conference, Srebrno jezero, Serbia, pp RO2.5- 1-6, (2015).*

*(sc3) K. Jovanovic, J. Vranic, “Muscle Models for Accurate Simulation of Human Movements”, The 1st IcETRAN Conference, Vrnjacka Banja, Serbia, pp RO2.4- 1-5, (2014).*

*(sc4) V. Petrovic, K. Jovanovic, V. Potkonjak, “ZMP approach to the critical design of a mobile platform for the semi-anthropomimetic robot”, The 57th ETRAN Conference, Zlatibor, Serbia, pp RO1.1- 1-6, (2013).*

*(sc5) P. Milosavljevic, N. Bascarevic, K. Jovanovic, G. Kvascev, “Neural networks in feedforward control of a robot arm driven by antagonistically coupled drives”, The 11th Symposium on Neural Networks Applications in Electrical Engineering (NEUREL), Belgrade, Serbia, pp 77-80, (2012). (10.1109/NEUREL.2012.6419967)*

(sc6) N. Bascarevic, K. Jovanovic, V. Potkonjak, “A tip-over stability analysis of an anthropomimetic wheeled robot based on zmp”, *The 56th ETRAN Conference, Zlatibor, Serbia, pp RO2.9 - 1-4, (2012).*

(sc7) K. Jovanovic, N. Bascarevic, “Modeling Contact Dynamics of the Anthropomimetic Robot – ECCEROBOT”, *The 55th ETRAN Conference, Teslic, Bosnia and Herzegovina, pp RO1.8- 1-4, (2011).*

(sc8) P. Milosavljevic, K. Jovanovic, V. Potkonjak, “The Puller-Follower Control Concept in the Multi-Jointed Anthropomimetic Robot Body”, *The 55th ETRAN Conference, Teslic, Bosnia and Herzegovina, pp RO1.7- 1-4, (2011).*

(sc9) K. Jovanovic, B. Svetozarevic, “Humanoid Robot Model with Antagonistic Drives”, *The 54th ETRAN Conference, Donji Milanovac, Serbia, pp RO1.3 - 1-4, (2010).*

In summary, the contributions of the present thesis can be grouped into several main topics, as follows (each corresponding to one of the following sections in the thesis):

**Contribution set 1 (Section 2):** Development of simulation-based models of antagonistically driven compliant robots in free motion and in contact/interaction tasks.

Here, Stepanjenko’s approach to robot modeling, known for efficient calculation of robot dynamics, is applied. Models of typical antagonistic joints in humans are developed and integrated into a full robot body model. As an upgrade of author's master thesis [104], models of contact dynamics are elaborated through approach, impact and in-contact-motion phases, and then integrated into the simulation-based model of the anthropomimetic robot in a contact task. In according to the type of surface in the contact zone contact dynamics is considered as rigid, elastodynamic or soft. Topic-related publications include: (j1), (j2), (sj1), (sj2), (c2), (c5), (c6), (sc3), (sc4), (sc6), (sc7), and (sc9).

**Contribution set 2 (Section 3):** Engineering approaches to the control of a robot with antagonistically coupled compliant drives.

Starting with the initially introduced concept in control of antagonistic drives with inelastic and elastic transmission by Svetozarevic in [4], conventional non-linear, multi-variable and robust control techniques are applied to control the position and antagonistic tendon force. Such control is developed for both linear and non-linear antagonistic drive configurations resembling typical human joints driven by antagonistically coupled muscles. The control approach is demonstrated for linear and non-linear elastic elements in antagonistic tendons. Then the control concept is modified for simultaneous position and stiffness control of the antagonistic compliant actuators. The developed puller-follower control algorithm synthesizes feedback-linearization, model-based gravity compensation, joint effective inertia estimation, and  $H_\infty$  loop-shaping robust control. The presented control approach is then effectively demonstrated on a multi-joint system through simulations. The publications that have come out of this work are: (b1), (j3), (j4), (sj3), (c4), (c5), (c7), (c8), and (sc8).

**Contribution set 3 (Section 4):** Cognitive approaches to the control of a robot with antagonistically coupled compliant drives.

Since anthropomorphic robots are built to resemble the human structure, anthropomorphic robot control algorithms are also expected to copy the way the human body works. To that end, fundamental research on control is extended to include techniques based on learning, cognition and heuristic. Therefore, the exploitation of optimization (in the nearest-neighbor method), neural networks, fuzzy logic and heuristics based on an experience base in anthropomorphic robot control are elaborated. Papers related to these contributions include: (b1), (j3), (c1), (c3), and (sc5).

**Contribution set 4 (Section 5):** Control of robots with antagonistically-coupled compliant drives in contact tasks.

This part of the thesis presents a mixture of state-of-the-art conventional and widely adopted impedance control techniques, implemented in antagonistic drives in a bio-inspired manner. The results of this recent research have not yet been published, although some preliminary investigations on the topic have been prepared and

presented, including (sc1) and (sc2).

In addition to scientific contributions, there are also a few awards worth mentioning, which constitute direct results of the author's work on the thesis. The award list follows:

Winner at the SAPHARI NMMI Winter School on Robotics: Variable Stiffness Actuators, Sapienza University of Rome, February 2015, Rome, Italy.

*Competition in control of low-cost variable stiffness robot using bi-directional antagonistic actuation – qb robots.*

Best Young Researcher Paper Award – Section: Robotics and Flexible Automation, 1<sup>st</sup> International Conference on Electrical, Electronic and Computing Engineering (IcETRAN 2014), Jun 2014, Vrnjacka Banja, Serbia.

*For the paper: K. Jovanovic, J. Vranic, "Muscle Models for Accurate Simulation of Human Movements", The 1st IcETRAN Conference, Vrnjacka Banja, Serbia, June, 2014. pp RO2.4- 1-5.*

German Exchange Academic Service (DAAD) grant for research stay at DLR Institute on Robotics and Mechatronics, May-November 2013, Wessling, Germany.

Belgrade University Award for the best student's scientific work in the field of technical & technological sciences at Belgrade University in 2010/2011, 2011, Belgrade, Serbia.

*As the presenting author of the paper: V. Potkonjak, B. Svetozarevic, K. Jovanovic, O. Holland, "Biologically-inspired control of a compliant anthropomorphic robot", The 15th IASTED International Conference on Robotics and Applications, Cambridge, Massachusetts, USA, November 2010. pp 182-189.*

All the presented contributions and results are expected to have an impact on the development and control of future anthropomorphic robots, envisaged as robots for environments fully-ergonomically designed for humans. Our anthropomorphic robot models will initially help to analyze and understand human biomechanical patterns and then extract and adapt them to the design and control of such robots. Not only can

robots benefit from the results, but also the new generation of exoskeletons and particularly the new concept of the so-called “exotendon exoskeleton” [105]. Such an exoskeleton recognized the benefits of anthropomimetic design, in order to adapt to natural movements of patients, but also to exploit energy storage and release in the way a human musculoskeletal system does.

## **2 Dynamics model of a robot with antagonistic joints in non-contact and contact tasks**

Anthropomorphic robots have been built as an engineering copy of the human body and designed to achieve a significant level of human performance. In order to facilitate the process and make it feasible, we first need to fully understand human motor control and then trade-off between desired levels of robot similarity to human appearance, performance, and reliability. As already pointed out, given the necessary human-like appearance of a future service robot, it must be designed and controlled carefully, to achieve high-level maneuverability, along with safety. In view of such demanding requirements, a thorough approach in analysis is indispensable. Since the human body, and consequently its robot replica, is not shaped following engineering patterns, an approximate model of robot dynamics should be derived. It is needed not only to simulate the behavior of the anthropomorphic robot, but also for analysis of human motor control patterns, developing and testing control methods, estimation of robot performance limits, etc. Since the aim is for compliant and anthropomorphic robots to interact with humans on a regular basis, a comprehensive analysis of interaction tasks is particularly important. Consequently, the analysis of anthropomorphic robots was approached from a modeling perspective, making compromises between the ultimate complex structure of anthropomorphic (musculoskeletal) robots and feasible modeling solutions and approximations.

There are multiple advantages of the analytical approach discussed in this thesis. First, contrary to most existing models derived inductively for particular purposes, the approach is deductive. Namely, the initial, general model is easy to upgrade and modify, making it possible to: add new contact points, add new links/joints in the robot structure, reconfigure drives, etc. It relies on well-known Newton-Euler equations, so it is rather easy to understand, expandable, and, finally, convenient for computer-based algorithm implementation. The main contributions to modeling of anthropomorphic

robot dynamics elaborated in this section are summarized in the author's papers [3], [106], and their applications presented in [107], [2].

This section first offers an overview of the related work (in Subsection 2.1). Then the point of view and main contribution to modeling of the anthropomimetic robot in contact and non-contact tasks are presented. The structure of one of the most advanced anthropomimetic robots – the Eccerobot, as the focus of the work, is depicted in Subsection 2.2. Subsection 2.3 introduces several approximations in modeling of musculoskeletal robots, as a tradeoff between model accuracy and feasible and convenient modeling solutions. Models for common antagonistic actuation structures are proposed. The final outcome of this subsection is a full analytical model of robot dynamics, for a freely-moving robot with antagonistically-coupled compliant drives. Analytical models for analysis of the anthropomimetic robot in contact tasks are derived in the next subsection (2.4). The developed models are verified in contact and non-contact tasks in Subsection 2.5. Computer-based models implemented in Matlab demonstrate a full dynamic model interacting with the environment through the modeled contact dynamics. The treatment includes all multi-joint effects, as well as contact phenomena and impacts. This section ends with conclusions in Subsection 2.6.

## **2.1 Background work**

This subsection presents an overview of models, considering the dynamics of humanoid robots and musculoskeletal robots in particular.

Modeling of a complex musculoskeletal robot body introduces numerous challenges. A fully-humanlike replica requires mapping of tendons that cross several rotation axes, even several joints. Also, bi-articular and multi-articular muscles/tendons are difficult to incorporate into a multi-body model. Including multi-axes joints in a model is not a trivial task and generally needs some approximations. Furthermore, moment arms in particular joints change according to the robot's pose, so the non-linearities could lead to numerical issues. In view of the above-mentioned facts, analytical models of

anthropomimetic robots, which are full copies of a musculoskeletal body, require approximations.

Two mainstreams in modeling of complex humanoid robots dynamics are analytics and physics-based engines. While analytical models may be considered as “dedicated models”, models based on physics engines are “general-purpose models”. The former group includes models mainly derived to describe a particular robotic mechanism, while the latter group is comprised of models employed to simulate various systems (a robot, a car, a ball hitting a brick wall, etc.). Therefore, if the need is to consider the dynamics of a body only in superficial terms, “general-purpose models” are the choice. However, if interaction tasks are considered, such models calculate all interaction forces between bodies, consistently dealing with a huge number of equations and variables. On the other hand, analytical models of dynamics eliminate contact forces, such that the number of equations that need to be solved is minimal and the computation demand is reduced. Moreover, analytical models are suitable for all tasks based on analytics, such as control design, stability analysis, dynamic balance analysis, etc. Physics-based engines rely on numerical calculation and, consequently, cannot compete with analytical models. Although from that perspective an analytical model appears to be a prime solution for comprehensive analysis of complex robot dynamics, such models would be unable to deal with the above-mentioned challenges of musculoskeletal mechanisms: multi-articular muscles, multi-axes joints, drive redundancy, etc. Physics engines would handle such structures more easily. Taking into consideration the characteristics of both approaches, analytical models for basic analysis are suggested, particularly for the control design phase, while in final testing and simulation physics-based engines prevail. However, since the focus is on simulation, and especially control of novel compliant robotic actuators (with special attention given to antagonistically coupled drives), the analytics approach was selected.

After an initial search for related literature, it was not hard to conclude that there are only a few analytical models of full musculoskeletal robot dynamics. One of the main goals of this thesis was the development of a computer-based model of anthropomimetic robot dynamics, or at least an approximation that represents the key features of an

anthropomimetic robot. This was finally accomplished by expanding existing analytical models, developed for the dynamics of classical robot structures, and considering constraints introduced by interaction.

A humanoid robot is in general a highly-complex dynamic system, regardless of whether its structure includes elasticity and/or antagonistic actuation or not. Accordingly, many authors have confronted their opinions about basic well-known approaches to analytical modeling of humanoid dynamics: Lagrange equations and Newton-Euler equations.

The benefits of Lagrange's approach to modeling of robot dynamics are highlighted first in the algorithms of Uicker [108], Vukobratovic and Potkonjak [109], and Hollerbach [110]. More recently [111], [112] pointed out the usefulness of a Lagrangian as a function of generalized coordinates, their time derivatives, and time in robot dynamics. On the other hand, Lagrange's approach is less general and intuitive. The Newton-Euler algorithm is often favored because it is intuitive and could be characterized as "algorithmically-oriented" (see well-known Featherstone Newton-Euler recursive schemes [113], [114], [115]). Originating from these two basic and well-known approaches, there are several other approaches known in the literature regarding humanoid dynamics: the Kane approach [116] implemented in robots by Houston and Kelly [117] and dynamics based on Apell's equations [118], [119]. The algorithms for robot dynamics presented here also favor the Newton-Euler approach, as an extension of previously well-known results of Serbian robotics in the domain of modeling of robot dynamics [120], [121], [122]. The thesis exploits those results and develops a new analytical form for bio-inspired robot models, using a human-like muscular actuation system. Most importantly, the model provides a tool for dealing with robot interactions with the external world through contact analysis.

The main feature of the present approach is the introduction of Stepanjenko's parameters [123] for characterizing robot geometry and, consequently, kinematics and dynamics, using Newton-Euler equations. Since a detailed approach to Stepanjenko's algorithm was presented in [104], it will not be discussed in detail, except to point out

the main characteristics that distinguish Stepnjenko's from widely-accepted Denavit-Hartenberg's (DH) formalism. The DH approach provides a convenient formulation of robot kinematics since coordinate frame transformation between joints is calculated easily in the closed form. However, since the coordinate frames refer to joints, inertia tensors are mostly full matrices that require a full computational effort, which could hardly be reduced. On the contrary, Stepnjenko's approach is link related, i.e. coordinate frames refer to robot links and axes can be directed arbitrarily. Therefore, link-frame axes are commonly set along the principal axes of inertia, thus providing an inertia tensor of diagonal form. Although such an approach is compromised from a kinematics perspective, its benefits stand out when we come to dynamics. In the model implementation phase, diagonal inertia tensors significantly improve the required time, which is an essential feature where a control algorithm exploits model-based dynamics. The algorithm efficiency of the method was confirmed by its implementation to the well-known six-DoF Stanford manipulator in [120].

However, complex humanoid robots are now often simulated using physics engines. Physics engines are widely used for computer game graphics and other rough dynamics applications. The best known among the physics engines are Bullet, PhysX, Havoc, Open Dynamics Engine (ODE), etc. They provide rigid and occasionally soft body simulation, with discrete or continuous collision detection. However, collision detection and in-contact motions are computationally demanding, so that the collision geometry is often simplified using shapes like cylinders, spheres, boxes, etc., rather than the complex shapes of real objects. This can lead to inaccuracies or anomalous behavior. Generally, physics-engine solvers repeatedly iterate basic physical relations to estimate new system states and arrive at that which best satisfies a set of constraints (e.g. joints) and forces (e.g. motor torques), describing the system at that point. In accordance with a particular application, the engine setting for the number of solver iterations and/or step time is generally selected as a trade-off between performance and accuracy. It is clear that even with these approximation tools, the simulation of an anthropomorphic robot would be a great challenge due to numerous constraints introduced by the complex mechanical structure, tendon compliance and many DoFs. Physics-based engines do offer easy-to-use solutions to analytically intractable problems and enable 3D objects to

be imported, to simplify the modeling and design process, but there are usually very limited facilities for analysis of intrinsic robot dynamics (tendon forces, joint reaction forces, dynamic coupling, etc.). Other drawbacks from a robotics perspective are limited methods for approximating friction and poor support of joint damping [124]. Nevertheless, largely due to their ease of use, physics engines are widely employed in contemporary humanoid robotics research; for example, WABIAN-2 at Waseda University [125] and the iCub simulator [126] use a robot simulation platform based on an open dynamics engine (ODE), whereas the complex human-like mechanism of Eccerobot utilizes some features of the Bullet physics engine (see [127]). In [127] Wittmeier et al. integrate user-shaped individual sub-models of robot components (e.g. artificial muscles, tendons, ligaments, etc.), which are validated separately against measurements. The greatest progress in the application of physics-based engines was made by Diamond et al. [128] who provide an approximate model of a fully-anthropomorphic robot using the Bullet physics engine and point out the numerical, design and implementation issues they faced. A CAD model of their work is shown in Figure 2.1.

However, with current emphasis on the safety of human-robot interaction and growing interest in tendon-driven compliant actuation and musculoskeletal robotics, it seems likely that future work in these areas will require sound analytical treatment of both robot and contact dynamics. Thus, analytical models would be employed rather than data that rely on limited empirical evidence from simulations using available physics engines, which may have compromised accuracy for speed. Moreover, with advances in hardware capabilities and performance, computationally demanding analytical models can be treated more easily and even exploited in real time.

When considering musculoskeletal models of targeted anthropomorphic robot design, available biomechanical simulation models need to be pointed out. Biomechanical modeling and computer simulations complement observations from physical experiments. Although there are numerous biomechanical models of individual human body parts or their simplified forms, only a few full-body human models exist. One of them is the fully-open platform OpenSim, offered by Stanford University [129].

OpenSim provides musculoskeletal modeling elements such as biomechanical joints, muscle actuators, ligament forces, compliant contact, and controllers, as well as tools for fitting generic models to subject-specific data, etc. It additionally enables inverse kinematics and forward dynamics simulations using the Simbody physics engine adapted to multi-body system dynamics [130]. Even well-known software for musculoskeletal systems, such as AnyBody [131], is not designed and can hardly be used as a control platform. Such software rather serves as a medical or sporting tool and takes real captured motions as inputs, rather than the direct muscle activation signals needed for control purposes.

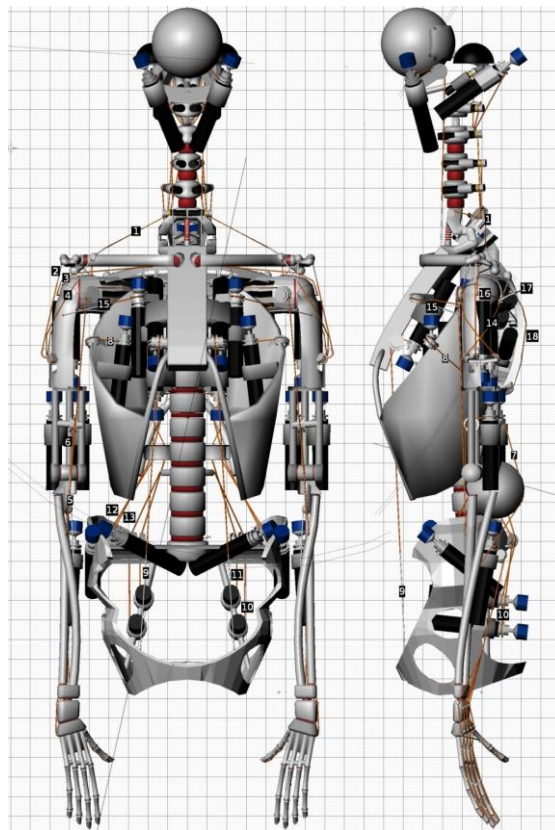


*Figure 2.1. Front and side views of the complete anthropomorphic robot model implemented by Diamond et al. in [128]. The authors initially captured Eccerobot morphology and, accordingly, created a static CAD model. The model was then exploited in the Bullet physics engine with user-shaped constraints; complex kinematics dependencies, as well as compliant elements, were introduced.*

Antagonistic joints are represented as a pair of opposing drives that pull against each other and provide overall joint torque, while extending compliant elements in associated

tendons. Therefore, if an antagonistic joint has electrical drives, the drives are often SEA units whose model is introduced in [12]. In accordance with the force-length relation of elastic elements in tendons, models of joints with antagonistically-coupled SEA are presented in [77], [132], [133]. On the other hand, pneumatic actuators as antagonistic drives are far more complex to control and model. Moreover, they are non-stationary and not the focus of this thesis.

Radkhah et al. presented an analytical model of a bio-inspired biped using mono-articular and bi-directional tendons in [134]. This model resulted from the BioBiped project at the Technical University of Darmstadt, whose objective was to analyze the contribution of each serial elastic tendon element, compare the contributions of active and passive compliance in human-like actuation, and finally suggest possible improvements in the design and construction of next-level bio-inspired bipeds. Similarly, the goal of the present research was to derive an analytical model of musculoskeletal robot dynamics, but in this case the target was the full robot's upper body.

Modeling of robot dynamics in contact tasks, as well as modeling of the contacts themselves, is also an increasingly growing topic in the robotic society, since contemporary robots are mostly designed for sensitive interaction tasks. Bouyarmane et al. discuss in [135] the realization of a humanoid dynamics model based on the Lagrange formalism in arbitrary contact states with the environment. To treat contacts, the authors deal with equality constraints and search for optimal solutions, which could additionally jeopardize prospective real-time implementation. Sugiama et al. at Waseda University proposed an algorithm for estimating contact dynamics in novel robotic systems, which are predominantly designed and manufactured for applications involving intensive interaction with the environment [136]. There, robots actually take advantage of these interactions. In that paper the authors identified the importance and benefits of the active body-environment contact scheme of the TWENDY-ONE system. Their motion planning strategy first deals with the contact between the robot and the environment and then, additionally, with the contact with the desired object. In both cases impact forces play important roles; a lack of analytical methods for exact

treatment of these forces hinders further improvement. Modeling contact dynamics is also one of the key issues and the most difficult aspect of generic simulators in robotics. The problem of contact modeling is especially important and challenging in space operations. Such a special-purpose simulator developed by McDonald Dettwiler Space and Advanced Robotics Ltd. is described in [137]. Similar to the approach of the present thesis, presented in the following subsections, software models each of the contact points with a spring-damping element and a friction (and stiction) model, while also modeling and simulating both impact and sustained in-contact motion (according to the pioneering work of Hertz's contact mechanics). In spite of a good match between experimental and simulation results, contact models in an analytical form are not provided but captured in the software. To create a database that includes appropriate model parameters for particular objects, different materials, geometries and interaction trajectories are pre-examined. In the work of De Luca and Manes [138], a general approach to modeling of robot-environment interaction, which is not restricted to kinematic constraints but includes dynamic coupling, is proposed. The authors introduce parameters of force and displacement in the interaction area, which are control-oriented and can be more easily exploited in hybrid position/force control. Also, energy exchange based on the Lagrangian between the robot and environment dynamics is exploited and a model of in-contact motion is derived. Finally, the directions in which there are both active interaction forces and hand tip motions, at the same time, are specified and modeled. However, the environment is considered to be a non-actuated system with known inertia and the establishment of contacts, including impact, is not mentioned. On the other hand, the final analytical model relates the robot and environment coordinates to motor torque inputs, which is convenient for inverse dynamics consideration and, consequently, the feedforward control component. A paper which deals with a very similar topic as this section of the thesis – robot dynamics in interaction tasks, but applied particularly to the stable-stance walking phase, has been published by Lee et al. [139]. However, they present an algorithm based on Lagrange's equations, which, due to complexity and for easier implementation, is divided into two models that represent humanoid constrained motion in the frontal and sagittal planes. Nonetheless, the model is restricted to an ideal constraint when contact surfaces are non-deformable and the impact phenomenon is neglected.

In summary, the vast majority of the mentioned contact-oriented works do not consider the impact phenomenon as an essential part of dealing with interaction modeling. Even though contacts are often planned to occur with zero velocity in practical applications, that is rarely the case when impact occurs.

The remainder of Section 2 introduces the proposed approach for dealing with robot dynamics of an anthropomimetic robotic mechanism, in non-contact and contact tasks, using analytical models. First the structure of the Eccerobot, as a fully anthropomimetic robot, is described and then several approximations are introduced to enable analytical modeling.

## **2.2 Structure of the anthropomimetic robot – Eccerobot**

Although the idea about anthropomimetic robots is discussed in more detail in Subsection 1.3, some of the key features that guided the modeling work on the thesis are reiterated here.

Following the anthropomimetic principle, the Eccerobot project [11], [52], [55] attempted to create an upper torso robot (Figure 2.2), very similar in its mechanical functioning to the human body, by replicating the skeleton and its compliant and redundant tendon drives. The Eccerobot was the target system, which the research group, including the author, intended to model and control in accordance with their role in the project. The human-like skeleton is made of a caprolactone polymer (polymorph or friendly plastic), which was hand-molded to form accurate shapes of the main human bones. As muscles can only pull, and not push, the controlled motion of a human joint requires the muscles to be arranged in such a way as to provide antagonistic components. In the simplest cases, the body uses pairs of antagonistically-arranged muscles. However, most instances involve complex components of several muscles. In Eccerobot, the arrangement of the major muscles and tendons copies, as far as possible, those of the human body. Each Eccerobot ‘artificial muscle’ consists of a DC motor with

a gearbox that drives a spindle, around which an inelastic cord (kiteline) is wound and terminated at the other end with an elastic spring (e.g. shock cord) connected to a limb section. The spring provides passive compliance and some damping.

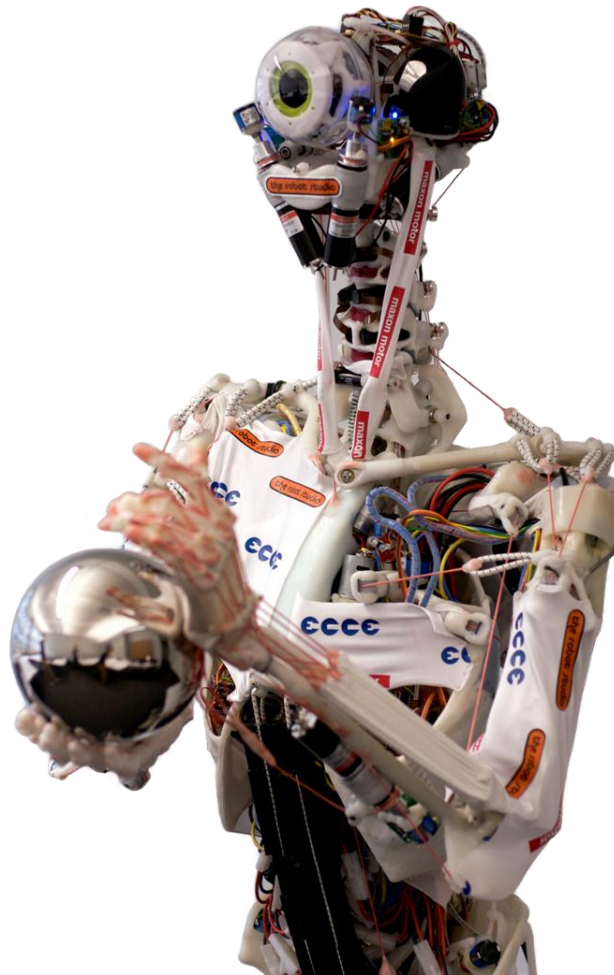


*Figure 2.2. Eccerobot – an upper-body anthropomorphic robot. This prototype served as the target system for modeling of a typical anthropomorphic robot.*

At this point a certain convention will be introduced to facilitate reading and understanding of the thesis. Musculoskeletal systems abound in kinematic redundancy (a human movement could be a result of numerous combinations of muscle activations). Therefore, there is no compromise about the precise number of human degrees of freedom. Furthermore, if only one antagonistic joint is considered, it has at least two degrees of freedom (in robotic applications generally the joint position and its stiffness are considered to be two independent terms controlled by the activity of antagonistic

muscles). Hereafter, we will use term “degree of freedom” (DoF) only for independent movements of robot joints (each rotational axis in the robot’s kinematic chain). Also, one agonist or antagonist actuator could be the physical structure consisting of its muscle and tendon, whereas a technical realization could have a non-elastic thread or a cord and elastic element, resembling a tendon and introducing intrinsic compliance. Hereafter the generic term “tendon” will be used to cover all cases.

## **2.3 Analytical approach to modeling in non-contact tasks**

The aim of this subsection is to deal with the modeling of a freely-moving humanoid robot with compliant antagonistically-coupled tendon drives, which resembles the human musculoskeletal structure. Although the inspiration for this work came from the advanced anthropomorphic Eccerobot, some of the complexity of a real robot (complex joints and multi-articular actuation) were omitted to enable strict mathematical treatment. In practice, this means that each DoF is now modeled as controlled by a single antagonistically-coupled pair of actuators. Multi-DoF joints are approximated by serial connection of antagonistically actuated hinge joints, whereas intermediary links are considered as links of negligible size and inertia. In the widely-adopted approximation used in humanoid robots, the waist, neck, and shoulder joints possess three DoFs each, while the elbow and wrist joints possess two. In order to resemble the musculoskeletal (anthropomorphic) actuation of the robot upper’s body as much as possible, a “triangular” mechanical model (see Figure 2.3, right) is adopted for the elbow rotations. One motor represents the biceps-brachii muscle (bending the arm), whereas the other mimics the triceps (straightening the arm). This is a convenient illustrative example of the role of antagonistically-coupled muscles in the human body, although the actual biology is rather more complex. For other rotations in the robot’s body, the more general “circular model” (see Figure 2.3, left) is used as a reasonable approximation.

This subsection first considers the application to single-joint systems of the circular and triangular mechanical models described above. Later, single-DoF drive equations are combined with dynamic equations of the robot’s spatial linkage to develop the dynamic

model of a full multi-jointed robot (Figure 2.2), actuated by antagonistically coupled compliant drives.

### 2.3.1 Models of antagonistically-driven compliant joints

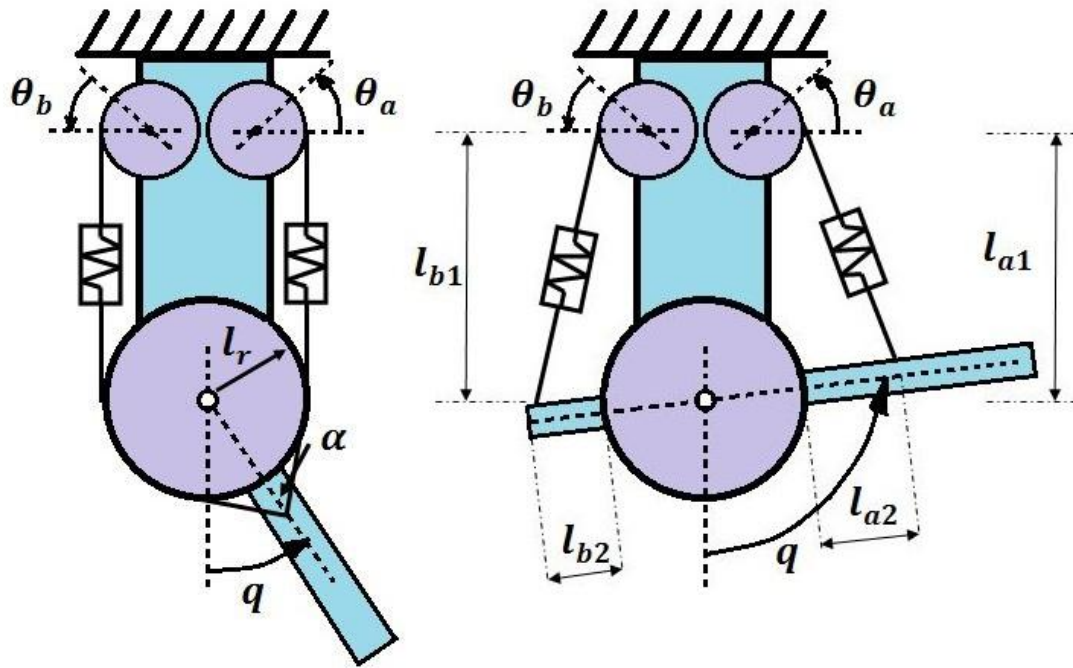


Figure 2.3. Circular joint structure: simplified linear antagonistic hinge joint geometry with two compliant tendons acting on a pulley. The moment arm is the same for both muscles and remains constant during joint movement. Non-linearity can be introduced by non-linear elastic elements (left); Triangular joint structure: non-linear antagonistic hinge joint geometry. Two moment arms are different and vary as a function of the joint angle due to tendon attachment points (right).

Once again, since the contraction of muscles or its technical counterpart develops unidirectional pulling forces, at least two antagonistic muscles are needed to move a link around the associated joint in two opposite directions. Here we introduce models of two of the most common antagonistic joint structures, which could in approximation mimic human-like musculoskeletal antagonistic actuation systems. Each muscle/tendon produces a torque, a product of the pulling force and its moment arm (i.e. the distance from the point of force application to the axis of rotation). For the first joint setup

(circular joint), this moment arm is constant. In the second joint setup (triangular joint), the moment arm varies as a function of the geometry or, more precisely, the joint position. The simplest joint geometry is a rotational hinge joint, which is fully linear and widely adopted in engineering as a typical antagonistic joint, whereas a triangular structure depicts a closer approximation to biological musculoskeletal antagonistic setups (elbow joint, ankle joint). In the latter configuration, the moment arms at which the muscles/tendons pull are a non-linear function of the joint angle.

The dynamics of the two antagonistically-paired drives are the starting point for the full model. A set of equations is introduced here, which describe the dynamics of the DC motors, followed by gear-boxes and pulleys. Equations (2.1) and (2.2) stand for mechanical and electrical characteristics of the DC motor, and the gear-boxes are introduced in (2.3) and (2.4). Geared motors turn pulleys that wind-up cords and stretch tendons (2.5). Since this set of equations apply to both the agonist  $a$  and the antagonist  $b$  of the same form, the superscripts  $a$  and  $b$  can be omitted.  $C^M$  is the torque constant,  $I^{rot}$  the rotor moment of inertia,  $B$  the viscous friction coefficient,  $\tau_m$  the motor output torque,  $u$  the input voltage,  $R$  the armature resistance,  $i$  the motor current,  $C^E$  the back-EMF constant,  $\theta$  the angle of the motor shaft rotation,  $N$  the gearbox ratio,  $\mu$  the gearbox efficiency coefficient,  $r$  the motor spindle radius,  $\theta^r$  the gearbox output angle,  $\tau_m^r$  the gearbox output torque, and  $F$  the tension force in the tendon.

$$C^M i = I^{rot} \ddot{\theta} + B \dot{\theta} + \tau_m \quad (2.1)$$

$$u = R i + C^E \dot{\theta} \quad (2.2)$$

$$\theta^r = \theta / N \quad (2.3)$$

$$\tau_m^r = \mu N \tau_m \quad (2.4)$$

$$F = \tau_m^r / r \quad (2.5)$$

Generally, elastic (tension) forces in the tendons each have two components: one proportional (stiffness) and the other differential (damping). Different force-deflection relations can be set, according to the elastic elements that introduce intrinsic compliance to the joints. For demonstration purposes, pure linear force-deflection characteristics are assumed. Furthermore, this linear approximation is based on real measurements from

experiments on the first prototype Eccerobot's elastic elements that showed the shock cord deformation to be almost linear up to a deformation of 100%. However, the linear characteristic of the spring restricts control, making stiffness control impossible [77]. Thus, expressions (2.6) and (2.7) describe linear spring characteristics, where  $k^a$  and  $k^b$  are the spring force constants,  $d^a$  and  $d^b$  the damping coefficients, and  $\Delta l^a$  and  $\Delta l^b$  the deformations (tendon extensions). The spring deformation (tendon extension) for both models can be described using the actual tendon length and pulley (motor) position, where  $\xi_0^{a/b}$  is the initial length of tendon  $a/b$  :  $\xi_0 = \xi(q(t = 0))$  as in (2.8) and (2.9). Therefore:

$$F^a = k^a \Delta l^a + d^a \dot{\Delta l}^a \quad (2.6)$$

$$F^b = k^b \Delta l^b + d^b \dot{\Delta l}^b \quad (2.7)$$

$$\Delta l^a = \xi^a(q) - \xi_0^a + r^a \theta^{ra} \quad (2.8)$$

$$\Delta l^b = \xi^b(q) - \xi_0^b - r^b \theta^{rb} \quad (2.9)$$

### 2.3.1.1 *Circular (linear) joint model*

This paragraph introduces a full model of the circular-joint model dynamics. It is a classical scheme of an antagonistic joint commonly considered in papers that discuss antagonistic actuation [132], [140], [106]. Since the moment arms are constant, the linear relation between the motor/joint positions and tendon extensions, and consequently the overall joint torque, is as shown below. Although very simple, this model approximately fits the structure of shoulder or knee joints.

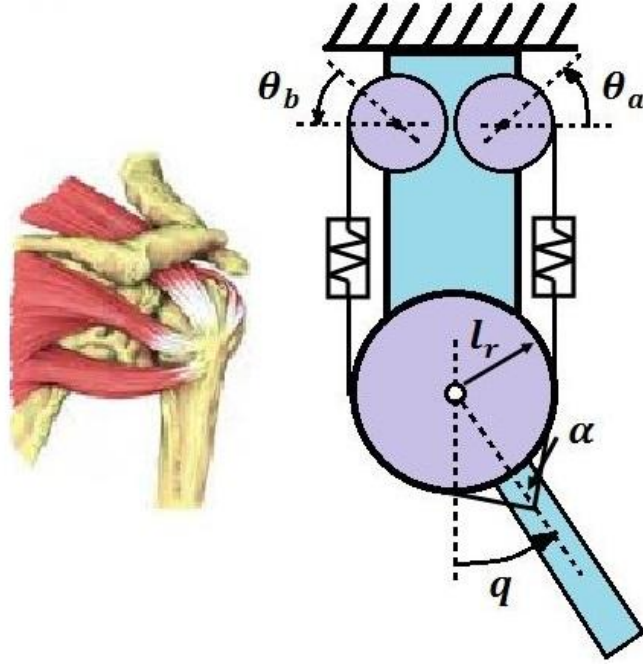


Figure 2.4. Demonstration of a human joint with constant moment arms (shoulder joint) - (left); Circular joint structure as a classical scheme of antagonistic joints with constant moment arms (right). This model is suggested as an approximation for shoulder or knee joint modeling.

The kinematics of joint rotation in the circular model depicted in Figure 2.4 is described by (2.10) and (2.11), where  $l_r$  is the sphere radius, and  $l_p$  is the distance between the sphere's centre and the place where the tendons are attached to the next link of the robot.  $\alpha$  represents the angle between  $l_r$  and  $l_p$ , so it is a constant and therefore  $l_p = l_r / \sin(\alpha)$  holds.

$$\xi^a(q) = (\pi/2 + \alpha - q)l_r + \sqrt{l_p^2 - l_r^2} \quad (2.10)$$

$$\xi^b(q) = (\pi/2 + \alpha + q)l_r + \sqrt{l_p^2 - l_r^2} \quad (2.11)$$

The overall joint torque for the circular joint configuration is calculated according to (2.12).

$$\tau = F^a l_p \sin(\alpha) - F^b l_p \sin(\alpha) = (F^a - F^b) l_r \quad (2.12)$$

If we define a set of state variables  $\mathbf{x}$ , which comprises motor positions  $\theta^a$ ,  $\theta^b$  and velocities  $\dot{\theta}^a$ ,  $\dot{\theta}^b$ , as well as joint position  $q$  and velocity  $\dot{q}$ , then the state variables vector is:  $\mathbf{x} = [x_1 \ x_2 \ x_3 \ x_4 \ x_5 \ x_6]^T = [\theta^a \ \dot{\theta}^a \ \theta^b \ \dot{\theta}^b \ q \ \dot{q}]^T$ . Using drives and spring dynamics given by (2.1) through (2.9) and the model geometry described in (2.10) and (2.11), the complete state-space form of the circular model can be written as in (2.13). Equations (2.14) through (2.16) are introduced for the sake of clarity and readability. Note that the number of DoFs is tripled when antagonistically-coupled drives with intrinsic elasticity are introduced (instead of the joint position only, there are agonist and antagonist motor positions as well).

$$\dot{\mathbf{x}} = \begin{bmatrix} \dot{x}_1 \\ \dot{x}_2 \\ \dot{x}_3 \\ \dot{x}_4 \\ \dot{x}_5 \\ \dot{x}_6 \end{bmatrix} = \begin{bmatrix} x_2 \\ x_{2dotC}(x_1, x_2, x_5, x_6) \\ x_4 \\ x_{4dotC}(x_3, x_4, x_5, x_6) \\ x_6 \\ x_{6dotC}(x_1, x_2, x_3, x_4, x_5, x_6) \end{bmatrix} + \begin{bmatrix} 0 & 0 \\ \frac{C^{Ma}}{R^a I_{rot a}} & 0 \\ 0 & 0 \\ 0 & \frac{C^{Mb}}{R^b I_{rot b}} \\ 0 & 0 \\ 0 & 0 \end{bmatrix} [u^a \ u^b] \quad (2.13)$$

$$\begin{aligned} x_{2dotC}(x_1, x_2, x_5, x_6) &= -\frac{r^a k^a}{\mu^a N^a I_{rot a}} x_1 - \frac{1}{I_{rot a}} \left( \frac{r^a d^a}{\mu^a N^a} + \left( B^a + \frac{C^{Ma} C^{Ea}}{R^a} \right) \right) x_2 \\ &\quad - \frac{r^a k^a}{\mu^a N^a I_{rot a}} (\xi^a(x_5) - \xi_0^a) + \frac{r^a d^a l_r}{\mu^a N^a I_{rot a}} x_6 \end{aligned} \quad (2.14)$$

$$\begin{aligned} x_{4dotC}(x_3, x_4, x_5, x_6) &= -\frac{r^b k^b}{\mu^b N^b I_{rot b}} x_3 - \frac{1}{I_{rot b}} \left( \frac{r^b d^b}{\mu^b N^b} + \left( B^b + \frac{C^{Mb} C^{Eb}}{R^b} \right) \right) x_4 \\ &\quad + \frac{r^b k^b}{\mu^b N^b I_{rot b}} (\xi^b(x_5) - \xi_0^b) + \frac{r^b d^b l_r}{\mu^b N^b I_{rot b}} x_6 \end{aligned} \quad (2.15)$$

$$\begin{aligned} x_{6dotC}(x_1, x_2, x_3, x_4, x_5, x_6) &= \frac{l_r r^a k^a}{N^a I} x_1 + \frac{l_r r^a d^a}{N^a I} x_2 + \frac{l_r r^b k^b}{N^b I} x_3 + \frac{l_r r^b d^b}{N^b I} x_4 - \frac{l_r^2}{I} (d^a + d^b) x_6 \\ &\quad + \frac{l_r}{I} [k^a \xi^a(x_5) - k^b \xi^b(x_5) - k^a \xi_0^a + k^b \xi_0^b] \end{aligned} \quad (2.16)$$

### 2.3.1.2 Triangular (non-linear) joint model

This paragraph introduces a full model of triangular joint dynamics. The model corresponds to the typical antagonistic structure – the structure one thinks of when speaking about antagonism in humans. It faithfully matches the elbow joint, which is a prime example of an antagonistically-driven joint but is also a good approximation of the ankle joint. Furthermore, since the moment arms change as joint position varies according to a non-linear relation, the model can be used to cover actuation of most joints of the musculoskeletal robot in an approximation.

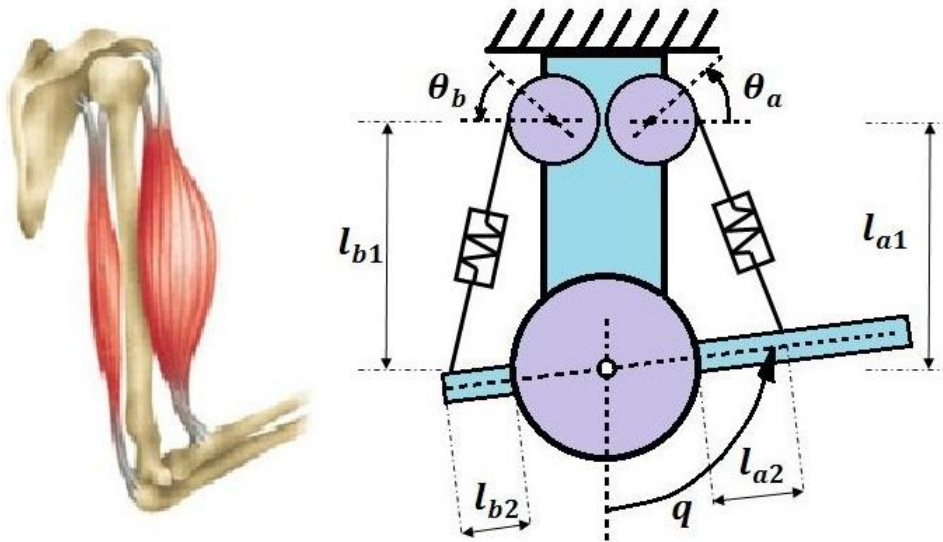


Figure 2.5. Demonstration of a human joint with changeable moment arms, which depends on the joint position (elbow joint) - (left); Triangular joint structure as a realistic scheme of antagonistic joints with variable moment arms. Moment arms change with the change of joint position according to non-linear relations (right). This model is suggested as an approximation for the elbow or ankle joint.

Expressions (2.17) through (2.20) describe the joint geometry for the triangular model depicted in Figure 2.5. Two tendons are denoted by ‘a’ and ‘b’. For a,  $l_{a1}$  is the distance from the joint axis to a’s motor spindle, and  $l_{a2}$  is the distance from the joint axis to the place where a is attached to the forearm. The same formulation is used for b.  $q$  to denote the joint angle.  $\xi^a$  ( $\xi^b$ ) denotes the actual length of tendon a (b), including the spring length; it is, of course, a function of the joint angle. Angles  $\varphi^a$  and  $\varphi^b$  are angles between the forearm and cords a and b, respectively. Therefore:

$$\xi^a(q) = \sqrt{l_{a1}^2 + l_{a2}^2 + 2l_{a1}l_{a2}\cos(q)} \quad (2.17)$$

$$\xi^b(q) = \sqrt{l_{b1}^2 + l_{b2}^2 - 2l_{b1}l_{b2}\cos(q)} \quad (2.18)$$

$$\varphi^a = \arcsin\left(\frac{l_{a1}\sin(q)}{\xi^a(q)}\right) \quad (2.19)$$

$$\varphi^b = \arcsin\left(\frac{l_{b1}\sin(q)}{\xi^b(q)}\right) \quad (2.20)$$

The overall joint torque for the triangular joint configuration is calculated according to (2.21).

$$\tau = F^a l_{a2} \sin(\varphi^a) - F^b l_{b2} \sin(\varphi^b) \quad (2.21)$$

Again, if we define a set of state variables  $\mathbf{x}$ , which comprises motor positions  $\theta^a$ ,  $\theta^b$  and velocities  $\dot{\theta}^a$ ,  $\dot{\theta}^b$ , as well as joint position  $q$  and velocity  $\dot{q}$ , then the state variables vector is:  $\mathbf{x} = [x_1 \ x_2 \ x_3 \ x_4 \ x_5 \ x_6]^T = [\theta^a \ \dot{\theta}^a \ \theta^b \ \dot{\theta}^b \ q \ \dot{q}]^T$ . Using drives and spring dynamics given by (2.1) through (2.9) and model geometry (2.17) through (2.20), the complete state-space form of the triangular model can be written as in (2.22). Equations (2.23) through (2.27) are introduced for the sake of clarity and readability. As in the case of the circular structure, by introducing antagonistically-coupled drives with intrinsic elasticity, the number of DoFs is tripled (instead of the joint position only, there are agonist and antagonist motor positions as well).

$$\dot{\mathbf{x}} = \begin{bmatrix} \dot{x}_1 \\ \dot{x}_2 \\ \dot{x}_3 \\ \dot{x}_4 \\ \dot{x}_5 \\ \dot{x}_6 \end{bmatrix} = \begin{bmatrix} x_2 \\ x_{2dotT}(x_1, x_2, x_5, x_6) \\ x_4 \\ x_{4dotT}(x_3, x_4, x_5, x_6) \\ x_6 \\ x_{6dotT}(x_1, x_2, x_3, x_4, x_5, x_6) \end{bmatrix} + \begin{bmatrix} 0 \\ C^{Ma} \\ \frac{R^a I^{rot a}}{R^a I^{rot a}} \\ 0 \\ 0 \\ 0 \\ 0 \\ \frac{C^{Mb}}{R^b I^{rot b}} \\ 0 \\ 0 \end{bmatrix} [u^a \ u^b] \quad (2.22)$$

$$\begin{aligned}
& x_{2dotT}(x_1, x_2, x_5, x_6) \\
&= -\frac{r^{a^2} k^a}{\mu^a N^{a^2} I^{rot a}} x_1 - \frac{1}{I^{rot a}} \left( \frac{r^{a^2} d^a}{\mu^a N^{a^2}} + \left( B^a + \frac{C^{Ma} C^{Ea}}{R^a} \right) \right) x_2 \\
&+ \frac{r^a}{\mu^a N^a I^{rot a}} (-k^a \xi^a(x_5) + d^a C_{Sa}(x_5) x_6 + k^a \xi_0^a)
\end{aligned} \tag{2.23}$$

$$\begin{aligned}
& x_{4dotT}(x_3, x_4, x_5, x_6) \\
&= -\frac{r^{b^2} k^b}{\mu^b N^{b^2} I^{rot b}} x_3 - \frac{1}{I^{rot b}} \left( \frac{r^{b^2} d^b}{\mu^b N^{b^2}} + \left( B^b + \frac{C^{Mb} C^{Eb}}{R^b} \right) \right) x_4 \\
&+ \frac{r^b}{\mu^b N^b I^{rot b}} (k^b \xi^b(x_5) + d^b C_{Sb}(x_5) x_6 - k^b \xi_0^b)
\end{aligned} \tag{2.24}$$

$$\begin{aligned}
& x_{6dotT}(x_1, x_2, x_3, x_4, x_5, x_6) \\
&= \frac{C_{Sa}(x_5) r^a k^a}{N^a I} x_1 + \frac{C_{Sa}(x_5) r^a d^a}{N^a I} x_2 + \frac{C_{Sb}(x_5) r^b k^b}{N^b I} x_3 + \frac{C_{Sb}(x_5) r^b d^b}{N^b I} x_4 \\
&+ \frac{1}{I} C_{Sa}(x_5) k^a \xi^a(x_5) - \frac{1}{I} C_{Sb}(x_5) k^b \xi^b(x_5) - \frac{1}{I} C_{Sa}(x_5) k^a \xi_0^a \\
&+ \frac{1}{I} C_{Sb}(x_5) k^b \xi_0^b - \frac{1}{I} \left( \frac{C_{Sa}(x_5) d^a l_{a1} l_{a2}}{\xi^a(x_5)} + \frac{C_{Sb}(x_5) d^b l_{b1} l_{b2}}{\xi^b(x_5)} \right) \sin x_5 \cdot x_6
\end{aligned} \tag{2.25}$$

$$C_{Sa}(x_5) = \frac{l_{a1} l_{a2} \sin x_5}{\xi^a(x_5)} \tag{2.26}$$

$$C_{Sb}(x_5) = \frac{l_{b1} l_{b2} \sin x_5}{\xi^b(x_5)} \tag{2.27}$$

### 2.3.2 Multi-joint robot model

This subsection derives the dynamic model of the full robot body mechanism and integrates it with the joint-drive models based on antagonism, defined by (2.13) or (2.22).

The starting point for the development of a complete dynamic model is a ‘‘classical’’ dynamic model that considers the joint torques as control inputs and relates them to joint motions (2.29). It is the so-called *Flier* concept [141], which is deductive, general, and applicable to an arbitrary humanoid robot in an arbitrary motion task. The idea of the *Flier* approach is to first consider the humanoid freely flying in space, and then introduce contacts with environment objects in order to model any desired movement task, such as walking, running, manipulation, sporting movements, and the like.

As already elaborated, the computer-based formulation of the proposed concept is founded upon Stepanjenko's parameters suitable for efficient calculation of robot dynamics [123], which can be adjusted to any robot configuration. Replicating the Eccerobot prototype and its functional DoFs, the robot structure presented in Figure 2.6. is adopted. The model contains three DoFs in the waist, neck, and shoulders; and two DoFs in the elbow and wrist joints. Therefore, the number of functional DoFs is 20, whereas 26 parameters are needed for a full description of the robot's spatial position ( $n = 20; N = 26$ ).

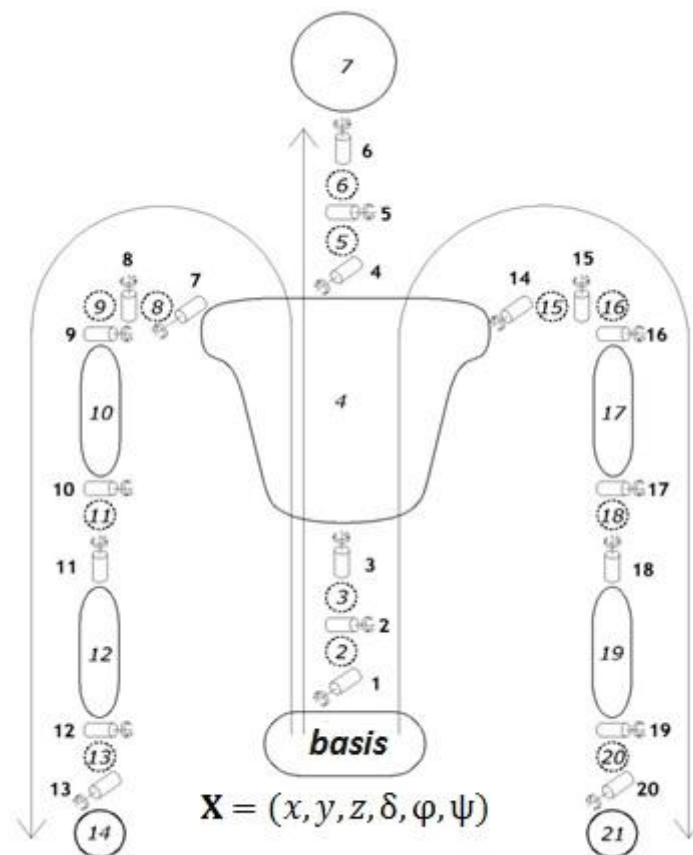


Figure 2.6. Robot model: three DoFs in the waist, neck, and shoulders; and two DoFs in the elbow and wrist joints. Six additional coordinates of the basic segment (basis) are introduced to fully describe the robot's spatial position.

If a robot has  $n$  single-rotation joints, as in the case of our approximation of the anthropomimetic robot, then its position is defined by expression (2.28) with vector  $\mathbf{Q}$  of dimension  $N = 6 + n$ , where  $\mathbf{X}_{6 \times 1} = [x \ y \ z \ \delta \ \varphi \ \psi]^T$  defines the absolute position of

the basis or basic link in the kinematic chain (the pelvis in this case), and  $\mathbf{q}_{nx1} = [q_1 \ q_2 \ \dots \ q_n]^T$  represents the joint angles.

$$\mathbf{Q}_{Nx1} = [x \ y \ z \ \delta \ \varphi \ \psi \ q_1 \ \dots \ q_n]^T = [\mathbf{X}_{6x1} \ \mathbf{q}_{nx1}]^T \quad (2.28)$$

If  $\boldsymbol{\tau} = [\tau_1 \ \tau_2 \ \dots \ \tau_n]^T$  represents the joint torques and consequently a generalized vector of the torque drives could be written as  $\mathbf{T}_{Nx1} = [0 \ 0 \ \dots \ 0 \ \tau_1 \ \tau_2 \ \dots \ \tau_n]^T = [\mathbf{0}_{6x1} \ \boldsymbol{\tau}_{nx1}]^T$ , then the general dynamic model has the matrix form (2.29). Note that for this initial model interaction forces are not considered.

$$\mathbf{H}_{NxN}(\mathbf{Q}) \ddot{\mathbf{Q}}_{Nx1} + \mathbf{h}_{Nx1}(\mathbf{Q}, \dot{\mathbf{Q}}) = \mathbf{T}_{Nx1} \quad (2.29)$$

Following this computer-aided algorithm for robot dynamics, elaborated in [142] or [104], Equation (2.29) can be derived for any humanoid robot model. We now focus on our anthropomorphic model and introduce the models of antagonistically-coupled compliant drives presented in Subsection 2.3.1. Keeping in mind the equations of the joint drives (2.1) through (2.9) and models of the kinematics ((2.10) and (2.11) for the circular joint model, (2.17) through (2.20) for the triangular joint model), it is clear that each joint torque ((2.12) for the circular joint model, (2.21) for the triangular joint model) can be written as a function of the joint and motor positions  $(q, \theta^a, \theta^b)$  and velocities  $(\dot{q}, \dot{\theta}^a, \dot{\theta}^b)$ . Therefore, each joint torque can be expressed as in (2.30) for the circular joint model and (2.31) for the triangular joint model. Depending on the joint model applied to each of the robot axes, the matrix of generalized joint torques can be written in the form of (2.32).

$$\begin{aligned} \tau(q, \dot{q}, \theta^a, \dot{\theta}^a, \theta^b, \dot{\theta}^b) &= l_p \sin(\alpha) \cdot [k^a \left( \xi^a(q) - \xi^a_0 + \frac{r^a}{N^a} \theta^a \right) - k^b \left( \xi^b(q) - \xi^b_0 - \frac{r^b}{N^b} \theta^b \right)] \\ &+ d^a \left( -l_r \dot{q} + \frac{r^a}{N^a} \dot{\theta}^a \right) - d^b \left( l_r \dot{q} - \frac{r^b}{N^b} \dot{\theta}^b \right) \end{aligned} \quad (2.30)$$

$$\begin{aligned}
& \tau(q, \dot{q}, \theta^a, \dot{\theta}^a, \theta^b, \dot{\theta}^b) \\
& = l_{a1} l_{a2} \sin(q) \cdot [k^a \left( \xi^a(q) - \xi^a_0 + \frac{r^a}{N^a} \theta^a \right) - k^b \left( \xi^b(q) - \xi^b_0 - \frac{r^b}{N^b} \theta^b \right)] \\
& + d^a \left( -\frac{l_{a1} l_{a2} \sin(q)}{\xi^a(q)} \dot{q} + \frac{r^a}{N^a} \dot{\theta}^a \right) - d^b \left( -\frac{l_{b1} l_{b2} \sin(q)}{\xi^b(q)} \dot{q} - \frac{r^b}{N^b} \dot{\theta}^b \right)
\end{aligned} \quad (2.31)$$

$$\mathbf{T}_{N \times 1} = \mathbf{T}(\mathbf{q}, \dot{\mathbf{q}}, \boldsymbol{\theta}^a, \dot{\boldsymbol{\theta}}^a, \boldsymbol{\theta}^b, \dot{\boldsymbol{\theta}}^b) = \mathbf{T}(\mathbf{Q}, \dot{\mathbf{Q}}, \boldsymbol{\theta}^a, \dot{\boldsymbol{\theta}}^a, \boldsymbol{\theta}^b, \dot{\boldsymbol{\theta}}^b) \quad (2.32)$$

The vectors  $\mathbf{q}$  (or  $\mathbf{Q}$ ),  $\boldsymbol{\theta}^a$ ,  $\boldsymbol{\theta}^b$  are proper position vectors for the joints and both motors in each joint. Note that compliance in the tendons makes the motor angles independent of the joint positions and thus triples the dimensionality of the problem. For a given joint, instead of joint position and velocity only, we now have six state-space coordinates: the joint position, the agonist motor position, and the antagonist motor position, all with corresponding velocities. Note that the generality of the method means that solutions for joint torques, other than those derived from the specified antagonistic models, can be used at this point.

Substituting each joint torque in vector  $\mathbf{T}$  in (2.29) by the appropriate expression (2.30) or (2.31), the adjoint matrix  $\mathbf{h}_{N \times 1}(\mathbf{Q}, \dot{\mathbf{Q}})$  is changed to  $\tilde{\mathbf{h}}_{N \times 1}(\mathbf{Q}, \dot{\mathbf{Q}}, \boldsymbol{\theta}^a, \dot{\boldsymbol{\theta}}^a, \boldsymbol{\theta}^b, \dot{\boldsymbol{\theta}}^b)$ , and robot dynamics can be rewritten to (2.34), in the absence of external influences.

$$\tilde{\mathbf{h}}_{N \times 1}(\mathbf{Q}, \dot{\mathbf{Q}}, \boldsymbol{\theta}^a, \dot{\boldsymbol{\theta}}^a, \boldsymbol{\theta}^b, \dot{\boldsymbol{\theta}}^b) = \mathbf{h}_{N \times 1}(\mathbf{Q}, \dot{\mathbf{Q}}) - \mathbf{T}_{N \times 1}(\mathbf{Q}, \dot{\mathbf{Q}}, \boldsymbol{\theta}^a, \dot{\boldsymbol{\theta}}^a, \boldsymbol{\theta}^b, \dot{\boldsymbol{\theta}}^b) \quad (2.33)$$

$$\mathbf{H}_{N \times N}(\mathbf{Q}) \ddot{\mathbf{Q}} + \tilde{\mathbf{h}}_{N \times 1}(\mathbf{Q}, \dot{\mathbf{Q}}, \boldsymbol{\theta}^a, \dot{\boldsymbol{\theta}}^a, \boldsymbol{\theta}^b, \dot{\boldsymbol{\theta}}^b) = \mathbf{0}_{N \times 1} \quad (2.34)$$

To enable numerical integration of the system,  $2n$  additional equations are needed. The necessary equations are obtained from motor dynamics. Combining Equations (2.1) through (2.9) for each two antagonistic motors per  $n$  joints, additional  $2n$  differential equations are introduced into the  $2n$ -dimensional matrix form (2.35).

$$\bar{\bar{\mathbf{H}}}_{2n \times 2n} \ddot{\boldsymbol{\theta}}_{2n \times 1} + \bar{\mathbf{h}}_{2n \times 1}(\mathbf{Q}, \dot{\mathbf{Q}}, \boldsymbol{\theta}^a, \dot{\boldsymbol{\theta}}^a, \boldsymbol{\theta}^b, \dot{\boldsymbol{\theta}}^b) = \mathbf{C}_{2n \times 2n} \mathbf{u}_{2n \times 1} \quad (2.35)$$

For the sake of clarity, the following notation is used:  $\boldsymbol{\theta}_{2n \times 1}$  – vector of  $n$  agonist and  $n$

antagonist motor positions,  $\bar{\mathbf{H}}_{2nx2n}$  – motor inertia matrix,  $\bar{\mathbf{h}}_{2nx1}$  – motor adjoint matrix comprising position and velocity dependent components of drive dynamics,  $\mathbf{C}_{2nx2n}$  – motor control matrix, and, finally,  $\mathbf{u}_{2nx1}$  – matrix of control voltages.

$$\bar{\mathbf{H}}_{2nx2n} = \begin{bmatrix} \mathbf{I}^{rot a} & \mathbf{0}_{nxn} \\ \mathbf{0}_{nxn} & \mathbf{I}^{rot b} \end{bmatrix}_{nxn}; \mathbf{I}^{rot a/b} = \text{diag}\{I^{rot a/b}_k\}; k = 1, \dots, n \quad (2.36)$$

$$\boldsymbol{\theta}_{2nx1} = \begin{bmatrix} \boldsymbol{\theta}^a \\ \boldsymbol{\theta}^b \end{bmatrix}_{nx1} \quad (2.37)$$

$$\bar{\mathbf{h}}_{2nx1}(\mathbf{q}, \dot{\mathbf{q}}, \boldsymbol{\theta}^a, \dot{\boldsymbol{\theta}}^a, \boldsymbol{\theta}^b, \dot{\boldsymbol{\theta}}^b) = \begin{bmatrix} \bar{\mathbf{h}}_{a2nx1}(\mathbf{q}, \dot{\mathbf{q}}, \boldsymbol{\theta}^a, \dot{\boldsymbol{\theta}}^a, \boldsymbol{\theta}^b, \dot{\boldsymbol{\theta}}^b) \\ \bar{\mathbf{h}}_{b2nx1}(\mathbf{q}, \dot{\mathbf{q}}, \boldsymbol{\theta}^a, \dot{\boldsymbol{\theta}}^a, \boldsymbol{\theta}^b, \dot{\boldsymbol{\theta}}^b) \end{bmatrix} \quad (2.38)$$

$$\mathbf{C}_{2nx2n} = \begin{bmatrix} \frac{\mathbf{C}^{Ma}}{\mathbf{R}^a} & \mathbf{0}_{nxn} \\ \mathbf{0}_{nxn} & \frac{\mathbf{C}^{Mb}}{\mathbf{R}^b} \end{bmatrix}_{nxn}; \frac{\mathbf{C}^{Ma/b}}{\mathbf{R}^{a/b}} = \text{diag}\left\{\frac{C^{Ma/b}_k}{R^{a/b}_k}\right\}; k = 1, \dots, n \quad (2.39)$$

$$\mathbf{u}_{2nx1} = \begin{bmatrix} \mathbf{u}^a \\ \mathbf{u}^b \end{bmatrix}_{nx1}; \mathbf{u}^{a/b} = [u^{a/b}_k]; k = 1, \dots, n \quad (2.40)$$

Ultimately, by combining (2.34) and (2.35), a total of  $3n + 6$  (or  $N + 2n$ ) relations are specified to enable numerical integration of the system and, consequently, simulations, assuming that the position of the basic link  $\mathbf{X}_{6x1}$  is known. Otherwise, if the basic link is moved by the external actuation system, the model should be extended by six additional equations that describe basic segment dynamics. To that end, these equations are recalled in (2.41).

$$\begin{aligned} \mathbf{H}_{NxN}(\mathbf{Q}) \ddot{\mathbf{Q}} + \tilde{\mathbf{h}}_{Nx1}(\mathbf{Q}, \dot{\mathbf{Q}}, \boldsymbol{\theta}^a, \dot{\boldsymbol{\theta}}^a, \boldsymbol{\theta}^b, \dot{\boldsymbol{\theta}}^b) &= \mathbf{0}_{Nx1} \\ \bar{\mathbf{H}}_{2nx2n} \ddot{\boldsymbol{\theta}}_{2nx1} + \bar{\mathbf{h}}_{2nx2n}(\mathbf{Q}, \dot{\mathbf{Q}}, \boldsymbol{\theta}^a, \dot{\boldsymbol{\theta}}^a, \boldsymbol{\theta}^b, \dot{\boldsymbol{\theta}}^b) &= \mathbf{C}_{2nx2n} \mathbf{u}_{2nx2n} \end{aligned} \quad (2.41)$$

## 2.4 Analytical approach to modeling in contact tasks

Since anthropomorphic robots are intended to work in a close human environment and often interact with humans, analysis of the interaction tasks is of the essence. To enhance the robot's safety but also the safety of its surroundings, this interaction has to be well planned, analyzed and controlled. Actually, most robotic tasks involve

intentional contact with the environment and, furthermore, involve the force output necessary to complete the tasks, such as assembling, polishing, deburring, etc.

In [143], Diamond et al. explain the benefits of an accurate model of a complex mechanical system in interaction with its environment. They argue that a sophisticated cognitive system must possess models of itself and the world, along with the necessary infrastructure, to use the modeled interactions between these two components to select relatively advantageous actions. Within the Eccerobot project, the group of Prof. Holland suggested twofold use of such models: representations of the future (imagination) and the past (memory).

In this subsection we extend the model of the freely-moving anthropomorphic robot with antagonistically-coupled compliant drives to enable analytical treatment of contact tasks. The presented theory considers the contacted object as prone to deformations, and robot contact surfaces as infinitely stiff objects. To allow comprehensive treatment of the interaction tasks, all phases are considered analytically:

- approach phase (the robot and the contacted object are considered to be two independent dynamic objects, while their relative positions are observed);
- impact phase (infinitely short, the conservation of momentum and angular momentum stands when impact occurs between the robot and the object);
- “in-contact motion” phase (the robot and the object are considered to be inseparable dynamic systems and the interaction forces are calculated).

One or more contacts with the environment are now introduced, following the theory explained in [144], where the basic features of contact dynamics are described. One can distinguish between instantaneous and prolonged contact. Instantaneous contact involves two objects interacting for an infinitely short time (impact), and subsequently becoming two separate dynamic systems (an example is a volleyball player hitting the ball). A prolonged contact includes the impact and a finite period of contact motion, while the two objects have joint dynamics (an example is a basketball player who catches and then holds the ball). The presented theory can be exploited to deal with

contacts between a robot and a mobile or stationary object, as well as between two robots (see Figure 2.7). Finally, one can distinguish between situations where the robot can influence the movement of a contacted object (e.g. a robot opening a door by pushing the door handle) and situations where it cannot, such as if the object has a much larger mass, if it is driven by extremely strong actuators, or, finally, if the object is immobile (e.g. a robot pushing against a wall).

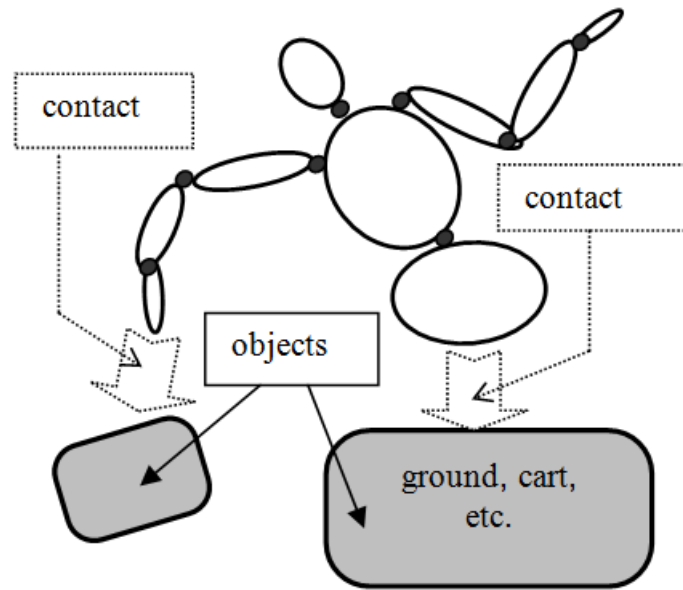


Figure 2.7. Schematic representation of a robot interacting with mobile or stationary objects treated as dynamics objects according to the analytical approach presented in Subsection 2.4.

For contact analysis we need a new set of coordinates – external coordinates, which describe the robot’s position in a global frame. We first define the external position of the link of interest and the point of interest on it – the point that will be contacted (e.g. robot gripper and its tip). By “external position” we mean the Cartesian coordinates  $(x, y, z)$  of the point of interest, and the orientation of the link of interest defined by  $\theta, \varphi,$  and  $\psi$  as yaw, pitch and roll angles, respectively. The external position vector is therefore  $\mathbf{X} = [x \ y \ z \ \theta \ \varphi \ \psi]^T$ . Since the robot contact point (CP) with external position  $\mathbf{X}$  depends on the robot’s position vector  $\mathbf{Q}$  ( $\mathbf{X} = \mathbf{X}(\mathbf{Q})$ ), Equations (2.42) and (2.43) hold. Here,  $\mathbf{J} = \frac{\partial \mathbf{X}}{\partial \mathbf{Q}}$  is a  $6 \times N$  Jacobian matrix and  $\mathbf{A} = \frac{\partial^2 \mathbf{X}}{\partial \mathbf{Q}^2} \dot{\mathbf{Q}}^2$  is a  $6 \times 1$  adjoint vector.

$$\dot{\mathbf{X}} = \mathbf{J}(\mathbf{Q})\dot{\mathbf{Q}} \quad (2.42)$$

$$\ddot{\mathbf{X}} = \mathbf{J}(\mathbf{Q})\ddot{\mathbf{Q}} + \mathbf{A}(\mathbf{Q}, \dot{\mathbf{Q}}) \quad (2.43)$$

However, in contact tasks it is more appropriate for the position of the robot point of interest (CP) to be defined relative to the object that will be contacted. Hence, it is useful to introduce a frame fixed to the object. Since the object might be mobile, the new frame will also move. Let the coordinates  $\mathbf{s} = [s_1 \ s_2 \ s_3 \ s_4 \ s_5 \ s_6]^T$  define this relative position, and let them be called functional coordinates (often referred to as  $s$ -coordinates).

In general, the object will be mobile and so its position will be described by the external coordinates:  $\mathbf{Q}_{\text{obj}} = [x_{\text{obj}} \ y_{\text{obj}} \ z_{\text{obj}} \ \theta_{\text{obj}} \ \varphi_{\text{obj}} \ \psi_{\text{obj}}]^T$ . Its motion has to be known (or calculated from the appropriate mathematical model (2.44), in a way similar to that described for a freely-moving robot (2.29)).

$$\mathbf{W}(\mathbf{Q}_{\text{obj}}) \ddot{\mathbf{Q}} + \mathbf{w}(\mathbf{Q}_{\text{obj}}, \dot{\mathbf{Q}}_{\text{obj}}) = \mathbf{T}_{\text{obj}} \quad (2.44)$$

Here we introduce a generalized inertial matrix of the object  $\mathbf{W}(\mathbf{Q}_{\text{obj}})$ , the corresponding adjoint matrix  $\mathbf{w}(\mathbf{Q}_{\text{obj}}, \dot{\mathbf{Q}}_{\text{obj}})$ , and the vector of driving torques applied to the object  $\mathbf{T}_{\text{obj}}$ . Regardless of the type of contacted object (other robot, moving object, stationary object, etc.), all the properties that characterize robot dynamics (2.29) hold for the object as well.

An  $s$ -frame fixed to the object is introduced to describe the relative position of the robot CP in the most useful and convenient way. The functional coordinates  $\mathbf{s}$  depend on both the robot position  $\mathbf{Q}$  (actually  $\mathbf{X}(\mathbf{Q})$ ) and the object position  $\mathbf{Q}_{\text{obj}}$  (2.45). An approach phase precedes the contact task or, more precisely, the impact task. The approach phase considers the robot and the object as two separate dynamic systems, whose models are independently integrated and functional coordinates are observed. The contact/impact occurs if any of the functional coordinates reaches zero. Before impact (before one of the functional coordinates reaches zero), we consider the robot and the object as two

independent dynamic systems, which could consequently be simulated separately. Concurrently, functional coordinates  $\mathbf{s}$  are calculated and we continue the procedure until one of them reaches zero. We call this phase the approach phase. When the contact occurs, the actual contact restricts some of the relative coordinates – let it be the subset  $\mathbf{s}^c$ , while the rest remain unrestricted (free). Thus, the subset of free coordinates  $\mathbf{s}^f$  is the relative complement of  $\mathbf{s}^c$  with respect to a set  $\mathbf{s}$  (see Figure 2.8). If a coordinate is restricted, there is no relative motion between the robot contact point and the object contact point, or, in other words, the restricted coordinate is zero, as are its velocity (2.46) and acceleration (2.47).

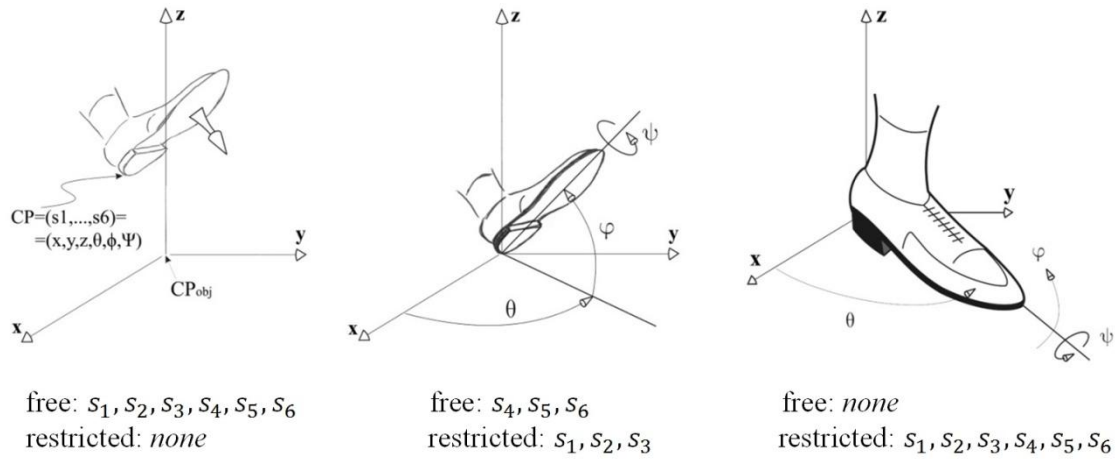


Figure 2.8. Identification of functional coordinates  $s$  – free and restricted. Impact occurs if any of the free coordinates reaches zero. Thereby the functional coordinate exchanges its set: from free to restricted functional coordinates. Each exchange between these sets requires a new corresponding mathematical model.

$$\mathbf{s}^c(\mathbf{Q}, \mathbf{Q}_{\text{obj}}) = \mathbf{0} \quad (2.45)$$

$$\dot{\mathbf{s}}^c = \mathbf{J}(\mathbf{Q}, \mathbf{Q}_{\text{obj}})\dot{\mathbf{Q}} + \mathbf{J}_{\text{obj}}(\mathbf{Q}, \mathbf{Q}_{\text{obj}})\dot{\mathbf{Q}}_{\text{obj}} = \mathbf{0} \quad (2.46)$$

$$\ddot{\mathbf{s}}^c = \mathbf{J}(\mathbf{Q}, \mathbf{Q}_{\text{obj}})\ddot{\mathbf{Q}} + \mathbf{J}_{\text{obj}}(\mathbf{Q}, \mathbf{Q}_{\text{obj}})\ddot{\mathbf{Q}}_{\text{obj}} + \mathbf{A}(\mathbf{Q}, \dot{\mathbf{Q}}, \mathbf{Q}_{\text{obj}}, \dot{\mathbf{Q}}_{\text{obj}}) = \mathbf{0} \quad (2.47)$$

If there are  $m$  restricted directions, the matrices  $\mathbf{J} = \frac{\partial \mathbf{s}^c}{\partial \mathbf{Q}}$  and  $\mathbf{J}_{\text{obj}} = \frac{\partial \mathbf{s}^c}{\partial \mathbf{Q}_{\text{obj}}}$  are Jacobians of dimensions  $m \times N$  and  $m \times k$ , respectively,  $\mathbf{A}$  is an adjoint matrix that contains second partial derivatives and  $k$  is the number of object coordinates (if the object is a single-DoF body, then  $k = 6$ ). The contact introduces reactions in the restricted directions  $\mathbf{s}^c$ :

reaction forces along restricted translations and moments around restricted rotations. This partition between free and restricted functional coordinates is of essential importance for hybrid position/force control. One of the popular papers of Yoshikawa et al. [145] is based on this very partition approach to the linearization of robot dynamics for a nonlinear-state feedback controller.

If an interaction force exists between the robot and the object, then the equations of robot and object dynamics are modified accordingly, by adding this force via the appropriate Jacobian, applying the principle of virtual work. Let  $\mathbf{R}_{m \times 1}$  be the vector of the interaction force. Equation (2.34) that originates from (2.29) becomes (2.48) for the anthropomorphic robot with antagonistic actuators, and the object dynamics is changed from (2.44) to (2.49).

$$\begin{aligned} \mathbf{H}_{N \times N}(\mathbf{Q}) \ddot{\mathbf{Q}} + \tilde{\mathbf{h}}_{N \times 1}(\mathbf{Q}, \dot{\mathbf{Q}}, \theta^a, \dot{\theta}^a, \theta^b, \dot{\theta}^b) &= \mathbf{0}_{N \times 1} + \mathbf{J}^T(\mathbf{Q}, \mathbf{Q}_{obj}) \mathbf{R} \\ \bar{\mathbf{H}} \ddot{\boldsymbol{\theta}} + \bar{\mathbf{h}}(\mathbf{Q}, \dot{\mathbf{Q}}, \theta^a, \dot{\theta}^a, \theta^b, \dot{\theta}^b) &= \mathbf{C} \mathbf{u} \end{aligned} \quad (2.48)$$

$$\mathbf{W}(\mathbf{Q}_{obj}) \ddot{\mathbf{Q}} + \mathbf{w}(\mathbf{Q}_{obj}, \dot{\mathbf{Q}}_{obj}) = \mathbf{T}_{obj} + \mathbf{J}_{obj}^T(\mathbf{Q}, \mathbf{Q}_{obj}) \mathbf{R} \quad (2.49)$$

In general, several interaction forces can be treated simultaneously. As such, the right side of Equations (2.48) and (2.49) would be expanded with the forces multiplied by the corresponding Jacobians.

When speaking about modeling of robot and external object interaction, we have to mention collision detection in robotic systems as an essential part of dealing with robot contact tasks. Although collision detection is not elaborated in this thesis, it is still a current topic of research and industry. Collision detection in commercial robots is already available, but it often comes only with very advanced robots from vendors such as KUKA or ABB, for instance. In order to detect that a collision has occurred, robots usually have to use noisy acceleration measurements and perform on-line inversion of the robot's inertia matrix. Since we know that an external force affects all preceding joints in the static case, and all joints in the dynamic case, we can examine collision detection. The most common algorithm for collision detection is a variation in the

commanded and actual drive torques or currents. Collision can be observed by comparing actual motions and, in parallel, simulated robot dynamics, by numerically estimating accelerations, etc. However, all these algorithms are sensitive to models of robot dynamics, applied references, and control algorithms. Significant results in this domain, and even more so in the isolation of collisions, have been achieved by introducing torque sensors in robot joints (e.g. DLR LWR-III robot).

#### 2.4.1 Models of in-contact motions

Contacts are further divided into groups: rigid, elastodynamic and soft, depending on whether or not elastic deformations occur at the time of contact (see Figure 2.9). A rigid contact assumes that stiffness of the parts in contact is so high that no elastic deformation occurs on either the robot or object side. In this case the motion of the robot link is geometrically constrained. Of course, no contact can be completely rigid, but in many cases approximation can be justified. In a real situation, some elastic deformation will occur in both the robot and the contacted object. A contact is characterized as soft if the object is likely to be deformed immediately, with certain impedance described by stiffness and damping in the contact zone. The most demanding mathematical treatment is required if the contact is characterized as elastodynamic, where impedance on the object side indicates some inertial mass besides stiffness and damping. Most contacts can be interpreted as elastodynamic, with associated parameters: inertia –  $M$ , stiffness –  $K$ , and damping –  $B$ , on the object side. Note that due to non-negligible inertia in the contact zone, impulse conservation must be treated in the case of rigid or elastodynamic contacts. To that end, we elaborate the impact phenomena for rigid and elastodynamic contacts, where discontinuities of velocity are possible.

The question that naturally arises is how the type of contact could be predicted in advance. So far, the present approach is based on predefined clustering of the already known object, which is the subject of interaction. In the Eccerobot project, a Microsoft Kinect camera was integrated purposely, to model the environment of the robot [146].

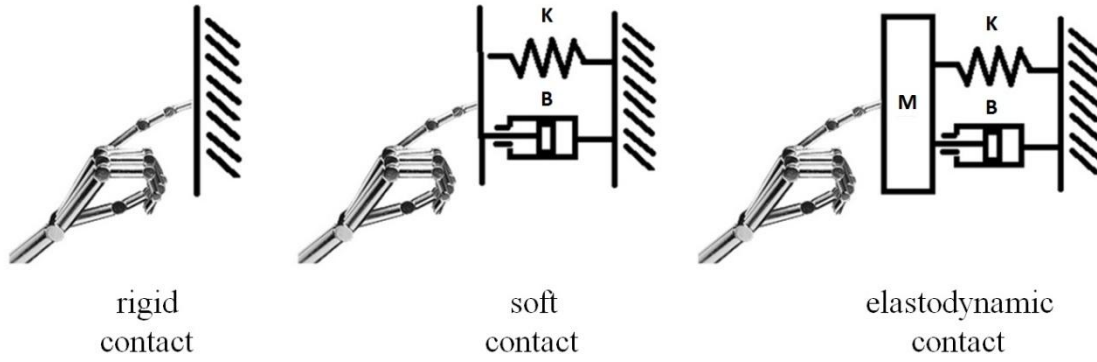


Figure 2.9. Division of contacts according to the type of elastic deformations in the contact zone.

#### 2.4.1.1 Rigid contact

If robot dynamics (2.48) and object dynamics (2.49) are considered when there is an interaction force  $\mathbf{R}$ , the system becomes underdetermined. More precisely, the introduced reaction force causes a lack of equations. This can be overcome by considering the constraints (2.47) in functional coordinates. Equation (2.47) provides exactly  $m$  additional relations between the robot and object coordinates due to the restricted contact motion, and therefore compensates for the  $m$  unknown interaction forces in (2.48) and (2.49). Finally, the dynamics of the rigid contact motion are described by a set of scalar equations, represented by model (2.50).

$$\begin{aligned}
 \mathbf{H}(\mathbf{Q}) \ddot{\mathbf{Q}} + \tilde{\mathbf{h}}(\mathbf{Q}, \dot{\mathbf{Q}}, \boldsymbol{\theta}^a, \dot{\boldsymbol{\theta}}^a, \boldsymbol{\theta}^b, \dot{\boldsymbol{\theta}}^b) &= \mathbf{J}^T(\mathbf{Q}, \mathbf{Q}_{\text{obj}}) \mathbf{R} \\
 \bar{\mathbf{H}} \ddot{\boldsymbol{\theta}} + \bar{\mathbf{h}}(\mathbf{Q}, \dot{\mathbf{Q}}, \boldsymbol{\theta}^a, \dot{\boldsymbol{\theta}}^a, \boldsymbol{\theta}^b, \dot{\boldsymbol{\theta}}^b) &= \mathbf{C} \mathbf{u} \\
 \mathbf{W}(\mathbf{Q}_{\text{obj}}) \ddot{\mathbf{Q}}_{\text{obj}} + \mathbf{w}(\mathbf{Q}_{\text{obj}}, \dot{\mathbf{Q}}_{\text{obj}}) &= \mathbf{T}_{\text{obj}} + \mathbf{J}_{\text{obj}}^T(\mathbf{Q}, \mathbf{Q}_{\text{obj}}) \mathbf{R} \\
 \ddot{\mathbf{s}}^c = \mathbf{J}(\mathbf{Q}, \mathbf{Q}_{\text{obj}}) \ddot{\mathbf{Q}} + \mathbf{J}_{\text{obj}}(\mathbf{Q}, \mathbf{Q}_{\text{obj}}) \ddot{\mathbf{Q}}_{\text{obj}} + \mathbf{A}(\mathbf{Q}, \dot{\mathbf{Q}}, \mathbf{Q}_{\text{obj}}, \dot{\mathbf{Q}}_{\text{obj}}) &= \mathbf{0}
 \end{aligned} \tag{2.50}$$

The model (2.50) includes  $N$ -dimensional robot dynamics,  $2n$ -dimensional drive dynamics,  $k$ -dimensional object dynamics, and the  $m$ -dimensional geometry of the contact, respectively. In general,  $m$  denotes the number of restricted coordinates ( $m_{\text{max}} = 6$  if all three translations and three rotations are restricted due to contact), while  $k$  denotes the number of DoFs of the contacted object (for a simple rigid body  $k$  is

6, but in the case of a contact with another robot it can be much more). The model relates input voltages –  $\mathbf{u}$  (as controlled inputs) of the anthropomorphic robot approximated by its structure with compliant antagonistic joints, and object driving torques –  $\mathbf{T}_{obj}$  in general, to system motion –  $\mathbf{Q}$  and  $\mathbf{Q}_{obj}$ , and contact reactions –  $\mathbf{R}$  on the other side. If the behavior of the contacted object is robust to the robot’s actions (e.g. if the contacted object has a disproportionately larger mass, or is driven by sufficiently strong actuators), then system dynamics can be decoupled. In such a case the object dynamics represented by the third equation in (2.50) can be solved independently, and then the equations for robot dynamics and contact dynamics from the prescribed object motion. Note that since a rigid contact is elaborated, discontinuities in velocities are possible and the impact phase needs to be considered before switching from the approach phase to the in-contact motion phase.

Thus, the system of differential equations (2.50) enables numerical integration and, consequently, the simulation of the dynamics of the anthropomorphic mechanism that interacts with an external object, if no deformations occur in the contact zone.

#### **2.4.1.2 Soft contact**

Although elastic deformations in the contact zone are usually small and in most cases negligible, they certainly exist. If the required task is to control the contact force, then the importance of precise contact modeling increases significantly.

A simplified approach to the definition of the “soft” contact is to introduce the elasticity of the contacted surfaces in the form of massless springs and dampers. In this way, the micro motion of particles in the contact zone is introduced but their inertia is neglected. In order to demonstrate the algorithms, we introduce elasticity on the object side only, that is, the object surface is considered to be deformable, whereas the robot tip is considered as rigid (see Figure 2.9). For a small deformation, deviations in different directions are regarded as mutually independent. The fact that deformation allows the robot’s hand to move means that the relative coordinates  $\mathbf{s}$  are no longer geometrically constrained during the interaction. While theoretically all free, the strong elastic contact

forces keep some of them small – their coordinates form the restricted vector  $\mathbf{s}^c$ . The deviations of these coordinates from zero represent the deformation; their values are negative since the robot link produces a force  $\mathbf{R}$  that acts on the surface.

$$\mathbf{R} = -\mathbf{K}\mathbf{s}^c - \mathbf{B}\dot{\mathbf{s}}^c \quad (2.51)$$

Then, there are the  $m$ -dimensional (in the case of  $m$  contact reactions) stiffness matrix  $\mathbf{K} = \mathbf{diag}\{k_i\}$  and damping matrix  $\mathbf{B} = \mathbf{diag}\{b_i\}$ , of the same dimension ( $k_i$  and  $b_i$  are the spring and damping coefficients of the contacted object for the relevant axes, which depend on the material of the object). If a contact restricts translation, then the reaction is a force  $[N]$ , and the coefficients are  $k_i$   $[N/m]$  and  $b_i$   $[Ns/m]$ . If a contact restricts rotation, then the reaction is a torque  $[Nm]$  and the coefficients are  $k_i$   $[Nm/rad]$  and  $b_i$   $[Nms/rad]$ .

Certain important differences appear when elastic properties are added to the object. The velocity does not change instantaneously and becomes continuous. This means that unlike a rigid contact, there is no impact phase. The simulation is therefore based on the approach phase, until one of the relative coordinates becomes zero, at which time the simulation model switches from two independent models ((2.41) for robot dynamics and (2.44) for object dynamics) to in-contact motion (2.52). We can model in the same manner any nonlinear effects during contact, instead of a linear spring damper system. Therefore, for in-soft-contact motion the following holds:

$$\begin{aligned} \mathbf{H}(\mathbf{Q}) \ddot{\mathbf{Q}} + \tilde{\mathbf{h}}(\mathbf{Q}, \dot{\mathbf{Q}}, \theta^a, \dot{\theta}^a, \theta^b, \dot{\theta}^b) &= \mathbf{J}^T(\mathbf{Q}, \mathbf{Q}_{obj})\mathbf{R} \\ \bar{\mathbf{H}} \ddot{\boldsymbol{\theta}} + \bar{\mathbf{h}}(\mathbf{Q}, \dot{\mathbf{Q}}, \theta^a, \dot{\theta}^a, \theta^b, \dot{\theta}^b) &= \mathbf{C} \mathbf{u} \\ \mathbf{W}(\mathbf{Q}_{obj}) \ddot{\mathbf{Q}}_{obj} + \mathbf{w}(\mathbf{Q}_{obj}, \dot{\mathbf{Q}}_{obj}) &= \mathbf{T}_{obj} + \mathbf{J}_{obj}^T(\mathbf{Q}, \mathbf{Q}_{obj})\mathbf{R} \\ \ddot{\mathbf{s}}^c &= \mathbf{J}(\mathbf{Q}, \mathbf{Q}_{obj})\ddot{\mathbf{Q}} + \mathbf{J}_{obj}(\mathbf{Q}, \mathbf{Q}_{obj})\ddot{\mathbf{Q}}_{obj} + \mathbf{A}(\mathbf{Q}, \dot{\mathbf{Q}}, \mathbf{Q}_{obj}, \dot{\mathbf{Q}}_{obj}) \\ \mathbf{R} &= -\mathbf{K}\mathbf{s}^c - \mathbf{B}\dot{\mathbf{s}}^c \end{aligned} \quad (2.52)$$

Note that restricted functional coordinates are still calculated using (2.47), but now they are not restricted to zero, whereas the interaction force is calculated according to (2.51). This way, additional  $m$  equations are introduced to enable the evaluation of  $N$  robot coordinates,  $2n$  antagonistic motor coordinates,  $k$  object coordinates, and  $m$  restricted

functional coordinates, in addition to  $m$  interaction forces. In conclusion, the system of differential equations (2.52) enables numerical integration and, consequently, simulation of the anthropomorphic mechanism dynamics during in-contact motion with an external object, if “soft” deformations occur in the contact zone.

### 2.4.1.3 *Elastodynamic contact*

As indicated in the previous subsection, accurate contact modeling is required if the actual task is control of the contact force, as is the case in many robotic applications. To that end, in a more thorough analysis, the inertia of deformation should not be disregarded. A more complex approach—an elastodynamic contact—takes into account the inertial properties of the particles in the contact zone (Figure 2.9). Therefore, deformation is considered as a dynamic process. Let the previous assumptions (small and mutually independent deviations in different directions) still apply. In addition to soft contact analysis, we now model an elastodynamic contact. In light of the previous discussion of soft contact, we introduce several changes. Taking into account the masses of the particles moved by the deformation in the contact zone, Equation (2.51) is modified to include inertial forces; this results in Equation (2.53), which is a single-mass approximation. A serial-masses approximation would allow the calculation of deformation propagation. At this point, nonlinearity can be included in the model as well. As with the stiffness and damping matrices, we can define an inertial lumped matrix with the same dimension of  $m$ :  $M = \text{diag}\{m_i\}$ , where  $m_i$  is in [kg] in the case of translation, and in [kgm<sup>2</sup>] for rotation.

$$\mathbf{R} = -\mathbf{K}\mathbf{s}^c - \mathbf{B}\dot{\mathbf{s}}^c - \mathbf{M}\ddot{\mathbf{s}}^c \quad (2.53)$$

Consequently, model (2.54) enables the simulation of a robot driven by antagonistically-coupled compliant drives in in-elastodynamic-contact motion:

$$\begin{aligned}
\mathbf{H}(\mathbf{Q}) \ddot{\mathbf{Q}} + \tilde{\mathbf{h}}(\mathbf{Q}, \dot{\mathbf{Q}}, \theta^a, \dot{\theta}^a, \theta^b, \dot{\theta}^b) &= \mathbf{J}^T(\mathbf{Q}, \mathbf{Q}_{obj}) \mathbf{R} \\
\bar{\mathbf{H}} \ddot{\boldsymbol{\theta}} + \bar{\mathbf{h}}(\mathbf{Q}, \dot{\mathbf{Q}}, \theta^a, \dot{\theta}^a, \theta^b, \dot{\theta}^b) &= \mathbf{C} \mathbf{u} \\
\mathbf{W}(\mathbf{Q}_{obj}) \ddot{\mathbf{Q}}_{obj} + \mathbf{w}(\mathbf{Q}_{obj}, \dot{\mathbf{Q}}_{obj}) &= \mathbf{T}_{obj} + \mathbf{J}_{obj}^T(\mathbf{Q}, \mathbf{Q}_{obj}) \mathbf{R} \\
\ddot{\mathbf{s}}^c = \mathbf{J}(\mathbf{Q}, \mathbf{Q}_{obj}) \ddot{\mathbf{Q}} + \mathbf{J}_{obj}(\mathbf{Q}, \mathbf{Q}_{obj}) \ddot{\mathbf{Q}}_{obj} + \mathbf{A}(\mathbf{Q}, \dot{\mathbf{Q}}, \mathbf{Q}_{obj}, \dot{\mathbf{Q}}_{obj}) & \\
\mathbf{R} = -\mathbf{K} \mathbf{s}^c - \mathbf{B} \dot{\mathbf{s}}^c - \mathbf{M} \ddot{\mathbf{s}}^c &
\end{aligned} \tag{2.54}$$

With this model of in-elastodynamic-contact motion, discontinuous change in velocity is possible due to inertial mass in the contact zone. Therefore, modeling of the impact phenomenon is unavoidable for a more accurate analysis. Impact modeling is discussed in the following subsection (2.4.2). In summary, for comprehensive treatment of elastodynamic interaction, it is necessary to consider all three phases of the interaction task: approach, impact, and in-contact motion.

## 2.4.2 Models of impact phenomena

Although motion is often planned to achieve zero-velocity contact, that goal is rarely achieved and thus impact occurs. Once again, regarding contact dynamics, any contact can be regarded as consisting of three phases: approach, impact, and contact motion. While in-contact motion of the robot and the contacted object are described by model (2.50), (2.52) or (2.54), depending on the type of elastic deformation in the contact zone, the impact needs additional explanation. If the inertia on the object side cannot be neglected, there will be velocity discontinuities and additional explanation of the contact phenomenon is needed. As stated in the previous subsection (2.4.1), treatment of the impact is required for both rigid and elastodynamic deformations in the contact zone and, therefore, the analysis in Subsections 2.4.1.1 and 2.4.1.3 needs to be supplemented. To trade-off between accuracy and complex analysis, we restrict the impact consideration to a non-elastic problem.

We first elaborated modeling of impact with a rigid object as a complement to in-rigid-contact motion. The present formulation assumes that an infinitely short impact occurs: two rigid bodies establish contact, transient effects disappear in an infinitely short time, and then contact motion lasts for some finite period of time. Such an impact results in

infinitely high reaction forces  $\mathbf{R}$  but due to the infinitely short impact time  $\Delta t$ , the impact momentum  $\mathbf{R}\Delta t$  is not infinite. The momentum and the resulting changes in the system velocities can then be calculated from the impact model. Since drive velocities are not affected by the impact phenomenon, due to deformable transmission between a robot joint and its antagonistic drives, the drive velocities remain unchanged. The impact model is generated by integrating the in-contact motion model (2.50) over the impact period  $\Delta t = (t', t'') \rightarrow 0$ . Integration yields:

$$\begin{aligned}
\mathbf{H}(\mathbf{Q})\Delta\dot{\mathbf{Q}} &= \mathbf{J}^T(\mathbf{Q}, \mathbf{Q}_{\text{obj}})\mathbf{R}\Delta t \\
\bar{\mathbf{H}}\Delta\dot{\boldsymbol{\theta}} &= \mathbf{0} \\
\mathbf{W}(\mathbf{Q}_{\text{obj}})\Delta\dot{\mathbf{Q}}_{\text{obj}} &= \mathbf{J}_{\text{obj}}^T(\mathbf{Q}, \mathbf{Q}_{\text{obj}})\mathbf{R}\Delta t \\
\mathbf{J}(\mathbf{Q}, \mathbf{Q}_{\text{obj}})\Delta\dot{\mathbf{Q}} + \mathbf{J}_{\text{obj}}(\mathbf{Q}, \mathbf{Q}_{\text{obj}})\Delta\dot{\mathbf{Q}}_{\text{obj}} &= \Delta\dot{\mathbf{s}}^c = \\
-\dot{\mathbf{s}}^c(t') &= -\mathbf{J}(\mathbf{Q}, \mathbf{Q}_{\text{obj}})\dot{\mathbf{Q}}' - \mathbf{J}_{\text{obj}}(\mathbf{Q}, \mathbf{Q}_{\text{obj}})\dot{\mathbf{Q}}_{\text{obj}}'
\end{aligned} \tag{2.55}$$

Note that the matrices  $\mathbf{H}$ ,  $\mathbf{J}$ ,  $\mathbf{J}_{\text{obj}}$ , and  $\mathbf{W}$  are calculated for the instant before impact ( $t = t'$ ), since the positions do not change in this infinitely short period  $\mathbf{Q}(t') = \mathbf{Q}(t'')$ , and  $\mathbf{Q}_{\text{obj}}(t') = \mathbf{Q}_{\text{obj}}(t'')$ . The impact model can then be solved for the change in velocities  $\Delta\dot{\mathbf{Q}}$ ,  $\Delta\dot{\mathbf{Q}}_{\text{obj}}$ ,  $\Delta\dot{\boldsymbol{\theta}}$  and the impact momentum  $\mathbf{R}\Delta t$ . Constraint (2.46) is used here, since immediately after impact for in-rigid-motion  $\dot{\mathbf{s}}^c(t'') = \mathbf{0}$ , so  $\Delta\dot{\mathbf{s}}^c = \dot{\mathbf{s}}^c(t'') - \dot{\mathbf{s}}^c(t') = -\dot{\mathbf{s}}^c(t')$  holds. The impact phase is infinitely short and therefore the velocities will change instantaneously, but the positions will not change. These new velocities, along with joint and motor positions, are the initial conditions for the next phase –in-rigid-contact motion. Finally, after the approach phase (any functional coordinate has reached zero), the impact model (2.55) should be resolved and then in-rigid-contact-motion considered according to (2.50).

An analogous procedure is followed for impact analysis, if the contact zone is characterized as deformable, with inertial mass (if an elastodynamic contact occurs). However, the impact refers only to particles in the contact zone. The impact is considered as infinitely short and non-elastic, and therefore the impact model is obtained by integrating the contact model (2.54) over the impact period  $\Delta t = (t', t'') \rightarrow 0$ .

$$\begin{aligned}
\mathbf{H}(\mathbf{Q})\Delta\dot{\mathbf{Q}} &= \mathbf{J}^T(\mathbf{Q}, \mathbf{Q}_{\text{obj}})\mathbf{R}\Delta t \\
\bar{\bar{\mathbf{H}}}\Delta\dot{\boldsymbol{\theta}} &= \mathbf{0} \\
\mathbf{W}(\mathbf{Q}_{\text{obj}})\Delta\dot{\mathbf{Q}}_{\text{obj}} &= \mathbf{J}_{\text{obj}}^T(\mathbf{Q}, \mathbf{Q}_{\text{obj}})\mathbf{R}\Delta t \\
\mathbf{J}(\mathbf{Q}, \mathbf{Q}_{\text{obj}})\Delta\dot{\mathbf{Q}} + \mathbf{J}_{\text{obj}}(\mathbf{Q}, \mathbf{Q}_{\text{obj}})\Delta\dot{\mathbf{Q}}_{\text{obj}} &= \Delta\dot{\mathbf{s}}^c \\
\mathbf{R}\Delta t &= -\mathbf{M}\Delta\dot{\mathbf{s}}^c
\end{aligned} \tag{2.56}$$

Contrary to the case with rigid contacts, immediately thereafter the impact relation  $\dot{\mathbf{s}}^c(t'') = \mathbf{0}$  does not hold any more. Therefore, relation  $\mathbf{R}\Delta t = -\mathbf{M}\Delta\dot{\mathbf{s}}^c$  is introduced directly by integrating (2.53) over this infinitely short time interval  $\Delta t$ . Equivalent to the previous paragraph in the case of rigid bodies, the impact model (2.56) should be considered when the approach phase ends. The new robot and object velocities obtained in this manner, along with the joint and motor positions that remain unchanged during the infinitely short impact, are the initial conditions for the next phase in-elastodynamic-contact motion (2.54).

## 2.5 Verification of developed analytical models through simulations

This subsection presents the results of simulation using models of the anthropomorphic robot approximation elaborated in Section 2 of the thesis. The structure of one of the first anthropomorphic robots, Eccerobot, is depicted in detail in Subsection 2.2, and its approximation that represents typical human-like actuation systems (antagonistic joints) is discussed in Subsection 2.3. Simulation of the robot interacting with its surroundings is described here to verify the models from Subsection 2.4, as a key feature for future application of the modeling approach proposed in this thesis. Therefore, two case studies are presented in detail. In both cases, the anthropomorphic robot model is controlled by the theory presented in Section 3 of this thesis. Since the control algorithm is discussed in the following section, it will not be elaborated in the examples illustrated in this subsection. Thus, emphasis is placed on the analytical model of robot dynamics.

### 2.5.1 Case study 1: Analysis of robot's dynamic balance in non-contact and contact tasks

The first case study considers the dynamic balance of the anthropomorphic robot's upper-body on a mobile base. More precisely, it elaborates the critical balance analysis of a mobile anthropomorphic robot exposed to external disturbances, which emulate the robot working in a real environment. The following analysis summarizes the results of the present research published in [107], [2].

The zero moment point (ZMP) approach [147], [148] is used to provide critical design criteria for the mobile base. In the analysis, the ZMP point is observed for different robot tasks and a conclusion is drawn about the required shape and size of the mobile base, to ensure that the ZMP stable region is inside the boundaries of the mobile base. Due to intensive movement of the mobile base, the robot's waist joint is the most affected and critical, from the standpoint of control and dynamic balance [149]. It also has a crucial effect on the resulting inertial force and ZMP position. The performance of the waist joint is highlighted to demonstrate satisfactory and stable behavior of the robot's torso.

With regard to the current configuration of the mobile wheeled base, [107] shows that the effects of robot behavior on the mobile base are negligible, so that control of the base may be synthesized independently. Thus, the mobile base can perform any assigned motion with insignificant influence of the robot, and any disturbances coming from the robot's movement can be easily overcome. On the other hand, base motion strongly influences the behavior of the robot. The assumption about base decoupling allows us to explore the robot's motion, considering the base motion as prescribed. From a theoretical point of view, this assumption advocates the use of a set of differential equation labeled by (2.50). Here the object dynamics are solved independently from the rest of the system. As such, the robot dynamics can be solved assuming that a rigid contact with the mobile base is established, considering the case where all functional coordinates are restricted  $\mathbf{s}^c = \mathbf{s}$ .

The mobile base is supposed to ensure universal motion of the robot in some environment (coming to a place where some work is to be done, maneuvering among objects, etc.). Since base motion has a considerable impact on the robot's behavior, it is necessary to examine the influence. The first group of experiments is intended to explore the influence of base motion on the robot's behavior and the design of the system, including base dimensions. The group consists of the most intensive base movements that the robot control system (particularly in the waist) can withstand. So, we choose the following base motions to demonstrate the key effects in a realistic scenario. First the examples try to isolate different effects and later simulation experiments comprise a combination of several effects:

- The base starts to move in the longitudinal direction, forward or back, applying constant acceleration. Such motion is present in the majority of everyday tasks.
- The base performs a forward-backward oscillation in the longitudinal direction. This motion emulates the inertial effects of non-uniform motion.
- Motion in the lateral direction with constant acceleration. This example emulates the effect of the centrifugal force.
- Oscillation in the lateral direction, which emulates the inertial effects of driving along a winding road.
- Yaw angle oscillation, which represents a twisting motion and reveals the influence of a change in base direction.
- Gyration (circular motion), which combines some of the previously mentioned basic motions and emulates the effects of turning.
- Pitch and roll angle changes, which occur when the robot moves over bumpy or winding terrain.

The second group of experiments explores the interaction of the robot with the environment and its ability to maintain balance while operating and completing assigned contact tasks. This group generalizes the previous experiments – in addition to base motion, external forces are imposed. Two types of forces are considered: impact impulse forces and long-term forces. External forces act horizontally, but from different directions (longitudinal and lateral). These two types cover the majority of real

situations, irrespective of whether the forces are expected as part of a task or occur accidentally. Regardless, from a robot balance perspective, external forces are seen as a disturbance. Again, the waist joint is the most affected and, hence, in our experiments external forces will be imposed on the torso segment. Examples of planned actions, which involve an external force, include pushing a supermarket cart (long-term force) and hitting a ball in sports (impact force). Accidental external forces can occur when the robot moves through a crowd of people or in an unstructured environment.

A compromise is needed to ensure safe and effective robot behavior. The size and shape of the mobile base should be as small as possible, to facilitate robot maneuverability, but, on the other hand, the mobile base should be big enough to cover the ZMP stability region in all possible cases. Therefore, the compromise requires a detailed simulation analysis. The prototype of the anthropomorphic robot on a three-wheel base and its schematic representation as a target of external influence are depicted in Figure 2.10.

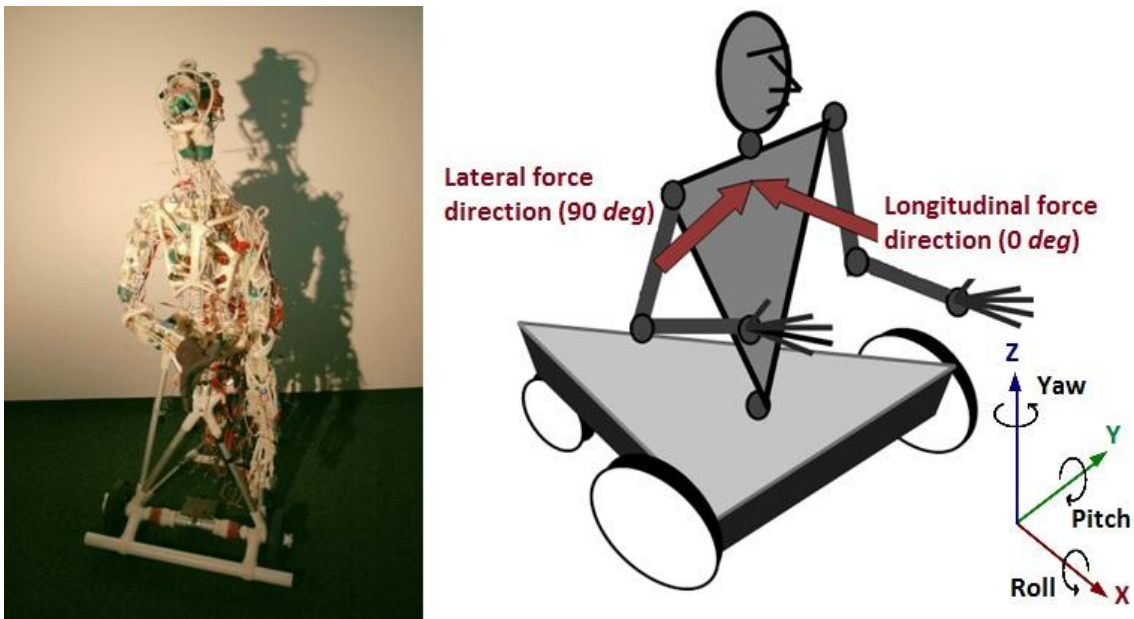


Figure 2.10. Eccerobot prototype standing on a three-wheel base as a moving base (left); Schematic representation of the model exposed to external disturbances, emulating the robot working in a real environment (right).

The main parameters for the simulation of robot dynamics are given in Table 2.1. Kinematic and dynamic parameters of each particular link are adopted following a basic

muscle-length link distribution in accordance with the work of Gravez et al. reported in [150], for a musculoskeletal mechanism of known height and weight. Their research was carried out within the framework of digital modeling of humanoid robots for which the inertial and geometrical properties are close to those of a human, based on only two input parameters – mass and height. However, since they do not consider the inertial distribution (positions of the centers of mass, moments and products of inertia of each link), in this thesis the parameters are slightly modified, as shown in Table 2.1. The robot's upper-body is assumed to be about 80cm high and to weigh 50kg.

*Table 2.1. Main parameters of robot dynamics, necessary for simulation-aimed models from Subsections 2.3 and 2.4. Since each kinematic chain approximates a multi-axes joint by a series of single-axis antagonistic joints, imaginary segments of negligible dynamic properties are added to match the exact number of DoFs per joint. Link numbers match the notations in Figure 2.6.*

Link/Property	$m$ (kg)	$J_x$ (kgm <sup>2</sup> )	$J_y$ (kgm <sup>2</sup> )	$J_z$ (kgm <sup>2</sup> )
1 - Pelvis	11.96	0.06900	0.06565	0.12800
2 and 3 (imaginary)	≈ 0	≈ 0	≈ 0	≈ 0
4 - Trunk	26.60	0.13060	0.11810	0.02440
5 and 6 (imaginary)	≈ 0	≈ 0	≈ 0	≈ 0
7 - Head	4.25	0.01700	0.01700	0.01700
8 and 9 (imaginary)	≈ 0	≈ 0	≈ 0	≈ 0
10 – Right upper arm	2.07	0.00200	0.00200	0.00022
11 (imaginary)	≈ 0	≈ 0	≈ 0	≈ 0
12 - Right forearm	1.14	0.00250	0.00425	0.00014
13 (imaginary)	≈ 0	≈ 0	≈ 0	≈ 0
14 - Right hand	0.35	0.00050	0.00100	0.00003
15 and 16 (imaginary)	≈ 0	≈ 0	≈ 0	≈ 0
17 – Left upper arm	2.07	0.00200	0.00200	0.00022
18 (imaginary)	≈ 0	≈ 0	≈ 0	≈ 0
19 – Left forearm	1.14	0.00250	0.00425	0.00014
20 (imaginary)	≈ 0	≈ 0	≈ 0	≈ 0
21 – Left hand	0.35	0.00050	0.00100	0.00003

The drive dynamics parameters that fit Equations (2.1) through (2.5) are summarized in Table 2.2. The motor and gearbox parameters are extracted from the Maxon Motor catalog [151] and they match the existing drives mounted on the presented prototype of Eccerobot. Waist joints include a 148877 DC motor RE40 48V and 203116 Gearbox GP42C 15:1 (set 1), shoulder joints use a 268193 DC motor RE30 12V and 326664 Gearbox GP32HP 51:1 (set 2), whereas small joints, such as neck, elbow, and wrist joints, use a 118637 DC motor RE13 12v and 110315 Gearbox GP13A 67:1 (set 3). The elastic element of linear characteristics is assumed to have a stiffness coefficient of  $k = 4000 \text{ N/m}$ .

*Table 2.2. Drive parameters used for simulations in Section 2. Waist joints include a 148877 DC motor RE40 48V and 203116 Gearbox GP42C 15:1 (set 1), shoulder joints use a 268193 DC motor RE30 12V and 326664 Gearbox GP32HP 51:1 (set 2), and small joints, such as neck, elbow, and wrist joints, use a 118637 DC motor RE13 12v and 110315 Gearbox GP13A 67:1 (set 3). All product codes match Maxon Motor catalog.*

Label	Set 1	Set 2	Set 3
$I^{rot} [\text{kg} \cdot \text{m}^2]$	$137 \cdot 10^{-7}$	$33.7 \cdot 10^{-7}$	$0.545 \cdot 10^{-7}$
$C^M [\text{Nm/A}]$	$60.3 \cdot 10^{-3}$	$13.9 \cdot 10^{-3}$	$8.27 \cdot 10^{-3}$
$B [\text{Nm} \cdot \text{s/rad}]$	$3216 \cdot 10^{-6}$	$936 \cdot 10^{-6}$	$7.13 \cdot 10^{-6}$
$R [\Omega]$	1.13	0.2	9.56
$C^E [\text{V} \cdot \text{s/rad}]$	$60.3 \cdot 10^{-3}$	$13.9 \cdot 10^{-3}$	$8.27 \cdot 10^{-3}$
$N [-]$	15	51	67
$\mu [-]$	0.81	0.7	0.75
$r [\text{m}]$	$42 \cdot 10^{-3}$	$32 \cdot 10^{-3}$	$13 \cdot 10^{-3}$

Table 2.3 summarizes the movements applied to the mobile base: forward-backward motion with constant acceleration/deceleration (15% of the movement time), forward-backward oscillations, motion in the lateral direction (both oscillating and with constant acceleration/deceleration), gyration, and travel over bumpy or winding terrain (changes in pitch, roll, and yaw angles). For each of the applied movements, the  $x$  and  $y$  ZMP coordinates are observed to set boundaries of the mobile base design that ensures dynamic balance of the robot. Namely, all possible ZMP positions need to lie within a

stable polygon or, in other words, they must be within the boundaries set by a triangle formed by the wheels in its vertices (in the case of a three-wheel mobile base). Critical cases for maintaining robot balance include moving over a bumpy road (changes in pitch angle) and moving around a circle, when centrifugal forces come into play.

*Table 2.3. Typical movements of the robot's mobile base and their influence on ZMP coordinates. Maximal ZMP deviations set boundaries for critical design of mobile base, which ensures dynamic balance of the robot.*

<b>Motion</b>	<b>Distance [m]</b>	<b>Time [s]</b>	<b> x<sub>zmp</sub>  [cm]</b>	<b> y<sub>zmp</sub>  [cm]</b>
<b>Longitudinal trapezoidal</b>	2	2.2	5.6	0.9
<b>Lateral trapezoidal</b>	2	2.3	2.5	2.2
	<b>Amplitude [m]</b>			
<b>Forward-backward</b>	1	2.5	2.8	1.4
	2	3.2	3.4	1.1
<b>Right-left</b>	1	2.6	2.5	1.5
	2	3.2	2.5	1.8
	<b>Radius [m]</b>			
<b>Gyration</b>	1	3.5	10.6	4
	<b>Amplitude [deg]</b>			
<b>Roll</b>	10	1.4	2.5	5.8
	20	2.2	2.5	9.3
<b>Pitch</b>	10	1.2	10.5	0.4
	20	2	15.3	0.8
<b>Yaw</b>	45	0.9	2.5	2
	60	1	2.5	2.2

Table 2.4 and Table 2.5 present maximal deviations of ZMP coordinates when long-term external forces and impulse forces that act from different directions disturb the robot's upright position. Maximal ZMP deviations set the boundaries for the critical design of the mobile base, which ensures the robot's dynamic balance. Applied forces emulate the robot acting in a real environment, when the forces mimic both planned interaction and unexpected external disturbances during the execution of common tasks. Similar to a human, the robot can handle more easily a disturbance coming from the front line

(angles  $0 \div \pi/4$ ), than forces applied from the back (angles  $3\pi/4 \div \pi$ ). This fact is attributable to hand activities compensating for a violation of the robot's dynamic balance.

*Table 2.4. Influence of long-term external forces acting on the robot's torso on deviations of ZMP coordinates. Maximal ZMP deviations set the boundaries for the critical design of the mobile base, which ensures the robot's dynamic balance, while applied forces emulate the robot acting in a real environment.*

Direction [deg]	$F_{\max}$ [N]	$x_{zmp}$ [cm]		$y_{zmp}$ [cm]	
		min	max		
$0$	150	-16	2.5	-1.7	1.3
$\pi/8$	160	-12	2.5	-1.3	1.3
$\pi/4$	180	-2	2.5	-4	8
$3\pi/8$	140	1.6	2.5	-4.8	9.5
$\pi/2$	140	2.1	2.5	-1.7	5.7
$5\pi/8$	130	2.1	2.8	-1.7	5.7
$3\pi/4$	220	2	18.4	-3.2	10.5
$7\pi/8$	140	2.5	21.9	-1.2	0.6
$\pi$	130	2.5	22.5	-0.8	1

*Table 2.5. Influence of long-term external forces acting on the robot's torso on deviations of ZMP coordinates. Maximal ZMP deviations set the boundaries for the critical design of the mobile base, which ensures the robot's dynamic balance, while applied forces emulate the robot acting in a real environment.*

Direction [deg]	$F_{\max}$ [N]	$x_{zmp}$ [cm]		$y_{zmp}$ [cm]	
		min	max	min	max
$0$	2700	-15	2.5	-1.5	0.4
$\pi/8$	3100	-21	2.5	0	2.8
$\pi/4$	2500	-2.8	2.5	-15.6	6.5
$3\pi/8$	1600	1.5	2.5	-5.3	4.5
$\pi/2$	1600	1.8	2.6	-6.6	8.9
$5\pi/8$	1800	1.6	3.9	-7.2	8
$3\pi/4$	2500	1.6	9.1	-8	9.6
$7\pi/8$	2800	2.5	24	-0.2	2.4
$\pi$	2500	2.5	21.8	-1.1	1

In order to make the acquired data more picturesque, following are several figures that demonstrate the influence of external forces on the ZMP position, as a decisive factor in the evaluation of the robot's balance.

Figure 2.11 depicts a change in the robot's ZMP position, while an external force acts on the robot. The left part of the figure illustrates a short-term impulse force of 1500N of  $\Delta t = 0.01s$  duration, acting on the robot's torso from four different directions: strictly laterally from the robot's right side (90 deg), 45 deg from the right, strictly frontally (0 deg), and 45 deg from the robot's left. The right-hand part of the figure shows the influence of a long-term external force on the robot's balance, described by its ZMP position. Three different force levels (magnitudes of 120N, 160N, and 200N) act in the same direction – 135 deg from the right, as shown in the figure. The robot compensates for the disturbance after some time, but the ZMP deviation is significant during the transient phase.

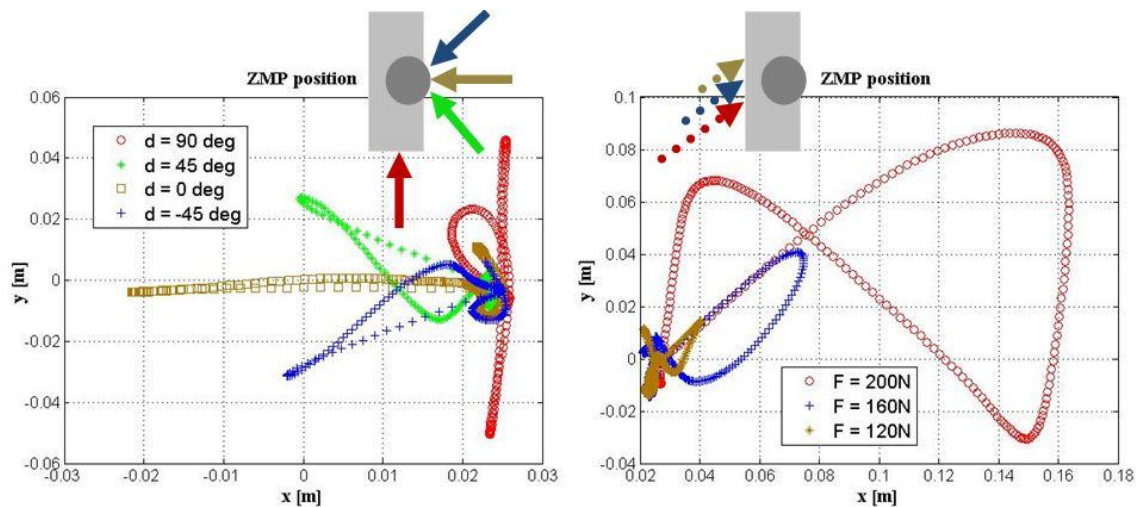


Figure 2.11. Robot's ZMP position while external forces act on the robot. Different force directions are displayed in different colors, as well as ZMP positions corresponding to the force of the same color: ZMP position while a short-term impulse force of 1500N and  $\Delta t = 0.01s$  duration acts on the robot's torso from four different directions: strictly laterally from the robot's right side (90 deg) – red, 45 deg from the right – green, strictly frontally (0 deg) – brown, and 45 deg from the robot's left – blue (left); ZMP position while a long-term external force violates the robot's balance. Three different force levels (magnitudes of 120N – brown, 160N – blue, and 200N – red) act in the same direction – 135 deg from the right (right).

Figure 2.12 presents the waist joint position, as a joint which is primarily affected by forces that act on the robot's torso. Movements along all rotational axes are displayed for both an impulse force and a long-term force. According to the direction of the external force (colors match force directions and magnitudes depicted in Figure 2.11), a different waist axis is affected and requires an extra effort to compensate for the deviation from the initial upright stance.

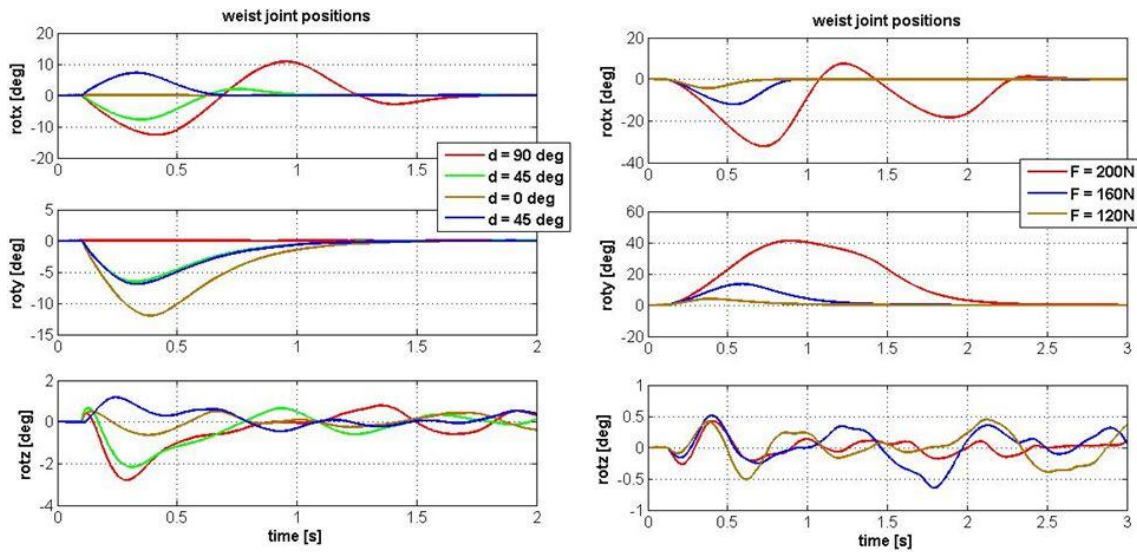


Figure 2.12. Position of the waist joint, primarily affected by forces that act on the robot's torso: Waist joint positions along all rotational axes, while compensating for a short-term impulse force of 1500N and  $\Delta t = 0.01s$  duration. Four different directions are tested: strictly laterally from the robot's right side (90 deg) – red, 45 deg from the right – green, strictly frontally (0 deg) – brown, and 45 deg from the robot's left – blue (left); Waist joint axes while the robot compensates for long-term external force disturbances that violate the robot's balance. Three different force levels (magnitudes of 120N – brown, 160N – blue, and 200N – red) act in the same direction – 135 deg from the right (right).

The target configuration of the Eccerobot base contains three wheels (a differential drive and supporting wheel), which form an equilateral triangle. The wheels create a triangle of dynamic balance, according to the ZMP theory. Although this stable region is sufficient to prevent the robot and base from overturning, we introduce a more restricted safety area  $S$  – a circle inscribed in the triangle. Let its radius be  $r$ . Using this safety region, we prevent situations in which the ZMP point goes to the corners of the triangle, where the stability region becomes narrow and where balance could be easily

compromised due to unpredictable external disturbances. There is another advantage of using a circle as a safety region. It does not restrict the applicability of the results to some particular base shape. The results support a triangular shape (three wheels), square shape (four wheels), etc. Therefore, this approach facilitates the redesign of the mobile wheel-base, keeping in mind the inscribed circle as the safety region. Quite similar approaches are proposed in [152] and [153]. For the described convention, the following stands:

$$S: x_{zmp}^2 + y_{zmp}^2 \leq r^2 \quad (2.57)$$

where  $x_{zmp}$ ,  $y_{zmp}$  denote the  $x$  and  $y$  coordinates of ZMP,  $S$  represents the safety region and  $r$  is its radius. If the ZMP point goes out of the region, then the robot starts to overturn. To arrive at a final decision about the minimum radius  $r_{min}$  of the safety region  $S$ , we use the maximum values of the  $x$  and  $y$  coordinates of ZMP, in all the tested situations:  $r_{min}^2 = x_{zmp-max}^2 + y_{zmp-max}^2$ . It should be noted that  $x_{zmp-max}$  and  $y_{zmp-max}$  are maximal absolute values of the  $x$  and  $y$  coordinates. This is due to the need to cover not just separate experiments, but all their combinations as well.

When the simulation results of this case study are analyzed, it becomes apparent that the most critical situation (the largest required range of ZMP changes) occurs when the robot is affected by an external impulse force. Also, robot motion in the longitudinal direction and oscillation of the pitch angle cause  $x_{zmp}$  to reach high values. Analogously,  $y_{zmp}$  reaches its maximum while the robot moves in the lateral direction or robot motion comprises the oscillations in roll angle. A comprehensive analysis of the results yields the maximal absolute values of the ZMP coordinates:  $x_{zmp-max} \approx 24\text{cm}$ ,  $y_{zmp-max} \approx 16\text{cm}$ . Therefore, according to (2.57), the minimum radius of the safe region is  $r_{min} \approx 28.5\text{cm}$ . This means that the Eccerobot mobile base needs to be designed so that a circle with a radius  $r \approx 28.5\text{cm}$  can be inscribed, ensuring balance of the robot in typical situations. The idea of having a triangular wheel base requires an equilateral triangle whose sides are  $a = 2\sqrt{3}r \approx 1\text{m}$ . Alternatively, in the case of a square design, the sides need to be  $a = 2r \approx 57\text{cm}$ , to ensure safe robot behavior. However, the final design of the robot base addresses these restrictions, as well as the

desired maneuverability and ultimate purpose of the robot.

The above case study demonstrated how the analytical models developed in this section of the thesis can be used for the critical design of a robot's mobile base. This approach was followed in the robot Cassius (see Figure 2.13), designed by Morena Engineering Company managed by Mr. Nikola Petrovic. Cassius was developed as one of the first robots that assist tennis players [1]. Since the robot needs to be quick and minimize the time required to roll a clay tennis court, its mobile base has to be optimally designed to ensure dynamic balance, but to also maintain a minimalistic design for the functionalities. So far, Cassius is capable of rolling clay courts efficiently, but a future objective is for it to collect tennis balls and throw them to tennis players. Thus, the introduction of any new interaction tasks would require a redesign of the robot's shape, as well as of its mobile base, which should ensure dynamic balance of the entire system in interaction tasks.



*Figure 2.13. Robot Cassius – one of the first robots that assists tennis players. It has been developed by Morena Engineering and is capable of rolling clay tennis courts between games. The dynamic balance of the robot needs to be thoroughly analyzed and its mobile base shaped to cover every possible, added, highly inertial interaction task, such as throwing tennis balls.*

### 2.5.2 Case study 2: Analysis of grasping an object in the vertical plane, demonstrating the phases of contact: approach, impact, and in-contact motion

The following paragraphs illustrate the simulation of a typical contact task in a robotic application. A robot arm moves towards an object, grasps it, and carries it to another location. In such a task, all contact phases have to be considered: approach (while the robot and object move as two decoupled dynamic systems, functional coordinates are observed); impact (infinitely short phase, when any functional coordinate reaches zero, so a contact occurs and the impulse momentum is exchanged between the robot and the object); and in-contact-motion (the robot and the object are considered as coupled dynamic systems and interaction forces affect the movement of both bodies).

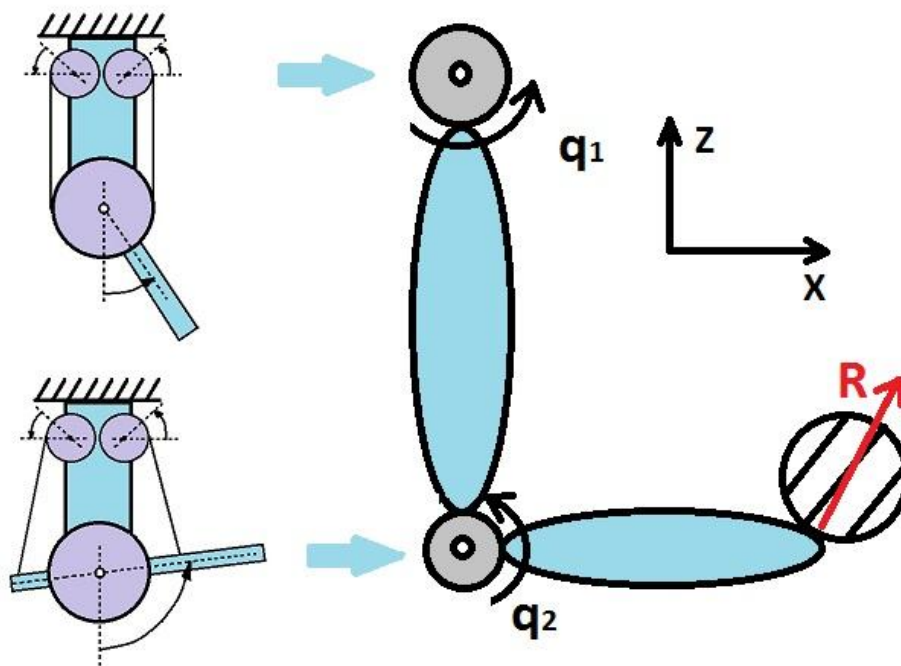


Figure 2.14. Two-DoF robot arm model in an interaction task. The shoulder is driven by a circular joint model of antagonistically-coupled compliant drives, whereas the elbow is fitted by a triangular antagonistic non-linear joint structure with changeable moment arms.

A two-DoF robot model driven by antagonistically-coupled compliant drives is used for demonstration purposes. In order to match the anthropomorphic structure, the shoulder joint is modeled after the classical antagonistic design of a circular joint model

(elaborated in Subsection 2.3.1.1), whereas a triangular joint model (Subsection 2.3.1.2) is adopted to more closely resemble a human elbow joint (see Figure 2.14). The parameters of the anthropomorphic robot structure and drive parameters are given in Table 2.6 and Table 2.7, respectively.

Table 2.6. Robot parameters used for simulations in the grasp experiment.

label	numerical value	units	description
$l_u$	0.3	[m]	Upper arm length
$m_u$	1.9	[kg]	Upper arm mass
$I_y$	0.057	[kg · m <sup>2</sup> ]	Upper arm inertia - shoulder y axis
$l_f$	0.32	[m]	Forearm length
$m_f$	1.6	[kg]	Forearm mass
$I_f$	0.036	[kg · m <sup>2</sup> ]	Forearm inertia - elbow y axis
$m_{obj}$	0.23	[kg]	Object mass

Table 2.7. Drive parameters used for simulations in the grasp experiment.

label	numerical value	units	description
$l_{a1}$	0.3	[m]	Triangular joint parameters
$l_{b1}$	0.3	[m]	
$l_{a2}$	0.1	[m]	
$l_{b2}$	0.07	[m]	
$k$	4000	[N/m]	
$l_r$	0.04	[m]	Circular joint parameters
$\alpha$	$\pi/4$	[m]	
$k$	2000	[N/m]	
$I^{rot}$	$33.5 \cdot 10^{-7}$	[kg · m <sup>2</sup> ]	Drive parameters
$C^M$	$13.9 \cdot 10^{-3}$	[Nm/A]	
$B$	$1.31 \cdot 10^{-5}$	[Nm · s/rad]	
$R$	0.198	[Ω]	
$C^E$	$13.9 \cdot 10^{-3}$	[V · s/rad]	
$N$	51	[–]	
$\mu$	1	[–]	
$r$	$5 \cdot 10^{-3}$	[m]	

The figures below show the results of simulations. While the robot arm rises, it catches a stationary object. Interaction is considered rigid (i.e. there is no elastic deformation). In the approach phase, the robot and the object are considered as two independent dynamic systems and, therefore, simulated according to (2.48) and (2.49), respectively. At the same time, the functional coordinates (Cartesian coordinates of the robot w.r.t. the object) are monitored and when one reaches zero, this initial phase ends. In this simulation task, a contact is indicated when both the horizontal coordinate  $x$  and vertical coordinate  $z$  become zero. This occurs at about  $t \approx 1s$ . The time change of the horizontal and vertical functional coordinates (as the difference between the robot's and the object's Cartesian positions) is shown in Figure 2.15. At the time of contact, the simulation switches to the analytical model of a rigid impact (2.55). Here, the momentum conservation law is applied and sudden jumps in velocity are possible. This effect is apparent in Figure 2.16 where a discontinuity in elbow velocity is especially prominent, since the contact is achieved with the succeeding link – forearm. However, due to dynamic coupling between the joints, the shoulder velocity also exhibits a sudden jump but it is less manifested. After the infinitely short impact phase, new initial conditions (updated system states representing joint velocities) are set and the final phase of the contact analysis occurs – in-contact motion. Consequently, in the case of a rigid contact, analytical model (2.50) takes effect and both the robot and the object comply with it. The robot and the object are two dynamics systems that interact with each other via the interaction forces depicted in Figure 2.15, while the functional coordinates are restricted to zero. Without considering the applied control (elaborated in Section 3 in details), we demonstrate the behavior of antagonistically-coupled drives that move the joints. Figure 2.16 shows motor positions; one can see that motor A (here acting as an agonist) winds up its tendon more, to provide sufficient agonist tendon force and, consequently, overall joint torque, to compensate for the gravity load but also the additional load introduced by the object.

In Figure 2.16 also note that joint positions are scaled by  $-90 \text{ deg}$  to enhance readability of the figures. The fully vertically extended arm fits the zero reference position  $[q_1 \ q_2]^T = [0 \ 0]^T$ . The resulting tendon forces are shown in Figure 2.17, along with the overall joint torques in the shoulder and elbow. The difference between

circular and triangular model configurations is apparent in Figure 2.17. Namely, the linear joint structure of the circular joint model provides a linear dependence of the shoulder torque on the difference between its agonistic and antagonistic tendon forces (2.12), whereas in the case of a triangular model with changeable moment arms there is a non-linear dependence (in accordance with (2.21)). In summary, the grasp analysis is considered through three phases of a contact task:

- approach phase (A) – analytical model (2.48) stands for robot dynamics, (2.49) stands for object dynamics, and the functional coordinates are calculated according to (2.47);
- impact phase (I) – model (2.55) is considered;
- in-contact-motion phase (C) – model (2.50) is considered.

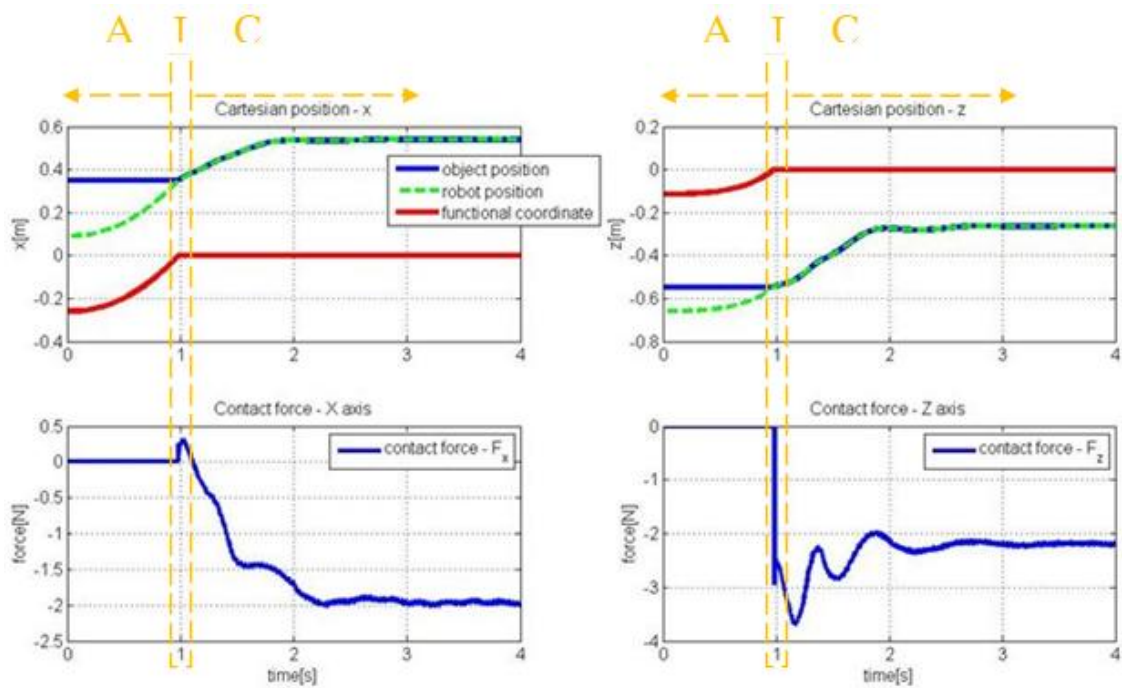


Figure 2.15. Time histories of the robot's and object's Cartesian positions (and their relative position – functional coordinates) during the grasp interaction task and the resulting interaction forces. Functional coordinates between the robot and the contacted object. When any of the functional coordinates reaches zero, the approach phase (A) ends and impact (I) occurs (top); When a contact occurs, there is an interaction force between the robot and the object, which influences both robot and object dynamics in in-contact motion (C) - (bottom).

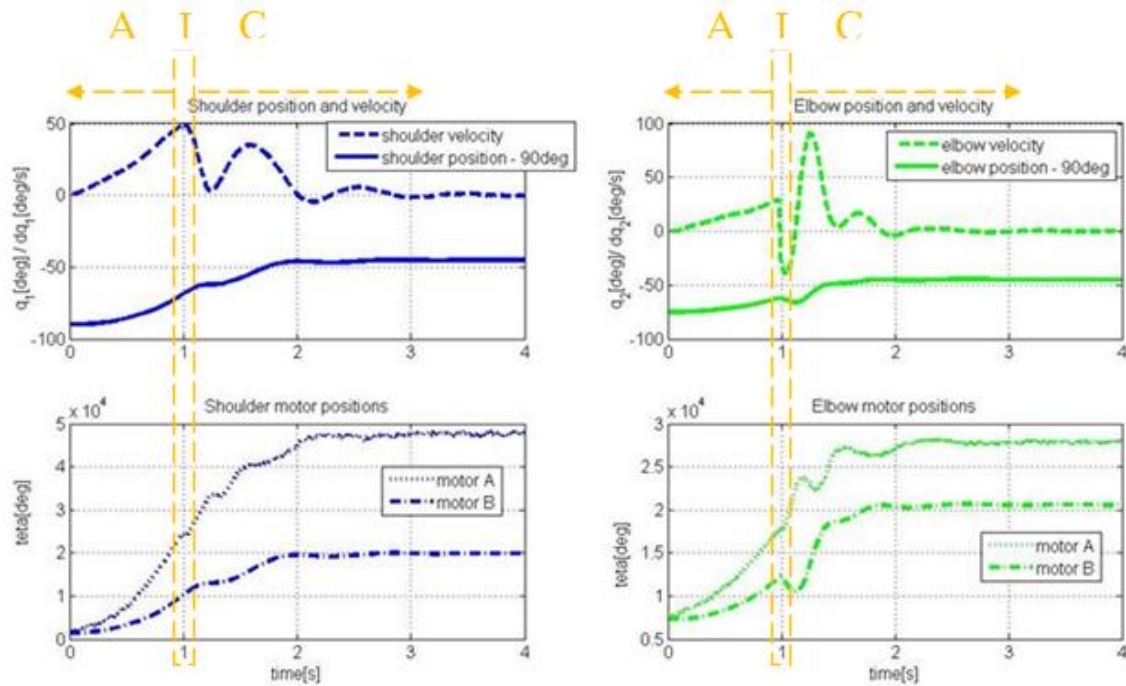


Figure 2.16. Shoulder and elbow velocities and corresponding positions during lifting of the arm in Cartesian space. When an impact occurs with the object (I), there are discontinuities in joint velocity due to the momentum conservation principle. Since the contact is achieved with the forearm tip, as the next link of the elbow joint, this effect is more pronounced than in the shoulder joint, where it occurs due to dynamic coupling between the joints (top); The antagonistically-coupled drives in the joints simultaneously contribute to the overall joint torque and stiffness. When the arm lifts, motor A (here acting as agonist) winds up tendons more, to provide enough agonist force to overcome gravity load (bottom).

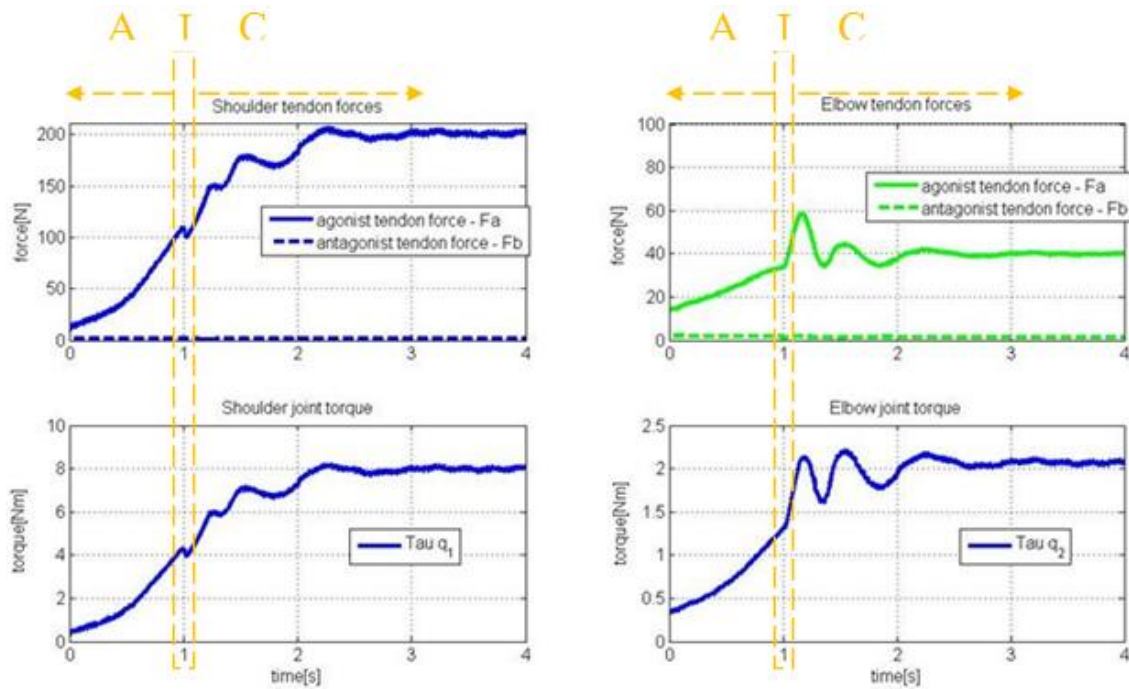


Figure 2.17. Resulting agonist and antagonist tendon forces of a grasp contact task in the vertical plane (relative ratios of agonist to antagonist tendons are the result of the puller-follower control method elaborated in Section 3) - (top); Overall shoulder and elbow joint torques, as a consequence of the difference between the agonistic and the antagonistic tendon activity, while grasping in the vertical plane. The linear joint structure of the circular joint model provides a linear dependence of shoulder torque on the difference between its agonistic and antagonistic tendon forces, whereas in the case of a triangular model with changeable moment arms applied to elbow joint modeling, there is a non-linear dependence (bottom).

## 2.6 Conclusion

An exact simulation tool for a robot driven by antagonistically-coupled compliant drives, which interacts with objects and the environment, was presented in this section. The inspiration for the research came from the anthropomorphic robot Eccerobot, which was built with a mechanical structure that closely resembles a human torso. The ultimate goal is to achieve human-like movement and maneuverability. The problems raised by this type of robot were a motivation to develop an exact computer-based model for efficient computing of the dynamics of anthropomorphic robots in contact tasks. A sound basis for further research in the fields of control and robot interaction

was established by modeling different types of contact, and considering contact dynamics in detail through analyses of impact effects and contact motion. Furthermore, other human-like drive configurations can be incorporated into the model and can make use of the same basic methods.

These computer-based models show that accurate simulations of a type of anthropomorphic robot that interacts with its environment are possible. Following the theoretical background presented here, one can exploit the model of contact and robot dynamics in fields such as control theory, dynamic coupling in compliant multiple DoF systems, motion planning, robot interaction, energy utilization and optimization, and the like. Some preliminary investigations in which the author already took advantage of the framework are reported in [154], [56] in the field of control theory, and in [106], [107], [2] in the field of dynamic coupling in compliant multiple DoF systems and contact analysis. Two case studies were presented for demonstration purposes. The first exploits a model of anthropomorphic robot dynamics, whose purpose is to explore the critical design of a robot mobile base, using dynamic balance within the scope of ZMP. The effects of dynamic coupling between a joint and external influences that emulate disturbances to the robot working in unstructured environment, were evaluated to propose a design of the mobile base. The second case study points out the analysis of a typical contact task – grasping of an object in the vertical plane. As a prime example, this task requires all phases of a contact task: approach, impact and in-contact-motion, to be considered.

As pointed out in the introductory section of the thesis, anthropomorphic robot models can help to not only simulate robot behavior but also understand and enhance human biomechanical patterns. Therefore, special attention with regard to the utilization of the model should be devoted to motion in sports. For instance, a load acting on human joints or antagonistic tendons can be analyzed and then reduced by optimizing the way movements are performed, which is of the essence these days in professional sports. As an added benefit, sport injuries could be reduced and endurance improved.

Computation of highly complex analytical models, such as those of the

anthropomorphic robot's upper-body structure, is demanding and time consuming. In particular, for a freely moving 20 DoF upper-body anthropomorphic robot with antagonistic joints according to model (2.41), there is a set of 66 differential equations that have to be numerically integrated. The initial software implementation was in Matlab/Simulink, but for reasons of computational efficiency, the functions for robot kinematics and dynamics were reprogrammed in C++ to speed-up the process about forty times. One second of simulated time took approximately 14 seconds on an Intel i3 M330 CPU working under Windows 7 OS. One of the future objectives will be further optimization towards faster execution of the developed algorithms.

In spite of the fact that analytical models were developed to enable detailed insight into the dynamics of future service anthropomorphic robots, some approximations had to be made. Another issue is the inevitable friction between the tendons and the robot's skeleton, which is not considered in the thesis. However, the extension of these models, based on antagonistic compliant joints, to an exact Eccerobot model (or other robot of a fully anthropomorphic structure), by including more of the unmodeled features (e.g., multi-articular actuation), will require significant future effort. So far, physics-based engines have demonstrated predominance in such simulations.

Finally, since anthropomorphic robots appear to be the choice for future safe service robotics, there is no doubt that analytical models will be of special importance in this field, not only for simulation and testing purposes, but for advanced control techniques that always exploit knowledge about systems through available models.

### 3 Engineering control approaches

The idea and motivation for this section came from the core activity of the research group, including the author, which worked on the ECCEROBOT project: to what extent could conventional engineering control approaches be used to control fully human-like robots? Of course, since musculoskeletal robots are built by copying human anatomy, it is expected that the control of such robots exploits some bio-inspired patterns of human movements and muscle activities. However, nobody can fully understand and describe the main principles of human behavior, distinguish between voluntary and involuntary actions, and define optimization processes solved by the human brain. Clearly, most of these points cannot be categorized under and considered as predominant conventional engineering issues. Also, the human body is not designed following any engineering policy.

However, the applicability of engineering control techniques to musculoskeletal robots is a particularly important topic, which will lead to a tradeoff between two mainstream directions. The first approach (e.g. JSK Tokyo Lab robot Kenshiro [62] and the European Eccerobot [11]) advocates a completely human-like robot design, which will allow the robot to easily move, act and fit in the environment that humans fully adapt to themselves, conforming to ergonomics and comfort. This mainstream also strives to examine the robot's human-like characteristics and reproduce certain human-like cognitive features. The second approach (e.g. electrically-actuated wheeled humanoid – Rollin' Justin [155], pneumatically-actuated biped Lucy [98]) supports a slower but reliable and robust breakthrough in conventional and trusted engineering technologies for humanoid robots, renouncing many of the benefits that an entirely human-like machine could offer.

Therefore, a straightforward question arose at the very beginning of research in the area: where should we draw the line between replicating nature and relying on the conventional engineering world? To that end, this section points out some limitations

and restrictions that apply to the design and control of human-like robots, in order to still be able to exploit known theoretical engineering approaches to control: nonlinear, multivariable, and robust.

Although the human body and, therefore, anthropomimetic robots are not shaped to comply with any engineering principle, some assumptions can be made for the purpose of gaining a better understanding of overall human behavior. Most human muscles are antagonistically coupled and movement is achieved using their co-contraction and reciprocal activation [156]. Considerable effort has already been put into optimizing muscle activity [157], [158]. Even though no finite solution has been offered, the consensus is that two basic principles are followed by different estimation cost approaches: minimal energy consumption and accuracy of motion. Therefore, we will focus on the control of antagonistically-actuated joints as prime movers in humans and a typical bio-inspired actuation structure. In order to simplify things, we will neglect any actuators other than these two per joint. Thus, we adopt a simplified human-like structure, which is still very demanding from a control point of view. We face an interesting and complex engineering challenge in general – control of a multivariable, compliant and nonlinear system.

Prior to presenting the contribution of this thesis, we will highlight some of the most important related works, aimed at developing control algorithms for antagonistically-coupled compliant drives. However, because of the complexity of certain methods, which are mostly non-linear and multivariable, most works focus on simulations and do not consider practical issues that arise from hardware. Such issues are, for example, the need to calculate higher-order derivatives for accurate tracking or the use of large matrix inversions, etc. Due to complex mechanics, all state variables are rarely measured, so their estimation and need for filtering is often critical to both accuracy and implementation in real time. Notwithstanding, previous research has not paid any attention to “switching” – the process of exchanging roles between two opposed actuators. Researchers rather assume that both tendons are always in tension. On the one hand, many of the approaches do not guarantee that tendons will not slacken and, on the other hand, if high pre-tension is used, the control methods could lead to energy

inefficient control because the level of co-contraction is significant, relative to the net torque. This thesis proposes to consider one actuator, the *puller*, as being responsible for joint motion, while the role of the other is to maintain some minimum tension in the inactive tendon. Moreover, an adaptive co-contraction value is introduced, which lowers the energy consumption arising from opposing forces in co-contraction, while keeping all tendons stretched all the time and keeping either the desired force in the antagonistic tendon or the desired joint stiffness. This arrangement can be seen as more human-like in some ways; however, it requires effective and efficient control of switching.

Subsection 3.2 points out the utilization of feedback linearization as an approach that has already been suggested for control of joints with intrinsic compliance. Since antagonistically-actuated compliant joints are multivariable systems, feedback linearization is employed as a tool for system decoupling and linearizing at the same time. After referencing previous results in this direction, Subsection 3.3 proposes a biologically-inspired and energy efficient method to simultaneously control the position and force of antagonistically-coupled tendon driven actuators: the puller-follower method. The novelties and enhancements that this approach introduces in simultaneous position and stiffness control of antagonistic joints are highlighted. Subsection 3.4 brings an extension of the puller-follower control method to include simultaneous decoupled position and stiffness control of an antagonistically-driven compliant joint as a key task of variable stiffness actuators. Finally, to adapt the control approach to multi-joint robot manipulators and deal with unmodeled dynamics and/or model uncertainties, additional control terms, such as gravity compensation, effective inertia estimation and robust control, are suggested to round-out the comprehensive approach to the puller-follower control proposed in Subsection 3.5. The directions of future work are summarized and final comments on the application of the proposed control concept are provided Subsection 3.6.

The present section offers a comprehensive overview of the author's contributions to the field, which have largely been presented in [159], [160], [161], [154].

### 3.1 Background work

As stated in Introduction, the first physical realization of a robotic hand with antagonistically-actuated joints (Utah/MIT Dexterous Hand) highlights the control challenge of antagonistic systems with intrinsic compliance [89]. The authors developed special-purpose pneumatic valves for corresponding pneumatic cylinders from the actuation side, as well as a tendon-tension sensing subsystem in combination with state-of-the-art Hall sensors for joint position sensing. With sophisticated hardware at the time, they point out the complexity of simultaneous setting of positions, tendon tensions, control loop gains, mechanically variable pneumatic damping of the system, etc. The same group at the University of Utah was the first to tackle the control problem of tendon-driven and antagonistic actuators [70], [162]. Jacobsen et al. list the advantages of tendon driven systems (reduced inertia, reduced static load, low backlash, low friction, minimal end-effector volume, extended range of motion, etc.) and consider antagonism as a necessity for bi-directional cable actuation. In these papers, the authors present several controllers (Figure 3.1), which are predecessors of all novel control algorithms in the domain of antagonistically-actuated joints. The first control task – joint position control – was achieved by Position Controller A, but open-loop force commands could lead to high co-contraction or tendon slackening. Controller B (position and force control with rectifiers) involves force feedback control, which prevents undesired effects and also minimizes force ripples. The remaining problems are external disturbances and unexpected interactions, which are compensated by one actuator only – depending on the direction in which it acts, and not by synergy of both actuators. This approach involves measuring of the joint position and tendon forces. The main controller is a position controller, implemented with proportional and differential compensation. The output of this controller, the “compensated” position error, was analyzed using flexion and extension rectifiers. The outputs of the rectifiers were positive and added to the co-contraction value, thus forming references for the tension forces. The force references created in this way is always positive and ensures that the tendons will always be in tension. This controller was employed on the Utah/MIT Dexterous Hand. Tendon management logic, which could generate push commands also but at the same time control and keep the desired level of co-contraction, was

introduced in Controller C – position, force, and torque control with tendon management logic. The second enhancement was additional torque feedback, which allowed both actuators to simultaneously respond to torque errors. Controller D (position, force, and torque control with tendon management absolute torque) represents a simplified version of Controller C – where tendon management logic was replaced with a feedforward command to contribute the co-contraction level, knowing the absolute value of the position error and representing the desired torque. The authors of the Utah/MIT Dexterous Hand exploited commercially-available linear springs and thereby reduced the control capabilities of the system.

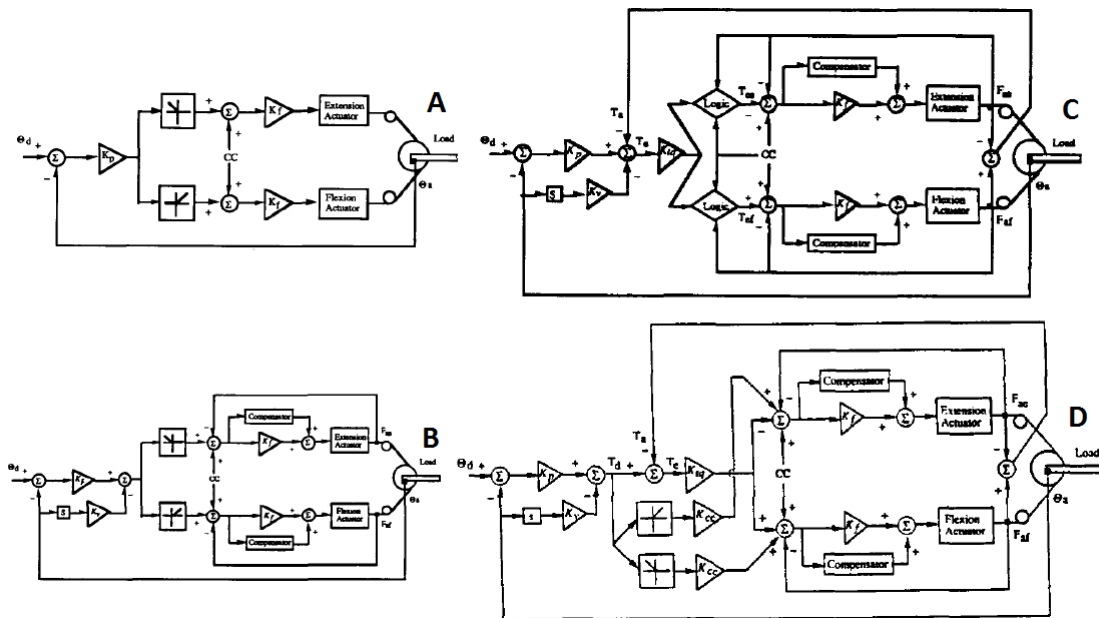


Figure 3.1. A series of pioneering controllers introduced by Utah University: A – Position controller (open-loop force commands can cause high co-contraction or tendon slackening); B – Position and force control with rectifiers (prevent tendon slackening and high co-contractions but external disturbances and unexpected interactions are still compensated by only one actuator – depending on the direction in which it acts, and not by synergy of both actuators); C – Position, force, and torque control with tendon management logic (Controller B is enhanced by tendon management logic, which can generate push commands also but at the same time control and keep the desired level of co-contraction); D – Position, force, and torque control with tendon management absolute torque (tendon management logic replaced with a feedforward command to contribute the co-contraction level, knowing the absolute value of the position error and representing the desired torque).

This work at the Massachusetts Institute of Technology (MIT) and Utah University introduced the basic principles of tendon-driven antagonistic robotic joints. Their ideas were later spread, modified and enhanced for both electric and pneumatic/hydraulic antagonistic drives.

### **3.1.1 Control of antagonistically-coupled electric drives**

While springs that featured linear force-displacement relation were commercially available, researchers were tackling with the design and manufacture of certain nonlinear springs with the characteristics needed for variation of overall joint stiffness. An additional challenge for a symmetric antagonistic design was a pair of elastic elements with identical force-displacement characteristics. To overcome the need for trade-off, Migliore et al. [77] designed a device for shaping the force-length relation of the elastic element in order to use commercially-available linear springs and achieve non-linear user-shaped elasticity, which is necessary for variable-joint stiffness. They used feedforward control to set the desired equilibrium joint position, as well as joint stiffness for a specific load torque. The authors even used FPGAs for efficient and fast calculations. That fact attested to the awareness of the authors about advanced computation that would be necessary for the next-generation device, upgraded with required measuring, conditioning and estimation of system state variables and related data. Although they did not use advanced force/torque sensors and/or an online stiffness estimator, they presented respectable results (especially for high stiffness settings, since at a low stiffness, friction and dissipation effects are more obvious). Yet, for reliable control in contact tasks and during unplanned interaction, an advanced sensing system and feedback are unavoidable.

Tonietti et al. propose in [81] the first feedback approach to stiffness/position control of VSA using antagonism. They introduce feedback for joint impedance and position control to deal with model parameter mismatches (unavoidable in such complex systems) and unmodeled dynamics and/or unforeseeable disturbances. They relate half of the sum of motor positions (antagonistically paired) to the resulting joint position and half of their difference to a variable proportional to the joint stiffness. Such intermediate

state variables are controlled by simple PD controllers, guaranteeing stability over the entire working range. A controller limited to a simple PD approach is also used to control next-generation VSAs, with two motors and two springs in an antagonistic configuration – VSA-II [82].

In order to control the anthropomorphic hand of the DLR hand arm structure [83], and particularly the drives that obtain variable impedance using antagonism, several control methods have been proposed. The following paragraphs summarize target system control efforts.

In [163], Chalon et al. propose a cascaded structure of the controller. The desired torque and stiffness are used to shape the desired pretension tendon forces. Thus, the inner control loop – tendon force control loop – is accompanied by the outer impedance control loop. The main challenge for the authors was how to cope with nonlinear tendon routing, where the non-linearity was configuration-dependent, i.e. depended on the hand position. Furthermore, the thumb position was not measured directly by a sensor but estimated from a model. However, this approach does not guarantee that the resulting tendon forces will satisfy the pulling constraints and might not create a sufficient force offset. Another evident issue in the above control approach is that the motor torque, as a control input, depends directly on estimated joint torque, whereas joint torque is estimated from measurements of tendon forces and tendon routing applying the principle of virtual work. Moreover, the outer impedance control loop would achieve the desired impedance behavior only if the real joint position and the estimated joint position are very close. Since the joint positions are estimated based only on motor positions, this error can deviate significantly, especially due to mechanical compliance of the thumb/tendons.

T. Wimböck et al. proposed in [140] an asymptotically-stabilizing adaptive nonlinear control law – immersion and invariance control (initially introduced by A. Astolfi and R. Ortega [164] at Imperial College, UK). Due to a rigorous mathematical apparatus, this approach, which considers the desired joint position and joint pre-tension as inputs, was applied only in simulations. In order to implement the immersion and invariance

control theory to an antagonistically-driven compliant joint, the authors assume that motor-side dynamics are much faster than the link-side dynamics, which could be misleading if the proposed solution is applied to real hardware. Although the simulation results are promising and demonstrate both performance and sensitivity, this approach would be very complex to implement on multi-DoF systems and integrate it into hardware.

Another work on the control of a joint driven by antagonistic tendons with non-linear stiffness attempted to bridge the gap towards experimental implementation and verification of control methods. It was the control of antagonistic joints within the DLR hand (more precisely the index finger of the Awiwi hand), using integrator backstepping presented at the 19<sup>th</sup> IFAC World Congress [165]. Backstepping is a recursive procedure that propagates the control error downward, by successively building Lyapunov functions and selecting intermediate control laws [166]. Namely, the authors first apply link-side impedance control, and then decouple systems to enable single-input-single-output control for individual motors. However, several issues from their previous work [163] are still present, especially those regarding the estimation of joint torque and position, as well as the limited tendon force range. Moreover, backstepping leads to high-order torques and position derivatives. Therefore, besides unavoidable computational errors, a compromise needs to be made between computationally-demanding analytical expressions and discrete measurement implementation, which amplifies measurement noise. Since joint stiffness derivatives were used for the control design, the commanded stiffness had to be constant or to at least be varied slowly. Although this approach enables control even in the case of failure of one of the antagonistic motors (when impedance would be compromised), it still does not give high priority to keeping tendons stretched, such that tendon slackening could occur and controllability would thereby be lost.

As stated in Subsection 1.4, QB Robotics announced several actuators from a series of compliant bidirectional antagonistic drives. They produced this low-cost platform to spread the technology and allow a wider audience to teach and do research on the topic. To that end, they trade-off more accurate and complex control for ease of use, so users

can control qb move actuators by setting the desired equilibrium position and stiffness preset (initial stiffness in the absence of external torque). Consequently, antagonistically-coupled motors are positioned via internal control loops, to ensure the desired characteristics according to Equations (3.1) and (3.2), which define the equilibrium position  $x_{eq}$  and stiffness preset  $\sigma_{pres}$ , respectively.

$$x_{eq} = \frac{q_1 + q_2}{2} \quad (3.1)$$

$$\sigma_{pres} = a_1 k_1 \cosh(a_1(x - q_1)) + a_2 k_2 \cosh(a_2(x - q_2)) \quad (3.2)$$

Thus, the achieved behavior is only approximate, since these algebraic equations are solved for static conditions in the absence of load torque and external disturbances, for initially estimated parameters of elastic spring characteristics. Several research teams have already exploited QB Robotics actuators to test and develop controlled compliant robotic mechanisms [167], [168], and [169]. For next level users, who are interested in more sophisticated control rather than the exploitation of robot compliance, the authors designated motor positions as control inputs. However, for more sophisticated control, one should integrate torque sensors or at least accurately estimate torque from available motor current sensors. Still, the low-cost design stands as a severe limitation on the hardware.

Petit et al. go a step further in [86] and propose “a helping antagonism stiffness adaptation scheme”. Here, the authors suggest a mechanism to shape stiffness characteristics and control a bidirectional antagonistic joint by calculating the desired pre-tension (expressed as motor positions) and facilitating motor cooperation to provide sufficient external torque. Again, internal control loops for motor position control are assumed to be fast and accurate enough, and are not considered. Still, bidirectional drives can compensate for some deficiencies of classical antagonistic unidirectional drives and prevent upgrading of such an actuation system to more human-like tendon routing mechanisms.

### 3.1.2 Control of antagonistically-coupled pneumatic/hydraulic drives

Although not the primary focus of this thesis, numerous designs of robotic manipulators driven by pneumatic artificial muscles (mostly actuated by their antagonistic coupling) were followed by a lot of effort invested in the control of such mechanisms. As pointed out in Subsection 1.4 where numerous antagonistic joints are presented, the key difference in the design and, consequently, control approaches between antagonistically-coupled pneumatic/hydraulic and electric drives is the source of compliance. Whereas compliance is always added via an additional elastic element in the case of electrical drives, pneumatic drives feature intrinsic compliance, which originates from the characteristics of the working fluid. However, this intrinsic compliance is a major cause of numerous control problems with pneumatic actuators in general, as well as their antagonistic configurations, as shown in the following paragraphs.

Control of pneumatic artificial muscles was initially tackled by Caldwell and his group at the University of Salford in [170] and [171]. In [170], a basic discrete time PID controller, tuned by trial and error, with a feedforward term, was implemented for pneumatic muscle control. The very first experiments showed that closed loop performance was quite sensitive to errors in the feedforward term, mainly due to supply pressure fluctuations, pipe length, temperature, etc. In [171], an alternative adaptive control scheme was investigated. Although this adaptive controller demonstrated significantly faster performance, its effectiveness was still dependent and limited due to the above factors.

Vitiello et al. from Scuola Superiore Sant'Anna came out with an idea for torque control based on torque estimation, using conventional position sensors [172]. However, for accurately known force-deflection spring characteristics and a combination of joint position and antagonistically-coupled motor positions, one can estimate the force in the spring. They advocate a two-step approach. The first step is experimental characterization of the non-linear elastic behavior of the actuation-transmission units, regardless of the technology and system layout. This was done by measuring the interaction force between the hand tip and the external object through a 6-axis load cell

and using the Jacobian matrix that relates the interaction force to the joint torques. Of course, such a procedure caused many inaccuracies due to the sensor resolution, choice of the force-deflection fitting polynomial, etc. The second part was direct control of the force exerted by each antagonistic actuation unit and the indirectly resulting torque of the antagonistically driven joint. Instead of using a force sensor, the force was indirectly estimated from the elongation of the tendon, as the elongation was evaluated from the commonly-used joint position and antagonistic position sensors. Finally, the tendon force was estimated from the obtained off-line experimental force-deflection curve. The evaluation of the proposed control approach was implemented and tested on a 2-DoF planar robot – NEURARM [90]. However, this set-up could hardly offer accurate and fast control; besides the stated inaccuracies, there is a limited bandwidth due to hydraulic actuation, as well as low resolution. The controller is based on a pure proportional compensator, which considers an error between the desired and estimated force as an input, and calculates the desired speed of the hydraulic piston. In addition, piston speed is controlled by the electro-valve voltage input, which features a non-linear relation to piston speed.

A very similar approach to the one presented in [167] for antagonistically coupled low-cost electrical drives for simultaneous position and open loop stiffness control, this time using antagonistically-paired McKibben artificial muscles, is proposed by Bicchi and Tonietti in [173] and [174]. In essence, they employ four-way servo valves, typically used to control a conventional pneumatic actuator, to control the actuator position via the difference in actuator pressures, while stiffness is controlled based on the sum of pressures. Here, the authors explore PID control strategies without considering the characteristics of pneumatic valves in the design of the controllers.

The entire preliminary research on the control of antagonistically-actuated PAMs indicated that these devices were difficult to control because of their nonlinear and uncertain models. To deal with this issue, numerous non-linear control approaches were adopted and implemented for testing purposes. Hasselroth et al. from the University of Illinois exploit neural networks in [175] to model and control their pneumatically-driven robot arm – SoftArm. In the work by Carbonell et al. [176] fuzzy logic is accompanied

by local backstepping controllers derived to set the equilibrium point of their PAM. Due to non-linearity and time invariance of the PAMs, another fuzzy controller demonstrated more effective results than conventional controllers – PD+I learning controller presented by Chan et al. [177]. The nonlinear characteristics of PAMs (and consequently their models), which are in general time-varying, are tackled and partly overcome by Lilly from Louisville University in [178]. He proposes an adaptive tracking algorithm for PAM control, which mimics a typical anthropomorphic antagonistic configuration – biceps and triceps. However, this approach was tested only in simulations, while the hardware has not yet been implemented to this author’s knowledge. Hildebrandt et al. demonstrate flatness-based control in [179], applied to FESTO’s pneumatic actuator. They advocate flatness-based control as a prime choice for tackling the system as a typical non-linear plant. One more control technique that does not linearize the model, with unavoidable model inaccuracies, is proposed in [180]. It uses the linear matrix inequality (LMI) optimization approach and robust PID controllers for every two antagonistically-coupled PAMs.

Although such sophisticated methods were being developed at the time, complex multi-DoF system driven by antagonistically coupled PAMs, such as Shadow Hand, were still driven in a basic intuitive way. It was a controller as a combination of two control variables – joint position and joint stiffness, motivated by the fact that the pressure difference correlated with the joint position, and the pressure sum correlated with the stiffness of the joint [99]. Here, most standard control approaches, focused on a single joint, could not be applied directly due to the unavoidably complex tendon routing in the hand and, consequently, friction, non-linearity and hysteresis.

Simultaneous torque and stiffness control of a robotic joint actuated by antagonistically-coupled PAMs was presented by a group from the Advanced Robotics Lab, Italian Institute of Technology. In [181], the authors cope with not only the non-linear nature and model uncertainties of PAMs but also the discontinuous on-off behavior of the solenoid valves, which generally makes smooth control of PAMs difficult to achieve. Regardless, PAMs used in robotics are mostly driven by solenoid valves because of their low cost, compactness, weight, and fast-switching capability. The presented

controller contains two stages: the first exploits mathematical models to determine the forces necessary at each antagonistic muscle, in order to obtain the required joint torque and stiffness. Consequently, a sliding-mode force controller was implemented on each muscle, since that was a well-known robust strategy, able to tackle the parametric and modeling uncertainties of a system such as PAM. Experiments on a single joint demonstrated promising results, but the application of such control to a multi-joint system and parameter time changes was questionable.

Honda et al. propose another biologically-inspired control method in [101]. They introduced two new terms: “antagonistic muscle ratio” and “antagonistic muscle activity”. Antagonistic muscle ratio is defined as the ratio of air pressures between the agonist to the sum of the agonist and antagonist, supposed to be related to the joint angle. Antagonistic muscle activity is defined as the sum of air pressures of the agonist and antagonist, supposed to be relevant to joint stiffness. However, this control approach suffered from many assumptions, which could hardly stand in a realistic case. First, a linear relation between the antagonistic muscle ratio and joint position was assumed, so the desired antagonistic joint ratio was estimated linearly, directly from the desired joint position in its full range. Moreover, the antagonistic joint ratio, related to a joint angle, and antagonistic muscle activity, related to joint stiffness, were assumed to be independent. Although these assumptions were largely proved in a single-joint control experiment, it was very hard to achieve system symmetry since PAM actuator properties vary in the manufacturing process, besides the fact that two actuators were designed to be the same. Therefore, the experimentally-tuned PID controller, which compensates for the joint tracking error, was implemented. In [182], the authors extend their research to include a five-fingered robot hand and implement feedforward control of the same kind. Theoretically, they prove the control concept on a multi-DoF system, provided that no external force is applied and model parameters are obtained with high accuracy. Professor Miyazaki’s team continued to perfect their control approach by transferring the muscle synergies and patterns, extracted from EMG signals, to commands of artificial muscles [183]. They decompose antagonistic muscles activities during certain repetitive tasks, such as a human walking and running, into two muscle synergies using Principal Component Analysis (PCA): antagonistic muscle ratio

(defined as the ratio of the EMGs for agonist to antagonist muscles) and antagonistic muscle activity (defined as the sum of the EMGs for agonist and antagonist muscles). They prove that one cannot treat a biological system and a robot system applying the common concepts of the antagonistic ratio and antagonistic activity. By carrying out special-purpose experiments with the robotic joint, they confirmed that the assumptions were valid for precise symmetric manufacture of antagonistic PAMs: the equilibrium joint angle is directly associated with the antagonistic ratio (in linear form), the joint stiffness at any equilibrium joint angle is directly dependent on antagonistic activity (in linear form), and the equilibrium joint angle and joint stiffness can be controlled separately, by setting the antagonistic ratio and the antagonistic activity parameter.

Finally, trends have definitely been moving towards electric drives that exploit additional compliant elements, rather than PAMs. The difficulties faced in fast and accurate control of pneumatically-driven antagonistic joints have mostly been intransitive (low control bandwidth, restricted workspace, low torque capacity, etc.). Time delays that can be measured in tenths of a second, as well as the unavoidable actuator hysteresis, prevented the use of feedback and led to various feedforward approaches, such as modes for each activity: walking, running or jumping [102]. Convincingly, further research toward effective use of antagonistically-coupled PAMs for simultaneous position and stiffness control depends on the enhancement of actuators and the drives themselves, rather than on the development of sophisticated control algorithms.

### **3.2 Feedback linearization for compliant robot joint control**

This subsection outlines the applications of feedback linearization in the control of compliant systems in general. Since compliant systems are predominantly nonlinear (to enable changeable stiffness) and multivariable (at least preferable to control position and stiffness, therefore at least two drives are needed), the fundamental challenges in the control of such systems are decoupling and linearization. Feedback linearization was first considered for a robot with elastic joints in the late 1980's [184], [185], [186]. These papers elaborate the control of robots with rigid links, but in the presence of joint

elasticity. Elasticity was first treated as a side effect of the transmission system (gearboxes, harmonic drives, long shafts, etc.). In other words, elasticity was perceived as a primary source of vibrations in robot joints. Not too long afterwards, engineers realized that elasticity could be a feature that everybody could take advantage of (e.g. to increase safety, reduce energy consumption, raise composite speed of robots, etc.). Some later works focused on the applicability of elastic transmissions and outlined important features of feedback linearization in the control of robots with elastic joints [187], [188], [189]. Comprehensive procedures for decoupling and linearization of robotic systems were proposed. However, none of these works consider stiffness as a variable parameter. An important observation that advocates the utilization of feedback linearization is (De Luca in [187]): “If the angular part of the kinetic energy of each rotor depends only on its relative rotation, or if there are no inertial couplings between the link and the motor dynamics, then the model is always feedback linearizable by static state feedback.”

In [190], Palli et al. analyze the feedback linearization problem of robotic manipulators with variable joint stiffness. The authors provide the theoretical background about how full state linearization of a robotic manipulator can be achieved and how both joint position and stiffness can be controlled via static or dynamic state feedback. There, the authors suppose that mechanical stiffness of the joint can be modulated by an external control input (i.e. without considering a detailed joint design and the actuation system). Also, the authors consider an ideal case – exact knowledge of the robot’s dynamics and lack of disturbances. Therefore, an extension of the work is needed, in light of robust and/or adaptive control, as confirmed in [187], [190]. These future research directions are partly covered and implemented in this thesis.

However, we restrict our target systems to those without dissipation effects in power transmission. In [191], De Luca and his group demonstrated that static state feedback achieves, at most, input-output linearization and decoupling for robots with visco-elastic joints, and internal nonlinear dynamics are left in the closed-loop system. Although they show that the stability of such unobservable dynamics is guaranteed in nominal conditions, a control design based on static feedback becomes ill-conditioned as joint

viscosity decreases. On the other hand, the use of dynamic state feedback leads to the same closed-loop properties, but with a regularized control effort for any level of the joint viscosity term. Therefore, feedback linearization is generally a viable nonlinear control technique for position tracking problems in robots with elastic joints.

Finally, we can say that feedback linearization is a very efficient tool for controlling robots with elastic antagonistically-coupled drives, but exact trajectory tracking is possible only in the nominal case. On the other hand, feedback linearization is a very demanding control strategy, since it requires full knowledge of the robot and drive dynamics. External disturbances and parameter uncertainties are challenges that feedback linearization should handle carefully, as highlighted in this thesis. Since feedback linearization relies on accurate system modeling, which is very difficult to accomplish, robust control of linearized and decoupled systems is essential for comprehensive control design.

### **3.3 Puller-follower control concept**

Before we move to the control concept itself, we first need to underline the features of the antagonistically-actuated compliant joint as the targeted control system. The joint driven by antagonistically coupled SEAs represents the most common human-like joint actuation source and is, therefore, an approximation of most musculoskeletal joint drives. A classical agonist-antagonist joint structure is recalled in Figure 3.2. Also, the antagonistically-actuated joint scheme is one of the most frequently considered among actuator schemes with variable compliance/stiffness, originating from human muscle antagonistic pairing. Once more, a robot link moves due to the activities (co-contraction and reciprocal activation) of two antagonistically-coupled drives, the so-called agonist and antagonist drives. Each drive comprises a DC motor, followed by a gearbox and a pulley that winds a cord. The cord, or tendon, is generally a non-elastic thread with an elastic element as a source of intrinsic compliance. Each linear, quadratic or exponential spring can be used as an elastic element, and each introduces some limitations and possibilities that one should be aware of. That is also highlighted in this section.

Although the thesis considers control of both a linear and slightly different structure, so called “triangular” [106], which fully matches the human elbow and introduces nonlinearities due to tendon mapping, we focus on the linear structure without loss of generality. For an application of the puller-follower control strategy to a “triangular” structure, please refer to [159].

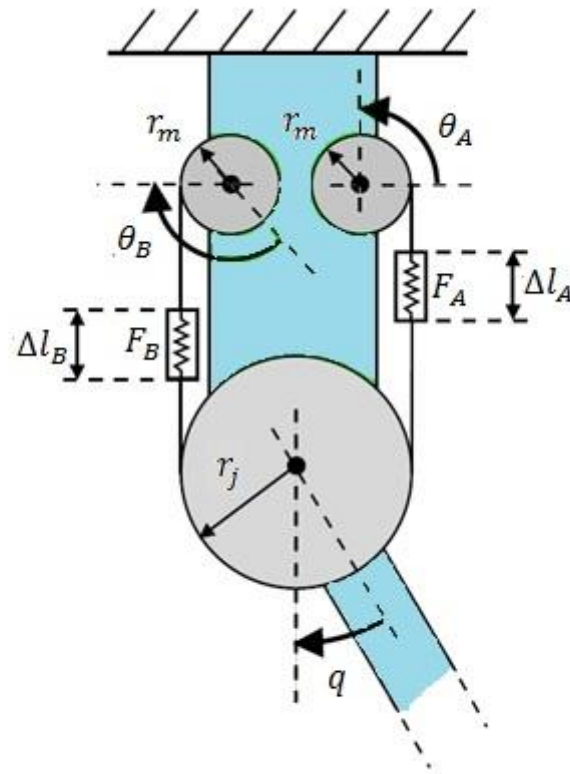


Figure 3.2. A classical representation of an antagonistically-actuated robot joint. Two motors, A and B, contribute equally to the overall joint torque and consequently move the joint, if their directions of rotation are opposite (for the adopted direction), whereas if the directions of motor rotation coincide, elastic elements co-contract and the joint stiffens.

Keeping in mind that there is still no fully-adopted robust control scheme, which has been successfully applied to antagonistically-actuated joints (despite some notable results, as shown in previous sections), we will try to improve an existing solution. Palli et al. [132] use feedback linearization to achieve simultaneous control of the position and stiffness of antagonistic robot joints. However, this theory is not fully applicable if the elastic element is linear (stiffness control is not possible since stiffness is constant

and depends directly on linear spring stiffness), and it does not consider the pulling limitation of the muscle force and its representatives in technical implementation (tension in tendons must always be positive as human muscles can only pull and not push). Also, in some conditions controllability can be lost, which is also subject of a potential enhancement. Furthermore, Palli and his contributors did not consider the application of robust control, further generalization to multi-joint systems, etc. Generally speaking, they provide solid groundwork for the topic, with numerous possibilities for future work.

Bearing in mind the above-mentioned restrictions and muscle-like features as a subject of transfer to the world of technology, this thesis proposes a novel control approach of antagonistically actuated compliant joints – puller-follower control. The puller-follower approach uses feedback linearization to independently control the joint position and pre-tension in the “follower” tendon. Two single actuators, in opposition to each other, produce a net torque at the joint while using tendons to transmit their force/torque. For a given motion, the actuator that initiates acceleration in the direction of motion is called the agonist (or “puller”), whereas the other actuator that can counteract the action and contribute to the overall motion is called the antagonist (or “follower”). After feedback linearization decouples the system into two linear subsystems, it is possible to control both joint position and force in the antagonistic tendon via two new intermediate inputs. Besides the numerous different approaches that can be employed to control these two decoupled systems, there are also several issues which should be treated very carefully. For most of them we refer to biology and biomechanics to look for answers. The first issue we should be aware of is planning of the tension (force) in the antagonistic tendon. While the “puller” controls joint position, the “follower” co-contracts the tendon to some prescribed tension level, which has to be low for reasons of overall energy efficiency, but sufficiently high to prevent slacking of the tendons and thus prevent the antagonistic system from becoming underactuated. Then, considering link movement in either direction, or even acceleration and deceleration phases during link movement in the same direction, or the influence of an external force, the puller and the follower need to change their roles occasionally (we will call the role change “switching”). This intuitive finding was checked in an experiment, which included recording of

electromyography (EMG) signal patterns of antagonistically-coupled human muscles for typical repetitive movements: knee flexion/extension, walking, etc. [192].

Switching is invariably followed by oscillations in tendon forces (switching shock), which can cause tendon slackening. Although the theoretical background of the influence of the relative ratio of the puller to follower force and the slopes of force changes has not been revealed, some simulation experiments at an optimal (relatively high) level of the follower tension that minimizes such a shock are noted in [161]. Therefore, to achieve energy efficiency and prevent tendon slackening during switching, adaptive reference tension is proposed in this thesis. The tension force in the follower tendon should be low during regular motion and should increase during periods of switching. The puller-follower control concept and the adaptive reference force are depicted in Figure 3.3.

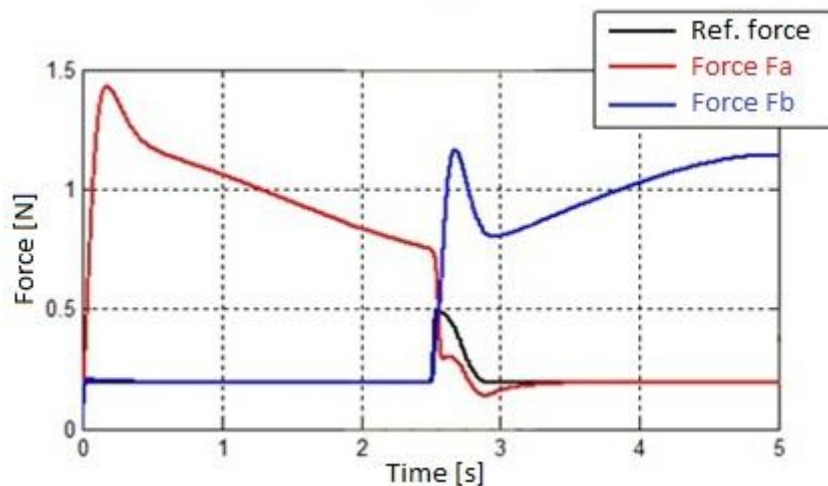


*Figure 3.3. Puller-follower principle. An antagonistic system is decoupled so one tendon the “puller” controls joint position, while the other - “follower” co-contracts the tendon to some prescribed tension level. To achieve good energy efficiency, the desired tension force in the “follower tendon” is always kept at a predefined low level. At the same time, the other tendon produces enough force to achieve the desired motion and ensure trajectory tracking. To avoid tendon slackening and retain controllability, the tendons sometimes switch roles. During switching, the adaptive reference force is increased to disable oscillation due to the switching shock and prevent slackening of the tendons.*

Finally, there are also some open issues that will definitively be the focus of the author's future work and research on bio-inspired robot control. To begin with, the switching roles between tendons are highlighted as an important feature of puller-follower control. The idea to implement switching originated precisely from biology and the behavior patterns of antagonistically-coupled muscles. However, the benefits of the time instant when tendons change their roles have not been sufficiently tested. The future work in this direction will begin with a comprehensive investigation of this issue during different tasks executed by humans. The possibility of exchanging roles (the follower tendon taking over the role of the "puller") before the forces are equal could be beneficial in certain cases that involve fast and radical movement or where the contribution of gravity or some external effect is significant. By examining the effect of switching, we can prevent the switching shock [159] and reduce oscillations that can arise naturally due to the compliant robot structure. So far, switching has been instant, when the puller tendon force drops below the follower tendon force.

Another open point is the adaptive tension force. A current topic of robotics research involves variable-stiffness actuators and how to trade-off between stiff actuation (high precision, fast) and compliant actuation (impact friendly, more energy efficient). The majority of guidelines for stiffness planning and, consequently, antagonistic force planning in the case of the puller-follower approach can be found in biological patterns. Although there is no generally accepted theory, it is highly intuitive that besides reducing discomfort while keeping maneuverability postures, humans also optimize energy consumption when they perform a common and regular task [193]. Therefore, the stiffness produced by muscle activity is as low as possible. However, while expecting unknown or insufficiently known interaction with their surroundings or intending to move very fast or precisely, humans stiffen their joint by co-contracting antagonistic muscles to achieve good trajectory tracking [194]. Note that a joint torque (necessary to execute a task) can be produced at different joint stiffness levels. In order to provide better insight into antagonistic tendon force patterns, the experiment described in [192] was carried out within the scope of this thesis. By measuring EMG activities of antagonistic muscles of the human knee during knee flexion and extension, the instances of flexor ("puller") and extensor ("follower") muscle activation were

observed. The experiment confirmed that simultaneous higher activation exists when muscles change their roles, and furthermore EMG signals corroborated the existence of the tri-phasic activation pattern of the antagonistic muscle, described by Hannaford and Stark [195], in movements where the influence of external forces (e.g. gravity) was reduced. An initial burst in the agonist, which initially accelerates the limb, is followed by a silent period that coincides with a burst in the antagonist, and finally by a second burst in the agonist. The magnitude of the antagonistic burst varies due to limb velocity. However, the timing and magnitudes of both the antagonistic burst and second agonist burst are subject to complex dependencies (e.g. the ones related to loads opposing movement, intended torque, etc.). Consequently, these relationships have been poorly understood so far. Hannaford and Stark went a step further by developing a simulation model of a joint driven by antagonistic muscles (Figure 3.4, left). The same tri-phasic EMG patterns in antagonistic muscles during isometric contractions were reported by Gordon and Ghez in [196]. In their experiment, when rapid force pulses were applied to examinee's arm, initial agonist bursts were of a constant duration and their magnitude was strongly related to the achieved peak force. The timing of the antagonist bursts was closely coupled to the dynamics of the force trajectory, and the rising phase of the force was determined by both agonist and antagonist bursts. When the peak force was kept constant and the rise time systematically varied, the presence and magnitude of the antagonist and late agonist bursts depended on the rate of rise of the force, occurring at a threshold value and then increasing in proportion to this parameter. The experiments showed that an initial agonist burst terminates at the time of the imposed force derivative peak  $dF/dt$ . The antagonist muscle exhibits a small amount of coactivation proportional to the magnitude of the agonist burst, but a large reciprocal burst (antagonistic burst) occurs at or just before the peak  $dF/dt$ . The antagonist burst lasts throughout the falling phase of  $dF/dt$ . A high correlation between the force magnitude and the first agonist burst magnitude was noted. The second agonist burst was reported only for a rapid change in the imposed force magnitudes (Figure 3.4, right). Consequently, the patterns of the adaptive desired tension force in the robot's antagonist tendon could be extracted in both contact and non-contact tasks. However, a further and more detailed analysis on the topic is required.

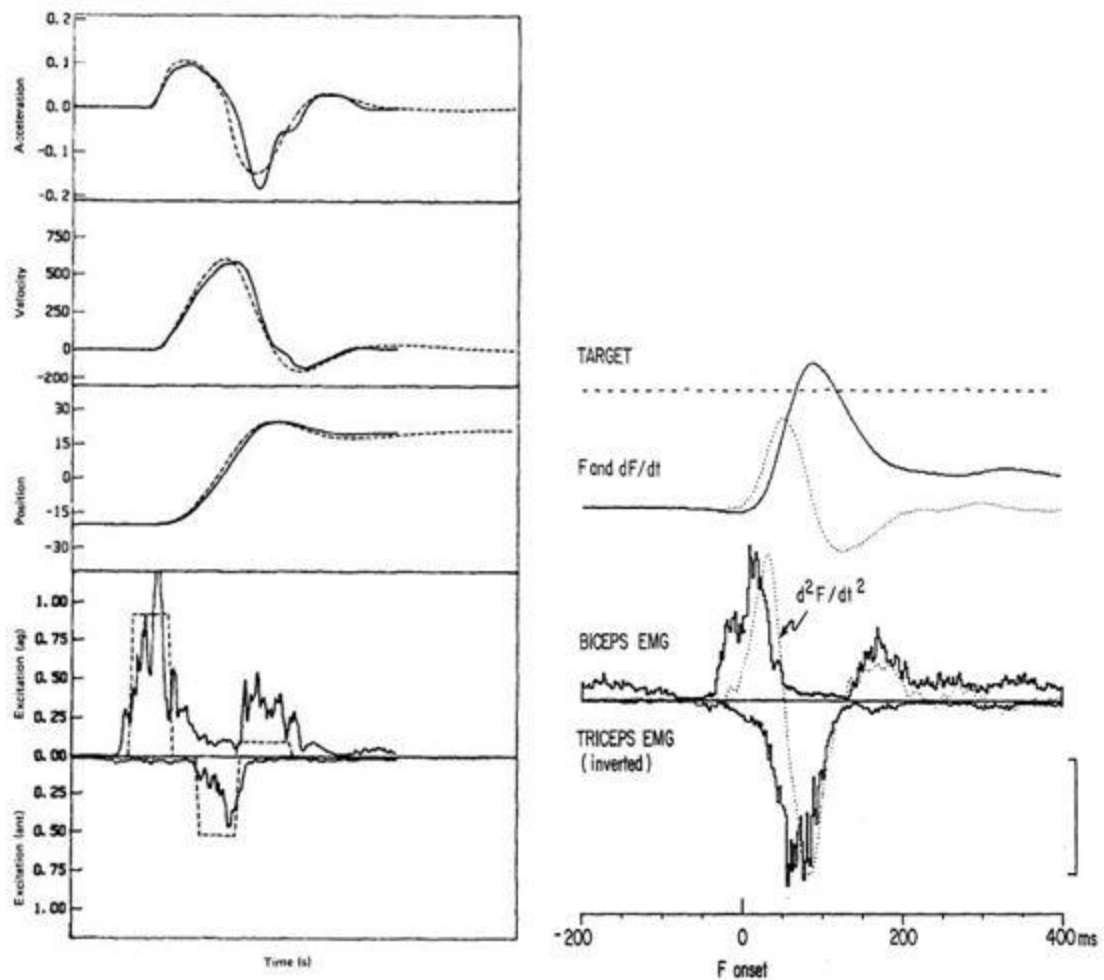


Figure 3.4. Experimental results of agonist and antagonist EMG muscle activity for typical tasks: Head movement dynamics measured by Hannaford and Stark [195]. Experimental records (solid lines) and simulation of the same movement (dashed lines) are depicted. Plotted are acceleration ( $10^3 \text{ deg/s}^2$ ), velocity ( $\text{deg/s}$ ), position ( $\text{deg}$ ), normalized EMGs from agonist (ag) and antagonist (ant) muscles, and rectangular approximations to EMG bursts used as inputs to the model. EMG signals clearly resemble three main areas: the first agonist burst (movement initiator), the antagonist burst (braking pulse), and the second agonist burst (fine joint position tuning) - (left); Triphasic EMG pattern in rapid force pulses applied to examinees – isometric experiment reported by Gordon and Ghez in [196]. The upper part of the figure shows force (solid line)  $F$  (peak force 58N) and force derivative (dotted line)  $dF/dt$  (peak 1575 N/s). The lower part of the figure shows the agonist (biceps) EMG, the antagonist (triceps) EMG, and the second force derivative (dotted line)  $d^2F/dt^2$  (peak 29800 N/s<sup>2</sup>) - (right).

The first research team that implemented a tri-phasic activation pattern to control a real

robot was Kawamura's group at Vanderbilt University. Their work describes a biologically-inspired control architecture for the McKibben actuated limbs of a humanoid robot [197]. The antagonistically-driven joints were actuated by pneumatic artificial muscles using biological control models observed in human muscle electromyograms of reaching movements in the vertical plane. The humanoid robot's muscles, actuated by pressure control, were controlled with feedforward pressure patterns analogous to those observed in human EMG activity. When the reached trajectory did not closely match the expected response that was associated in memory, and the feedback controller adjusted the activation patterns as necessary. However, the effects of misperception of loading conditions were examined to enhance bio-inspired feedforward control. The demonstrated results have only opened this direction of research, which is expected to reach its peak in very near future.

Following this biological paragon, we introduce an adaptive tension force in the antagonistic tendon – one that prevents tendon slackening and controls joint stiffness. The reference tendon force should thus retain a low value, to ensure good energy efficiency and prevent tendon slackening. However, when switching is likely to occur, the antagonistic tendon force should be increased to raise the overall joint stiffness and prepare the joint for the new situation. At the same time, by slightly increasing the force and keeping that ascending force slope, the follower tendon prepares to progressively take over the puller role. This is the ultimate way to achieve smooth trajectories and avoid abrupt force changes, necessary for good tracking as explained in Subsection 3.3.1, which clarifies the necessity for smooth reference trajectories of both joint position (4<sup>th</sup> order smoothness) and reference tendon force (2<sup>nd</sup> order smoothness). A smooth reference trajectory could be compromised by switching. To prevent this, the adaptive tension force must be well planned, smooth and shaped according to the descending pulling force. However, the time instant in which the reference tension force should start rising, and the level of its rising slope, is still the subject of debate. Some of the criteria that can be used are the difference between the forces in the puller and follower tendons, the decreasing slope of the puller tendon force, the previous maximum tension force, the joint velocity, the estimated effective joint inertia, etc. However, until a comprehensive study on this open issue is undertaken, we will deal

with the adaptive tension force using intuition and heuristics to create fuzzy rules with the above input parameters and the output reference tension force with a logarithmic slope [161]. Hopefully even such a heuristic approach can contribute to significant findings in this research direction that targets both biomechanics and engineers.

Distribution of the overall joint torque into agonist and antagonist portions has also been studied by Komiya et al. [198] at Tokyo University. This research was carried out in parallel with that on the puller-follower approach and these authors came to very similar conclusions, but working with a pneumatically-actuated antagonistic joint. Namely, they calculated the required overall torque ( $\tau_{ref}$ ) and divided it into the agonist force ( $F_{2ref}$ ) and antagonist force ( $F_{1ref}$ ) by setting the minimal force ( $T_m$ ) in the antagonist tendon or the mean value of agonist and antagonist forces ( $T_o$ ) – see Figure 3.5. Finally, the authors opted for a minimal tension force also in the case of the pneumatically-driven antagonistic actuators. They proved this by both better system performance and safety against wire slackening.

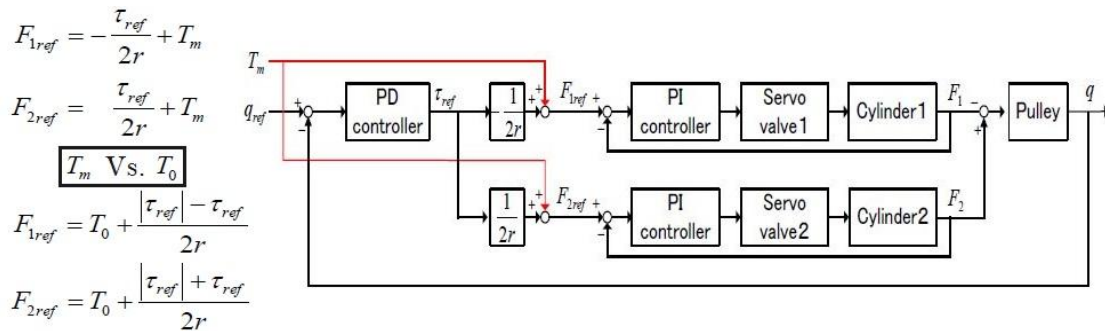


Figure 3.5. Force distribution between agonist and antagonist pneumatic drives using minimal or mean tension value. The approach presented by Komiya et al. [198] to antagonistic joint position control using a cascade controller: PI controlled force as the an inner loop and PD position control as the outer loop.

The puller-follower principle is demonstrated on a simple circular robotic joint driven by antagonistically-coupled tendons with linear springs as a source of compliance in Subsection 3.3.1. The driving torques of both motors are considered as control inputs (Figure 3.2). The same procedure and methodology apply even in the case of a nonlinear triangular joint structure (Figure 2.5), a different source of compliance

(nonlinear springs: quadratic or exponential springs), or a different level of control inputs (if control inputs are motor currents or voltages), as shown in [154]. The same control approach pertains to antagonistic joints with tendons of non-linear characteristics: quadratic (Subsection 3.3.2) and exponential (Subsection 3.3.3). The simulation results that validate this control design are given in Subsection 0.

### 3.3.1 Antagonistic joints with linear tendon characteristics

The complete model of joint dynamics in the case of a robotic joint driven by antagonistically-coupled compliant drives with elastic elements of linear characteristics is given by Equations (3.3) through (3.11). Equation (3.3) represents joint dynamics; (3.4) and (3.5) are equations of the dynamic balance of the two motors:  $A$  and  $B$ ; the contribution of both tendons to overall joint dynamics is given by (3.6) and (3.9); (3.7) and (3.10) introduce elastic properties of the springs as a source of compliance, which are basic linear relations here; and, finally, (3.8) and (3.11) demonstrate elastic element elongations due to joint and motor movement. For easier understanding, we recall the symbols from Figure 3.2:  $q$  – joint position,  $\theta_A(\theta_B)$  – motor  $A$  ( $B$ ) position,  $I_j$  – effective inertia of the link,  $I_m^A(I_m^B)$  – rotor  $A$  ( $B$ ) inertia,  $B_m^A(B_m^B)$  – motor  $A$  ( $B$ ) viscous friction,  $r_j$  – joint radius,  $r_m$  – motor pulley radius,  $F_A(F_B)$  – tendon  $A$  ( $B$ ) force (its contribution to the net joint torque is denoted by  $\tau_A(\tau_B)$ , and  $\Delta l_A(\Delta l_B)$  spring  $A$  ( $B$ ) elongation). Note that springs in antagonistically coupled tendons are always of the same kind and assumed to have the same characteristics.

$$I_j \ddot{q} = r_j (F_B - F_A) \quad (3.3)$$

$$I_m^A \ddot{\theta}_A + B_m^A \dot{\theta}_A + \tau_A = \tau_m^A \quad (3.4)$$

$$I_m^B \ddot{\theta}_B + B_m^B \dot{\theta}_B + \tau_B = \tau_m^B \quad (3.5)$$

$$\tau_A = F_A r_m \quad (3.6)$$

$$F_A = k \Delta l_A \quad (3.7)$$

$$\Delta l_A = r_m \theta_A + r_j q \quad (3.8)$$

$$\tau_B = F_B r_m \quad (3.9)$$

$$F_B = k \Delta l_B \quad (3.10)$$

$$\Delta l_B = r_m \theta_B - r_j q \quad (3.11)$$

The state space form which joint and motor positions and velocities are considered as state space variables  $\mathbf{X} = [x_1 \ x_2 \ x_3 \ x_4 \ x_5 \ x_6]^T = [\theta_A \ \dot{\theta}_A \ \theta_B \ \dot{\theta}_B \ q \ \dot{q}]^T$ , motor torques  $\mathbf{u} = [\tau_m^A \ \tau_m^B]^T$  as control inputs, and the joint position  $q$  and the force in the antagonistic tendon  $F_{ANT}$  as outputs, is given by (3.12).

$$\dot{\mathbf{x}} = \mathbf{f}(\mathbf{x}) + \mathbf{g}(\mathbf{x})\mathbf{u} = \begin{bmatrix} \frac{x_2}{x_1} \\ -\frac{r_m^2 k}{I_m^A} x_1 - \frac{B_m^A}{I_m^A} x_2 - \frac{r_m r_j k}{I_m^A} x_5 \\ \frac{x_4}{x_3} \\ -\frac{r_m^2 k}{I_m^B} x_3 - \frac{B_m^B}{I_m^B} x_4 + \frac{r_m r_j k}{I_m^B} x_5 \\ \frac{x_6}{x_5} \\ -\frac{r_m r_j k}{I_j} x_1 + \frac{r_m r_j k}{I_j} x_3 - \frac{2 r_j^2 k}{I_j} x_5 \end{bmatrix} + \begin{bmatrix} 0 & 0 \\ \frac{1}{I_m^A} & 0 \\ 0 & 0 \\ 0 & \frac{1}{I_m^B} \\ 0 & 0 \\ 0 & 0 \end{bmatrix} \mathbf{u} \quad (3.12)$$

$$\mathbf{y} = [y_1 \ y_2] = [q \ F_{ANT}]$$

The idea of static feedback linearization is to decouple control of joint position and antagonistic tendon force, and transform system (3.12) into a new fully-controllable and observable system. This can be accomplished if the sum of the relative degrees of the outputs  $q$  and  $F_{ANT}$  is equal to the state dimension, and if the decoupling matrix of the system is non-singular. Finally, two decoupled single-input-single-output (SISO) systems are obtained, each of which is controlled by separate intermediate control inputs  $v_q$  and  $v_F$ . By straightforward application of feedback linearization [199], we differentiate outputs  $q$  and  $F_{ANT}$  until a linear relation to inputs  $\tau_m^A$  and/or  $\tau_m^B$  is obtained. To this end, the output  $q$  is differentiated four times (3.13) and the linear input/output relation for  $F_{ANT}$  is found in its second derivative (3.14). Therefore, the relative degree of the outputs is  $4+2=6$ , which is equal to the system order.

$$q^{(4)} = L_f^4 h_q(x) + E_{11} \tau_m^A + E_{12} \tau_m^B \quad (3.13)$$

$$F_{ANT}^{(2)} = L_f^2 h_F(x) + E_{21} \tau_m^A + E_{22} \tau_m^B \quad (3.14)$$

Let us introduce  $\mathbf{E}(\mathbf{x})$  as the decoupling matrix (3.15), and  $L_f h(\mathbf{x})$  as the Lie derivative

of  $h(\mathbf{x})$  along vector function  $f(\mathbf{x})$  - (3.16). The second condition that must be fulfilled for feedback linearization is non-singularity of the decoupling matrix  $\mathbf{E}(\mathbf{x})$ . The decoupling matrix for the described system is the upper triangular matrix and obviously nonsingular (3.15).

$$\mathbf{E} = \begin{bmatrix} E_{11} & E_{12} \\ E_{21} & E_{22} \end{bmatrix} = \begin{bmatrix} -\frac{kr_j r_m}{I_j I_m} & \frac{kr_j r_m}{I_j I_m} \\ 0 & \frac{kr_m}{I_m} \end{bmatrix} \quad (3.15)$$

$$L_f^4 h_q(x) = \frac{k r_j}{I_j} \left( \frac{B r_m (x_2 - x_4) + k r_m^2 (2r_j x_5 + r_m (x_1 - x_3))}{I_m} + \frac{2 k r_j^2 (2 r_j x_5 + r_m (x_1 - x_3))}{I_j} \right) \quad (3.16)$$

$$L_f^2 h_F(x) = k \left( \frac{-B r_m x_4 + k r_m^2 (r_j x_5 - r_m x_3)}{I_m} + \frac{k r_j^2 (2 r_j x_5 + r_m (x_1 - x_3))}{I_j} \right)$$

Therefore, the input  $\mathbf{u}$  can be transformed as in (3.17), to achieve independent control of both the joint position and antagonistic force via the newly-defined intermediate input  $\mathbf{v} = [v_q \ v_F]^T$ . The new state vector becomes  $\mathbf{z} = [q \ \dot{q} \ \ddot{q} \ q^{(3)} \ F_{ANT} \ \dot{F}_{ANT}]^T$ , and the complete state space model (3.18) is:

$$\mathbf{u} = \mathbf{E}^{-1} \left( - \begin{bmatrix} L_f^4 h_q(x) \\ L_f^2 h_F(x) \end{bmatrix} + \begin{bmatrix} v_q \\ v_F \end{bmatrix} \right) \quad (3.17)$$

$$\dot{\mathbf{z}} = \begin{bmatrix} 0 & 1 & 0 & 0 & 0 & 0 \\ 0 & 0 & 1 & 0 & 0 & 0 \\ 0 & 0 & 0 & 1 & 0 & 0 \\ 0 & 0 & 0 & 0 & 0 & 0 \\ 0 & 0 & 0 & 0 & 0 & 1 \\ 0 & 0 & 0 & 0 & 0 & 0 \end{bmatrix} \mathbf{z} + \begin{bmatrix} 0 & 0 \\ 0 & 0 \\ 0 & 0 \\ 1 & 0 \\ 0 & 0 \\ 0 & 1 \end{bmatrix} \mathbf{v} \quad (3.18)$$

It follows from (3.13) through (3.18) that  $[q^{(4)} \ F_{ANT}^{(2)}]^T = [v_q \ v_F]^T$ . Thus, if we choose  $q_d$  as the desired joint position and  $F_{ANT,d}$  as the desired pre-tension of the antagonistic tendon, a basic control law (3.19) can be applied. Therefore, state feedback linearization allows control of both the positions and the force in the antagonist tendon of the compliant robot joint, by means of two totally independent linear controllers, composed of static state feedback and feedforward action:

$$\begin{aligned}
v_q &= q_d^{(4)} + K_{q3} \left( q_d^{(3)} - L_f^3 h_q(x) \right) + K_{q2} \left( \ddot{q}_d - L_f^2 h_q(x) \right) + K_{q1} \left( \dot{q}_d - L_f h_q(x) \right) + K_{q0} \left( q_d - h_q(x) \right) \\
v_F &= \ddot{F}_{ANT\_d} + K_{F1} \left( \dot{F}_{ANT\_d} - L_f h_F(x) \right) + K_{F0} \left( F_{ANT\_d} - h_F(x) \right)
\end{aligned} \tag{3.19}$$

Stability and convergence to zero tracking error are ensured for (3.19) if the gains  $K_{q0}$ ,  $K_{q1}$ ,  $K_{q2}$ ,  $K_{q3}$ ,  $K_{F0}$ ,  $K_{F1}$  are chosen so the polynomials (3.20) are Hurwitz's.

$$\begin{aligned}
s^4 + K_{q3}s^3 + K_{q2}s^2 + K_{q1}s + K_{q0} &= 0 \\
s^2 + K_{F1}s + K_{F0} &= 0
\end{aligned} \tag{3.20}$$

As explained in [190], not only do the reference trajectories for joint position and antagonistic tendon force need to be smooth, but also their derivatives up to the derivative that directly depends on the control input. Theoretically, if the desired joint positions are continuous up to the 4<sup>th</sup> order  $q_{ref}(t) \in \mathbb{C}^4$ ;  $t \in [0, T]$ , and the pre-tension is planned to be continuous up to the 2<sup>nd</sup> order  $F_{ref}(t) \in \mathbb{C}^2$ ;  $t \in [0, T]$ , asymptotic trajectory/force tracking is achieved. These reference trajectories can be the result of a higher control level, an optimization process as in the case of [35], etc. In this thesis, we set the trajectories manually without considering higher control levels and optimization issues.

Finally, feedback linearization to the multiple-input-multiple-output (MIMO) system (robot joint actuated by antagonistically-coupled compliant drives) reduces the required control design to two decoupled single-input-single-output (SISO) subsystems – two integrator chains. The first represents joint position tracking  $G_p$  and the second stands for antagonistic tendon force tracking  $G_f$ . Two target systems can be described by (3.21) and (3.22), respectively.

$$G_p(s) = \frac{1}{s^4} \tag{3.21}$$

$$G_f(s) = \frac{1}{s^2} \tag{3.22}$$

The same approach can be used for elastic elements of different characteristics. In view of the required space, a discussion is omitted and only the final results are presented for

quadratic and exponential springs. Nonlinear springs are of special interest since linear springs, although easier to design and manufacture, do not provide variable joint stiffness.

### 3.3.2 Antagonistic joints with quadratic tendon characteristics

In the case of quadratic springs, Equations (3.3) through (3.11) still hold; only the force-displacement characteristics are changed according to (3.23) and (3.24) instead of (3.7) and (3.10). The index  $QA$  stands for quadratic spring characteristics.

$$F^A_{QA} = \text{sign}(\Delta l_A)[k_2(\Delta l_A)^2 + k_1|\Delta l_A| + k_0] \quad (3.23)$$

$$F^B_{QA} = \text{sign}(\Delta l_B)[k_2(\Delta l_B)^2 + k_1|\Delta l_B| + k_0] \quad (3.24)$$

The following control system analysis assumes that both tendons are stretched all the time ( $\Delta l_A > 0$ ,  $\Delta l_B > 0$ ), since that is the main requirement for tendon-driven joint control and the preservation of controllability. Consequently, the state-space form of an antagonistically-actuated joint with quadratic springs is given by (3.25):

$$\begin{aligned} \dot{\mathbf{x}} &= \mathbf{f}(\mathbf{x}) + \mathbf{g}(\mathbf{x})\mathbf{u} = \\ & \begin{bmatrix} -\frac{r_m^3 k_2}{I_m^A} x_1^2 - \frac{r_m^2 k_1}{I_m^A} x_1 - \frac{2r_m^2 r_j k_2}{I_m^A} x_1 x_5 - \frac{B_m^A}{I_m^A} x_2 - \frac{r_m r_j k_1}{I_m^A} x_5 - \frac{r_m r_j^2 k_2}{I_m^A} x_5^2 - \frac{r_m}{I_m^A} k_0 \\ -\frac{r_m^3 k_2}{I_m^B} x_3^2 - \frac{r_m^2 k_1}{I_m^B} x_3 + \frac{2r_m^2 r_j k_2}{I_m^A} x_3 x_5 - \frac{B_m^B}{I_m^B} x_4 + \frac{r_m r_j k_1}{I_m^B} x_5 - \frac{r_m r_j^2 k_2}{I_m^B} x_5^2 - \frac{r_m}{I_m^B} k_0 \\ -\frac{r_m r_j k_1}{I_j} x_1 - \frac{r_m^2 r_j k_2}{I_j} x_1^2 - \frac{2r_m r_j^2 k_2}{I_j} (x_1 + x_3)x_5 + \frac{r_m r_j k_1}{I_j} x_3 + \frac{r_m^2 r_j k_2}{I_j} x_3^2 - \frac{2r_j^2 k_1}{I_j} x_5 \end{bmatrix} + \begin{bmatrix} 0 & 0 \\ \frac{1}{I_m^A} & 0 \\ 0 & 0 \\ 0 & \frac{1}{I_m^B} \\ 0 & 0 \\ 0 & 0 \end{bmatrix} \mathbf{u} \\ \mathbf{y} &= [y_1 \quad y_2] = [q_{QA} \quad F_{ANTQA}] \end{aligned} \quad (3.25)$$

In the same manner, the outputs  $q_{QA}$  and  $F_{ANTQA}$  are differentiated until linear relations to the inputs  $\tau_m^A$  and/or  $\tau_m^B$  are obtained. Again, the output  $q_{QA}$  needs to be differentiated four times (3.26), and the linear input-output relation for  $F_{ANTQA}$  is found in its second derivative (3.27).

$$q_{QA}^{(4)} = L_f^4 h_{q_{QA}}(x) + E_{11QA}(x) \tau_m^A + E_{12QA}(x) \tau_m^B \quad (3.26)$$

$$F_{ANTQA}^{(2)} = L_f^2 h_{F_{QA}}(x) + E_{21QA}(x) \tau_m^A + E_{22QA}(x) \tau_m^B \quad (3.27)$$

Therefore:

$$\begin{aligned} \mathbf{E}_{QA}(\mathbf{x}) &= \begin{bmatrix} E_{11QA}(\mathbf{x}) & E_{12QA}(\mathbf{x}) \\ E_{21QA}(\mathbf{x}) & E_{22QA}(\mathbf{x}) \end{bmatrix} \\ &= \begin{bmatrix} \frac{r_j r_m (k_1 + 2 k_2 r_j x_5 + 2 k_2 r_m x_1)}{I_m I_j} & \frac{r_j r_m (k_1 - 2 k_2 r_j x_5 + 2 k_2 r_m x_3)}{I_m I_j} \\ 0 & \frac{r_m (k_1 - 2 k_2 r_j x_5 + 2 k_2 r_m x_3)}{I_m} \end{bmatrix} \end{aligned} \quad (3.28)$$

$$\begin{aligned} L_f^4 h_{q_{QA}}(x) &= \frac{2 r_j^3}{I_j^2} (k_1 + k_2 r_m (x_1 + x_3)) (2 r_j x_5 + r_m (x_1 - x_3)) (k_1 + k_2 r_m (x_1 + x_3)) \\ &+ \frac{r_m r_j}{I_m I_j} (k_1 + k_2 r_m (x_1 + x_3)) (2 k_2 r_j r_m^2 x_5 (x_1 + x_3) + k_1 r_m (2 r_j x_5 + r_m (x_1 - x_3)) + B_m (x_2 - x_4)) \\ &+ \frac{k_2 r_j r_m}{I_m I_j} (2 r_j x_5 + r_m (x_1 - x_3)) (B_m (x_2 + x_4) + r_m (2 k_0 + k_2 (2 r_j^2 x_5^2 + 2 r_j r_m x_5 (x_1 - x_3) + r_m^2 (x_1^2 + x_3^2) + \\ &k_1 r_m (x_1 + x_3))) - \frac{2 k_2 r_j r_m}{I_j} (2 r_j x_6 + r_m (x_2 - x_4)) (x_2 + x_4) \end{aligned} \quad (3.29)$$

$$\begin{aligned} L_f^2 h_{F_{QA}}(x) &= k_2 (2 r_j^2 x_6^2 + 2 r_m^2 x_4^2 - 4 r_j r_m x_6 x_4) \\ &+ \frac{r_m}{I_m} (2 k_2 (r_j x_5 - r_m x_3) - k_1) (B_m x_4 + r_m (k_0 + k_2 (r_j^2 x_5^2 - 2 r_j r_m x_5 x_3 + r_m^2 x_3^2) - k_1 (r_j x_5 - r_m x_3))) \\ &- \frac{r_j^2}{I_j} (2 k_2 (r_j x_5 - r_m x_3) - k_1) (2 r_j x_5 + r_m (x_1 - x_3)) (k_1 + k_2 r_m (x_1 + x_3)) \end{aligned}$$

Obviously, the relative degree of the outputs (4+2=6) is again equal to the system order, and the decoupling matrix is singular only if either equality from (3.30) is fulfilled.

$$k_1 + 2 k_2 r_j x_5 + 2 k_2 r_m x_1 = 0 \quad \vee \quad k_1 - 2 k_2 r_j x_5 + 2 k_2 r_m x_3 = 0 \quad (3.30)$$

According to (3.30), the decoupling matrix becomes singular if joint position ( $q \equiv x_5$ ) is related to motor positions ( $\theta_A \equiv x_1, \theta_B \equiv x_3$ ) according to (3.31):

$$q = -\frac{r_m}{r_j} \theta_A - \frac{k_1}{2 k_2 r_j} \quad \vee \quad q = \frac{r_m}{r_j} \theta_B + \frac{k_1}{2 k_2 r_j} \quad (3.31)$$

Note that  $\frac{k_1}{2k_2r_j} \geq 0$  is always valid, due to quadratic spring characteristics ( $k_1 \geq 0$ ,  $k_2 > 0$ ). However, if the switching logic is applied as explained earlier in this section, both tendons remain stretched. Therefore, it follows from (3.23) and (3.24) that  $\Delta l_A > 0$  and  $\Delta l_B > 0$ , or, recalling (3.8) and (3.11), we can prove the non-singularity of the decoupling matrix  $\mathbf{E}_{QA}(\mathbf{x})$  and, consequently, the validity of puller-follower control since neither equalities given by (3.30) can be satisfied.

$$q > -\frac{r_m}{r_j}\theta_A \wedge q < \frac{r_m}{r_j}\theta_B \Rightarrow -\frac{r_m}{r_j}\theta_A - \frac{k_1}{2k_2r_j} < -\frac{r_m}{r_j}\theta_A < q < \frac{r_m}{r_j}\theta_B < \frac{r_m}{r_j}\theta_B + \frac{k_1}{2k_2r_j} \quad (3.32)$$

Finally, the control input given by (3.33) linearizes and decouples the system into the form of (3.18). The basic control law to the new intermediate inputs, as already given in (3.19) can be applied.

$$\mathbf{u} = \mathbf{E}_{QA}^{-1} \left( - \begin{bmatrix} L_f^4 h_{q_{QA}}(x) \\ L_f^2 h_{F_{QA}}(x) \end{bmatrix} + \begin{bmatrix} v_q \\ v_F \end{bmatrix} \right) \quad (3.33)$$

### 3.3.3 Antagonistic joints with exponential tendon characteristics

In the case of springs with exponential characteristics, (3.34) and (3.35) hold instead of (3.7) and (3.10), while everything else remains the same. The index *EXP* stands for exponential spring characteristics.

$$F^A_{EXP} = \text{sign}(\Delta l_A) k_e (e^{\alpha_e |\Delta l_A|} - 1) \quad (3.34)$$

$$F^B_{EXP} = \text{sign}(\Delta l_B) k_e (e^{\alpha_e |\Delta l_B|} - 1) \quad (3.35)$$

The form (3.36) represents the state-space form of an antagonistically-actuated joint with exponential springs (again  $\Delta l_A > 0$  and  $\Delta l_B > 0$  are assumed and proved in further control system analysis):

$$\dot{\mathbf{x}} = \mathbf{f}(\mathbf{x}) + \mathbf{g}(\mathbf{x})\mathbf{u} = \begin{bmatrix} x_2 \\ -\frac{r_m k_e}{I_m^A} (e^{\alpha_e(r_m x_1 + r_j x_5)} - 1) - \frac{B_m^A}{I_m^A} x_2 \\ x_4 \\ -\frac{r_m k_e}{I_m^B} (e^{\alpha_e(r_m x_3 - r_j x_5)} - 1) - \frac{B_m^B}{I_m^B} x_4 \\ x_6 \\ \frac{r_j k_e}{I_j} (-e^{\alpha_e(r_m x_1 + r_j x_5)} + e^{\alpha_e(r_m x_3 - r_j x_5)}) \end{bmatrix} + \begin{bmatrix} 0 & 0 \\ \frac{1}{I_m^A} & 0 \\ 0 & 0 \\ 0 & \frac{1}{I_m^B} \\ 0 & 0 \\ 0 & 0 \end{bmatrix} \mathbf{u} \quad (3.36)$$

$$\mathbf{y} = [y_1 \quad y_2] = [q_{EXP} \quad F_{ANTEXP}]$$

It is worth mentioning that if one of the tendons slackens, controllability is lost and models (3.12), (3.25) and (3.36) do not hold any more.

By differentiating the outputs  $q_{EXP}$  and  $F_{ANTEXP}$ , linear relations to the inputs  $\tau_m^A$  and/or  $\tau_m^B$  are obtained in their 4<sup>th</sup> (3.37) and 2<sup>nd</sup> differential (3.38), respectively.

$$q_{EXP}^{(4)} = L_f^4 h_{q_{EXP}}(x) + E_{11EXP}(x) \tau_m^A + E_{12EXP}(x) \tau_m^B \quad (3.37)$$

$$F_{ANTEXP}^{(2)} = L_f^2 h_{F_{EXP}}(x) + E_{21EXP}(x) \tau_m^A + E_{22EXP}(x) \tau_m^B \quad (3.38)$$

The decoupling matrix  $\mathbf{E}_{EXP}(\mathbf{x})$  and Lie derivatives of the appropriate order can be extracted from (3.37) and (3.38). Feedback linearization can thus be applied as an integral part of the puller-follower approach:

$$\mathbf{E}_{EXP}(\mathbf{x}) = \begin{bmatrix} E_{11EXP}(\mathbf{x}) & E_{12EXP}(\mathbf{x}) \\ E_{21EXP}(\mathbf{x}) & E_{22EXP}(\mathbf{x}) \end{bmatrix}$$

$$= \begin{bmatrix} \frac{\alpha_e k_e r_j r_m e^{\alpha_e(r_j x_5 + r_m x_1)}}{I_m I_j} & \frac{\alpha_e k_e r_j r_m e^{-\alpha_e(r_j x_5 - r_m x_3)}}{I_m I_j} \\ 0 & \frac{\alpha_e k_e r_m e^{-\alpha_e(r_j x_5 - r_m x_3)}}{I_m} \end{bmatrix} \quad (3.39)$$

$$L_f^4 h_{q_{EXP}}(x) = \frac{k_e r_j \alpha_e}{I_j} e^{\alpha_e(r_j x_5 + r_m x_1)} \left( \frac{r_m (B x_2 + k_e r_m (e^{\alpha_e(r_j x_5 + r_m x_1)} - 1))}{I_m} + \frac{k_e r_j^2 (e^{\alpha_e(r_j x_5 + r_m x_1)} - e^{-\alpha_e(r_j x_5 - r_m x_3)})}{I_j} - \alpha_e (r_j x_6 + r_m x_2)^2 \right) - \frac{k_e r_j \alpha_e}{I_j} e^{-\alpha_e(r_j x_5 - r_m x_3)} \left( \frac{r_m (B x_4 + k_e r_m (e^{-\alpha_e(r_j x_5 - r_m x_3)} - 1))}{I_m} - \frac{k_e r_j^2 (e^{\alpha_e(r_j x_5 + r_m x_1)} - e^{-\alpha_e(r_j x_5 - r_m x_3)})}{I_j} - \alpha_e (r_j x_6 - r_m x_4)^2 \right)$$

$$L_f^2 h_{F_{EXP}}(x) = \alpha_e^2 k_e e^{-\alpha_e(r_j x_5 - r_m x_3)} (r_j x_6 - r_m x_4)^2 \tag{3.40} - \alpha_e k_e e^{-\alpha_e(r_j x_5 - r_m x_3)} \left( \frac{r_m (B x_4 + k_e r_m (e^{-\alpha_e(r_j x_5 - r_m x_3)} - 1))}{I_m} - \frac{k_e r_j^2 (e^{\alpha_e(r_j x_5 + r_m x_1)} - e^{-\alpha_e(r_j x_5 - r_m x_3)})}{I_j} \right)$$

To satisfy the preconditions for feedback linearization, the relative degree of the outputs (4+2=6) is conformed to equal the system order – 6, which ensures the absence of zero dynamics. The fact that the decoupling matrix (3.39) is always nonsingular goes in favor of exponential springs as elastic elements. Like in the case of systems with linear (3.17) or quadratic (3.33) springs, full linearization and decoupling are achieved by the control input (3.41).

$$\mathbf{u} = \mathbf{E}_{EXP}^{-1} \left( - \begin{bmatrix} L_f^4 h_{q_{EXP}}(x) \\ L_f^2 h_{F_{EXP}}(x) \end{bmatrix} + \begin{bmatrix} v_q \\ v_F \end{bmatrix} \right) \tag{3.41}$$

### 3.3.4 Simulation results

A schematic of the puller-follower control approach is presented in *Figure 3.6* for illustration purposes. The same schematic stands for all types of elastic elements (linear, quadratic or exponential), as well as for any antagonistic joint configuration (circular or triangular). One can distinguish several core blocks of puller-follower control: the feedback linearization block, which linearizes and decouples the system; four single-input-single-output controllers (two position controllers and two force controllers); the switching logic block that keeps tension in both tendons to ensure controllability; and

the adaptive reference tension force that trade-offs between energy efficiency and controllability of the system, which is of particular importance when tendons exchange their roles. The target system can be any type of antagonistic joint (circular or triangular joint configuration) driven by any of the compliant elements (linear, quadratic or exponential). The sensor block provides motor and joint positions, and consequently the tendon forces, knowing the force-deflection relation of the elastic elements. The switching logic block preserves tension in both tendons by alternating the puller and follower roles of the tendons, to ensure controllability. The adaptive reference tension force block trade-offs between energy efficiency (by keeping the reference tension force low) and controllability of the system (by raising the reference tension force in cases of switching, where oscillation could occur and jeopardize system performance and stability). In support of high energy efficiency, the reference tension force is always kept at a predefined low level. At the same time, the other tendon produces enough force to achieve the desired motion and ensure trajectory tracking. To avoid tendon slackening and maintain controllability, the tendons sometimes switch their roles.

*Table 3.1. Joint, link and spring parameters used for simulations in Subsection 0.*

Label	Numerical value	Unit	Description
$l_r$	0.15	[m]	Circular joint parameters
$\alpha$	$\pi/2$	[rad]	
$m$	3	[kg]	Link parameters
$I$	0.015	[kgm <sup>2</sup> ]	
$k$	200	[N/m]	Linear spring coeff.
$k_2$	100	[N/m <sup>2</sup> ]	Quadratic spring coeff.
$k_1$	0	[N/m]	Quadratic spring coeff.
$k_0$	0	[N]	Quadratic spring coeff.
$k_e$	5	[N]	Exponential spring coeff.
$\alpha_e$	2	[1/m]	Exponential spring coeff.

In order to validate the puller-follower approach, simulation experiments were carried out for all types of elastic elements: linear (Figure 3.7), quadratic (Figure 3.8) and exponential (Figure 3.9) springs. The demonstrated example involved the desired smooth changes in joint position in the range from  $-90deg$  to  $90deg$ , whereas the

reference tension force was assumed to be constant, keeping the force at  $F_{ref} = 3N$ . The results demonstrated only the basic concepts and validated the approach. More detailed insight into position and force control is provided in the following subsections. Also, the adaptive tension force is omitted from the results, to facilitate comparison and observe the results obtained for different types of elastic transmission more clearly. It is apparent that both position and force tracking are satisfactory. The main difference between the figures lies in motor positioning, since motors A and B were positioned so as to ensure trajectory and force tracking via different elastic elements between the antagonistic drives and the joint. Exchanging the roles between the tendons, or “switching”, is depicted for the sake of illustration in the graphic called Puller-follower modes. The simulation parameters applied are shown in *Table 3.1*. Controllers (3.78) and (3.81) for the decoupled force subsystem and position subsystem were used, although any controller that satisfies (3.20) can be employed.

In summary, some important features of the puller-follower approach need to be pointed out. It should be noted that the puller-follower approach is strongly model-dependent, as in the case of all feedback linearization methods. To control a multi-joint system, the phenomena of dynamic coupling between joints, the variable effective joint inertia (depending on the position of the entire distal mechanism), and the influence of gravity need to be addressed. An interesting point raised by this research is the moment in which the adaptive tension force should be applied. Although a heuristic solution in proposed by the author in [106], this topic should be considered carefully and addressed in patterns of antagonistic muscle activity. The issues are outlined and some improvements of the puller-follower approach suggested in [159], [106], and also summarized in Subsection 3.5 of this thesis. In particular, robust control utilizing the  $H_\infty$  loop shaping method [161] (a combination of the loop shaping and robust stabilization proposed in [200]), gravity compensation, estimation of effective joint inertia, and the like have been discussed.

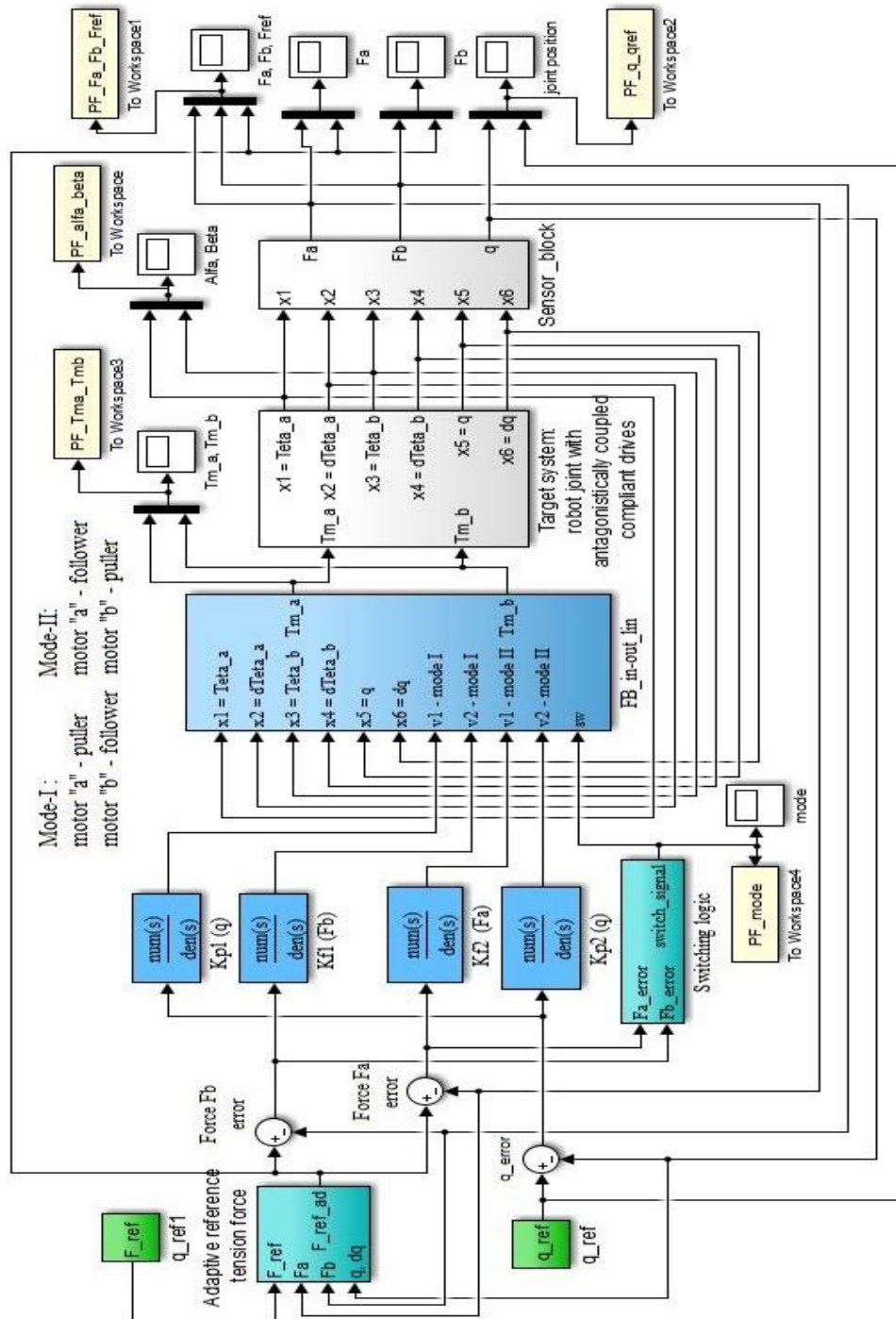


Figure 3.6. Puller-follower control scheme. Alternatively, tendon forces can be measured directly by strain gauges. The basic control part contains two components (shown in blue): the feedback linearization block that linearizes and decouples the position and force subsystems, and four single-input-single-output controllers (two position controllers and two force controllers), whose activation alternates depending on the active mode. Additional control logic includes the switching logic block and the adaptive tension force block, both depicted in green.

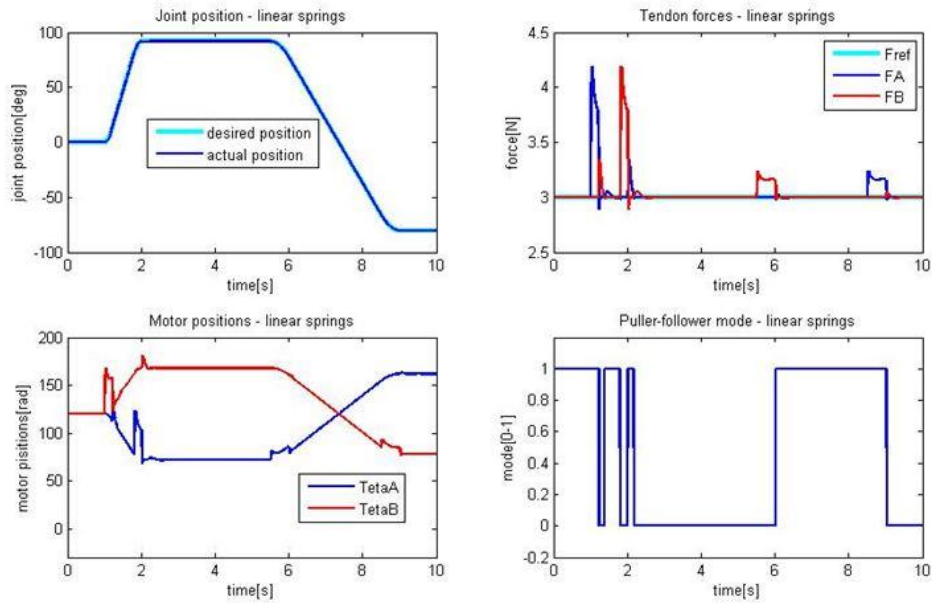


Figure 3.7. Puller-follower control applied to an antagonistically-coupled drive using linear springs as elastic elements (3.7), (3.10). Validation is demonstrated by trajectory tracking (top left); Force control in the antagonistic tendon (top right); The positions of motor A and motor B, whose simultaneous action ensures proper joint position and antagonistic force (bottom left); Changing of the roles of motor A and motor B (“switching”) – mode 1 stands for motor A as the puller, and motor B as the follower, or vice-versa if mode 0 is active (bottom right).

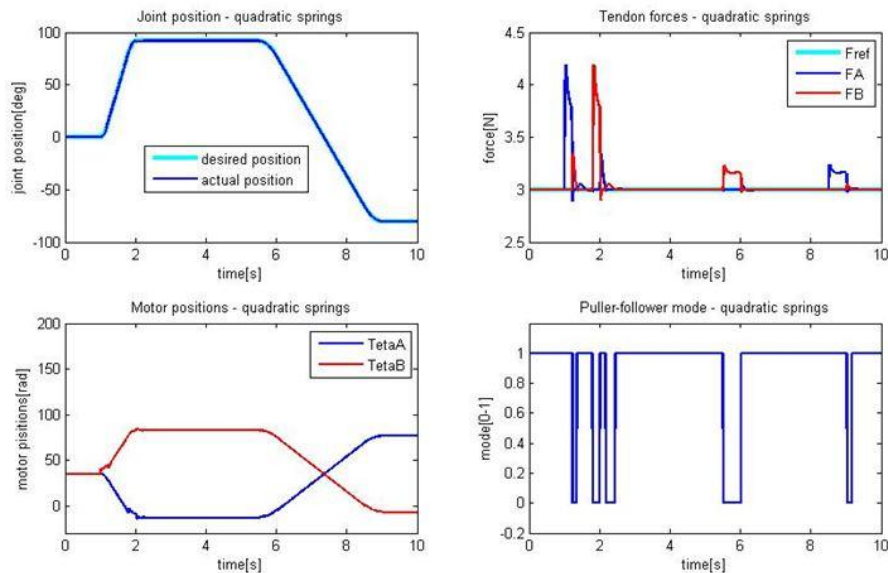


Figure 3.8. Puller-follower control applied to antagonistically-coupled drive using quadratic springs as elastic elements (3.23), (3.24). Validation is demonstrated by trajectory tracking (top left); Force control in the antagonistic tendon (top right); The positions of motor A and motor B, whose simultaneous action ensures proper joint position and antagonistic force (bottom left); Changing of the roles of motor A and motor B (“switching”) – mode 1 stands for motor A as the puller, and motor B as the follower, or vice-versa if mode 0 is active (bottom right).

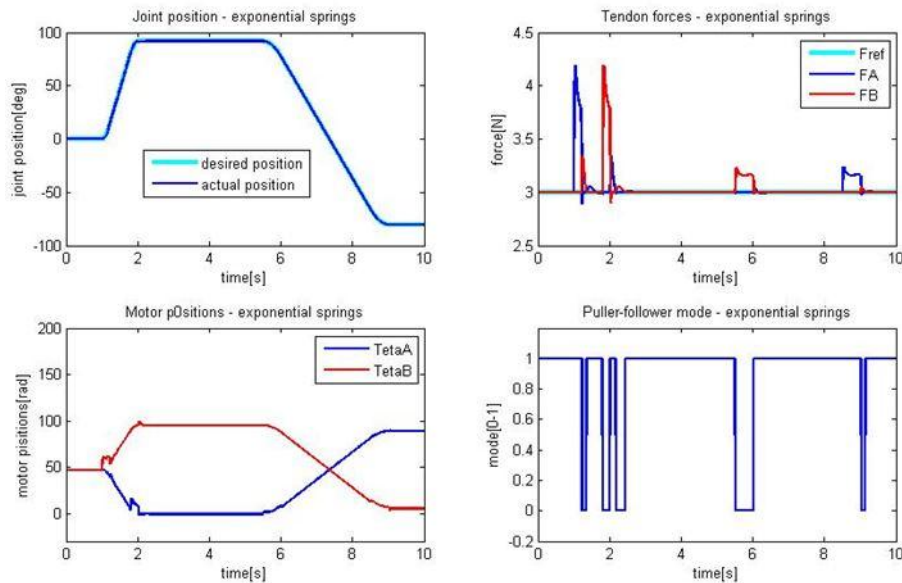


Figure 3.9. Puller-follower control applied to antagonistically-coupled drive using exponential springs as elastic elements (3.34), (3.35). Validation is demonstrated by trajectory tracking (top left); Force control in the antagonistic tendon (top right); The positions of motor A and motor B, whose simultaneous action ensures proper joint position and antagonistic force (bottom left); Changing of the roles of motor A and motor B (“switching”) – mode 1 stands for motor A as the puller, and motor B as the follower, or vice-versa if mode 0 is active (bottom right).

Even though the main idea and motivation for the puller-follower approach were biomechanically inspired, from the design and control of distinguishable human-like systems, the application of the puller-follower concept in musculoskeletal robots still has certain limitations. The most striking among them is the inability to apply the concept in a straightforward manner to the control of spherical joints or multi-articular muscles, or for precise biomechanical system modeling. Consequently, the ultimate solution for controlling such systems should be sought by considering not only conventional control techniques, but also experience and learning – which is, again, how the control of any biological system evolves and advances.

### 3.4 Puller-follower control concept for decoupled position and stiffness control

Subsection 1.2.3 pointed out the key benefits of variable stiffness. Among VSAs, actuators based on the antagonistic principle can take advantage of copying biomechanical principles and patterns. As such, they are a preferable source of action for future service robot design to fit an environment fully adapted to humans. The activities of both antagonistic drives are equally employed to trade-off between rigid-like/precise motion and compliant motion that favors interaction tasks. Therefore, simultaneous stiffness and position control of antagonistically-coupled drives is desired. From a user's point of view, besides position control, the necessity for stiffness control is dominant, compared to antagonistic force control, as in the case of the puller-follower approach. However, this subsection will demonstrate how puller-follower control can be extended to include simultaneous control of both joint position and stiffness. Therefore, the same goal using feedback linearization like in [132] by Palli et al. is achieved (simultaneous control of position and stiffness via antagonistically-coupled drives), but the modified puller-follower approach includes several enhancements, rectifies certain omissions, and introduces new possibilities. For instance, controllability and elimination of tendon slackening can be ensured by switching and an adaptive tension force, and there is the option to trade-off between exact stiffness tracking and energy efficiency.

Let us briefly recall the definition of joint stiffness, which is equivalent to the stiffness of a translational spring. The force acting on the spring depends on its extension and this static dependence is defined as the spring stiffness  $k[N/m]$ . Thus, the spring of length  $x_0$  in its equilibrium position ( $F = 0$ ) stays undeformed, whereas if the spring is extended to a length  $x$ , it generates a force  $F \neq 0$ . If this relation is linear, then we consider the spring as linear (3.42) and the stiffness is constant. Otherwise, the spring is considered as non-linear (3.43) and the stiffness is variable.

$$F = k \cdot (x - x_0) \Rightarrow k = dF/dx = const \quad (3.42)$$

$$F = k(\Delta x) \cdot (x - x_0) \Rightarrow k(\Delta x) = dF/dx \neq const \quad (3.43)$$

Likewise, the stiffness of the robot joint (usually denoted in the literature as  $S[Nm/rad]$ ) is defined by (3.44), where  $\tau_j$  stands for the torque generated in the joint and  $q$  denotes the joint position.

$$S = d\tau_j/dq \quad (3.44)$$

Analogously, joint stiffness can be constant or changeable (which is a desirable feature from an exploitation point of view, as previously explained in Subsection 1.2). At this point, it is useful to recall that joint stiffness can be achieved in a variety of ways (see Subsection 1.2.3). Since we focus on compliant joints that exploit antagonism, the stiffness of such joints is presented in accordance with the source of mechanical stiffness in antagonistically-coupled tendons: linear (3.45), quadratic (3.46), and exponential (3.47).

$$F_{LIN} = k\Delta l \quad (3.45)$$

$$F_{QA} = k_2(\Delta l)^2 + k_1\Delta l + k_0 \quad (3.46)$$

$$F_{EXP} = k_e(e^{\alpha_e\Delta l} - 1) \quad (3.47)$$

Using the general definition of joint stiffness (3.44), and recalling the joint configuration from Figure 3.2, the overall joint stiffness can be obtained for each source of compliance: linear (3.48), quadratic (3.49), and exponential (3.50). Here the pulling constraint of tendons is assumed ( $\Delta l_A > 0, \Delta l_B > 0$ ).

$$S_{LIN} = 2r_j^2 k \quad (3.48)$$

$$\begin{aligned} S_{QA} &= r_j^2(k_1 + 2k_2\Delta l_A + k_1 + 2k_2\Delta l_B) \\ &= 2r_j^2(2k_2 r_m(\theta_A + \theta_B) + k_1) \end{aligned} \quad (3.49)$$

$$\begin{aligned} S_{EXP} &= k_e\alpha_e r_j^2(e^{\alpha_e\Delta l_A} + e^{\alpha_e\Delta l_B}) \\ &= k_e\alpha_e r_j^2(e^{\alpha_e(r_m\theta_A+r_jq)} + e^{\alpha_e(r_m\theta_B-r_jq)}) \end{aligned} \quad (3.50)$$

Evidently, the stiffness/compliance range, as well as torque capacity, can be increased by utilizing a larger joint radius/joint pulley  $r_j$ . On the other hand, a larger joint radius

magnifies the required space rapidly, so one should deal with this trade-off carefully. Comprehensive research on the topic was carried out at Khatib's laboratory at Stanford University and is reported by Shin et al. in [201].

For the sake of illustration, a comparative analysis of force-deflection characteristics of all three springs is shown in Figure 3.10. The resulting stiffness-deflection dependence for an antagonistically-actuated joint, with all three sources of compliance, is depicted in Figure 3.11. It is assumed that both the agonist and antagonist tendons are stretched equally for some  $\Delta l$ .

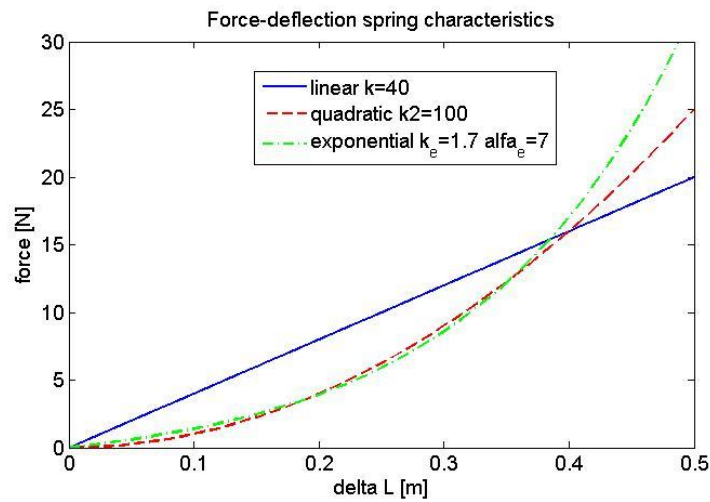


Figure 3.10. Force-deflection characteristics of: linear, quadratic and exponential spring.

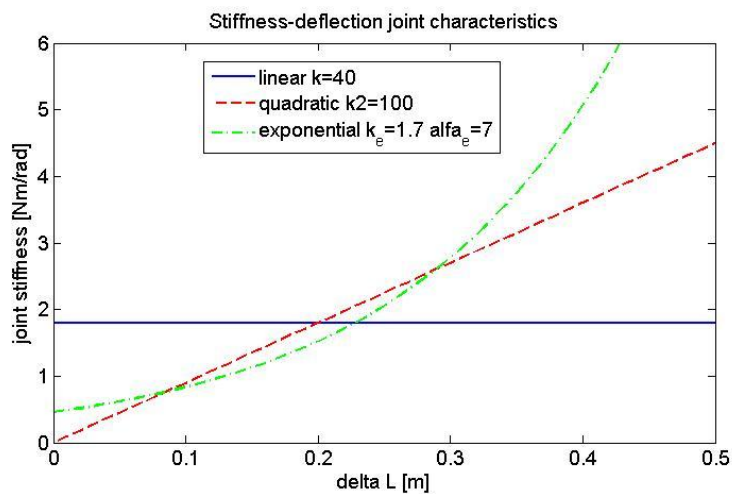


Figure 3.11. Resulting stiffness-deflection dependence for an antagonistically-actuated joint with all three sources of compliance: linear, quadratic and exponential springs.

While considering stiffness control, we should note that stiffness (3.44) is generally not a measurable quantity. However, it can be computed directly by measuring torques and joint positions [33] or estimated by relating stiffness to system state variables as in [77], [81]. The topic of stiffness estimation in VSAs was elaborated at the Italian Institute of Technology (IIT). Flacco et al. present in [202] a robust stiffness estimator for robot joints with flexible transmissions. The estimator is implemented in two stages. The first stage is estimation of the main driving torque using a residual-based method. In the second stage this estimated torque, the transmission deformation and the position of the second drive (for stiffness tuning) are the parameters used for final stiffness estimation based on an RLS algorithm. However, this estimator is limited to the specific drive configuration: a principal motor used to control link motion and a secondary motor used to adjust stiffness separately. Specifically, Menard et al. consider the problem of estimating nonlinear stiffness in an agonistic–antagonistic joint configuration in [203]. They propose an algorithm to avoid the need for a numerical derivative based on modulating functions. Besides the difficulties associated with direct measurement/estimation of joint stiffness, we note another obstacle in determining stiffness in the literature, and that is improper use of the stiffness term or misleading interpretations. This is especially prominent for stiffness term in the field of human motor control.

Although linear elastic springs are most widely used and the easiest to manufacture, it directly follows from (3.48) that for a joint driven by antagonistically-coupled linear springs, joint stiffness is constant and cannot, therefore, be controlled in the desired manner. Consequently, only the original puller-follower control for joint position and antagonistic force tracking can be applied, whereas position-stiffness control for such a system is generally not applicable.

Thus, antagonistic coupling of nonlinear springs is required for variable joint stiffness. Note that knowing the exact model of the nonlinear elastic element (from technical documentation or by direct identification of the elastic curve), the overall joint stiffness can be calculated on the basis of the motors and joint positions, as state variables. For instance, Equations (3.49) and (3.50) stand for antagonistically-actuated joints that use

quadratic and exponential springs, respectively. The following section shows how stiffness can be controlled applying the puller-follower principle to quadratic or exponential springs directly. The extension of the puller-follower control to include simultaneous joint position and stiffness control is demonstrated for nonlinear spring elasticity, as two case studies elaborated in the thesis: quadratic (Subsection 3.4.1) and exponential (Subsection 3.4.2) springs. The simulation results of this concept applied to both quadratic and exponential tendon characteristics are given in Subsection 3.4.3. The main idea of the concept is to calculate the desired force in the antagonistic tendon directly, from the desired stiffness and state space variables. All other features of the puller-follower principle are retained. This way, one can manage the trade-off between stiffness tracking and keep the antagonistic tendon force in an energy efficient manner, as well as prevent tendon slackening. The modified puller-follower control scheme for simultaneous position-stiffness control is displayed in Figure 3.12. Additional blocks, which represent simultaneous position and stiffness control adaptation to genuine puller-follower control, are highlighted in orange. These function blocks are based on Equations (3.51) through (3.54) for quadratic springs as the source of compliance, and on Equations (3.55) through (3.58) in the case of exponential springs as the source of compliance in tendons.



### 3.4.1 Antagonistic joints with quadratic tendon characteristics

Let us first consider an antagonistically-actuated joint driven by tendons using springs of quadratic characteristic (3.25). The overall joint stiffness (3.44) can be expressed as a function of spring extensions (3.49). Without limiting the generality of the problem, we assume that tendon “A” is the agonist or puller and that tendon “B” is the antagonist or follower. If the desired stiffness  $S_{QA_{des}}$  is known and the positions of the motors and joint are measured, it is possible to obtain the desired elongation of the antagonistic tendon from (3.51) and, consequently, also the desired force in the antagonistic tendon (3.52) based on (3.46). Thus, since the desired joint position is already specified, the puller-follower control scheme can be applied in a straightforward manner to achieve simultaneous position and stiffness control of the antagonistically-actuated compliant joint.

$$\Delta l_{B_{des}} = \frac{S_{QA_{des}}}{2r_j^2 k_2} - \frac{k_1}{k_2} - \frac{1}{2k_2} \left( -k_1 + \sqrt{k_1^2 - 4k_2(k_0 - F^A(\theta_A, q))} \right) \quad (3.51)$$

$$F^B_{QA_{des}} = k_2(\Delta l_{B_{des}})^2 + k_1 \Delta l_{B_{des}} + k_0 \quad (3.52)$$

Precisely in the same manner, if switching occurs, the tendon denoted by “B” takes over the puller role, so tendon “A” becomes the one that follows. Therefore, by commanding the desired joint position and stiffness, the desired force of the antagonistic tendon (this time tendon “A”) is calculated according to (3.53) and (3.54). Consequently, the puller-follower approach can be applied directly.

$$\Delta l_{A_{des}} = \frac{S_{QA_{des}}}{2r_j^2 k_2} - \frac{k_1}{k_2} - \frac{1}{2k_2} \left( -k_1 + \sqrt{k_1^2 - 4k_2(k_0 - F^B(\theta_B, q))} \right) \quad (3.53)$$

$$F^A_{QA_{des}} = k_2(\Delta l_{A_{des}})^2 + k_1 \Delta l_{A_{des}} + k_0 \quad (3.54)$$

### 3.4.2 Antagonistic joints with exponential tendon characteristics

It is also possible to apply the puller-follower approach for simultaneous control of joint position and stiffness in the case of a robot joint actuated by an antagonistic configuration that exploits exponential springs. Again, very similar to the analysis of quadratic springs, the main idea is to determine the desired force in the antagonistic tendon, which will ensure the desired joint stiffness at the desired joint position. Considering the overall joint stiffness in the case of a system that exploits exponential springs (3.36), it is possible to show that the expression can be amended to a form where stiffness is expressed as a combination of state space variables and, consequently, spring extensions (3.50). If the desired joint stiffness  $S_{EXP_{des}}$  and the desired joint position are known, and if all available system variables are measured, one can derive the desired elongation of the antagonistic tendon (3.55) and, therefore, its force (3.56). The equations are given considering tendon “A” to be the puller and tendon “B” the follower.

$$\Delta l_{B_{des}} = \frac{1}{\alpha_e} \ln \left( \frac{S_{EXP_{des}}}{k_e \alpha_e r_j^2} - \frac{F^A(\theta_A, q)}{k_e} - 1 \right) \quad (3.55)$$

$$F^B_{EXP_{des}} = k_e (e^{\alpha_e \Delta l_{B_{des}}} - 1) \quad (3.56)$$

The same approach is possible in the case where the tendons exchange their roles due to switching (tendon “B” being the puller and tendon “A” the follower). By commanding the desired joint position and stiffness, the desired force of the antagonistic tendon (this time tendon “A”) is calculated according to (3.57) and (3.58). Again, the puller-follower approach can be applied directly.

$$\Delta l_{A_{des}} = \frac{1}{\alpha_e} \ln \left( \frac{S_{EXP_{des}}}{k_e \alpha_e r_j^2} - \frac{F^B(\theta_B, q)}{k_e} - 1 \right) \quad (3.57)$$

$$F^A_{EXP_{des}} = k_e (e^{\alpha_e \Delta l_{A_{des}}} - 1) \quad (3.58)$$

### 3.4.3 Simulation results

Before we turn to the simulation results which prove the theory presented in this section, we should mention physical implementations of some antagonistic joints and their feasible stiffness ranges, in addition to real physical stiffness of human joints actuated by antagonistically coupled muscles.

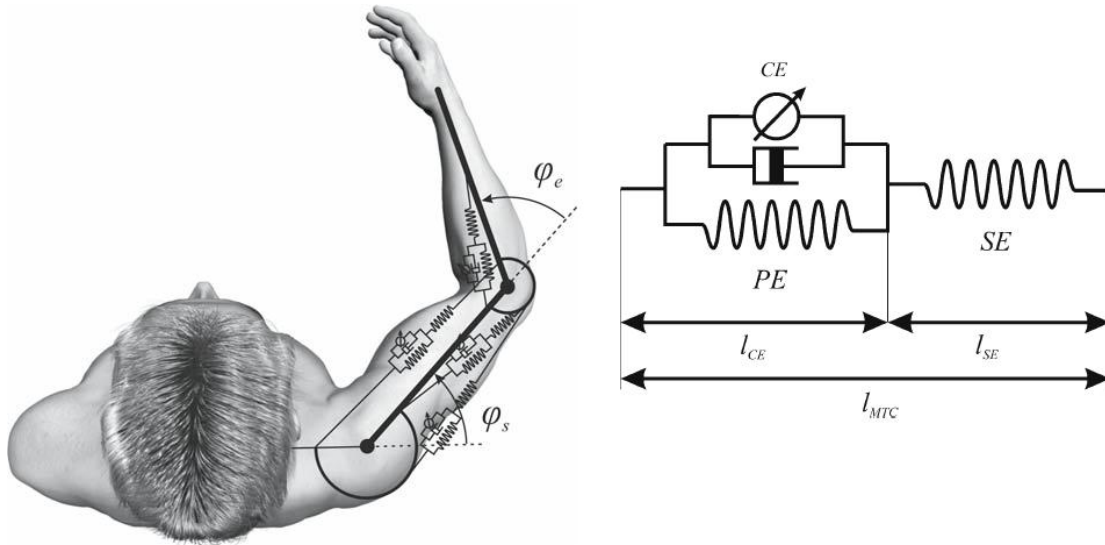


Figure 3.13. Schematic of musculoskeletal arm model (left); Hill's muscle model used for simulations [204] - (right).

In a study by Lan and Crago [205], stiffness of the elbow joint is estimated to be in the range of  $[20 \text{ Nm/rad} \div 80 \text{ Nm/rad}]$ , but this result came out from numerical simulation. Similarly, the estimation of elbow stiffness based on simulation and a comprehensive model of the human arm are presented in [204]. The model developed in this study contains shoulder and elbow joints actuated by four muscles, as shown in Figure 3.13 (left): two extensors and two flexors. Each muscle was represented by Hill's muscle model that contains a contractile element (CE) and parallel element (PE), where a tendon was represented by a serial element (SE). The functional muscle scheme is depicted in Figure 3.13 (right). Hill's model parameters were extracted from literature. Muscle stiffness is examined for different co-contraction indices (CCI) of two antagonistic muscles. As intuitively expected, a positive correlation between CCI and joint stiffness was noted and elbow stiffness reached maximum values around  $40 \text{ Nm/rad}$ .

Depending on the technical implementation, variable stiffness can vary significantly. Initial experiments with NEURARM [90], described in Subsection 1.4.2, demonstrated the theoretical joint stiffness range in the interval  $6.22 - 35.1 \text{ Nm/rad}$ . This achievable range of one of the rare antagonistic manipulators driven by hydraulics, was evaluated by taking into account the results of static characterization for a certain dimension of the pulley radius and prescribed maximum deformation of the elastic springs as reported in [206]. One of the first biologically-inspired technical implementations of a rotational joint, using antagonistic series elastic actuation designed by Migliore et al. [77] has a very small stiffness range  $[0.1 \text{ mNm/deg} \div 0.7 \text{ mNm/deg}]$ . Tonietti et al. claim in [81] to have achieved a stiffness range of  $[200 \text{ Nm/rad} \div 3000 \text{ Nm/rad}]$  with their VSA design that makes use of pre-tension springs to control stiffness. Indeed, an experimental evaluation of the setup demonstrated a feasible stiffness range of  $[500 \text{ Nm/rad} \div 2200 \text{ Nm/rad}]$ . As pointed out in Subsection 1.4.1, the same research team presented a new generation of VSAs (VSA-II), where the antagonistic principle is applied and exhibits better performance than its predecessor. It could achieve a stiffness up to  $10000 \text{ Nm/rad}$ , according to the initial tests reported in [82]. In [86], Petit et al. highlight the possibility of extending the principle of classical antagonistic joints towards bidirectional antagonistic joints. The main contribution of the paper is an increase in the joint load range, accomplished by the so-called “helping mode” in which two motors support each other to generate a higher torque. Preliminary experiments with the DLR bidirectional setup showed a significant range of achieved stiffness  $[20 \text{ Nm/rad} \div 60 \text{ Nm/rad}]$ . Bidirectional springs in an antagonistic configuration were also exploited by QB Robotics to build an entire line of VSAs. The basic idea of the authors was to create a low-cost solution and help spread VSA technology to a wide audience. The initial model, QBmove maker, is capable of changing its stiffness range from  $0.2 \text{ Nm/rad}$  to  $2 \text{ Nm/rad}$ , while delivering a nominal torque of  $0.6 \text{ Nm}$  and a velocity of  $3 \text{ rad/s}$ . Its successor, QBmove maker pro, which doubles the nominal torque and velocity, can adjust its stiffness in a significantly wider range  $[0.6 \text{ Nm/rad} \div 8 \text{ Nm/rad}]$ . The newest actuator in this series is QBmove advanced, released this year. Besides enhancing the nominal torque and velocity, the technical implementation of the actuator enables variable stiffness up to  $30 \text{ Nm/rad}$ . On the other hand, if controlled by

pneumatic artificial muscles, antagonistic joint setups provide a stiffness range of  $[3 \text{ Nm/rad} \div 20 \text{ Nm/rad}]$  at a working pressure of around  $4 \text{ bar}$ , as referenced by Sardellitti et al. [181].

The following figures demonstrate the puller-follower control scheme for simultaneous position and stiffness control, which is a typical requirement for compliant robot joint control. The demonstration example comprises the desired joint position as a smooth trajectory and sine trajectory sequence in the range from  $0 \text{ deg}$  to  $-120 \text{ deg}$ . The desired stiffness also combines an interval of smoothly varied values and sine in the range from  $3 \text{ Nm/rad}$  to  $6.5 \text{ Nm/rad}$ . The results demonstrate the basic concepts and validate the approach. Results are given for both quadratic and exponential springs. One can note that both position and stiffness tracking are satisfactory and that the main difference between the figures lies in motor positioning, since motors A and B are positioned to ensure trajectory and stiffness tracking via different elastic elements between the antagonistic drives and the joint. The exchange of roles between the tendons, or “switching”, is depicted for the sake of illustration in the graphic called Puller-follower modes. The simulation parameters are shown in Table 3.2. Controllers (3.78) and (3.81) are used for the decoupled force/stiffness subsystem and position subsystem, although any controller that satisfies (3.20) can be employed. Figure 3.14 and Figure 3.15 demonstrate simultaneous position and stiffness control of a robot joint actuated by antagonistically-coupled drives with compliant elements of quadratic and exponential characteristics, respectively.

*Table 3.2. Joint, link and spring parameters used for simulations in Subsection 3.4.3.*

Label	Numerical value	Unit	Description
$l_r$	0.15	$[m]$	Circular joint parameters
$\alpha$	$\pi/2$	$[rad]$	
$m$	3	$[kg]$	Link parameters
$I$	0.015	$[kgm^2]$	
$k_2$	100	$[N/m^2]$	Quadratic spring coeff.
$k_1$	0	$[N/m]$	Quadratic spring coeff.
$k_0$	0	$[N]$	Quadratic spring coeff.
$k_e$	10	$[N]$	Exponential spring coeff.
$\alpha_e$	2	$[1/m]$	Exponential spring coeff.

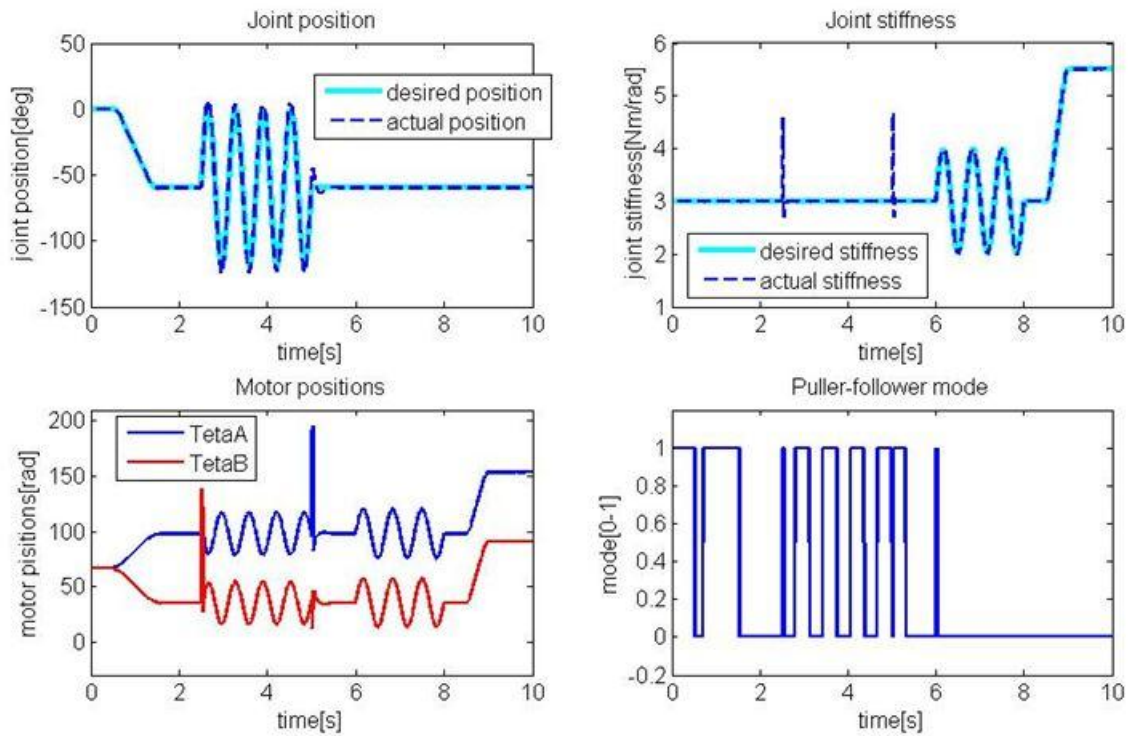


Figure 3.14. Puller-follower control method for simultaneous position and stiffness control of a joint actuated by antagonistically-coupled drives with an elastic element of quadratic characteristics. The approach is validated by: joint trajectory tracking (top left); desired and achieved joint stiffness (top right); Both position and stiffness references contain a sinusoidal and a polynomial part. One can notice the additional effort in the motor position when the reference motion is not a smooth curve of the 4<sup>th</sup> order, as explained in Subsection 3.3. The rise in stiffness influences tendon co-contraction (motors A and B rotate in the same, positive direction, according to Figure 3.2), while rotation directions differ to produce joint movements - (bottom left); Puller and follower roles are assigned to tendons A and B, according to the switching mode (bottom right).

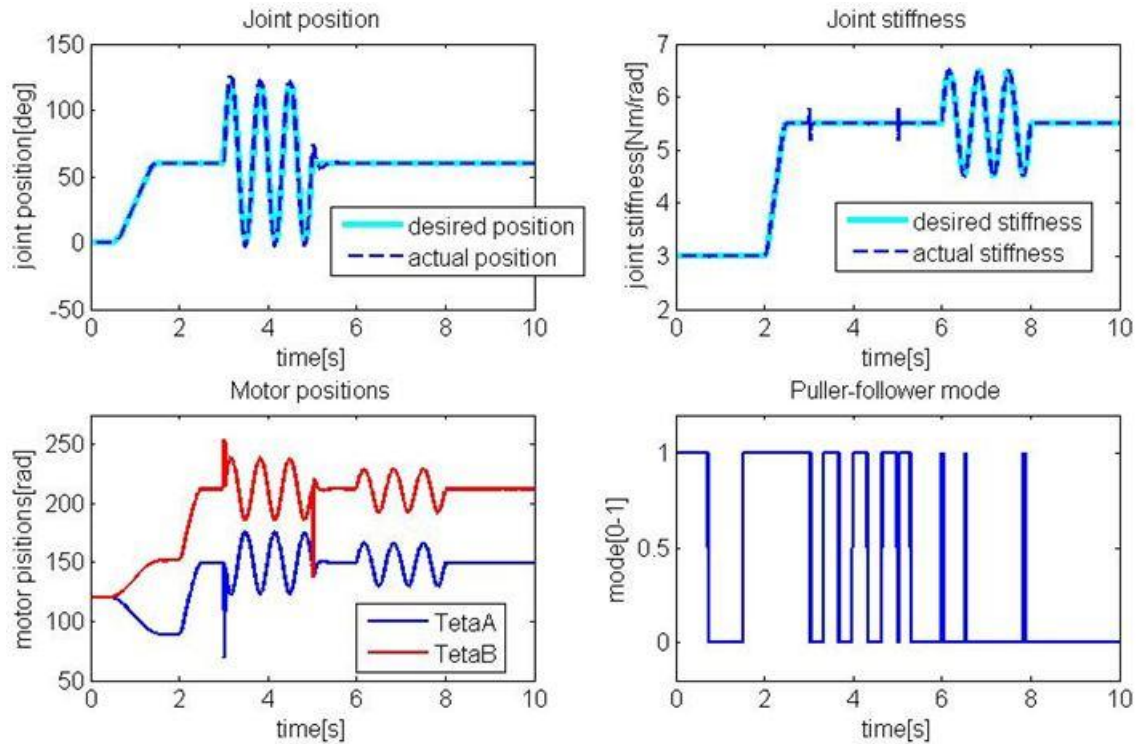


Figure 3.15. Puller-follower control method for simultaneous position and stiffness control of a joint actuated by antagonistically-coupled drives with an elastic element of exponential characteristics. The approach is validated by: joint trajectory tracking (top left); desired and achieved joint stiffness (top right); Both position and stiffness references contain a sinusoidal and a polynomial part. One can notice the additional effort in the motor position when the reference motion is not a smooth curve of the 4<sup>th</sup> order, as explained in Subsection 3.3. The rise in stiffness influences tendon co-contraction (motors A and B rotate in the same, positive direction, according to Figure 3.2), while rotation directions differ to produce joint movements - (bottom left); Puller and follower roles are assigned to tendons A and B, according to the switching mode (bottom right).

Figure 3.16, Figure 3.17, and Figure 3.18 demonstrate the superiority of puller-follower control, compared to direct application of feedback linearization to simultaneous position and stiffness control of antagonistically-driven joints. As stated at the beginning of the section, application of puller-follower control prevents tendon slackening, as a dominant source of controllability loss in target systems of the same kind. Furthermore, switching of roles between the motors can improve energy efficiency. However, if puller-follower control limits the tendon force to above some prescribed minimal level, controllability is indeed ensured, but stiffness tracking is compromised as a trade-off effect. The figures below show how typical disturbances can adversely affect system

behavior. Namely, if an external disturbance occurs or if higher control levels or disturbances cause references that are not smooth enough ( $q_{ref}(t) \in \mathbb{C}^4$ ,  $F_{ref}(t) \in \mathbb{C}^2$ ;  $t \in [0, T]$ ), the tendons could slacken and the controllability of the system would be lost. Figure 3.16 shows joint position and stiffness tracking when the system is controlled by direct feedback linearization for simultaneous position-stiffness control vs the puller-follower approach. Results are presented for a joint driven by two antagonistically-coupled tendons with quadratic springs. The desired stiffness is a sinusoidal signal of a  $2.5 \text{ Nm/rad}$  mean value and an amplitude of  $1.5 \text{ Nm/rad}$ . The desired joint position comprises a smooth ramp and a damped sinusoidal part with an amplitude of about  $80 \text{ deg}$  and a period of about  $1.2 \text{ s}$ . The first challenge for the system is the imposed reference change. The first derivative of the desired joint position is not a continuous function, although the trajectory itself is continuous (at  $t = 2\text{s}$ ). The second challenge is an external torque of  $-50 \text{ Nm}$  applied to the joint axis from  $t_{start} = 7\text{s}$  to  $t_{stop} = 10\text{s}$ . The figures demonstrate that since a classical control scheme cannot deal with external disturbances, the tendons will slacken and the system become underactuated. On the other hand, a puller-follower controlled system will withstand the external disturbance, trading-off stiffness tracking. However, the tendons remain stretched and system controllability is, therefore, preserved. Intervals of interest are zoomed in and shown individually in Figure 3.17 (trajectory change – denoted by green frames) and Figure 3.18 (external load applied to the joint – denoted by orange frames). Again, the parameters given in Table 3.2 were used for the simulations.

A very similar analysis applies to other types of non-linear elastic elements, as well as to springs of exponential characteristics. The advantages of puller-follower control over the basic approach of feedback linearization for simultaneous position-stiffness control can be demonstrated in an analogous manner. Such an analysis is therefore omitted.

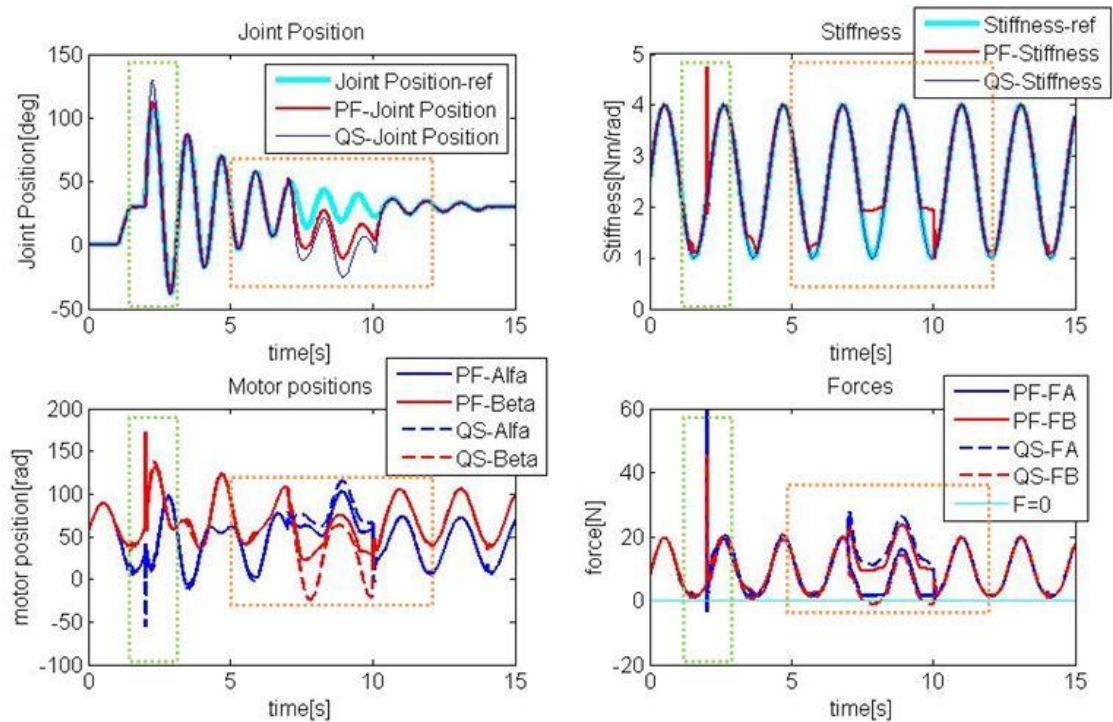


Figure 3.16. Puller-follower control (PF) vs. direct feedback linearization for simultaneous position-stiffness control (QS) employed to drive an antagonistic joint with non-linear (quadratic) springs as the source of intrinsic elasticity. A rapid change in the desired trajectory ( $t = 1.2$  s), and the externally applied torque ( $t = 7$  s  $\div$  10 s) are introduced to test system performance. The results comprise: the desired joint position shown in cyan, the actual PF joint positions in red and the actual QS joint position in blue (top left); The desired and actual PF and QS stiffness values - it is apparent that QS control maintains the desired stiffness throughout, while PF control trades-off by allowing stiffness deviation in order to ensure tension in the tendons and preserve controllability (top right); The positions of the antagonistic motors for both PF and QS (bottom left); The tendon forces pointing out the key benefit of PF control – tendons remain stretched, whereas in order to ensure perfect stiffness tracking, QS fails in controllability (tendons slacken  $F_a < 0$  or  $F_b < 0$ ) - the benefit of switching tendon roles, a feature of PF control (bottom right).

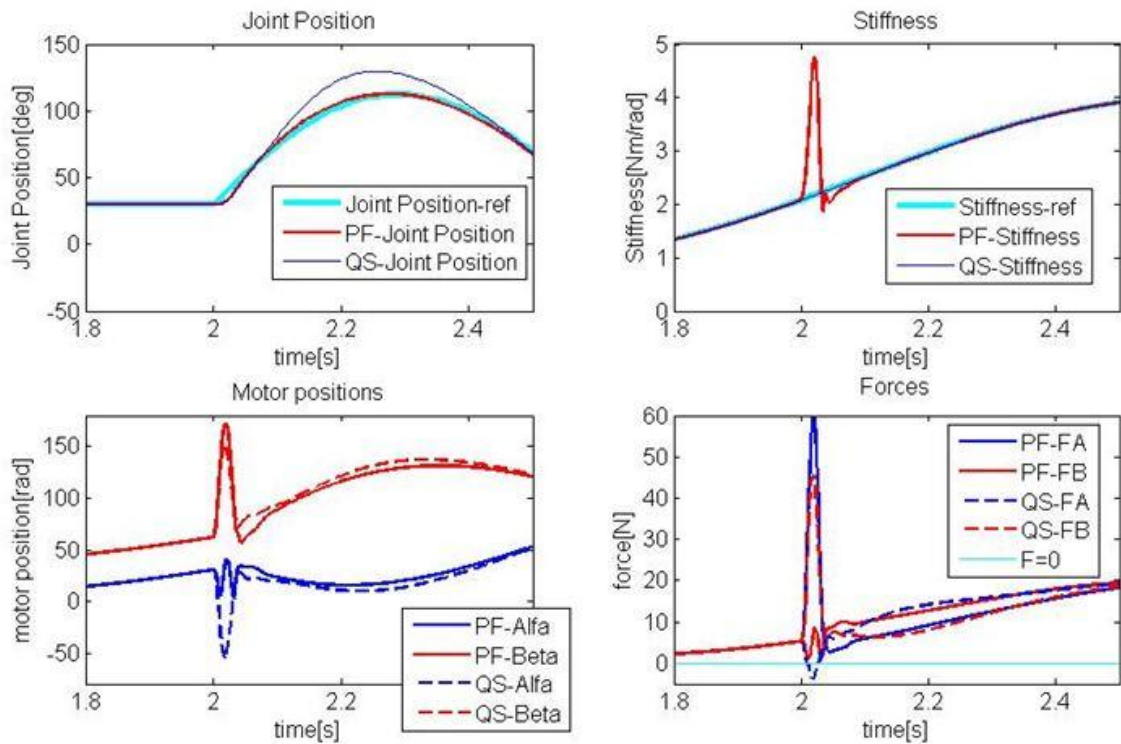


Figure 3.17. Puller-follower control (PF) vs. direct feedback linearization for simultaneous position-stiffness control (QS) employed to drive an antagonistic joint with non-linear (quadratic) springs as the source of intrinsic elasticity – zoomed in segment (Figure 3.16 green frame). A rapid change in the desired trajectory leads to slackening of tendon A in the case of QS control, whereas in the case of PF control, controllability is ensured by switching. It is apparent that to handle this sudden change, PF reacted by indirectly increasing the force in tendon A (puller role assigned to tendon A). However, in order to deal with the risk of tendon slackening, there was a short divergence in stiffness tracking.

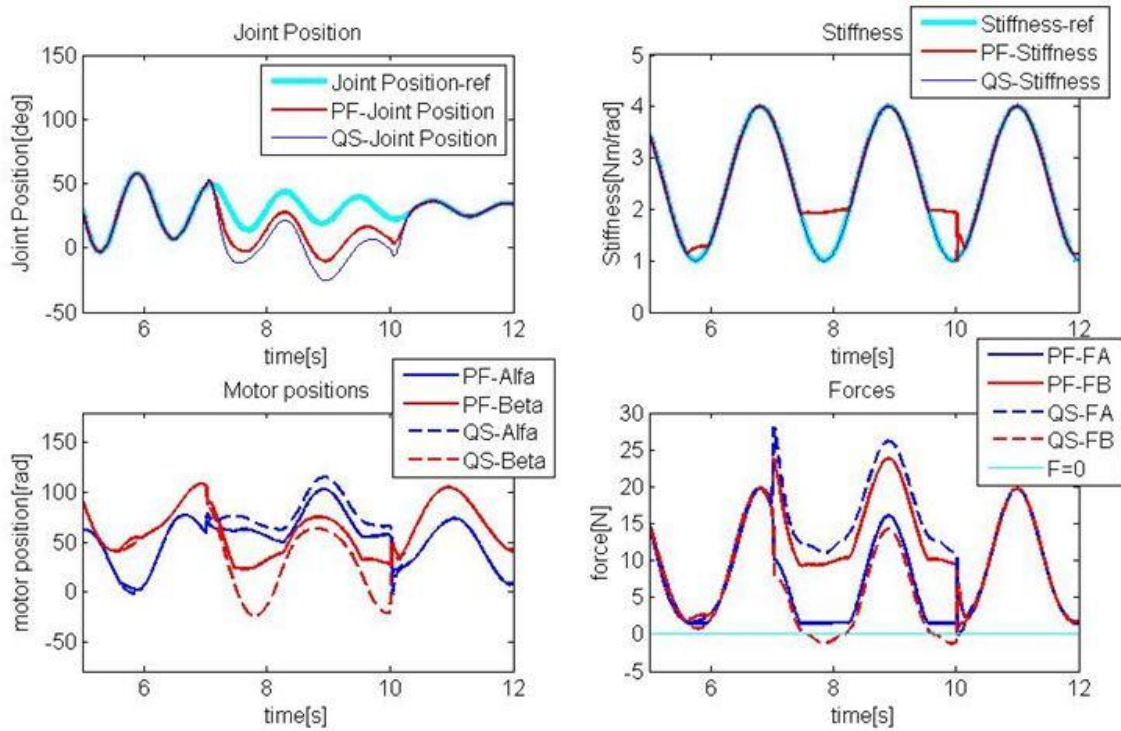


Figure 3.18. Puller-follower control (PF) vs. direct feedback linearization for simultaneous position-stiffness control (QS) employed to drive an antagonistic joint with non-linear (quadratic) springs as the source of intrinsic elasticity – zoomed in segment (Figure 3.16 orange frame). The external disturbance represented by the applied external torque to the joint led to slackening of tendon B in the case of QS control, whereas in the case of PF control controllability was ensured by switching. Also, a minimal tension margin ( $F_{min} = 2N$ ) in the zone of low forces is notable, to avoid slackening of the tendons. PF reacted by indirectly increasing the force in tendon B (puller role assigned to tendon B), to achieve reciprocal activation and counteract the external torque. Again, in order to deal with the risk of tendon slackening, there was a short divergence in stiffness tracking.

### 3.5 Enhancement of the puller-follower approach

As in the case of any control based on feedback linearization, the puller-follower approach is very model-dependent. This dependence is expected since model knowledge is used to deal with nonlinearities in the system, as well as with decoupling. So far, the puller-follower principle has been demonstrated for the control of a single joint in the horizontal plane. Moving towards a multi-joint configuration and a system in three dimensional space, there are several aspects that need to be considered. To begin with,

gravity should be compensated. Then, a multi-joint system introduces dynamic coupling between joints as well as changes in effective joint inertia, which are “seen” in a single-joint model. Finally, to deal with these challenges, the robust theory should be employed to control two decoupled subsystems. On the other hand, decoupling presents an additional obstacle since it blurs model parameterization. Thus, conventional robust control techniques based on parameter uncertainties (structured uncertainties) cannot be applied. An evaluation of the enhanced puller-follower approach is demonstrated in a multi-joint robot simulation, while grasping an object in the vertical plane.

### 3.5.1 Gravity compensation

The state space model (3.12), or (3.25) and (3.36) in cases that involve nonlinear springs, applies to the joint in horizontal plane and does not consider gravity at all. However, a general case that addresses gravity must be handled. In order to compensate the effects of gravity, the feedback linearization part should be extended in an appropriate way. Initially, the gravity load in each joint should be estimated and then compensated. Since the gravity load depends only on the robot’s pose, it is actually easy to evaluate. For the purposes of demonstration, a robot joint model driven by antagonistically-coupled linear springs, including gravity, is given in (3.59). Even in the case of a multi-joint robot, the driving torque needed to compensate for gravity can be estimated easily from the model of robot dynamics (reduced to statics by setting accelerations and velocities to zero), as explained in Subsection 2.3. So, if  $\tau_g(q \equiv x_5)$  is the estimated static gravitational torque in the joint, feedback linearization is modified according to (3.60) to make the control system aware of the influence of gravity. In the case of a multi-joint system, the influence of gravity is even more pronounced. To deal with gravity compensation in a multi-joint system, once again the influence of gravity torque on each robot axis needs to be estimated and compensated. This favors the importance of modeling of robot dynamics. However, if the results from Subsection 2.3.2 are used, gravity torques can be extracted from the robot model (2.41) and then compensated through the feedback linearization control section in a similar manner (3.60).

$$\dot{\mathbf{x}} = \mathbf{f}(\mathbf{x}) + \mathbf{g}(\mathbf{x})\mathbf{u} = \begin{bmatrix} -\frac{r_m^2 k}{I_m^A} x_1 - \frac{B_m^A}{I_m^A} x_2 - \frac{r_m r_j k}{I_m^A} x_5 \\ -\frac{r_m^2 k}{I_m^B} x_3 - \frac{B_m^B}{I_m^B} x_4 + \frac{r_m r_j k}{I_m^B} x_5 \\ -\frac{r_m r_j k}{I_j} x_1 + \frac{r_m r_j k}{I_j} x_3 - \frac{2 r_j^2 k}{I_j} x_5 - \frac{1}{I_j} \tau_g(x_5) \end{bmatrix} + \begin{bmatrix} 0 & 0 \\ \frac{1}{I_m^A} & 0 \\ 0 & \frac{1}{I_m^B} \\ 0 & 0 \\ 0 & 0 \end{bmatrix} \mathbf{u} \quad (3.59)$$

$$L_f^4 h_q(x) = \frac{k r_j}{I_j} \left( \frac{B r_m (x_2 - x_4) + k r_m^2 (2 r_j x_5 + r_m (x_1 - x_3))}{I_m} + \frac{2 k r_j^2 (2 r_j x_5 + r_m (x_1 - x_3))}{I_j} \right) + \frac{1}{I_j} \left( \frac{2 k r_j^2}{I_j} \tau_g(x_5) + \frac{1}{I_j} \left( \tau_g(x_5) + k r_j (2 r_j x_5 + r_m (x_1 - x_3)) \right) \frac{\partial \tau_g(x_5)}{\partial x_5} - \frac{\partial^2 \tau_g(x_5)}{\partial x_5^2} \right) \quad (3.60)$$

$$L_f^2 h_F(x) = k \left( \frac{-B r_m x_4 + k r_m^2 (r_j x_5 - r_m x_3)}{I_m} + \frac{k r_j^2 (2 r_j x_5 + r_m (x_1 - x_3))}{I_j} \right) + \frac{k r_j}{I_j} \tau_g(x_5)$$

Although Lie derivatives have changed, the relative degree remains the same and is still equal to the system order. The decoupling matrix  $\mathbf{E}(\mathbf{x})$  remains unchanged (3.15), so gravity does not influence the controllability of the system.

An analogous procedure can be followed to compensate for gravity if a robot joint with antagonistically-coupled nonlinear springs is considered.

### 3.5.2 Estimation of effective joint inertia

In a single joint system, the moment of inertia of a moving segment is a constant parameter which is easy to evaluate. However, in a multi-joint system, effective joint inertia changes generally depend on the current position of the entire system. More precisely, the “seen” inertia in a particular joint depends on all the succeeding links in the kinematic chain of the robot. If effective joint inertia is considered, one more important feature of compliant robots needs to be taken into account. Namely, for a rigid transmission between an actuator and the corresponding robot link, effective inertia of the joint is the sum of link inertia and actuator inertia, multiplied by the squared gearbox

ratio. On the other hand, if transmission compliance is incorporated, effective joint inertia equals link inertia only (now decoupled from actuator inertia). Therefore, for a robot driven by antagonistically-coupled compliant drives, the effective inertia in each joint can be obtained accurately, knowing only the robot's position and individual link inertia parameters. As explained in Subsection 2.3, the estimated "seen" inertia in each joint  $j \in 1, \dots, n$  of a total of  $n$  joints is a diagonal element of the basic inertial matrix  $\mathbf{H}(\mathbf{Q}) - H_{jj}(\mathbf{Q})$ . Consequently, to enhance multi-joint system control, feedback linearization is modified by replacing the constant link inertia  $I_j$  with the estimated effective inertia in each joint  $H_{jj}(\mathbf{Q})$  in the feedback linearization scheme (e.g. (3.15) and (3.16) for linear springs). Note that all diagonal elements of the inertial matrix  $\mathbf{H}(\mathbf{Q})$  are strictly positive, so the preconditions for the application of feedback linearization are still satisfied: the sum of relative degrees of each output derivative is still equal to the system order and the decoupling matrix  $\mathbf{E}(\mathbf{x})$  remains nonsingular.

### 3.5.3 $H_\infty$ loop shaping robust control

Enhancements of the puller-follower control approach for application to a multi-joint robot, based on gravity compensation and effective joint inertia, have so far been elaborated and introduced. It is apparent that both improvements rely on information that can be extracted from an accurate model of the robot dynamics, peculiarly inertial and geometrical link characteristics and robot joint positions. All these parameters can be easily estimated and/or measured in each time instant. However, any inaccuracy in parameter evaluation can lead to deviations in the robot's behavior. Furthermore, if one looks back to the overall model of robot dynamics (2.41), there are other effects that should be compensated, such as dynamic coupling between the joints. Since dynamic coupling includes cross-joint inertial terms and velocity related dependencies between the joints (centrifugal forces, Coriolis forces, viscous friction, etc.), it is very difficult to model, estimate and eventually compensate. Even if such effects could be obtained with certain credibility, it would require a lot of computation. In the other words, the task would be very challenging to handle, especially in real time.

Considering these arguments, we face the problem from a different perspective. We consider dynamic coupling between joints as unmodeled dynamics, and refer to the robust control theory to compensate for model discordance. Because of the applied input-output feedback linearization, the uncertainty in the system cannot be described as a function of the system's parameters. Therefore, the  $H_\infty$  loop-shaping method proposed by McFarlane and Glover [200] is used. It is a combination of loop shaping and robust stabilization, where the  $H_\infty$  optimization problem guarantees closed-loop stability and a certain level of robust stability at all frequencies. In general,  $H_\infty$  norm optimization is often used to minimize the closed loop impact of a perturbation with regard to stabilization or performance. In a loop shaping approach, one specifies closed-loop objectives as requirements for open-loop singular values of the compensated system. In simplistic terms, one selects a controller that achieves a sufficiently high open-loop gain at low frequency and therefore ensures the desired closed-loop performance, while obtaining sufficiently low open-loop gain at higher frequencies and achieving good robust stability.

Flexible-joint robot control using  $H_\infty$  loop shaping is also discussed by Axelsson et al. in [207]. They propose an  $H_\infty$  loop shaping approach, as well as a mixed- $H_\infty$  design, for the control of a compliant joint position only, and demonstrate its predominance in standard PID control. The choices of weighting functions are discussed briefly and the need to reduce the controller order is highlighted as a consequence of the control method.

Typically, as suggested by McFarlane and Glover, the control design has two main stages. The first is the loop shaping stage, which is used to shape the nominal system singular values to provide the desired open-loop properties at frequencies of both high and low loop gains. During this stage, the designer chooses a pre-compensator  $W_1$  and/or post-compensator  $W_2$  to achieve the desired open-loop properties. Therefore, the nominal target model  $G$  is reshaped to a new model –  $G_s = W_2GW_1$ , which is the target system for the feedback compensator (see Figure 3.19). The second stage is solving the normalized coprime factor  $H_\infty$  problem introduced in [208], to design the feedback controller  $K_\infty$  used to robustly stabilize the shaped plant. Consequently, the final

feedback controller  $K$  integrates the pre-compensator  $W_1$ , feedback controller  $K_\infty$  and post-compensator  $W_2$ .

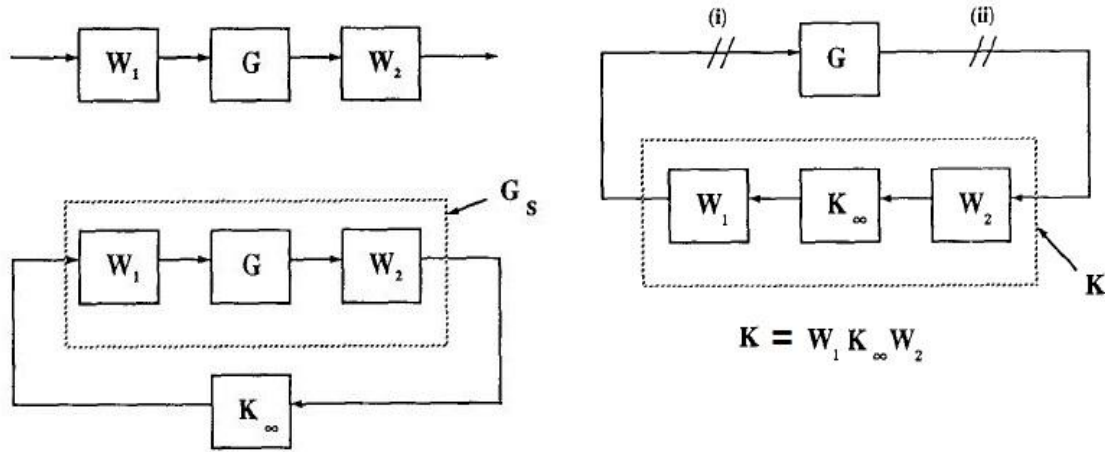


Figure 3.19.  $H_\infty$  loop shaping procedure uses pre-compensator  $W_1$  and/or post-compensator  $W_2$  to reshape the open loop of the target system for the feedback controller  $K_\infty$ . Robust stabilization of the shaped system is achieved by compensator  $K_\infty$  according to the procedure introduced by McFarlane and Glover [200]. The end result of the  $H_\infty$  loop shaping design procedure is controller  $K$ , which assimilates all the compensators:  $K = W_1 K_\infty W_2$ .

Since our final target system is a complete semi-anthropomorphic robot, whose kinematic chains contain up to four links (Figure 2.6) and where the effective inertia of particular joints varies significantly and the Coriolis and centrifugal forces influence high dynamic coupling, controllers of different bandwidths have to be designed to cover all joint drive requirements. To that end, we set three pre-compensators of different dynamics for both the force subsystem –  $G_f$  (3.21) and the position subsystem –  $G_p$  (3.22). In particular, according to the nature of our target system (anthropomorphic robot), we opt for several general requirements as guidelines for the loop-shaping design of controllers, as explained in the following paragraphs:

- High gain at low frequencies;
- Rapidly decreasing gain after bandwidth frequency;
- 20 dB/dec slope at bandwidth frequency; and
- Phase margin greater than 0.5 rad (ca. 30 deg).

Following these guidelines, we adopt three pre-compensators for both force ( $W_{pre\_F}$ ) and position ( $W_{pre\_P}$ ) regulation; the concepts are similar but the bandwidth differs. Our primary goal is to avoid tendon slackening and, therefore, maintain controllability of the system. Thus, higher priority is given to force control and higher control bandwidths are therefore set for the antagonist force control loop than the joint position control loop. Force control pre-compensators are given by (3.61) through (3.63), which shape open-loop performance to achieve bandwidth frequencies of  $10 \frac{rad}{s}$ ,  $100 \frac{rad}{s}$  and  $700 \frac{rad}{s}$ , respectively. Equations (3.64) through (3.66) stand for position control pre-compensators that accomplish bandwidths of  $10 \frac{rad}{s}$ ,  $65 \frac{rad}{s}$  and  $190 \frac{rad}{s}$ , respectively. The post-compensators of both the force controller and position controller,  $W_{post\_F}$  and  $W_{post\_P}$ , respectively, are assumed to be equal to the identity matrix  $I$  for reasons of simplicity.

$$W_{pre\_F1} = 378 \frac{(s + 2.6)}{(s + 36)} \quad (3.61)$$

$$W_{pre\_F2} = 19800 \frac{(s + 39)}{(s + 207)} \quad (3.62)$$

$$W_{pre\_F3} = 7.45 \cdot 10^5 \frac{(s + 401)}{(s + 943)} \quad (3.63)$$

$$W_{pre\_P1} = 1.18 \cdot 10^7 \frac{(s + 3)(s^2 + 4s + 7)}{(s + 99)(s^2 + 150s + 10000)} \quad (3.64)$$

$$W_{pre\_P2} = 6.41 \cdot 10^8 \frac{(s + 10)(s^2 + 22s + 81)}{(s + 149)(s^2 + 250s + 62500)} \quad (3.65)$$

$$W_{pre\_P3} = 3.35 \cdot 10^{10} \frac{(s + 76)(s^2 + 52s + 2590)}{(s + 439)(s^2 + 376s + 403000)} \quad (3.66)$$

The final open-loop characteristics achieved by shaping the system using pre-compensators (3.61) through (3.63) and (3.64) through (3.66) in the frequency domain are given in Figure 3.20 for the force control open loop and in Figure 3.21 for the joint position open loop.

By selecting pre- and post-compensators, the desired loop shaping performance is finalized and so is the first step of the robust  $H_\infty$  loop shaping control design. If nominal performance is not achieved, pre- and post-compensators need to be reshaped.

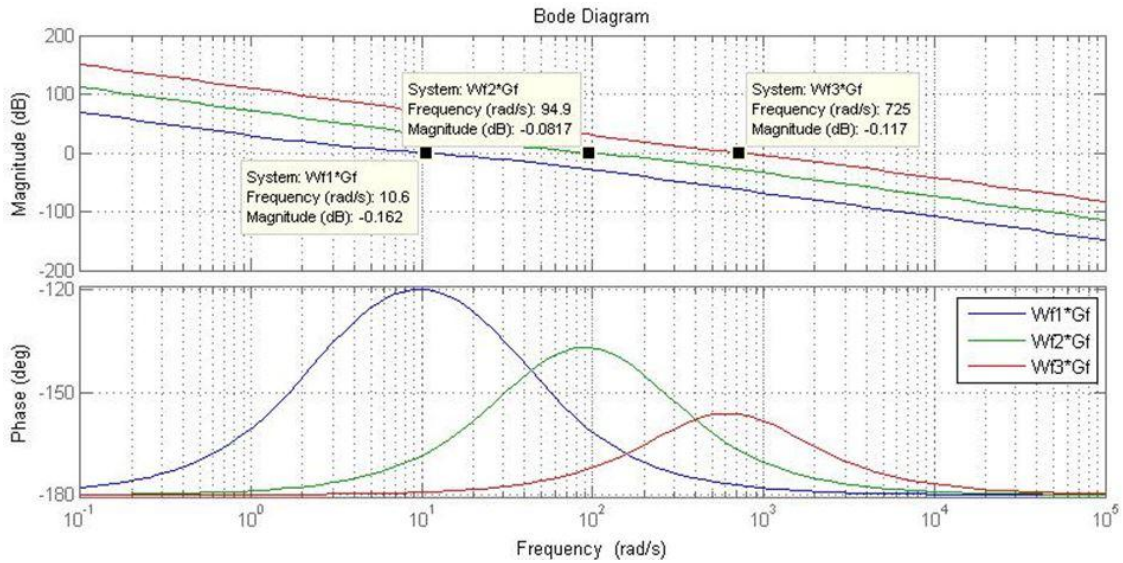


Figure 3.20. Loop-shaping procedure using pre-compensator  $W_f$  to reshape the target system of antagonistic force control  $G_f$ . Three pre-compensators, resulting in different bandwidths, are selected. The ultimate controllers of different dynamics (bandwidths) are selected to cover all necessary joint dynamics requirements – from the beginning (where high loads and low frequency motion/disturbances are expected) to the end of the kinematic chain (where low loads but high frequency motion/disturbances are anticipated).

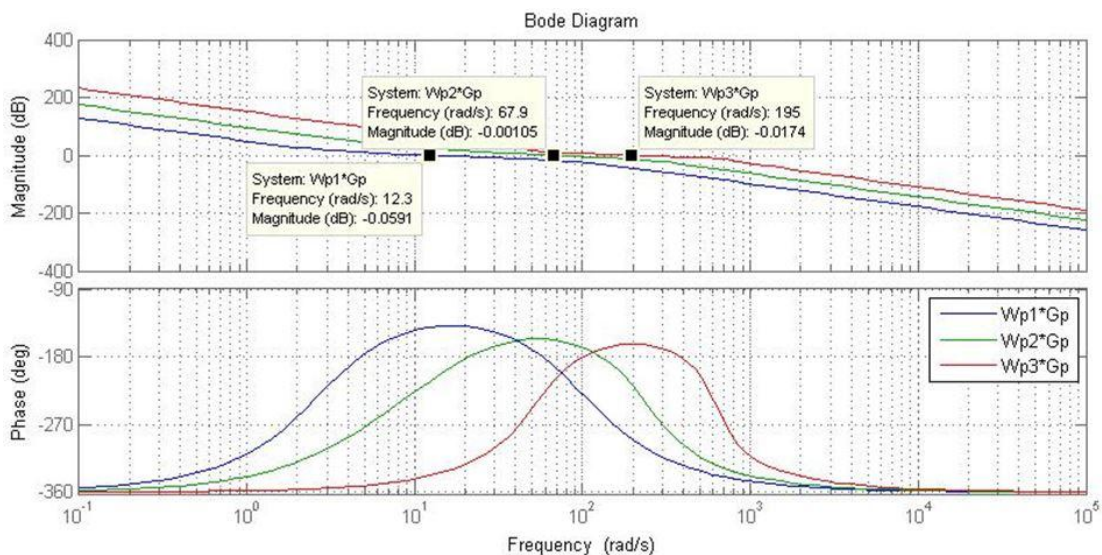


Figure 3.21. Loop-shaping procedure using pre-compensator  $W_p$  to reshape the target system of joint position control  $G_p$ . Three pre-compensators, resulting in different bandwidths, are selected. The ultimate controllers of different dynamics (bandwidths) are selected to cover all necessary joint dynamics requirements – from the beginning (high load, low frequency motion/disturbances) to the end of the kinematic chain (low load, high frequency motion/disturbances).

The second step of the control design is the selection of the feedback controller –  $K_\infty$ . The goal of the  $K_\infty$  compensator is to ensure robust stability of the closed-loop system. Therefore, according to [200],  $K_\infty$  has to satisfy inequality (3.67), where  $\gamma$  represents the  $H_\infty$  norm of the transfer function from disturbances to the input and output of the system. Glover and McFarlane in [208] explain the selection of  $\gamma_{min}$  in accordance with (3.68), or the maximal discrepancy between the model and the corresponding real process  $\varepsilon_{max}$  ( $H_\infty$  norm of the model uncertainty or supremum of the largest singular value over all frequencies). At the same time,  $\varepsilon_{max}$  represents the stability margin of the so-called normalized coprime factor for the robust stability problem. Here,  $X$  and  $Y$  stand for unique positive solutions to Riccati's algebraic equations (3.69) and (3.70), respectively. The target system given by the transfer function  $G(s)$  is represented in its state space form, defined by the matrices  $A, B, C, D$ . The symbols  $S = I + D^T D$  and  $R = I + D D^T$  are introduced to allow more compact writing, and  $\bar{\sigma}$  denotes the maximal singular values.

$$\gamma = \left\| \begin{bmatrix} K \\ I \end{bmatrix} (I - GK)^{-1} M^{-1} \right\|_\infty \leq \varepsilon \quad (3.67)$$

$$\gamma_{min} = \varepsilon_{max}^{-1} = (1 + \bar{\sigma}(XY))^{1/2}; \quad (3.68)$$

$$X: (A - BS^{-1}D^T C)^T X + X(A - BS^{-1}D^T C) - XBS^{-1}B^T X + C^T R^{-1}C = 0 \quad (3.69)$$

$$Y: (A - BS^{-1}D^T C)Y + Y(A - BS^{-1}D^T C)^T - YC^T R^{-1}CY + BS^{-1}B^T = 0 \quad (3.70)$$

Therefore, after solving Riccati's equations (3.69) and (3.70) for  $X$  and  $Y$ , and for some  $\gamma > \gamma_{min}$ , the compensator that ensures robust stability  $K_\infty$  is specified in a closed form by its state space representation  $A_{K_\infty}, B_{K_\infty}, C_{K_\infty}, D_{K_\infty}$ :

$$A_{K_\infty} = A - BS^{-1}(D^T C + B^T X) + \gamma^2(XY + (1 - \gamma^2)I)^{-T} Y C^T (C - DS^{-1}(D^T C + B^T X)) \quad (3.71)$$

$$B_{K_\infty} = \gamma^2(XY + (1 - \gamma^2)I)^{-T} Y C^T \quad (3.72)$$

$$C_{K_\infty} = B^T X \quad (3.73)$$

$$D_{K_\infty} = -D^T \quad (3.74)$$

Finally, the compensator which satisfies (3.67) is given by:

$$K_\infty(s) = C_{K_\infty} (sI - A_{K_\infty})^{-1} B_{K_\infty} + D_{K_\infty} \quad (3.75)$$

The same procedure is applied for the antagonist tension force and joint position subsystems, and loop shaping pre-compensators (3.61) through (3.66), resulting in  $K_\infty$  compensators (3.76) through (3.81). Robust stability margins  $\varepsilon_{max}$  belong to the range  $0.36 \div 0.56$ , which corresponds to a good robust design.

$$- \varepsilon_{max\_F1} = 0.56608 \Rightarrow \gamma_{min\_F1} = 1.7665 \Rightarrow \gamma_{K_\infty\_F1} = 1.9432:$$

$$K_{\infty\_F1} = 90.507 \frac{(s + 36.49)(s + 1.786)}{(s + 2.578)(s^2 + 108.4s + 3758)} \quad (3.76)$$

$$- \varepsilon_{max\_F2} = 0.50754 \Rightarrow \gamma_{min\_F2} = 1.9703 \Rightarrow \gamma_{K_\infty\_F2} = 2.1673:$$

$$K_{\infty\_F2} = 999.48 \frac{(s + 211.5)(s + 22.63)}{(s + 38.44)(s^2 + 885.4s + 2.362e05)}; \quad (3.77)$$

$$- \varepsilon_{max\_F3} = 0.44807 \Rightarrow \gamma_{min\_F3} = 2.2318 \Rightarrow \gamma_{K_\infty\_F3} = 2.455:$$

$$K_{\infty\_F3} = 9281.1 \frac{(s + 975.7)(s + 212.1)}{(s + 396)(s^2 + 6273s + 1.074e07)} \quad (3.78)$$

$$- \varepsilon_{max\_P1} = 0.46555 \Rightarrow \gamma_{min\_P1} = 2.148 \Rightarrow \gamma_{K_\infty\_P1} = 2.3628:$$

$$K_{\infty\_P1} = 171.05 \frac{(s + 99.09)(s + 1.882)(s^2 + 2.593s + 4.936)(s^2 + 150.1s + 1.001e04)}{(s + 2.986)(s^2 + 3.994s + 6.975)(s^2 + 245.8s + 1.733e04)(s^2 + 106.6s + 9228)} \quad (3.79)$$

$$- \varepsilon_{max\_P2} = 0.40384 \Rightarrow \gamma_{min\_P2} = 2.4763 \Rightarrow \gamma_{K_\infty\_P2} = 2.7239:$$

$$K_{\infty\_P2} = 932.3 \frac{(s + 150.4)(s + 4.429)(s^2 + 15.54s + 88.84)(s^2 + 250.4s + 6.247e04)}{(s + 17.21)(s + 10.01)(s + 4.675)(s^2 + 696s + 1.33e05)(s^2 + 193.2s + 8.06e04)} \quad (3.80)$$

$$- \varepsilon_{max\_P3} = 0.36458 \Rightarrow \gamma_{min\_P3} = 2.7429 \Rightarrow \gamma_{K_\infty\_P3} = 3.0172:$$

$$K_{\infty\_P3} = 3462.5 \frac{(s + 441.1)(s + 42.36)(s^2 + 34.76s + 1732)(s^2 + 375.6s + 4.013e05)}{(s + 75.64)(s^2 + 52.09s + 2590)(s^2 + 2061s + 1.1e06)(s^2 + 354.6s + 5.95e05)} \quad (3.81)$$

As explained in the preceding paragraphs, the final feedback controller  $K$  is a combination of the pre-compensator  $W_1$ , feedback controller  $K_\infty$  and post-compensator  $W_2$ .

$$K = W_1 K_\infty W_2 \quad (3.82)$$

Therefore, for selected loop shaping compensators  $W_1$  (assuming post-compensators to be  $W_2 = I$ ) and their matching  $K_\infty$  compensators that enhance robust stability, we can design six different feedback controllers (three for the so-called “antagonistic force” intermediate input and three for the “joint position” intermediate input), which complement feedback linearization and achieve robust simultaneous positioning and antagonistic force tracking of a joint driven by antagonistically-actuated compliant drives. In order to demonstrate the contribution of  $K_\infty$  compensators that enhance robust stability to the previously applied loop shaping compensator  $W_1$ , Bode’s plots of one open loop force (Figure 3.22) and one open loop position robustly controlled system (Figure 3.23) are presented.

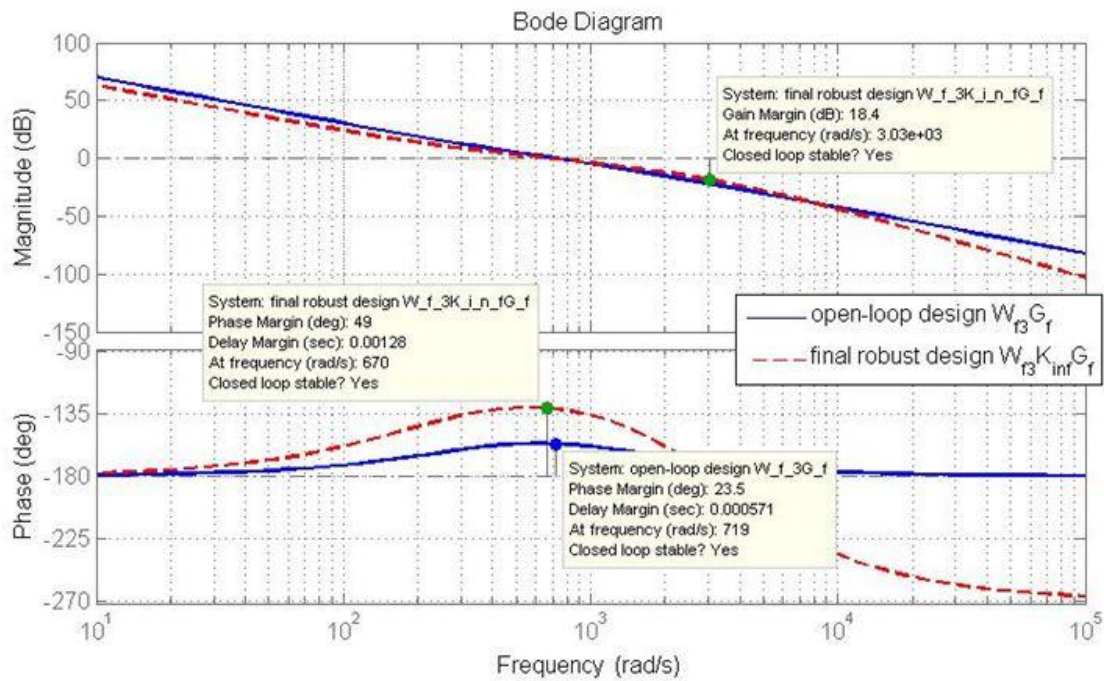


Figure 3.22. Contributions of  $H_\infty$  optimization to robust stability enhancements of the target system: lowered open-loop gain at high frequencies and improved stability margins. The frequency characteristics of the antagonistic force subsystem already shaped by the pre-compensator  $W_{f3} - W_{f3}G_f$  (solid blue line), is improved using the  $K_{\infty\_F3}$  robust stability compensator –  $W_{f3}K_{\infty\_F3}G_f$  (dashed red line).

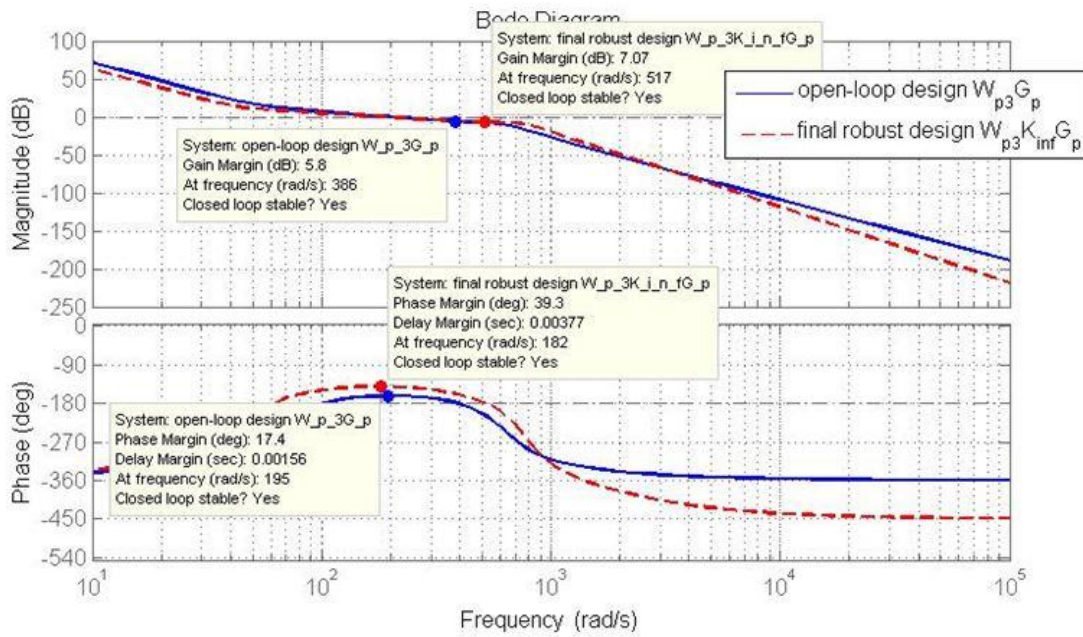


Figure 3.23. Contributions of  $H_{\infty}$  optimization to robust stability enhancements of the target system: lowered open-loop gain at high frequencies and improved stability margins. The frequency characteristics of the joint position subsystem already shaped by the pre-compensator  $W_{p3} - W_{p3}G_p$  (solid blue line) is improved using the  $K_{\infty_{p3}}$  robust stability compensator  $-W_{p3}K_{\infty_{p3}}G_p$  (dashed red line).

In the very least, it should be pointed out that the same control design procedure can be applied to different antagonistic structures, different compliance characteristics (linear, quadratic, exponential, etc.), various open-loop characteristics reshaped using pre- and/or post-compensators, etc. Here we defined three pre-compensators to achieve different dynamics of the final controllers by purpose. Namely, as stated in the preceding paragraphs, dynamic coupling between joints is crucial for optimal controller selection. For instance, joints of high effective (“seen”) inertia are usually of a low-frequency intrinsic nature. Therefore, they do not react to high-frequency disturbances, but absorb them very well, so controllers of a lower bandwidth should be applied. Waist joints or shoulder joints in this particular case are an example. On the other hand, joints of low effective inertia exhibit a higher natural frequency, so the selected controllers can be of a higher bandwidth and should be able to deal with high frequency disturbances. Anyway, whatever pairing of antagonistic force and joint position robust controllers is selected, the antagonistic force control should be of a magnitude order higher bandwidth, since the prevention of tendons slackening is of primary importance when

controlling tendon driven joints. Furthermore, this is significant because the adaptive tension force and tendon switching usually occur during fast joint motions.

Finally, we should highlight the benefits of  $H_\infty$  loop-shaping design for robust control in this particular case. As pointed out in Section 2, the anthropomorphic robot structure is highly complex, as is its model. Because feedback linearization is utilized to decouple the target system, as well as due to dynamic coupling in kinematic chains, it is impossible to extract structured model uncertainties. Therefore, we have to look for a robust control method that makes use of unstructured model uncertainties and an  $H_\infty$  loop-shaping design imposed as a robust control approach, which is relatively easy to implement and tune according to system change. Namely, it is very intuitive since it is based on a conventional loop-shaping approach, and system performance and robust stability are considered in different stages of the control design. Moreover, the  $H_\infty$  loop-shaping design is given in a closed form, which means that no iterative tuning is necessary as in the case with  $\mu$ -synthesis and DK iterations, for instance [209].

Of course, an accurate model of the system is very important for providing adequate knowledge, enabling feedback linearization and decoupling, and, therefore, shaping the target plant for the  $H_\infty$  loop-shaping compensator. According to this procedure, the designed controller is only optimal with respect to the prescribed objectives and does not necessarily represent the best controller in terms of other common performance measures, such as the settling time, overshoot, energy consumption, etc. There is one more general limitation that is not considered in this thesis – non-linear constraints like saturation of the control input. The comfort afforded by the  $H_\infty$  loop-shaping design, through successive tuning of system performance and stability, introduces another inhibitory implementation issue – an unavoidably high order of the controller. As a result, a task usually associated with this control design is to reduce the controller order.

However, the above limitations and shortcomings are not elaborated in this thesis; they remain open questions for some future research. Also, further elaboration on similar but also different control approaches is needed to handle such issues. For instance, the  $H_\infty$  loop-shaping design for multiple-input-multiple-output (MIMO) systems in light of the

robust multivariable control theory will be an intuitive sequel of this work.

### 3.5.4 Simulation results

In summary, the basic puller-follower control scheme is extended to include gravity compensation, awareness of effective joint inertia, and controller design based on the robust control theory. For demonstration purposes, a simulation experiment of a multi-jointed robot (2-DoF robot arm, shoulder and elbow in a plane, actuated by antagonistically-coupled drives with basic linear springs), controlled by the enhanced puller-follower approach, is carried out. Here the shoulder is modeled as a circular joint (see Subsection 2.3.1.1), whereas a triangular joint model (see Subsection 2.3.1.2) is used for the elbow. In addition to the existing uncertainty and unmodeled dynamics, external disturbances are introduced to test the robustness of the control system. The experiment consists of raising the arm in the sagittal plane, by moving the elbow from  $15^\circ$  to  $45^\circ$  and the shoulder from  $0^\circ$  to  $45^\circ$ , in two seconds, following a triangular velocity profile (uniform acceleration phase followed by uniform deceleration phase). Therefore, the control algorithm should compensate for gravity since the movement is planned in the vertical plane. Although the moment of inertia in the elbow is constant, the effective moment of inertia in the shoulder varies according to the elbow position. Finally, dynamic coupling of this multi-body system and the external disturbance are there to validate the robust controller. During movement, a challenging task is assigned to the robot. At time instant  $t = 1s$ , the robot grasps a  $0.25kg$  ball and holds it until the end of the task – this is regarded as a strong external disturbance. Note that the control system first deals with the impact phenomenon as the primary challenge, and then, while holding the object, a constant external load is imposed on the robot. Forearm and upper arm link parameters and joint parameters are given in Table 3.3. Controllers (3.78) and (3.81) for the decoupled force subsystem and position subsystem are used in the case of the shoulder, while (3.77) and (3.80) are used to control the force in the antagonistic tendon and the position of the elbow, respectively.

Table 3.3. Parameters used for simulations in Subsection 3.5.4.

Label	Numerical value	Unit	Description
$l_u$	0.308	[m]	Upper arm length
$m_u$	2.07	[kg]	Upper arm mass
$I_u$	0.0164	[kg · m <sup>2</sup> ]	Upper arm moment of inertia tensor
$l_f$	0.264	[m]	Forearm length
$m_f$	1.14	[kg]	Forearm mass
$I_f$	0.066	[kg · m <sup>2</sup> ]	Forearm moment of inertia
$l_r$	0.15	[m]	Circular joint parameters (shoulder joint)
$\alpha$	$\pi/4$	[rad]	
$l_{a1}$	0.3	[m]	Triangular joint parameters (elbow joint)
$l_{b1}$	0.3	[m]	
$l_{a2}$	0.07	[m]	
$l_{b2}$	0.05	[m]	
$k$	200	[N/m]	Linear spring coeff.

Trajectory tracking and force tracking in both elbow and shoulder joints during this grasping experiment are shown in Figure 3.24 and Figure 3.26. The control system exhibits very acceptable behavior – the influence of the external disturbance is reduced after 1s to less than a 2% position error, there are no steady-state position errors, and the tendons are taut at all times during the movement, even though the reference tension force is set at a very low value of 3 N (which makes the system highly energy efficient). Figure 3.25 displays Cartesian  $x$  and  $z$  positions. It demonstrates deviations in trajectory tracking due to unmodeled dynamics and the in-contact robot motion as an external disturbance which is compensated by the enhanced puller-follower control scheme. Figure 3.27 shows unavoidable effects on a multi-joint system compensated by the enhanced puller-follower algorithm, including gravity compensation, estimation of effective joint inertia and  $H_\infty$  loop shaping robust control: gravity load torque in the shoulder and elbow, changeable joint inertia (effective shoulder inertia changed due to elbow position change, while elbow inertia remained unchanged since it was the last link in the kinematic chain) and external forces of an unexpected interaction with an external object.

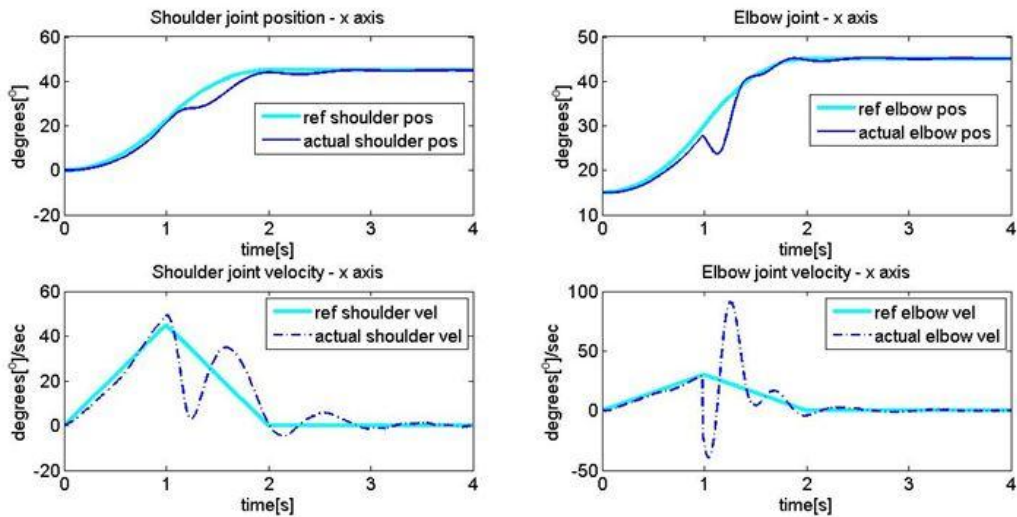


Figure 3.24. Puller-follower control applied to a 2-DoF robot arm actuated by antagonistic compliant drives. The top two windows depict shoulder and elbow positions, and the bottom windows show velocities during movement in the vertical plane. Trajectory tracking demonstrates how puller-follower control deals with a multi-joint system, nonlinearities caused by gravity, changeable effective joint inertia, and external disturbances (impact with an external object at  $t = 1$ s).

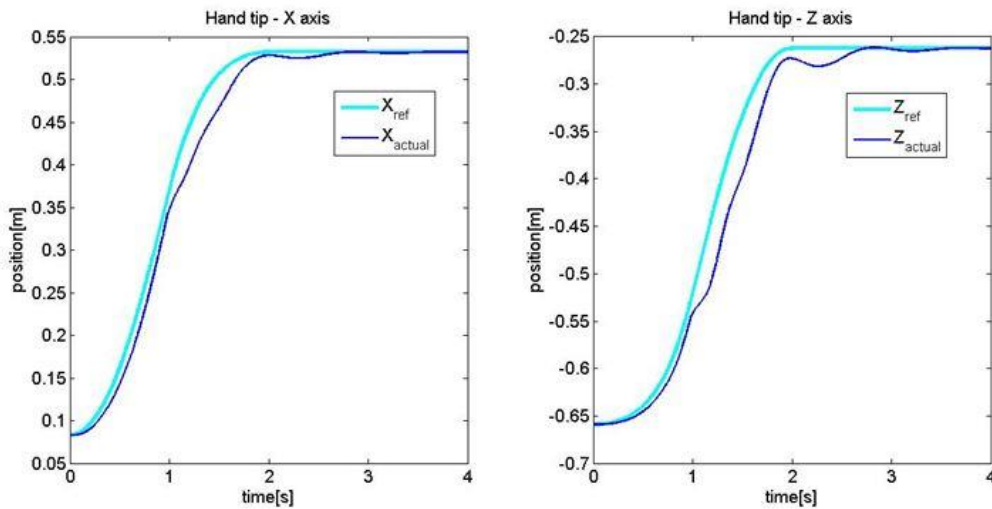


Figure 3.25. Puller-follower control applied to a 2-DoF robot arm actuated by antagonistic compliant drives. Horizontal (left window) and vertical (right window) Cartesian coordinates demonstrate the effects of gravity compensation, effective joint inertia and impact in the vertical plane.

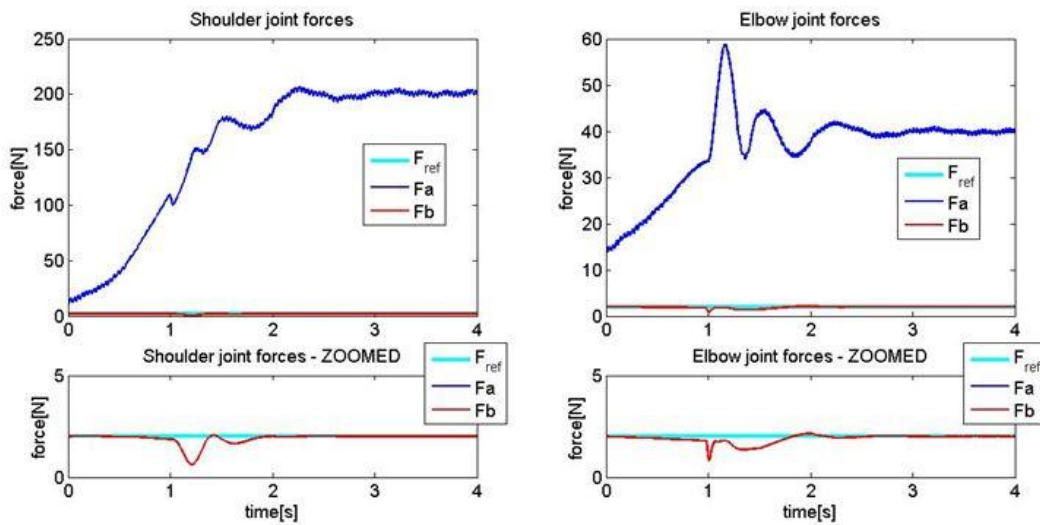


Figure 3.26. Puller-follower control applied to a 2-DoF robot arm actuated by antagonistic compliant drives. Agonist and antagonist tendon forces in shoulder and elbow joints during movement in the vertical plane (top windows); Zoomed in detail from the top – force tracking in antagonist tendons. Both antagonistic tendons remain tight even though impact occurs (bottom windows).

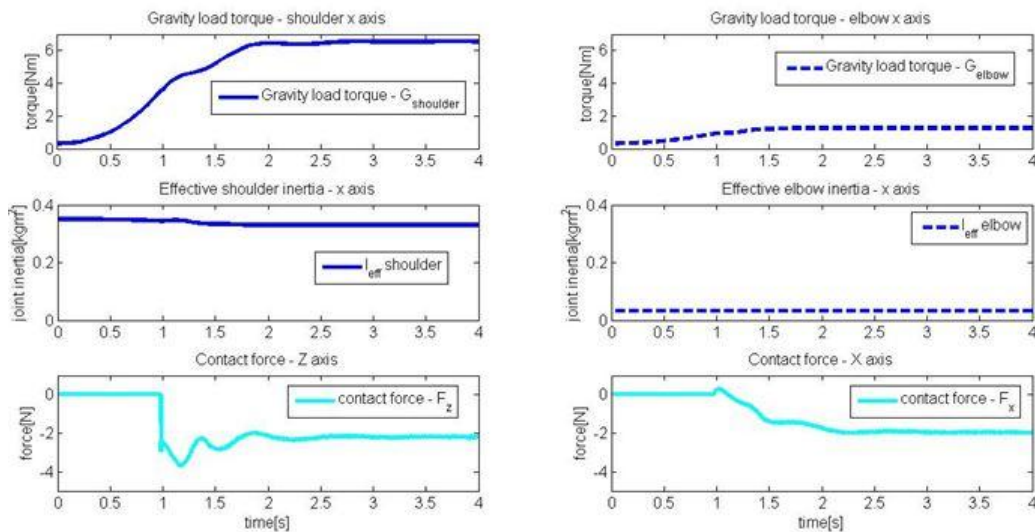


Figure 3.27. Puller-follower control applied to a 2-DoF robot arm actuated by antagonistic compliant drives. The figure shows unavoidable effects on a multi-joint system compensated by the enhanced puller-follower algorithm, including gravity compensation, estimation of effective joint inertia and  $H_\infty$  loop shaping robust control: gravity load torque in the shoulder and elbow (top windows); changeable joint inertia (effective shoulder inertia changed due to elbow position change, while elbow inertia remained unchanged since it was the last link in the kinematic chain) – (middle windows); external disturbance expressed by an unexpected impact with an external object at  $t = 1$ s and resulting in-contact motion that caused the interaction force compensated by puller-follower control (bottom windows).

### **3.6 Final comments on the puller-follower control concept for musculoskeletal system control**

Although we highlighted the possibilities of the puller-follower and extended puller-follower control concepts, the application to musculoskeletal robots is still limited.

Despite the fact that many humanoid robot joints are human-like (with reduced complexity and single-axis rotational joints) and, therefore, designed to exploit antagonism and be controlled in this manner, the application of puller-follower control to fully human-like multi-rotational joints or multi-articular muscles is still an open issue. Many human joints are multi-rotational and/or spherical (shoulder, hip, elbow, etc.). Yet, we do not consider such complex structures in this thesis. It is clear that such joints cannot be controlled in a conventional manner – a rigid connection with their actuator. “Artificial muscles” (tendon-driven and antagonistic actuators, and probably compliant as well) need to be used [210]. Therefore, all the work elaborated here on the control of antagonistically-coupled compliant joints can be adapted and used to support the design and, particularly, control of full human-like joints.

The control concepts applied to pure antagonistic joints might not be only a step towards control of complex human-like joints. Also, Lynch et al. show in [211] that functional electrical stimulation (FES) can be used to efficiently move a knee by controlling only one antagonistic muscle pair, instead of the whole musculoskeletal knee structure. Further analysis of knee co-contraction patterns of antagonistic muscles could contribute to a future FES based on a single antagonistic muscle group.

Another limiting factor is accurate system modeling. Biological systems are not designed according to engineering principles, they are highly nonlinear and coupled, and, as such, are very difficult to model and copy in the technical world. The lack of accurate models is a major obstacle for advanced control techniques, which are mostly model-dependent in order to achieve their ultimate performance.

Note that the antagonistically-driven compliant joint elaborated in this section is nothing but a joint driven by two antagonistic SEAs. Therefore, the same control issues and fundamental limitations apply, like those highlighted by Robinson in [212] for SEAs that use electric motors. The control system gain and the spring stiffness gain each contribute to the loop gain of the closed-loop system. With a lower spring stiffness, the controller gain can be increased by a proportional amount to bring the loop gain to the desired phase and gain stability margins. However, high controller gain/bandwidth could degrade system performance due to sensor noise. Also, in order to achieve a powerful actuator that generates high torques/forces at high velocities (called “large force bandwidth” in the literature), serial tendon stiffness should be rather high. Compromising the previous requirement, a lower output impedance is achieved with lower tendon stiffness. Therefore, in order to control a robot joint driven by two antagonistically coupled SEAs, one should follow performance limit guidelines set by Pratt and Williamson in [12], since movement dynamics are limited by mechanical properties of the setup. In the presented designs, these properties are: serial elasticity of the springs, joint inertia (or “effective” moment of inertia for kinematic chains), motor pulley’s diameter and, ultimately, the motor parameters themselves.

Following are some effects that should be considered with regard to antagonistically-actuated compliant joint control, in order to prevent reaching the limitations and thus causing unpredictable system behavior based on references [12] and [212]:

- Actuator dynamics – a motor has limits in its instantaneous force and position/velocity changes (as long as the motor operates within these limits, the overall bandwidth of the actuator is not affected; otherwise an increase in spring stiffness should be considered);
- Non-collocated dynamics (higher-order dynamics that may be excited as the closed-loop bandwidth of the actuator is increased);
- Bandwidth limitations of the power modulator (electric motor amplifiers operate in the kHz range, but if hydraulic drives are used as actuators, servo valve bandwidth should be considered);

- Finite sensor resolution and sensor noise (these apparent sensor characteristics, amplified with a high controller gain, could be a source of instability);
- Controller dynamics (it may be necessary to filter noisy signals (low pass filtering adds poles to the controller dynamics) or have an integral component in the controller (adds phase lag) to get zero steady-state error; so a trade-off between spring stiffness and control gains should be reconsidered); and
- Plant nonlinearities (i.e. transmission backlash and friction, actuator saturation, etc.)

The theory behind this advocates that at low forces or during contact tasks, low stiffness helps maintain stability. At much higher forces and/or at high velocities, low stiffness is unnecessary and may even be undesirable. This discussion about different limitations in the technical world tells us more about the perfection of biological systems. Namely, tendons as “biological springs” are non-linear in general, but their stiffness characteristics increase rapidly for high forces/elongations. This makes ideal serial elasticity, even from a control theory perspective.

Finally, the work presented in this section leads us to an unequivocal conclusion. In spite of the natural human wish to create a fully human-like musculoskeletal robot (an artificial human), which would easily fit in an environment completely adapted to humans, some compromises must be made. The puller-follower control approach, applicable to antagonistically-actuated joints, is proposed here as an engineering approximation of human prime movers, which are rarely driven solely by activation of two antagonistically-coupled muscles, but rather by a number of multi-articular muscles. The puller-follower is a synthesis of conventional control techniques (non-linear, multivariable, robust) and is perceived at the frontier of conventional engineering in the field of control of conspicuously non-engineered musculoskeletal mechanisms. In order to move closer to the control of bio-inspired mechanisms, we need to broaden this approach to include learning and cognition, as evident techniques that could advance the exploitation of such mechanism. Although these directions are not of primary interest here, they are something that should be called upon to assist and overcome the

limitations of conventional engineering. Moreover, it is intuitively expected that the final control scheme of human-like robots will be a symbiosis of control techniques based on conventional engineering, learning, and, finally, cognition.

## 4 Cognition-based control approaches

In accordance with the anthropomimetic robotic principle, to fully replicate the (non-engineered) human structure, the control of such a robot would have to rely on artificial intelligence, learning and experience, rather than on conventional engineering. The limitations and issues associated with engineering control design, pointed out in Section 3, support this point of view. Consequently, some cognitive-based approaches hold the most promise for the control of fully anthropomimetic robot structures, which are highly complex, compliant, non-linear, and multivariable systems. As part of the ultimate objective of this thesis – to suggest directions in the control of fully anthropomimetic robots, we will step away from conventional engineering and look toward some novel paths. Although not the primary focus of the thesis, this section explores the exploitation of neural networks, the fuzzy theory, experience and cognition in terms of control of future human-like mechanisms. The main findings and observations on the topic are elaborated in the present section and have also been summarized in the author's previous papers [5], [213], [214].

Even though a lot of effort is being invested in future service robots of distinguishable human-like appearance and such a mechanical design (anthropomimetic robots), conventional robots still prevail in our everyday lives. Most probably, the control of such robots is a stumbling block that hinders rapid progress of this emerging technology. Conventional control techniques cannot fully cope with the concept of robots that have multi-DoF joints, muscles (tendons) crossing several joints (so called multi-articular muscles), and, in general, features that go beyond the scope of conventional engineering. Modeling of such systems is demanding (if at all possible), so that one cannot rely on analytical models and numerous engineering robot-control techniques. For instance, this applies to the previously presented puller-follower control concept (Section 3). There is no doubt that anthropomimetic robot control will strongly rely on experience and cognition, as in the case with humans. A lot of effort has been made to first understand human motor control, extract similarities and understand the

differences of engineering control schemes, and ultimately copy and adapt biological patterns to the technical world, to a certain extent.

Not many control approaches based on human motor control strategies and learning strategies have ultimately been implemented in robots. Successful examples that have been presented include the DLR LWR, which utilizes a scheme for instantaneous adaptation of the reference motion trajectory, impedance and generated force [215], and the GuRoo project at the University of Queensland [216]. Furthermore, very few research teams target control approaches based on learning, experience and cognition, as applied to antagonistic joints, but with the growth in popularity of anthropomorphic robots, this number will increase. An overview of the background work is given in Subsection 4.1.

Section 4 is organized as follows. Subsection 4.1 describes the background work and ideas and concepts presented to date for cognition-based robot control, with special emphasis on anthropomorphic robots and antagonistic joint structures. Subsection 4.2 introduces our ideas that rely on previously presented works. The author's ideas for a non-conventional approach to feedforward and feedback control are discussed in Subsection 4.3 and Subsection 4.4, respectively. Subsection 4.3.1 deals in more detail with the experience acquisition phase, as a foundation for the generation of experience-based feedforward control. Feedforward methods that make use of the "nearest-neighbor" approach and neural networks are elaborated in Subsection 4.3.2 and Subsection 4.3.3, respectively. Feedback terms comprise the nearest-neighbor feedback approach presented in Subsection 4.4.1 and feedback control based on online estimation of kinematic coefficients and fuzzy logic proposed in Subsection 4.4.2. The simulation results of all the approaches are presented in Subsection 4.5. Subsection 4.6 concludes the section and highlights the author's point of view.

## **4.1 Background work**

This thesis supports the belief that evolution of control schemes and algorithms for

anthropomimetic robots will lead to a close resemblance of human control patterns as anthropomimetic robots move to higher levels of human-like design. This position is shared with Prof. Burdet from Imperial College, who recalled the words of the famous tennis player Chris Evert who jokingly said: “When I was younger, I was a robot”. Burdet claims in [215] that she might have been closer to reality than she thought. Infants progressively master their skills, and actually learn how to utilize information made available by their senses to improve control actions in certain tasks and, in particular, environments. Therefore, the study of human motor control and learning is closely related to robotics. Different learning technologies, acquired experience and cognition techniques will also unequivocally master the control of future anthropomimetic robots. To that end, several research directions can be distinguished, all leading to control of complex musculoskeletal humanoids. Let us briefly remind ourselves of some important works in the fields of forward-model exploitation, equilibrium-point hypothesis, trial-and-error or repetitive-learning methods, neural networks, etc. All the presented research efforts have targeted control of complex robotics structures and some have considered antagonistic joints as the main movers of anthropomimetic robots in particular.

For a complex mechanism such as a truly anthropomimetic robot, it would be extremely difficult to generate an analytical model. However, a forward-model<sup>1</sup> may be implemented in other ways, such as a trained neural network or a physics-based simulator. The existence and exploitation of internal forward models in humans were uncovered and discussed by Wolpert at MIT. In [217] and [218], they claim that the central nervous system internally simulates the dynamic behavior of the motor system in planning, control, and learning. The existence and use of such models are advocated by experiments in which participants estimate the location of one of their hands at the end of movement in the dark and under externally imposed forces. Although an inverse model is often required in the control design, to relate current and desired states to control inputs, some control techniques could benefit from this forward (or "black-box") model, too. Very often, an inverse model cannot be derived since inverse kinematics

---

<sup>1</sup> A forward-model enables the evaluation of resultant states based on a set of current states and a set of control signals.

cannot easily handle model redundancy that leads to numerous potential solutions. Wolpert and Kawato presented in [219] the utilization of a forward model to provide its inverse model by estimating an error signal for training and correction of the inverse model over time. Other applications of feedforward models in control cover improved state estimation through Kalman filtering [220], delay compensation [221], feedback error learning [222], and cost function minimization in optimal control [223]. Finally, Diamond et al. apply this idea of forward models to the complex anthropomorphic robot – Eccerobot in [224].

Another group of control methods rely on Feldman’s “equilibrium point hypothesis” – EP [225]. Briefly, an equilibrium point is a pair of muscle length and muscle force that would have been observed if the control process stopped and the system was given time to reach an equilibrium state. In addition, the explanatory and predictive capacity of the EP model has been enhanced by its extension to include multi-joint systems and muscles crossing several joints [226]. Gu and Ballard present in [227] a controller that uses the equilibrium point hypothesis and choose motor synergies for coordinated movements in humanoid robots. Researchers in different fields also support the existence of activity subsets or primitives. Thus, a complex movement can be parsed into many simple movements – so-called primitives, which can be controlled/activated easily and can even comprise the natural dynamics of the system [228]. Chhabra and Jacobs tried to reduce the complexity of multi-DoF system control by introducing libraries of primitives (i.e., motor synergies), which contain control sequences for different individual tasks or parts of tasks. They introduce a new learning model for a simulated two-joint robot arm referred to as a greedy additive regression (GAR) model [229]. GAR is used to learn the coefficients of a linear combination of library sequences that minimize the cost function. However, for an anthropomorphic robot driven by a large number of tendons, with high redundancy, inevitable friction, and blurred kinematic coupling, it would be very difficult to acquire the equilibrium and synergies.

Following biological patterns, one can also expect to find a solution for controlling an anthropomorphic robot through trial-and-error learning methods. As the name implies, this algorithm rewards successful trials, while repressing others. However, control of a

complex musculoskeletal robot does not appear to be a suitable candidate, since reinforcement learning control [230] needs to look for the entire sequence of action, which is a high-dimensional problem. More and Atkeson prove in [231] that computation and data requirements in reinforcement learning increase exponentially with the problem state size. A significant improvement in the application of generic reinforcement learning to high dimensional control systems, such as robots, is reported in [232]. On the other hand, if only the task parameters are varied even slightly after training, then learning must often be recommenced [233]. A form of modified reinforcement learning has already been tested on anthropomorphic robots [224], or, more precisely, on a reduced-complexity robot model. The authors use GPUs for fast simulation of possible scenarios of reaching/pointing tasks and rewarding of the best candidates. This algorithm is used to decide on the next activity of the robot.

Note that none of the previous efforts has targeted antagonistically-coupled drives. This is mainly due to the fact that input-output relations are not restricted to established and accurate models, so treatment of multi-articular muscles and multi-DoF joints is also feasible. Clearly, that has not been the case in modeling and control of the same systems using analytics. However, Shadmehr introduced learning technologies in [234] for the control of a two-DoF arm driven by antagonistic joints. He elaborates the possibilities of learning the inverse dynamics of such a system, while the kinematics are well known. To that end, he suggests a Cerebellar-modeled articulated controller (CMAC), which produces a virtual trajectory of joints as the controller output, rather than the intuitively expected joint torque. Chou and Hannaford [71] were among the first to implement the knowledge of the physiology of human motion control in antagonistic drives and robotics. Their antagonistic pneumatic actuators, acting as elbow flexor and extensor, are assumed to have the same timing and relative amplitude characteristics as a spatial summed and rectified EMG. They are controlled by artificial neural networks based on physiological laws, where the actuator pressures were analogous to muscle activation levels, so basic feedforward was implemented, resembling measured EMG patterns. Huh et al. apply in [235] RBN neural networks to compensate for model uncertainties and friction, in addition to a computed torque control scheme for simultaneous position and stiffness control of a VSA [81], which also exploits the antagonistic principle. The

authors demonstrate the predominance of such an actuation scheme over an experimentally-tuned PID controller.

Since classical control methods mostly ignore or are incapable of incorporating stochastic information, Vijayakumar and his group at the Institute of Perception, Action and Behaviour, University of Edinburgh, were the first to introduce the principles of stochastic optimization in the control of antagonistically-coupled drives and variable impedance actuators in general. In [236], Mitrovic et al. propose a methodology for generating optimal control commands for variable impedance actuators, with a prescribed trade-off between task accuracy and energy cost. Supervised learning is acquired to model both the plant dynamics and its stochastic properties. Their approach was evaluated using two antagonistically-coupled series elastic actuators of a classical mechanical structure. By changing weights between accuracy and energy consumption, the biological pattern and the role of the co-contractions of antagonistic drives is evident. These authors also list several directions, which could potentially avoid numerical issues and instability (not converge to a non-reasonable solution), which was noted when using fully-learned forward dynamics. They suggest a combination of locally-weighted projection regression (LWPR) learning and an analytic model, which supports the fact that an accurate model of system dynamics is a valuable tool for advanced control techniques applied to such a sophisticated mechanical system. However, the employment of a complex mathematical apparatus, such as machine learning and stochastic optimization, requires significant resources. In that work, machine-learning validated experiments were carried out on a single joint and two motors. Implementations in multi-DoF systems would be extremely demanding since high-dimensional systems would impose serious computational challenges on both optimal control methods and machine learning techniques.

Kawai and Fujita demonstrate the supremacy of control methods based on learning, over conventional control methods, for more complex joint structures. They consider a two-DOF robot manipulator with antagonistic bi-articular muscles. Actually, their simulation model considers two pairs of classical antagonistically-coupled muscles (one per DoF), plus one bi-directional muscle pair that affects both axes. In [237], they

propose Arimoto-type iterative learning control, where convergence analysis of the closed-loop system is discussed based on passivity. They rate this passivity-based iterative learning control as more robust and accurate than their previous work based on classical control, which again considered passivity but was not proven explicitly for antagonistic bi-articular muscles [238].

The coexistence of feedforward and feedback control in human motor control is explained by Burdet et al. in [215]. Feedback control in human motor control is evidently present and could be proved in tasks when a disturbed motion returns to the planned trajectory by reciprocal muscle activation. Since a reflex arc takes at least 60 ms, there must be some feedforward pattern to plan the forces for a task in advance. In light of antagonist actuators, as typical movers of the human body, the authors advocate the co-activation activity as the one that results mainly from a feedforward action, whereas the reciprocal activation is often referred as a feedback term. Furthermore, they distinguish two portions of feedback control action: the first originates from the mechanical properties of muscles and depends on the co-contraction level (passive compliance), and the second is the part learned through interaction with the environment (active compliance). By observing human behavior patterns from a robot perspective, the authors claim that both robots and humans simultaneously adapt the movement reference trajectory, impedance and generated force.

One more cognition-based approach, which resembles a bio-inspired design of robot control via a combination of feedforward and feedback learned terms, is presented in [216]. The feedforward subsystem relies on an on-line learning algorithm founded upon a CMAC-based (cerebellar model arithmetic computer) neural network, whereas, atypically, feedback is tuned off-line in a simulator. The feedback control is based on a classical PI compensator whose parameters are determined by a genetic control algorithm, utilizing a fitness function that minimizes the tracking error and vibration in each joint.

## 4.2 Introduction to cognitive approaches

Inspired by these ideas, several feedforward-feedback control approaches were developed under this thesis, which solved the point-to-point control problem (end-effector position without orientation) in the operational space. Here we primarily focus on hand-tip position control and no interaction is planned. For a comprehensive control design of an anthropomorphic robot deemed to be a black-box system, both the feedforward (FF) term and the feedback (FB) term are considered. FF control drives the hand tip to the vicinity of the prescribed final position. FF is followed by the contribution of the FB component, which enables fine tuning of the hand tip. Since the target system mimics its typical biological paragon, an attempt was made to follow the biological pattern, such that computational intelligence, experience, neural networks and fuzzy logic were used. The following paragraphs propose a few approaches, such as: heuristic methods for interpolation and neural network based FF, as well as a fuzzy logic approach to FB control. The presented control approaches are demonstrated on a multi-joint anthropomorphic robot arm with seven DoFs modeled after the Eccerobot arm structure (Figure 4.1). Thus, each robot axis is driven by antagonistically-paired tendons, wound up by pulleys, and the corresponding motor-gearbox coupling. Shoulder and hand joints are considered to be circular (Figure 2.3, left), whereas a triangular structure (Figure 2.3, right) is adopted for the elbow joints to resemble the actuation and structure of a human arm more closely. The targeted simulation model considers DC motor voltages as control inputs and therefore exploits the model given by (2.41). Such a model does not restrict the proposed control approaches in any manner and DC motor voltages were selected as control inputs to allow comparison to their physical paragon – electromyogram (EMG) signal.

Contrary to the majority of the previous methods, the proposed solution should be rather easy to extend and apply to various anthropomorphic structures. This means that the control approach does not consider the exact number of robot DoFs and takes care of each actuator unit, regardless of whether the robot configuration is redundant or not. System identification is omitted and special attention paid to the control of the system, characterized as a black-box system. Thus, the aim of this research is to achieve point-

to-point movement with a certain accuracy, whereas the model representation, and hence the kinematics, dynamics, and drive parameters of the robot, are deemed unknown or too complex to be considered. Therefore, the approach is planned to even deal with multi-articular tendons (muscles) or multi-DoF joints.

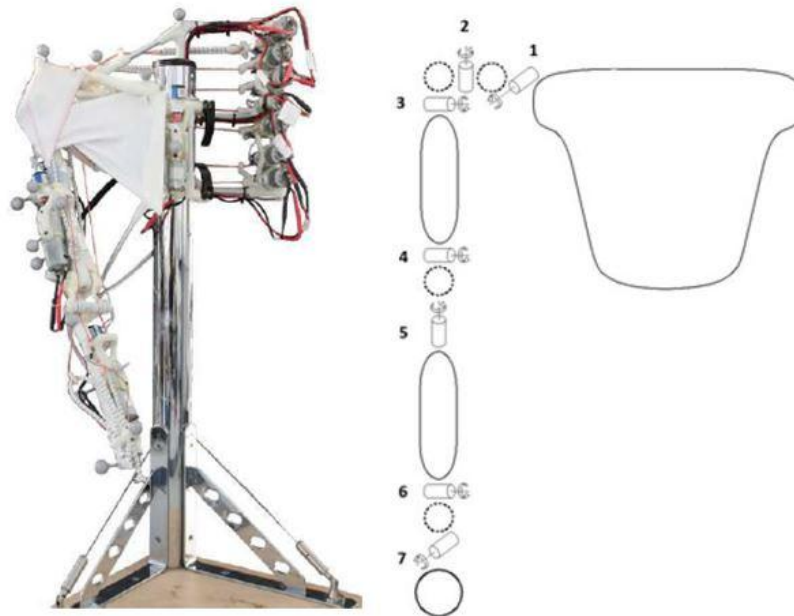


*Figure 4.1. Eccerobot arm test bed – robot arm with seven DoFs (three-DoF shoulder, two-DoF elbow and two-DoF hand), with fully anthropomorphic tendon routing. Each tendon contains an elastic element and is driven by a DC drive, gearbox and winding pulley (left); Graphical representation of the seven-DoF anthropomorphic arm approximation. Each multi-DoF joint is approximated with virtual segments (segments of negligible size and mass) between joint axes. Tendon routing is approximated by two antagonistically-coupled tendons per rotation axis (right).*

Two stages are distinguished in the proposed control designs. The first stage is “experience acquisition”, comprised of a set of experiments with the robot, which are performed applying different input sequences and measuring corresponding responses. The initial and final Cartesian positions as system outputs and input voltage sequences recorded for each motor create a database called the experience base. In the second stage, “system exploitation”, the robot is asked to reach a target point that had not previously been reached in training. The recorded data are used for training of a neural network in order to obtain the FF control component, but also kinematic coefficients for fuzzy control at the FB level. The same recorded data are also used for a heuristic control scheme, which has been named “the nearest-neighbor” method.

## 4.3 Feedforward control

Feedforward has been recognized [239] as a key component of fast reaching movement, as the most frequent motion of future service robots. This subsection brings two approaches to feedforward control dedicated to complex mechanical structures, such as fully-human-like robotic manipulators. Since both feedforward methods are intentionally model-free, we rely on the experience base. In both cases, the experience acquisition stage is the initial stage where an initial pool of movements is created as a foundation for following the required moves. The nearest-neighbor feedforward approach is elaborated in Subsection 4.3.2 and the utilization of neural networks in feedforward control of the anthropomorphic robot is discussed in Subsection 4.3.3. Both approaches rely on the experience base, which is created from point-to-point movements of the hand tip. The robot arm is driven by antagonistically-paired actuators whose control inputs resemble typical activities of human antagonistically-coupled muscles, as explained in Subsection 4.3.1.

### 4.3.1 Experience base

To tailor a robot to its own skills, the robot should consider its own experience that arises from previous trial-and-error exploration of possible scenarios. Using this experience-based learning, it is almost guaranteed that the robot will be capable of achieving the required tasks. Unfortunately, data gathering is often expensive, if even applicable, and the time required for the learning phase could be intolerably long.

To comply with the targeted system of the musculo-tendon structure, the experience base has been created by feeding DC drives with signals that resemble EMG activity patterns for common tasks, such as lifting an arm [240]. In that paper, Tal'nov et al. present the results of recorded flexor (agonist) and extensor (antagonist) EMGs during flexion of the elbow joint. It is apparent that the agonist's EMG signal achieves maximal values in the middle range of the joint angle and decreases noticeably afterwards. It is also easy to notice that the antagonist has a very similar EMG pattern

compared to the agonist, but it is delayed proportionally to the speed of the complete move. Following these bio-inspired patterns, we create patterns of input voltages to drive the system from the vicinity of an initial position to a targeted zone.

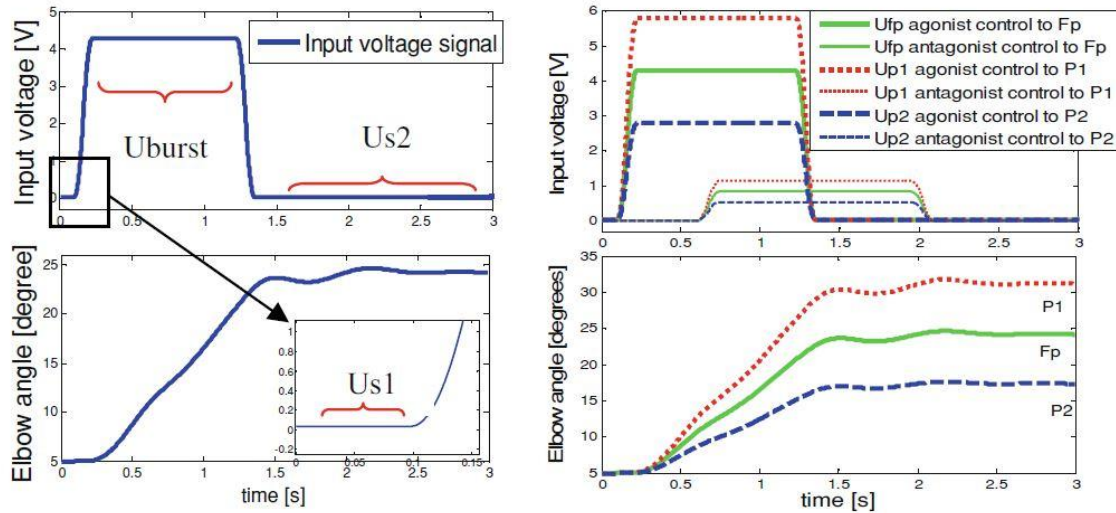


Figure 4.2. EMG-like control signal consists of several phases: a burst component before  $t < 1.5s$  ( $U_{burst}$ ), a silent period after approximately  $t > 1.5s$  ( $U_{s2}$ ), and a zoomed in period before the motion ( $U_{s1}$ ) - (top left); Agonist and antagonist input control voltages resembling EMG shapes of flexor and extensor muscles during elbow flexion (top right); Elbow position as a result of the presented input control pattern (bottom left); Elbow positions  $p_1$ ,  $p_2$  and  $f_p$  resulting from the presented control  $U_{p1}$ ,  $U_{p2}$  and  $U_{fp}$ , respectively (bottom right).

We apply the same pattern to control all joints of the robot model. The pattern of input voltage, which is fed into the actuators and generated by replicating the EMG signals, is shown in Figure 4.2 (top left). This pattern holds for both agonists and antagonists, while the timing and intensity differ. By observing the input signal, we can distinguish three input voltage components: initial silent period ( $U_{s1}$ ); control signal burst ( $U_{burst}$ ), mainly responsible for joint motion; and silent period ( $U_{s2}$ ). Therefore, these three parameters define the input voltage fed to the actuator. The supplied voltages that correspond to the agonist-antagonist pair and the resulting joint position are shown in Figure 4.2 (right). Such activity patterns of antagonistic muscles and their correlations were also confirmed by Smith. In his hypothesis [241], Smith says: “...*Cerebellum plays an important role in motor learning by forming and storing associated muscle*

*activation patterns for the time varying control of limb mechanics. By modulating the co-contraction of agonist-antagonist muscles through adjustments in the timing and amplitude of muscle activity, the viscoelastic properties of joints can be appropriately regulated throughout movement and adapted for transitions between postures and movements ...”.*

As previously stated, this author’s idea was demonstrated using a model of the anthropomorphic robot arm with seven single DoFs, modeled according to (2.41). The experience is acquired through a series of motion experiments performed from a set of initial hand-tip positions  $X_s$  that define the initial region of predefined radius, which end in the region of the final positions  $X_f$  of another radius. After a properly accomplished motion, the arm would be in an extended position so that the hand tip is located at the height of the right shoulder. The joints are controlled by heuristically-determined control voltages of the same pattern as presented in Figure 4.2. The pointing action does not specify the path, only the end point. However, since interpolation is based on human-like movements, it is expected from the robot arm to act in the same manner. These positions (Figure 4.3) define the acquired population (experience) as a grid of nodes. Namely, any initial position is in the sphere  $X_s$  with a  $0.1m$  radius and the center in the Cartesian point  $(0.2, -0.4, -0.45)$ , whereas each final position is in the sphere  $X_f$  with a  $0.05m$  radius, located around Cartesian coordinates  $(0.55, -0.2, 0)$ . In case of a larger sphere, the same algorithm can be applied but experience acquisition would be even more time-consuming. The set of experiments with the robot are performed applying different input controls and measuring the point reached by the hand tip in the global frame. Our forward model requires an initial position in the global frame and time histories of applied control inputs. Starting from different initial positions, we form the experience base by relating input voltages to initial positions, on one side, with the reached points (outputs) on the other. Learning, teaching or knowledge acquisition represents the training phase when initial and/or final sets are enlarged by adding new points. For each initial position there are about 100 final positions in the final sphere. The average distance between the reached points is called the base resolution. The distance between neighboring points in the initial sphere is up to  $3.5cm$ . The distance between neighbors that derive from the same initial position in the final sphere is up

to 2.5cm.

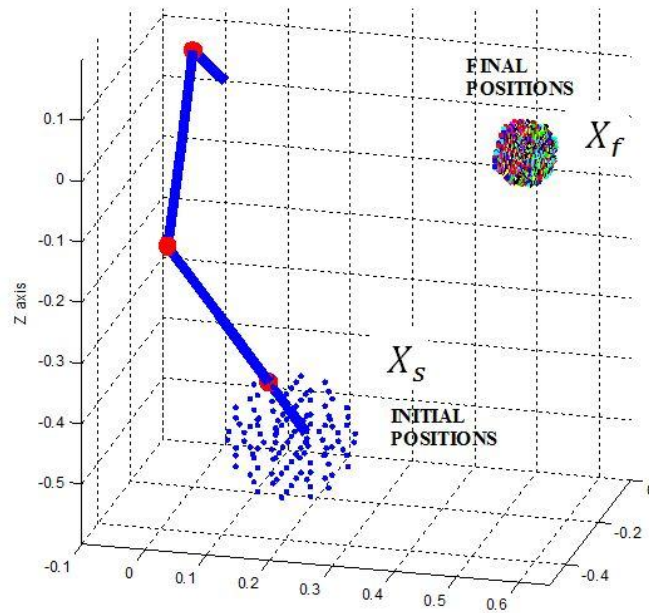


Figure 4.3. Spherical grids of initial and final hand-tip positions, formed in the experience acquisition stage. Sphere  $X_s$ , with a 0.1m radius and the center in the Cartesian point  $(0.2, -0.4, -0.45)$ , captures all initial positions in the training phase. The final sphere  $X_f$ , with a 0.05m radius, located around Cartesian coordinates  $(0.55, -0.2, 0)$ , consists of about 100 points from each of the initial positions within the sphere  $X_s$ .

In the exploitation phase, the robot is required to reach a target point that has not been previously reached in training, starting from a position that has not been previously used. Of course, it is assumed that both initial and final positions are within the initial and final sphere, respectively. Feedforward control is evaluated before the robot moves, i.e. off-line.

### 4.3.2 Nearest-neighbor feedforward approach

In this subsection, the proposed control synthesis is based on interpolation according to the so-called “nearest-neighbor” approach that exploits the experience base. Its application to an anthropomorphic robot arm is presented in [242]. The method is first introduced for a single-joint system and then expanded to a multi-joint system.

As shown in Figure 4.2, the joint position shift strongly depends on the burst components of the input voltages fed into the actuators, as in the case of real muscle-joint configurations and corresponding EMG signals. While these activation bursts are mainly responsible for joint motion, the appropriate steady-state position is held by the static component of post-burst voltages. In approximation, the ratio of the maximum values of the agonist to antagonist activation, as well as their activation time ratio, can be assumed constant for a particular joint. Therefore, in order to move the joint, the maximum activation of the agonist (maximum input voltage) and duration need to be selected, while the activation of the agonist and duration are proportionally modified. It is also assumed that antagonist activation will always make a proportional contrariwise contribution to the joint motion, compared to the contribution of the agonist. In order to demonstrate the nearest-neighbor approach on a single-joint, three elbow joint shifts with corresponding input voltages fed into agonist/antagonist actuators, presented in three different colors, are depicted in Figure 4.2 (right). Two of them ( $p_1$  and  $p_2$ ) are extracted from an experience base, while the third,  $f_p$ , is the desired joint position. Of course, the same initial (home) position is treated. If the distance from  $p_1$  to  $p_2$  is considered as a region of potentially-required final positions  $f_p$ , the appropriate joint control can be interpolated and should drive the joint to the vicinity of  $f_p$ . Namely, if we define  $d_1$  and  $d_2$  as the distance from the final position  $f_p$  to  $p_1$  and  $p_2$ , respectively, joint control of both the agonist and antagonist would be estimated as in (4.1). Since the same signal pattern stands for both agonist and antagonist drives, an expression in matrix form can be derived.

$$\mathbf{U}_{f_p}(t)_{2 \times 1} = \frac{d_1 \mathbf{U}_{p_2}(t)_{2 \times 1} + d_2 \mathbf{U}_{p_1}(t)_{2 \times 1}}{d_1 + d_2} \quad (4.1)$$

The first rows of the matrices  $\mathbf{U}_{f_p}$ ,  $\mathbf{U}_{p_1}$  and  $\mathbf{U}_{p_2}$  stand for agonists, and the second rows are antagonist voltage inputs, corresponding to the labels in Figure 4.2 (top right). As expected, the accuracy of the achieved target point depends on the experience base resolution (the distance between extracted positions  $p_1$  and  $p_2$ ), as elaborated in [242].

This basic principle of single-joint control (demonstrated in Figure 4.2) is now

generalized to a multi-joint robot arm. In the exploitation phase, it is expected from the robot to reach a target point ( $F_0$ ), within the final sphere  $X_F$ , which has not been previously reached in training, starting from a position ( $S_0$ ) within the initial sphere  $X_S$ , which has not been previously used (see Figure 4.4).

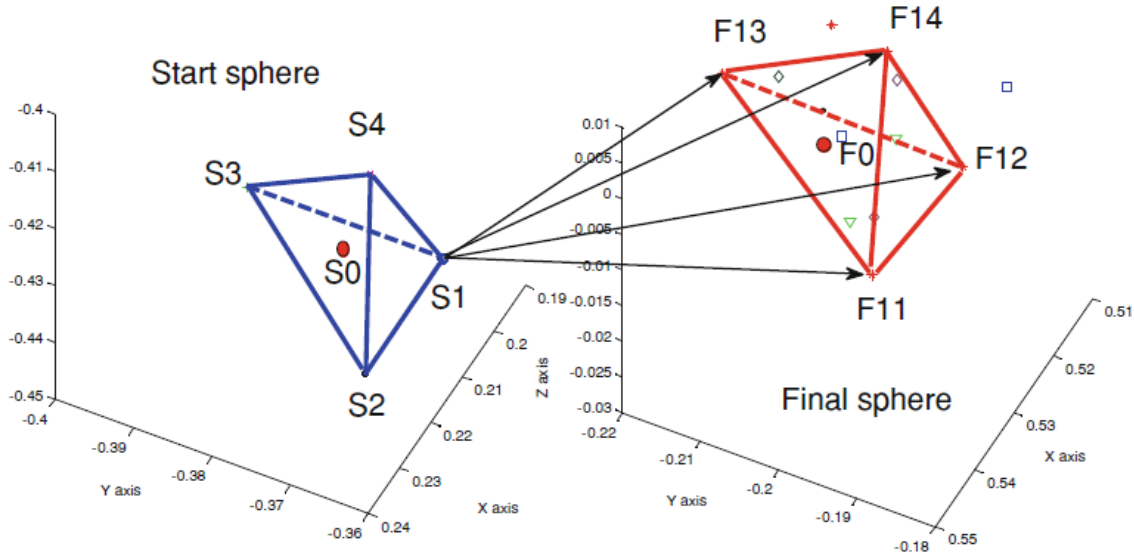


Figure 4.4. Four initial positions (the nearest-neighbors) –  $S_1$ ,  $S_2$ ,  $S_3$  and  $S_4$ , which create the tetrahedron depicted in blue, are selected for the prescribed initial position  $S_0$  according to the requirements (RS1) and (RS2) - (left); Four final positions ( $F_{11}$ ,  $F_{12}$ ,  $F_{13}$  and  $F_{14}$ ) that result from one of the initial positions –  $S_1$ , which create the tetrahedron depicted in red, are selected according to the requirements (RF1) and (RF2) - (right).

FF control signals are calculated before the robot moves, i.e. off-line. As in any interpolation, the nearest-neighbor yields an approximate solution – the resulting control will drive the robot to the vicinity of the target point. A deviation from the target point depends on the competency of the knowledge base (i.e. its resolution) and the selected interpolation method. Therefore, the first step of the nearest-neighbor algorithm is sequential selection of the nearest four initial positions from the data set  $X_S$ , following the requirements (RS1) and (RS2).

(RS1): Distance  $ds = \min(ds_1 + ds_2 + ds_3 + ds_4)$  is the minimum sum, where  $ds_1, ds_2, ds_3, ds_4$  are the distances from the prescribed initial position  $S_0$  to the first ( $S_1$ ), second ( $S_2$ ), third ( $S_3$ ) and fourth ( $S_4$ ) neighbor from the data set  $X_S$ , respectively.

(RS2): The prescribed initial position  $S_0$  must be inside the volume of the tetrahedron defined by  $S_1, S_2, S_3,$  and  $S_4$ .

The following step would be a nomination of corresponding final positions for each of the four selected initial neighbors. Therefore, one should first extract all the positions  $X_{fi}$  from the final sphere that originates from the initial position  $S_i, i \in (1,2,3,4)$ . Then, the four final positions  $F_{i1}, F_{i2}, F_{i3},$  and  $F_{i4}$  from each extracted subset  $X_{fi}$  should be selected to estimate the control sequence from  $S_i$  to  $F_0$  (see Figure 4.4). To that end, the requirements (RF1) and (RF2) should be met:

(RF1): Distance  $df = \min(df_{i1} + df_{i2} + df_{i3} + df_{i4})$  is the minimum sum, where  $df_{i1}, df_{i2}, df_{i3}, df_{i4}, i \in (1,2,3,4)$  are the distances from the prescribed final position  $F_0$  to the first ( $F_{i1}$ ), second ( $F_{i2}$ ), third ( $F_{i3}$ ) and fourth ( $F_{i4}$ ) neighbor from the extracted data set  $X_{fi}$ , respectively.

(RF2): The prescribed initial position  $F_0$  must be inside the volume of the tetrahedron defined by  $F_{i1}, F_{i2}, F_{i3},$  and  $F_{i4}$ , for each  $i \in (1,2,3,4)$ .

This way, four tetrahedrons of the smallest volume are established, each with the final position  $F_0$  inside. Finally, control signal evaluation for robot arm's motion from the initial (home) position  $S_0$  to the final position  $F_0$  is divided into two steps (Step Si-to- $F_0$ ) and (Step  $S_0$ -to- $F_0$ ).

(Step Si-to- $F_0$ ): Here the control from each of the selected initial neighbors  $S_i, i \in (1,2,3,4)$  to the desired point  $F_0$  is evaluated. To begin with, control from  $S_i$  to  $F_{i1}, F_{i2}, F_{i3}, F_{i4}$  is evaluated as follows: Auxiliary points  $A$  and  $B$  inside the tetrahedron specified by  $F_{i1}, F_{i2}, F_{i3}, F_{i4}$  are added (see Figure 4.5(left)).  $B$  is defined as the meeting point of the tetrahedron side defined by  $F_{i1}, F_{i2}, F_{i3}$  and the line defined by  $F_{i4}$  and  $F_0$ , and  $A$  is the meeting point of the line defined by  $F_{i1}$  and  $B$  and the line defined by  $F_{i2}$  and  $F_{i3}$ . With the selected auxiliary points  $A$  and  $B$ , the following distances are defined:  $d_1$  - distance from  $F_{i3}$  to  $A$ ;  $d_2$  - from  $F_{i2}$  to  $A$ ;  $d_3$  - from  $F_{i1}$  to  $B$ ;  $d_4$  - from  $B$  to  $A$ ,  $d_5$  - from  $F_{i4}$  to  $F_0$ ; and  $d_6$  - from  $B$  to  $F_0$ . Let us denote by  $\mathbf{U}_{X,Y}(t)_{2nx1}$  the control matrix

of  $2n$  rows ( $n$  rows for agonist motors and  $n$  for antagonist motors for each of  $n$  joints), with recorded/evaluated control from any point  $X$  to any point  $Y$  in time  $t$ . Control evaluation for a multi-joint robot moving in three dimensional space can be carried out analogously to the case of single-joint control evaluation (4.1). According to *Figure 4.5* (left) and for the already-defined distances  $d_k$ ,  $k \in (1,2,3,4,5,6)$ , the sequences of control inputs from the initial position  $S_i$  to position  $A$  ( $\mathbf{U}_{S_i-A}(t)$ ), position  $B$  ( $\mathbf{U}_{S_i-B}(t)$ ), and finally the target position  $F_0$  ( $\mathbf{U}_{S_i-F_0}(t)$ ) can be estimated by (4.2), (4.3) and (4.4), respectively. By repeating this algorithm for each of the selected neighbors in the initial sphere  $S_i$   $i \in (1,2,3,4)$ , it is possible to evaluate control from each of them to the desired position  $F_0$ :  $\mathbf{U}_{S_1-F_0}(t)$ ,  $\mathbf{U}_{S_2-F_0}(t)$ ,  $\mathbf{U}_{S_3-F_0}(t)$ , and  $\mathbf{U}_{S_4-F_0}(t)$ .

$$\mathbf{U}_{S_i-A}(t)_{2nx1} = \frac{d_2 \mathbf{U}_{S_i-F_{i3}}(t)_{2nx1} + d_1 \mathbf{U}_{S_i-F_{i2}}(t)_{2nx1}}{d_1 + d_2} \quad (4.2)$$

$$\mathbf{U}_{S_i-B}(t)_{2nx1} = \frac{d_4 \mathbf{U}_{S_i-F_{i1}}(t)_{2nx1} + d_3 \mathbf{U}_{S_i-A}(t)_{2nx1}}{d_3 + d_4} \quad (4.3)$$

$$\mathbf{U}_{S_i-F_0}(t)_{2nx1} = \frac{d_6 \mathbf{U}_{S_i-F_{i4}}(t)_{2nx1} + d_5 \mathbf{U}_{S_i-B}(t)_{2nx1}}{d_5 + d_6} \quad (4.4)$$

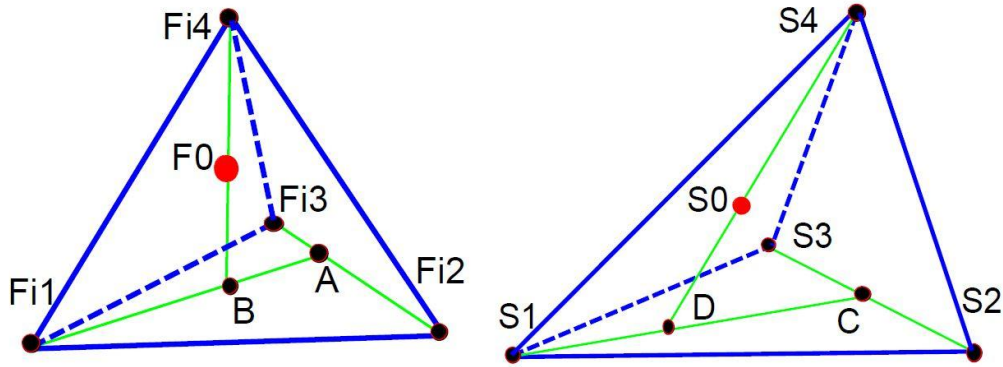


*Figure 4.5. Tetrahedron of minimal volume formed by points  $F_{i1}$ ,  $F_{i2}$ ,  $F_{i3}$ , and  $F_{i4}$ , selected from the subset of the final sphere  $X_{fi}$  that originates from the initial position  $S_i$  according to (RF1) and (RF2). Auxiliary points  $A$  and  $B$  are introduced for evaluation of the control sequence  $\mathbf{U}_{S_i-F_0}(t)$  from the initial neighbor  $S_i$  to the target position  $F_0$  (left); Tetrahedron of minimal volume formed by points  $S_1$ ,  $S_2$ ,  $S_3$ , and  $S_4$ , selected as the nearest neighbors of the robot's initial position  $S_0$  according to (RS1) and (RS2). Auxiliary points  $C$  and  $D$  are introduced for evaluation of the final control sequence  $\mathbf{U}_{S_0-F_0}(t)$  from the initial position  $S_0$  to the target position  $F_0$ , based on the weighted contribution of the selected initial neighbors  $S_1$ ,  $S_2$ ,  $S_3$ , and  $S_4$  (right).*

(Step S0-to-F0): Here the final control sequence from the initial position neighbor  $S_0$  to the desired position  $F_0$  is evaluated, after control from each of the selected nearest neighbors  $S_1, S_2, S_3$ , and  $S_4$  to  $F_0$  is obtained. Auxiliary points  $C$  and  $D$  inside of the tetrahedron specified by  $S_1, S_2, S_3, S_4$  are added (see *Figure 4.5* (right)).  $D$  is defined as the meeting point of the tetrahedron side defined by  $S_1, S_2, S_3$  and the line defined by  $S_4$  and  $S_0$ , and  $C$  is the meeting point of the line defined by  $S_1$  and  $D$  and the line defined by  $S_2$  and  $S_3$ . These auxiliary points  $C$  and  $D$  define the distances used to evaluate the final control sequences:  $dd_1$  - distance from  $S_3$  to  $C$ ;  $dd_2$  - from  $S_2$  to  $C$ ;  $dd_3$  - from  $S_1$  to  $D$ ;  $dd_4$  - from  $D$  to  $C$ ;  $dd_5$  - from  $S_4$  to  $S_0$ ; and  $dd_6$  - from  $D$  to  $S_0$ . For the defined  $dd_k, k \in (1, 2, \dots, 6)$  and according to *Figure 4.5* (right), the final control sequence that drives the robot hand tip from the robot's initial position  $S_0$  to the target position  $F_0$  is given by (4.7), with previously-calculated intermediate control sequences (4.5) and (4.6).

$$\mathbf{U}_{C_{F_0}}(t)_{2nx1} = \frac{dd_2 \mathbf{U}_{S_3_{F_0}}(t)_{2nx1} + dd_1 \mathbf{U}_{S_2_{F_0}}(t)_{2nx1}}{dd_1 + dd_2} \quad (4.5)$$

$$\mathbf{U}_{D_{F_0}}(t)_{2nx1} = \frac{dd_4 \mathbf{U}_{S_1_{F_0}}(t)_{2nx1} + dd_3 \mathbf{U}_{C_{F_0}}(t)_{2nx1}}{dd_3 + dd_4} \quad (4.6)$$

$$\mathbf{U}_{S_0_{F_0}}(t)_{2nx1} = \frac{dd_6 \mathbf{U}_{S_4_{F_0}}(t)_{2nx1} + dd_5 \mathbf{U}_{D_{F_0}}(t)_{2nx1}}{dd_5 + dd_6} \quad (4.7)$$

The nearest-neighbor feedforward approach is demonstrated on the seven-DoF anthropomorphic hand. The validity of the algorithm is proved through simulations in Subsection 4.5.

### 4.3.3 Neural network approach

This subsection considers neural networks as another approach to calculating FF using experience and learning. For the sake of comprehensiveness, neural networks appear to be a tool of choice for controlling complex, difficult to model, systems. Milosavljevic et al. (including the present author) [243] elaborate the utilization of neural networks (NN) for anthropomorphic robot control, with special emphasis on radial-basis neural

networks (RBN) and multi-layer perceptron networks (MLP). In this thesis we exploit RBN for the control of a seven-DoF simulator of the anthropomorphic robot arm recalled in the introductory part of this section and depicted in Figure 4.1. The initial experience base, previously created and introduced in Subsection 4.3.1, is used for neural network training. The NN was trained to perform a reaching movement, from an arbitrary point within the initial sphere  $X_s$  to the target position within the final sphere  $X_f$ . Again, proper positioning of the hand tip is considered, but not its orientation. Simulation results on the neural network as an integral part of the cognitive control of the anthropomorphic arm are highlighted in Subsection 4.5.

Neural networks have generally been used for black-box modeling of complex systems in robotics, as well as for forward models, estimation of inverse models, and, therefore, control. For instance, Wang et al. in [244] deal with the problem of inverse kinematic computation for redundant manipulators (the classical seven-DoF industrial robot arm), as a pronounced problem in robot control. Similarly, a method for the identification of industrial robot dynamics and control of an industrial robot manipulator, using a broad NN class, is proposed in [245]. The authors use sub-networks, like RBN, to represent the dynamic components. This method can be recommended as an effective approach to the identification of multi-jointed manipulator dynamics. A common problem encountered in the identification of multi-link industrial manipulator dynamics is a lack of even a small portion of prior knowledge about robot parameters, since robot behavior is a result of high dynamic coupling between links. The identification of robot dynamics using artificial NN is studied in [246], [247]. Jäntschi uses radial-basis functions for adaptive NN control of the musculoskeletal robot Anthrob, to compensate for joint and tendon friction [248]. These methods suffer from several limitations since they assume relatively small nonlinearities, compared to multi DoFs manipulators, tendon-driven robots and especially compliant systems. Therefore, we use previous results to create a new neural network for the evaluation of control signals, exploiting the experience base.

We opt for RBN because of good performance, despite the simple structure, comprised of input, output and hidden layers of normalized Gaussian activation functions [249]. Here in particular, the use of RBN is advisable due to insufficient data in the experience

base with regard to the complexity of the antagonistically-coupled compliant system. In addition, the utilization of a Gaussian RBN is proposed since it can smoothly approximate a wide range of functions. There are three parameters that define the input signal fed into the actuator, which resembles biological patterns of antagonistically-coupled muscles according to Figure 4.2:

- $U_{s1}$  – control signal while the arm is in its initial position
- $U_{s2}$  – control signal during the post-motion silent period
- $U_{burst}$  – amplitude of control signal burst

The joint motion amplitude depends mostly on the difference between the control signal burst  $U_{burst}$  and the initial control signal  $U_{s1}$  and its duration  $T$ . In the initial analysis, it is assumed that the related parameter  $E$  is an integral of the difference between the muscle burst activity and the initial control signal (4.8). Therefore, the parameter  $E$  is calculated for each motor and, here in particular, each antagonistic pair of motors that drive the 7-DoF anthropomorphic robot arm. However, voltage saturation, as a physical limitation of the control input in this case, is not considered.

$$E = \int_T (U_{burst}(t) - U_{s1}(t)) dt \quad (4.8)$$

To achieve the ultimate goal of driving the hand tip from the initial point  $S_0$  within the initial sphere  $X_s$  to the target point  $F_0$  within the final sphere  $X_f$ , all control input parameters need to be estimated for each motor of the robot arm. For the sake of simplicity and to provide a basic demonstration of the neural network approach, we assume that the duration of each phase of actuator activity ( $U_{s1}, U_{burst}, U_{s2}$ ) is fixed and that it matches the duration in the experience acquisition stage, when the motors are driven according to the profiles from Figure 4.2. The initial and final positions of the hand tip presented in Cartesian space are used as inputs and they, therefore, represent a neural network input vector (4.9). Since the final outcome of this algorithm should be control signal parameters for each motor of the anthropomorphic robot arm, the neural network output vector is defined by (4.10).  $Out = [Out_i]_{3xm}$ , where  $Out_i$  is the

notation for the control parameters defined for each of  $m$  drives (in this case of the 7-DoF anthropomorphic robot arm, each of  $n$  joints is driven by two antagonistically-coupled motors, so  $m = 2n$ ):

$$In = [x_{initial} \quad y_{initial} \quad z_{initial} \quad x_{final} \quad y_{final} \quad z_{final}] \quad (4.9)$$

$$Out_i = [U_{s1i} \quad U_{s2i} \quad E_i]^T, i \in (1, \dots, m) \quad (4.10)$$

Finally, the RBN defined in this manner is trained and tested using the experience pool presented in Subsection 4.3.1. For the initial position  $S_0$  and final position  $F_0$ , the network generates an output in the form of the control signal  $U_{s1new}$  during the silent period in position  $S_0$ , the control signal  $U_{s2new}$  in position  $F_0$  and the value of parameter  $E_{new}$  for each of the total of  $m$  actuators. The entire procedure and the possibility of using neural networks in the control of an antagonistically-coupled joint are reported in [243]. Simulation results are summarized in Subsection 4.5, in combination with the feedback approach, based on online estimation of kinematic coefficients (elaborated in Subsection 4.4.2).

Since the neural network approach was briefly discussed to round out the presentation of the algorithms we labeled as cognitive, there are many issues that remain open. Algorithm efficiency strongly depends on the training process, such that it needs to be reconsidered. In addition, not only can different kinds of neural networks be tested for the control of such complex systems as the anthropomorphic robots, but the output variables should also be re-assessed. In order to keep exploiting biological patterns of muscle activity, the correlation between a joint movement and the corresponding muscle activity needs to be examined comprehensively and then the parameter  $E$  reshaped.

## 4.4 Feedback control

The main obstacle in the control of anthropomorphic mechanisms is highly complex kinematics. For instance, the actuator that drives a multi-articular artificial muscle affects several rotation axes at the same time. Moreover, a hand tip motion or a single

joint motion could be a result of the activity of different muscles, so inverse kinematic is often redundant and non-trivial. Even if available information can be used to model such complex kinematics, conventional control techniques based on an estimated model would be very demanding and the procedure too complex and questionable for real-time implementation.

Since these issues are difficult to tackle from an engineering point of view, we will suggest two feedback control algorithms that do not require robot kinematics to be solved. Both approaches rely on experience and information available from sensors. In the first approach, the nearest-neighbor feedback approach, the deviation between the desired and the actual hand tip position achieved by feedforward is compensated by the control derived from an extended experience base (upgrade to experience base presented in Subsection 4.3.1). The second approach assumes measuring of both the position of the hand tip in the Cartesian frame and all joint positions. Kinematic coefficients that evaluate the contribution of each robot actuator to hand-tip movement in Cartesian space are then calculated on-line. This calculation is based on sensor data, but also on the experience base. Kinematic coefficients are then combined with fuzzy logic rules to provide a feedback control signal.

#### **4.4.1 Nearest-neighbor feedback approach**

This subsection shows how the nearest-neighbors method can be used to calculate the feedback control component. The only sensory information we consider available is the hand tip position in the Cartesian frame denoted by  $X_f$ . Joint positions are considered unknown, as are tendon forces. This was exactly the case with the prototype of the first anthropomorphic robot – ECCE1 [10]. Furthermore, in a number of musculoskeletal robots with multi-articular muscles and multi-DoF joints, joint positions are hardly available, whereas the hand tip position in Cartesian space can be accurately obtained from cameras [146]. FB starts contributing the final control signal and enables fine tuning of the hand tip once FF drives the hand tip to the prescribed vicinity of the desired final point  $F_0$ . The actual position of the hand tip is denoted by  $\hat{F}_0$ . In order to

reduce the Cartesian position error  $\Delta X = F_0 - \hat{F}_0$ , an appropriate set of input-to-output experiments and the corresponding experience base need to be formulated to provide the FB as function of the Cartesian position error  $\Delta U_{FB} = f(\Delta X)$ . To that end, we assume a basic linear relation between the Cartesian position error and the FB control signal  $\Delta U_{FB} = K\Delta X$ . Here,  $\Delta U_{FB}$  represents the FB contribution to the overall control signal and it is therefore a column vector of dimension  $m \times 1$ , where  $m$  is the number of actuators. Since only the Cartesian position is considered, and not the orientation,  $\Delta X$  is a column vector that contains three elements (Cartesian deviations on  $x$ ,  $y$ , and  $z$  axes). The following paragraphs demonstrate how matrix  $K$  (matrix of kinematic coefficients) can be evaluated. Although joint positions are unknown, the influence of each actuator on the robot hand tip in the global frame should be evaluated. One approach to the evaluation of matrix  $K$ , using an additional experience base, is described below. The feedback gain matrix  $K$  and thus FB control are evaluated on-line, from the actual Cartesian position, the desired position and the extended experience base. Similar to the nearest-neighbor method for the evaluation of FF control inputs discussed in Subsection 4.3.2, we distinguish two stages: experience acquisition and experience exploitation.

First, in order to estimate the contribution of each actuator to the hand tip motion along the Cartesian  $x$ ,  $y$  or  $z$  axis, a new set of experiments are conducted by making small shifts and relating them to the applied control inputs. This means that after a properly accomplished motion from the initial sphere  $X_s$  to the final sphere  $X_f$ , an additional increase in the input voltage  $dU$  to each actuator should be applied to cause an additional shift of the robot's hand tip. Repeating the procedure for each point of the final sphere makes this approach very time consuming, but it is necessary for an evaluation of the proposed feedback method. Although the approach is tested through simulations on the seven-DoF anthropomorphic robot arm strictly driven by antagonistically-coupled compliant drives (2.41), the control approach is generalized for any anthropomorphic structure with an arbitrary number of actuators –  $m$ . An applied voltage increment to actuator  $j$  over the time period  $T_{inc}$  would drive the hand tip to the new steady-state position  $\mathbf{X}(t + T_{inc})_{3 \times 1}$ , with the new FF static voltage level  $\mathbf{U}_{FF}(t + T_{inc})_{m \times 1}$ . For each point in the final sphere, the same procedure should be applied for each of the  $m$  actuators, so for an increase in the input voltage of the  $j^{th}$  actuator,  $j \in$

(1,2 ...  $m$ ), the following variables are recorded:

$$\Delta \widehat{\mathbf{U}}_{j_{mx1}} = \mathbf{U}_{\text{FF}}(t + T_{\text{inc}})_{mx1} - \mathbf{U}_{\text{FF}}(t)_{mx1} = \begin{bmatrix} \mathbf{0}_{[j-1 \times 1]} \\ dU_j \\ \mathbf{0}_{[m-j \times 1]} \end{bmatrix}_{mx1} ; j \in (1,2 \dots m) \quad (4.11)$$

$$\Delta \widehat{\mathbf{X}}_{j_{3x1}} = \mathbf{X}(t + T_{\text{inc}})_{3x1} - \mathbf{X}(t)_{3x1} = \begin{bmatrix} dx_j \\ dy_j \\ dz_j \end{bmatrix}_{3x1} ; j \in (1,2 \dots m) \quad (4.12)$$

After carrying out  $m$  experiments for each of the  $m$  actuators, the input voltage increment matrix  $\Delta \widehat{\mathbf{U}}_{mxm}$  (4.13) and position increment matrix  $\Delta \widehat{\mathbf{X}}_{3xm}$  (4.14) are defined for each final position.

$$\Delta \widehat{\mathbf{U}}_{mxm} = [\Delta \widehat{\mathbf{U}}_{1[mx1]} \quad \Delta \widehat{\mathbf{U}}_{2[mx1]} \quad \dots \quad \Delta \widehat{\mathbf{U}}_{m[mx1]}] \quad (4.13)$$

$$\Delta \widehat{\mathbf{X}}_{3xm} = [\Delta \widehat{\mathbf{X}}_{1[3x1]} \quad \Delta \widehat{\mathbf{X}}_{2[3x1]} \quad \dots \quad \Delta \widehat{\mathbf{X}}_{m[3x1]}] \quad (4.14)$$

Relation (4.15) stands for the matrices obtained in this manner. Matrix  $\widehat{\mathbf{H}}_{3xm}$  is the mapping matrix, which matches the shifts in actuator control inputs to hand tip displacements. Since the matrix  $\Delta \widehat{\mathbf{U}}_{mxm}$  is a diagonal matrix ( $u_{ij} = dU_j$ ;  $i = j$  and  $u_{ij} = 0$ ;  $i \neq j$ ; for  $j \in (1,2 \dots m)$ ), and also non-singular, the mapping matrix  $\widehat{\mathbf{H}}_{3xm}$  can be evaluated according to (4.16).

$$\Delta \widehat{\mathbf{X}}_{3xm} = \widehat{\mathbf{H}}_{3xm} \Delta \widehat{\mathbf{U}}_{mxm} \quad (4.15)$$

$$\widehat{\mathbf{H}}_{3xm} = \Delta \widehat{\mathbf{X}}_{3xm} (\Delta \widehat{\mathbf{U}}_{mxm})^{-1} \quad (4.16)$$

Experience-based feedback is established by calculating the mapping matrix  $\widehat{\mathbf{H}}_{3xm}$  for each point in the final sphere  $X_f$ . The following paragraphs will show how this experience can be exploited and how the feedback control component  $\Delta \mathbf{U}_{\text{FB}_{mx1}}$  can be evaluated for a Cartesian mismatch between the desired (target) position and its actual value –  $\Delta \mathbf{X}_{3x1}$ . In other words, mapping of  $\widehat{\mathbf{K}}_{mx3}$  (4.17) should be achieved.

$$\Delta \mathbf{U}_{\text{FB}_{mx1}} = f(\Delta \mathbf{X}_{3x1}) = \widehat{\mathbf{K}}_{mx3} \Delta \mathbf{X}_{3x1} \quad (4.17)$$

Since  $\hat{\mathbf{H}}_{3xm}$  is not a square matrix, there is no inversion  $\hat{\mathbf{K}}_{mx3} = (\hat{\mathbf{H}}_{3xm})^{-1}$ . A possible solution would be to calculate  $\hat{\mathbf{K}}_{mx3}$  as a modified pseudo inversion of  $\hat{\mathbf{H}}_{3xm}$ . In order to minimize the control effort  $\Delta\mathbf{U}_{\text{FB}mx1}$ , the weighted form  $\min(\frac{1}{2}\Delta\mathbf{U}_{\text{FB}}^T \mathbf{W}\Delta\mathbf{U}_{\text{FB}})$  should be minimized, where  $\mathbf{W} = \mathbf{I}_{mxm}$  stands for normal pseudo inversion. A properly modified pseudo inversion requires a well-estimated weight coefficient matrix  $\mathbf{W} = \mathbf{W}_1^T \mathbf{W}_1$ , in order to provide the smallest norm of  $\mathbf{W}_1 \Delta\mathbf{U}_{\text{FB}}$ . To deal with the optimization problem, the Lagrange multiplier ( $\lambda$ ) method can be used to find the minimum of a function subject to constraints in a form of (4.18). To evaluate the function, minimum stationary points (the points where the partial derivatives are equal to zero) need to be found (4.19).

$$J(\Delta\mathbf{U}_{\text{FB}}, \lambda) = \frac{1}{2}\Delta\mathbf{U}_{\text{FB}}^T \mathbf{W}\Delta\mathbf{U}_{\text{FB}} + \lambda(\hat{\mathbf{H}}\Delta\mathbf{U}_{\text{FB}} - \Delta\mathbf{X}) \quad (4.18)$$

$$\frac{\partial J(\Delta\mathbf{U}_{\text{FB}}, \lambda)}{\partial \Delta\mathbf{U}_{\text{FB}}} = 0; \quad \frac{\partial J(\Delta\mathbf{U}_{\text{FB}}, \lambda)}{\partial \lambda} = 0 \quad (4.19)$$

From (4.18) and (4.19), the FB gain  $\hat{\mathbf{K}}_{mx3}$  can easily be calculated for each particular final position from the sphere  $X_f$ , comparing the result (4.20) to the form (4.17). For the basic case  $\mathbf{W} = \mathbf{I}_{mxm}$ , mapping (4.21) from  $\hat{\mathbf{H}}_{3xm}$  to  $\hat{\mathbf{K}}_{mx3}$  is the right pseudo inverse -  $\hat{\mathbf{K}} = \hat{\mathbf{H}}^T(\hat{\mathbf{H}}\hat{\mathbf{H}}^T)^{-1}$ .

$$\Delta\mathbf{U}_{\text{FB}mx1} = (\mathbf{W}^{-1}\hat{\mathbf{H}}^T(\hat{\mathbf{H}}\mathbf{W}^{-1}\hat{\mathbf{H}}^T)^{-1})\Delta\mathbf{X}_{3x1} \quad (4.20)$$

$$\hat{\mathbf{K}}_{mx3} = \mathbf{W}^{-1}\hat{\mathbf{H}}^T(\hat{\mathbf{H}}\mathbf{W}^{-1}\hat{\mathbf{H}}^T)^{-1} \quad (4.21)$$

Finally, based on (4.21), feedback control for each of the  $m$  actuators  $\Delta\mathbf{U}_{\text{FB}mx1}$  is specified by measuring the deviation of the desired from the actual Cartesian position of the hand tip -  $\Delta\mathbf{X}_{3x1}$  according to (4.17). However, this evaluation is undertaken only for points in the experience base. Consequently, for arbitrary initial and final robot positions within the initial sphere  $X_s$  and final sphere  $X_f$ , weighted mapping of  $\mathbf{K}_{mx3}: \Delta\mathbf{X}_{3x1} \rightarrow \Delta\mathbf{U}_{\text{FB}mx1}$  has to be derived. To that end, the linear feedback gains  $\mathbf{K}_{mx3}$  are calculated from gains  $\hat{\mathbf{K}}_{mx3}$ , evaluated for the four nearest neighbors in the same manner as in Subsection 4.3.2.

In spite of the simulation experiments presented in Subsection 4.5, which validate the approach elaborated in this subsection, there are numerous limitations to its applicability. First, it is obvious that numerous experiments have to be carried out to establish an experience base of appropriate resolution, given that the control accuracy depends on the resolution. The repeatability of movements that create the experience base would be questionable in the case of complex tendon-driven mechanisms due to friction. Furthermore, although here we do not specify the actuator dynamics and performance, one should be fully aware of them while considering optimization and fit within the actuator saturation limits. There are also a few improvements that could enhance the presented control approach. Some of them would refer to potential updating of the experience base (learning process), extrapolation to targets outside the final sphere  $X_f$ , improvement of the approach by incorporating any knowledge about the model, etc.

#### **4.4.2 Approach based on online estimation of kinematic coefficients and fuzzy logic**

This subsection presents one more model-free approach to feedback control. The lack of a kinematic model introduces a new control challenge – how to determine the influence of each control input on hand tip motion in the Cartesian frame. In other words, how a particular control input should be changed to compensate for deviations from the desired position of the hand tip in the  $x$ ,  $y$ , and  $z$  directions needs to be evaluated. In order to solve the problem, this section introduces an experience-based estimation algorithm for the so-called kinematic coefficients. Afterwards, each control input will be evaluated according to a deviation of the hand tip from the desired position. This time, both Cartesian positions and joint positions are considered available. Again, the seven-DoF anthropomorphic arm depicted in Figure 4.1 was the test bed for the implementation and evaluation of the proposed control approach. The preliminary idea, which was the inspiration for the algorithm elaborated in this subsection, is outlined in [214].

#### 4.4.2.1 Kinematic coefficient estimation algorithm

The first step of the algorithm is the evaluation of the kinematic coefficients estimated from the experience base (elaborated in Subsection 4.3.1) and available sensor information. Here we come to another issue, associated with anthropomorphic robot sensorization. Namely, we have already noted that in the case of multi-axes joints, joint position measurement is not straightforward (e.g. shoulder position measurement in the case of a spherical joint structure). Although sensorization could be an application issue of this control approach to complex anthropomorphic robots, we will assume that joint positions can be obtained. Kinematic coefficients are defined as parameters that describe the relation between the control inputs and axes of the global frame. Thus, for each joint  $i$  (controlled by two antagonistically-coupled actuators), three normalized coefficients  $n_{c_{x_i}}, n_{c_{y_i}}, n_{c_{z_i}}$  are assigned to the  $x$ ,  $y$  and  $z$  axis, respectively.

Supposing that feedforward brings the hand tip to point  $\hat{F}_0 = (\hat{x}, \hat{y}, \hat{z})$  within the final sphere  $X_f$ , feedback starts to contribute to the evaluation of control inputs. The coordinates of the points from the narrow environment of  $\hat{F}_0$  (the nearest neighbors of  $\hat{F}_0$ ) are denoted as  $F_j=(x_j, y_j, z_j)$ ,  $j = 1, 2, \dots, N$  ( $j$  - neighbor number). The selection of the nearest neighboring points, in the case where four nearest neighbors ( $N=4$ ) need to be selected, is described in detail in Subsection 4.3.2 and reported in [213]. Therefore, the selected neighbors must satisfy two conditions: the sum of the distances between  $\hat{F}_0$  and each of the four neighbors must be minimal, and  $\hat{F}_0$  must be inside the volume of the tetrahedron formed by the four neighbors.

The following paragraphs depict the algorithm for calculating the kinematic coefficient for the  $x$  axis and  $i$ -th joint –  $n_{c_{x_i}}$ . Analogous procedures apply to the  $y$  and  $z$  axes. In order to avoid the inverse kinematics problem, all available and measurable data can be used to enhance the accuracy of this heuristic approach. Two types of sensors can be employed, as is often the case in robotics applications: one for the Cartesian position of the hand tip (e.g. camera) and the other group for the joint positions (e.g. encoders). The same data are available in the experience base. Therefore, to evaluate the kinematic

coefficients, we use:

- the desired and the actual hand tip position in the Cartesian frame (available from sensors),
- actual joint angles (available from sensors),
- positions of chosen neighbors in the Cartesian frame (available from the experience base), and
- corresponding joint angles (available from the experience base).

Assuming that all the above information is available, we can define several parameters that facilitate the evaluation of the feedback control signal and, primarily, the kinematic coefficients. The parameter denoted by  $K_{x_j}$  shows how much each selected neighbor  $j$  contributes to error compensation along the  $x$  axis, relative to error compensation along the  $y$  and  $z$  axes.  $L_{x_j}$  relates the discrepancy between the desired position and the position of neighbor  $j$  in the  $x$  direction, relative to the same discrepancy in the  $x$  direction of the other neighbors. Then, the parameter  $P_{q_{ij}}$  shows how much the actual position of joint  $i$  deviates from the position of the  $i$ -th joint of neighbor  $j$ , relative to the deviations of other joints of the particular neighbor  $j$ . The final data that can be extracted and exploited pertain to the discrepancy between the actual position of the  $i$ -th joint and the position of the  $i$ -th joint of the particular neighbor  $j$ , relative to the deviations of the same joint  $i$  in other neighbors –  $Q_{q_{ij}}$ . These four parameters relate information from the experience base and the positions of the nearest neighbors to the actual hand tip position and its deviation from the desired position. However, the final kinematic coefficients  $n_{c_{x_i}}, n_{c_{y_i}}, n_{c_{z_i}}$  can exploit these parameters ( $K, L, P, Q$ ) in a variety of ways and, consequently, the dependence of the hand tip position in Cartesian space on joint movements, would be estimated differently. Here we present only one possible pairing of the introduced parameters. For further enhancements of the algorithm, comprehensive research is needed to define each parameter  $K, L, P$ , and  $Q$ , and then their pairing.

The first parameter  $K_{x_j}$  defines the normalized discrepancy of the desired hand tip

position  $F_0=(x_0, y_0, z_0)$ , compared to the final point represented by the position of the  $j$ -th neighbor  $F_j=(x_j, y_j, z_j)$  along the  $x$  axis, relative to discrepancies in the  $y$  and  $z$  directions of the global Cartesian frame. Thus, the larger the deviation on the  $x$  axis of neighbor  $j$  ( $j = 1, \dots, N$ ), compared to deviations in the  $y$  and  $z$  directions, the less influence of the neighbor  $j$  in the  $x$  direction than in the  $y$  and  $z$  directions. Consequently, relation (4.22) is adopted and an exponential function is chosen to avoid numerical problems. Parameter  $\alpha$  is used to increase/decrease the contribution of the parameter  $K$  in the evaluation of the final kinematic coefficients.

$$K_{x_j} = \frac{1}{e^{\alpha \frac{|x_0 - x_j|}{|x_0 - x_j| + |y_0 - y_j| + |z_0 - z_j|}}} \quad (4.22)$$

The second parameter  $L_{x_j}$  again evaluates the deviation of the Cartesian  $x$  position of the  $j$ -th neighbor, labeled with  $x_j$ , from the desired hand tip position along the  $x$  axis denoted by  $x_0$ . This time, the parameter  $L_{x_j}$  depicts the relative deviation of neighbor  $j$  in the  $x$  direction from the sum of deviations in the  $x$  direction of all  $N$  joints selected as the nearest neighbors. This results in relation (4.23) Once more, an exponential function is chosen to avoid numerical problems and parameter  $\beta$  can be tuned to the weight contribution of the parameter  $L$  in the evaluation of the final kinematic coefficients.

$$L_{x_j} = \frac{1}{e^{\beta \frac{|x_0 - x_j|}{|x_0 - x_1| + |x_0 - x_2| + \dots + |x_0 - x_N|}}} \quad (4.23)$$

The following parameters compare the actual positions of all joints in the robot's kinematic chain with the corresponding joint positions of the chosen neighbors from the experience base. The total number of joints in the kinematic chain is denoted by  $n$ , while  $N$  is the number of selected neighbors. In particular, if a seven-DoF anthropomorphic robot arm is considered and if four neighbors are used as referring neighbors, these parameters are  $n = 7$  and  $N = 4$ .

The parameter  $E_{q_{ij}}$  determines the normalized deviation of the joint position ( $\hat{q}_i$ ),

reached by FF, where  $i$  denotes the joint number ( $i = 1, \dots, n$ ), from the position of the same joint of the  $j$ -th neighbor ( $j = 1, \dots, N$ ) labelled by  $q_{ij}$ .

$$E_{q_{ij}} = |\hat{q}_i - q_{ij}| \quad (4.24)$$

The parameter  $P_{q_{ij}}$  depicts the discrepancy between the actual position of the  $i$ -th joint and its counterpart – the position of the  $i$ -th joint of the  $j$ -th neighbor, and the sum of position discrepancies of all  $n$  joints in the kinematic chain of the  $j$ -th neighbor. This parameter is calculated for each of the  $N$  neighbors separately, using (4.25).

$$P_{q_{ij}} = \frac{E_{q_{ij}}}{E_{q_{1j}} + E_{q_{2j}} + \dots + E_{q_{nj}}} \quad (4.25)$$

Finally, one more useful correlation can be noted – the relative discrepancy between the actual position of the  $i$ -th joint and the position of the  $i$ -th joint of the  $j$ -th neighbor, and the sum of discrepancies in the corresponding joint of all the selected  $N$  neighbors. In other words, the parameter  $Q_{q_{ij}}$  shows how much the achieved motion of the  $i$ -th joint deviates from that of the  $i$ -th joint of the neighbor  $j$ , relative to the deviations of the same joint of all other selected neighbors. Note that the parameters  $P_{q_{ij}}$  in (4.25) and  $Q_{q_{ij}}$  in (4.26) are evaluated by basic algebraic relations. Both relations can be exponential, to emphasize the deviations in a particular joint. Only this basic equation is used in the present thesis, for demonstration purposes. Future research can elaborate further shaping of Equations (4.25) and (4.26).

$$Q_{q_{ij}} = \frac{E_{q_{ij}}}{E_{q_{i1}} + E_{q_{i2}} + \dots + E_{q_{iN}}} \quad (4.26)$$

The required coefficients ( $K_{x_j}, L_{x_j}, P_{q_{ij}}, Q_{q_{ij}}$ ) can be estimated using (4.22), (4.23), (4.25), and (4.26). Since different weights can be set for each of these parameters, as in (4.22) and (4.23) by parameters  $\alpha$  and  $\beta$ , the final kinematic coefficients can be calculated as the product of these parameters, without limiting the generality. Equation

(4.27) represents the influence of a particular joint  $i$  on the movement of the hand tip in the  $x$  direction, and is described by the coefficient  $C_{x_i}$ . An analogous procedure leads to the coefficients  $C_{y_i}$  and  $C_{z_i}$  for properly evaluated parameter sets  $(K_{y_j}, L_{y_j}, P_{q_{ij}}, Q_{q_{ij}})$  and  $(K_{z_j}, L_{z_j}, P_{q_{ij}}, Q_{q_{ij}})$ , according to (4.28) and (4.29). Eventually, the normalized form that defines the contribution of the  $i$ -th joint to the  $x$ ,  $y$ , and  $z$  Cartesian coordinates of the hand tip are given by (4.30), (4.31) and (4.32), respectively. Note that the normalized coefficients satisfy:  $n_{C_{x_i}} + n_{C_{y_i}} + n_{C_{z_i}} = 1$ .

$$C_{x_i} = \sum_{j=1}^N K_{x_j} L_{x_j} P_{q_{ij}} Q_{q_{ij}} \quad (4.27)$$

$$C_{y_i} = \sum_{j=1}^N K_{y_j} L_{y_j} P_{q_{ij}} Q_{q_{ij}} \quad (4.28)$$

$$C_{z_i} = \sum_{j=1}^N K_{z_j} L_{z_j} P_{q_{ij}} Q_{q_{ij}} \quad (4.29)$$

$$n_{C_{x_i}} = \frac{C_{x_i}}{C_{x_i} + C_{y_i} + C_{z_i}} \quad (4.30)$$

$$n_{C_{y_i}} = \frac{C_{y_i}}{C_{x_i} + C_{y_i} + C_{z_i}} \quad (4.31)$$

$$n_{C_{z_i}} = \frac{C_{z_i}}{C_{x_i} + C_{y_i} + C_{z_i}} \quad (4.32)$$

#### 4.4.2.2 An example of kinematic coefficient evaluation for a two-DoF planar robot

In order to demonstrate the elaborated algorithm, the kinematic coefficients are evaluated for a simple 2-DoF planar robot. For demonstration purposes, link lengths are set to  $l_1 = l_2 = 0.5m$ . Three nearest neighbors  $S_j$  ( $j=1,2,3$ ) are selected to comply with the algorithm and the requirements presented in Subsection 4.3.2. Figure 4.6 shows the point reached in the feedforward phase  $\hat{F}_0$ , the desired point  $F_0$ , and the three nearest neighbors  $S_1$ ,  $S_2$ , and  $S_3$ , selected from an experience base according the above rules. All parameters related to the points of interest and corresponding joint positions are

depicted in Table 4.1.

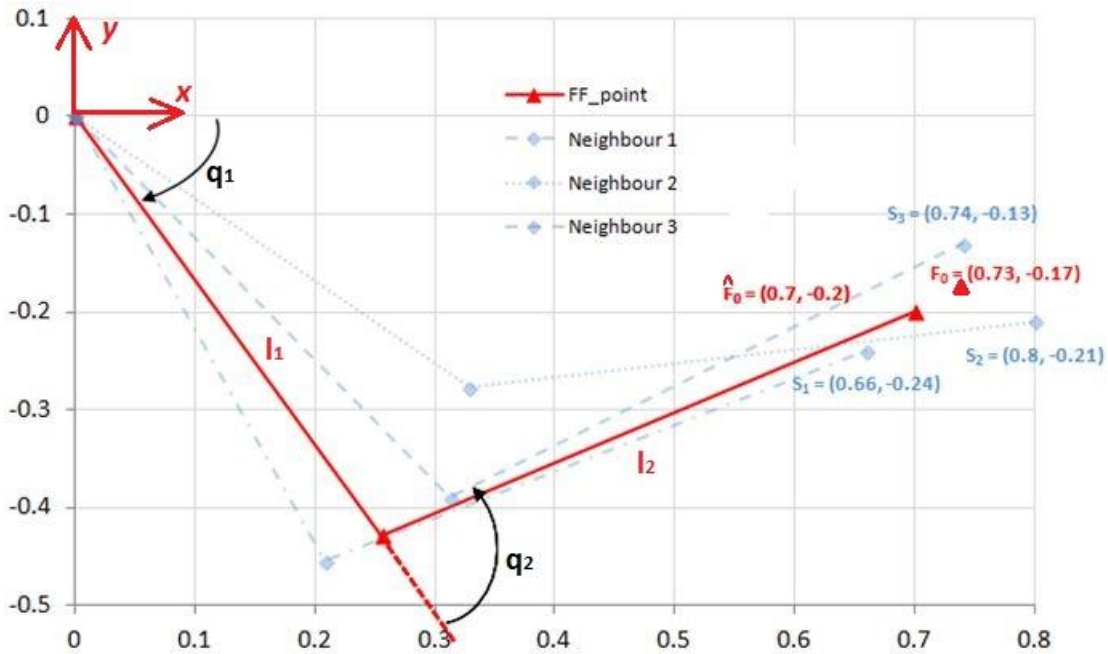


Figure 4.6. Two-DoF planar robot as a target system for estimating kinematic coefficients. The actual position ( $\hat{F}_0$ ) and the desired position ( $F_0$ ) of the hand tip are depicted by red triangles. The selected nearest neighbors  $S_1$ ,  $S_2$ , and  $S_3$  are marked by blue squares.

Table 4.1. Cartesian and joint coordinates of actual, desired and selected nearest neighbors points used for kinematic coefficients estimation in case of two DoF planar robot depicted in Figure 4.6.

Point of interest	Cartesian coordinates ( $x, y$ ) [m]	Joint coordinates ( $q_1, q_2$ ) [deg]
$F_0 = (x_0, y_0)$	(0.73, -0.17)	?
$\hat{F}_0 = (\hat{x}_0, \hat{y}_0)$	(0.7, -0.2)	(-59.26, 85.56)
$S_1 = (x_1, y_1)$	(0.66, -0.24)	(-65.37, 90.78)
$S_2 = (x_2, y_2)$	(0.74, -0.13)	(-48.91, 68.39)
$S_3 = (x_3, y_3)$	(0.8, -0.21)	(-51.26, 82.59)

The final evaluation of the kinematic coefficients is performed according to Equations (4.22) through (4.32). Note that the number of selected neighbors is three ( $N = 3$ ), that the robot has two joints in its kinematic chain ( $n = 2$ ), and that the weighted parameters

are selected arbitrarily:  $\alpha = \beta = 2$ . By straightforward application of the algorithm explained in the previous subsection, and for data listed in Table 4.1, the kinematic coefficients  $n_{c_{x_i}}$  and  $n_{c_{y_i}}$  are easily evaluated for each of the two joints. The kinematic coefficients are shown in Table 4.2. As intuitively expected from Figure 4.6, the estimated kinematic coefficients show that in this particular position the first joint contributes more in the  $x$  than  $y$  direction of the hand tip motion in the global Cartesian frame  $n_{c_{x_1}} (= 0.5776) > n_{c_{y_1}} (= 0.4224)$ , and that the second joint contributes significantly more in the  $y$  than  $x$  direction  $n_{c_{x_2}} (= 0.284) \ll n_{c_{y_2}} (= 0.716)$ .

*Table 4.2. Estimated kinematic coefficients of the two-DoF planar robot depicted in Figure 4.6, according to the algorithm presented in Subsection 4.4.2.1.*

<b>Kinematic coefficient</b>	<b>Estimated value</b>
$n_{c_{x_1}}$	0.5776
$n_{c_{y_1}}$	0.4224
$n_{c_{x_2}}$	0.2840
$n_{c_{y_2}}$	0.7160

#### **4.4.2.3 Fuzzy logic algorithm**

Once the kinematic coefficients are calculated to estimate the contribution of each actuator to the hand tip position in the Cartesian frame, deviation of the achieved motion from the desired motion should be estimated and then compensated. Kinematic coefficients tell us how each of the robot joints influences hand tip displacement in the  $x$ ,  $y$ , or  $z$  direction. Control logic should be applied to finally evaluate the feedback control signal in each of the actuators. A fuzzy controller [250] is implemented to achieve this. To demonstrate our idea, we use the basic implementation of a fuzzy controller that resembles PD conventional control. It is possible to elaborate on more complex fuzzy logic, but this is not the focus of the present thesis. Thus, the proposed fuzzy controller has two input variables (position error  $e_x$  and derivative of position error  $de_x$ ) and one output variable (corresponding to voltage) for each axis  $x$ ,  $y$ , and  $z$ .

The position error  $e_x$  denotes the deviation of the actual hand tip position from the desired hand tip position along the  $x$  axis of the Cartesian frame (4.33), while  $de_x$  denotes its derivative (4.34) calculated for two successive time instants  $(m - 1)T_s$  and  $mT_s$ , where  $T_s$  is the sampling time. Input and output membership functions are shown in Figure 4.7. The depicted boundaries for the inputs and outputs are set according to the resolution of the experience base and output control voltages. Both the inputs and outputs can either be scaled or modified to match particular needs. The triangular shapes of fuzzy sets, as well as the regions of overlapping, are adopted arbitrarily and are also a topic of further discussion. Furthermore, seven and five input sets are introduced for the position error  $e_x$  and its derivative  $de_x$ , respectively. The number of the fuzzy sets is also heuristically decided, as a compromise between computation efficiency and complexity.

$$e_x(mT_s) = x_0(mT_s) - \hat{x}(mT_s) \quad (4.33)$$

$$de_x(mT_s) = e_x(mT_s) - e_x((m - 1)T_s) \quad (4.34)$$

The pool of all implemented fuzzy rules, based on heuristics, is shown in Table 4.3. The gray column cells are the position error  $e_x$  input sets, while the gray row cells contain the position error derivative  $de_x$  input sets. AND operator is used to relate input sets. The meanings of the acronyms in Table 4.3 are consistent with Table 4.4. Corresponding if-then rules are activated to an appropriate level, in accordance with the membership degree of the input variables  $e$  and  $de$  to their inputs fuzzy sets. The min-max method is used for the aggregation of fuzzy rules (mathematical implementation of logical operators *AND* and *OR*), whereas the Centroid method (center of gravity) is implemented for the defuzzification process. For illustration purposes, all rules are considered without additional weighting factors, which could give preference to a specific fuzzy rule. Therefore, further shaping of the presented fuzzy logic is possible, especially by selecting other methods or introducing weighting factors.

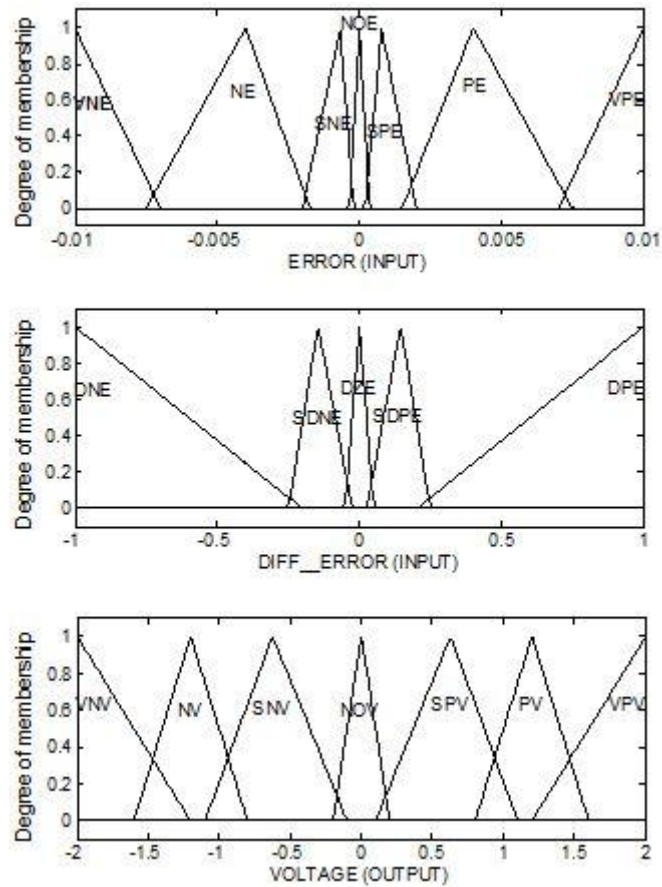


Figure 4.7. Fuzzy membership functions for two inputs (position error  $e_x$ , derivative of position error  $de_x$ ) and the output (voltage) for the  $x$  axis of the Cartesian frame. Analogous figures apply to  $y$  and  $z$  axes.

Table 4.3. Pool of fuzzy if-then rules that relate the position error and the position error derivative to the corresponding output fuzzy sets for a particular axis in Cartesian space –  $x$ ,  $y$  or  $z$ .

	Derivative of position error - $de$					
	AND	DNE	SDNE	DZE	SDPE	DPE
Position error - $e$	VNE	VNV	VNV	VNV	VNV	VNV
	NE	NV	NV	SNV	SNV	NOV
	SNE	NV	SNV	SNV	NOV	SPV
	NOE	NV	SNV	NOV	SPV	PV
	SPE	SNV	NOV	SPV	PV	PV
	PE	NOV	SPV	SPV	PV	PV
	VPE	VPV	VPV	VPV	VPV	VPV

Table 4.4. Meanings of acronyms that represent the input and output fuzzy sets given in Table 4.3.

<b><i>e</i> - input sets</b>	<b><i>de</i> - input sets</b>	<b><i>voltage</i> - output sets</b>
VNE-very_negative_error	DNE – diff_negative_error	VNV – very_negative_voltage
NE – negative_error	SDNE–Sdiff_negative_error	NV – negative_voltage
SNE – Snegative_error	DZE – diff_zero_error	SNV–Snegative_voltage
NOE – no_error	SDPE– Sdiff_positive_error	NOV – no_voltage
SPE – Spositive_error	DPE – diff_positive_error	SPV – Spositive_voltage
PE–positive_error		PV – positive_voltage
VPE – very_positive_error		VPV – very_positive_voltage

Finally, the fuzzy inference system maps an input vector to a crisp output value using the centroid defuzzification method and the fuzzy controller provides voltages as outputs on each axis, denoted by  $U_{fuzzy}(x)$ ,  $U_{fuzzy}(y)$ , and  $U_{fuzzy}(z)$ .

Along with kinematic coefficients, FB voltage can be calculated for each actuator  $i$  according to (4.35), for fine tuning of the hand tip position. The final control input  $U_i$  aggregates the contributions of both feedforward and feedback control as in (4.36). Thus, while the variable  $U_{i\_FF}$  as a feedforward voltage (see Subsection 4.3) keeps the  $i$ -th joint in a position that results in the Cartesian hand tip position  $\hat{F}_0$  in the vicinity of the desired position  $F_0$ ,  $U_{i\_FB}$  compensates for the deviation of the desired position  $\Delta X = F_0 - \hat{F}_0$ .

$$U_{i\_FB} = n_{C_{x_i}} U_{fuzzy}(x) + n_{C_{y_i}} U_{fuzzy}(y) + n_{C_{z_i}} U_{fuzzy}(z) \quad (4.35)$$

$$U_i = U_{i\_FF} + U_{i\_FB} \quad (4.36)$$

## 4.5 Simulation results

This subsection provides an overview of the results that illustrate all the control approaches presented in Section 4. Furthermore, a comparison with the engineering

puller-follower control concept is made. The crucial differences, as well as the typical features and implementation issues of the cognitive approaches and engineering puller-follower control, are pointed out.

Simulation experiments were carried out using a seven-DoF anthropomorphic robot arm as a test bed (Figure 4.1). The robot arm was driven by antagonistically-coupled compliant drives and model (2.41) was considered. The parameters of the anthropomorphic robot arm and corresponding drives, which are necessary for the simulations, are given in

Figure 4.9 shows a comparison of the results obtained using the presented cognitive control algorithms to the results when the engineering puller-follower control method was employed for the same task. The results are presented only for two joints, which are mostly affected by gravity load while the arm is lifting – shoulder and elbow rotations around the  $y$  axis (joints 3 and 4 from the arm model depicted in Figure 4.1, right). Figure 4.9 (left) shows joint coordinates in the pointing task case. The role of the left figure is to demonstrate that when the arm was controlled by either the puller-follower method or cognitive methods, both joint positions ended at the same value. However, the force distribution between the agonist and antagonist was different (Figure 4.9, right). The main advantage of the puller-follower approach is evident here – good energy efficiency. This was ensured by keeping the antagonistic force at the desired low level. Due to input control patterns in the experience base, the forces in the antagonistic tendons in the case of the cognitive approaches were significantly higher than the antagonistic tendon forces when puller-follower control was applied. Consequently, in order to provide the same joint torque, the agonist tendon forces were lower in the case of puller-follower control as well. This observation applies to the anthropomorphic arm controlled by either the nearest-neighbor approach or a combination of neural networks and fuzzy control with kinematic coefficient estimation. Conversely, while the engineering puller-follower approach is restricted to single-axis antagonistic joints, the cognitive control methods can be applied to highly complex musculoskeletal mechanism. Consequently, the need to deal with complex inverse kinematics is avoided.

Table 4.5 and Table 4.6. In order to closely resemble the structure of a human arm, the

shoulder, forearm elbow rotation and hand joints (joints denoted by 1, 2, 3, 5, 6, and 7 in Figure 4.1, right) were circular, and the main elbow rotation joint (joint denoted by 4 in Figure 4.1, right) was triangular, with changeable moment arms. Again for the sake of simulation, multi-axis joints are represented as a series of single-axis joints of negligible dynamic and kinematic properties. The drives were defined in accordance with Maxon drives integrated into the Eccerobot prototype [11], and the parameters were taken from the Maxon DC drive catalog [151]. The experience base was created as explained in Subsection 4.3.1. Thus, the initial sphere  $X_s$  was created with a  $0.1m$  radius, center point  $(0.2, -0.4, -0.45)$  and a grid of 100 points, and all final points were located within the final sphere  $X_f$  with a  $0.05m$  radius, centered at the point described by Cartesian coordinates  $(0.55, -0.2, 0)$ . There were about 100 final points that originated from each of the initial positions.

The robot was required to reach the desired final point  $F_0$   $(0.53, -0.22, 0)$  from the initial position  $S_0$   $(0.22, -0.35, -0.43)$ . The initial and final points were arbitrarily set within the initial and final sphere in the experience base, respectively. The points were selected to mimic a typical pointing human task – to lift an arm in front of the robot (see Figure 4.3 for illustration). Figure 4.8 shows the hand tip position while controlled by two cognitive control methods. The first utilizes the nearest-neighbor approach based on interpolation for both FF (Subsection 4.3.2) and FB (Subsection 4.4.1) and is depicted in blue (Figure 4.8, top), whereas the second combines the neural network control approach for FF (Subsection 4.3.3) and the fuzzy theory with kinematic coefficient estimation for FB (Subsection 4.4.2) depicted in red (Figure 4.8, bottom). In other words, the first control algorithm is based on the nearest-neighbor at both FF and FB levels, while the combination of neural networks for FF control and fuzzy logic with estimation of the kinematic coefficients as FB represents the second control approach. The entire motion of the robot arm lasts for 5 s. During the first phase, feedforward control was applied (the nearest-neighbor or the neural network) to drive the robot arm tip from the initial position  $S_0$  to the vicinity of the desired position  $F_0$ . This activity resulted in position  $\hat{F}_0$  within the final sphere  $X_f$ . Control was restricted to FF only during the first 3s. Afterwards (from 3s to 5s), assuming that FF brought the hand tip to the prescribed vicinity of the desired final position  $F_0$ , the robot arm was controlled by

FB in addition to FF. These two periods are distinguished in Figure 4.8 to clearly demonstrate the contributions of the feedforward control approaches (Subsection 4.3) and feedback approaches (Subsection 4.4).

Figure 4.9 shows a comparison of the results obtained using the presented cognitive control algorithms to the results when the engineering puller-follower control method was employed for the same task. The results are presented only for two joints, which are mostly affected by gravity load while the arm is lifting – shoulder and elbow rotations around the  $y$  axis (joints 3 and 4 from the arm model depicted in Figure 4.1, right). Figure 4.9 (left) shows joint coordinates in the pointing task case. The role of the left figure is to demonstrate that when the arm was controlled by either the puller-follower method or cognitive methods, both joint positions ended at the same value. However, the force distribution between the agonist and antagonist was different (Figure 4.9, right). The main advantage of the puller-follower approach is evident here – good energy efficiency. This was ensured by keeping the antagonistic force at the desired low level. Due to input control patterns in the experience base, the forces in the antagonistic tendons in the case of the cognitive approaches were significantly higher than the antagonistic tendon forces when puller-follower control was applied. Consequently, in order to provide the same joint torque, the agonist tendon forces were lower in the case of puller-follower control as well. This observation applies to the anthropomorphic arm controlled by either the nearest-neighbor approach or a combination of neural networks and fuzzy control with kinematic coefficient estimation. Conversely, while the engineering puller-follower approach is restricted to single-axis antagonistic joints, the cognitive control methods can be applied to highly complex musculoskeletal mechanism. Consequently, the need to deal with complex inverse kinematics is avoided.

*Table 4.5. Robot parameters used for simulations in Section 4.*

<b>Label</b>	<b>Numerical value</b>	<b>Unit</b>	<b>Description</b>
$l_u$	0.308	[m]	Upper arm length
$m_u$	2.07	[kg]	Upper arm mass
$I_u$	$\begin{bmatrix} 0.0164 & 0 & 0 \\ 0 & 0.0164 & 0 \\ 0 & 0 & 0.0015 \end{bmatrix}$	[kg · m <sup>2</sup> ]	Upper arm inertia tensor
$l_f$	0.264	[m]	Forearm length

$m_f$	1.14	[kg]	Forearm mass
$I_f$	$\begin{bmatrix} 0.0066 & 0 & 0 \\ 0 & 0.0066 & 0 \\ 0 & 0 & 0.0009 \end{bmatrix}$	[kg · m <sup>2</sup> ]	Forearm inertia tensor
$l_h$	0.1	[m]	Hand length
$m_h$	0.35	[kg]	Hand mass
$I_h$	$\begin{bmatrix} 0.0004 & 0 & 0 \\ 0 & 0.0004 & 0 \\ 0 & 0 & 0.0002 \end{bmatrix}$	[kg · m <sup>2</sup> ]	Hand inertia tensor

Table 4.6. Drive parameters used for simulations in Section 4.

Label	Numerical value	Unit	Description
$l_{a1}$	0.3	[m]	Triangular joint parameter (Figure 4.1: joint 4)
$l_{b1}$	0.3	[m]	
$l_{a2}$	0.07	[m]	
$l_{b2}$	0.05	[m]	
$l_r$	0.04	[m]	Circular joint parameter (Figure 4.1: joints 1,2,3,5,6,7)
$\alpha$	$\pi/4$	[rad]	
$I^{rot}$	$33.5 \cdot 10^{-7}$	[kg · m <sup>2</sup> ]	Motor parameters respectively: rotor moment of inertia, torque constant, viscous friction coefficient, armature resistance, back-EMF constant, gearbox ratio, gearbox efficiency coefficient, motor spindle radius
$C^M$	$14.3 \cdot 10^{-3}$	[Nm/A]	
$B$	$1.31 \cdot 10^{-3}$	[Nm · s/rad]	
$R$	9.07	[Ω]	
$C^E$	$8.42 \cdot 10^{-3}$	[V · s/rad]	
$N$	51	[-]	
$\mu$	1	[-]	
$r$	$5 \cdot 10^{-3}$	[m]	

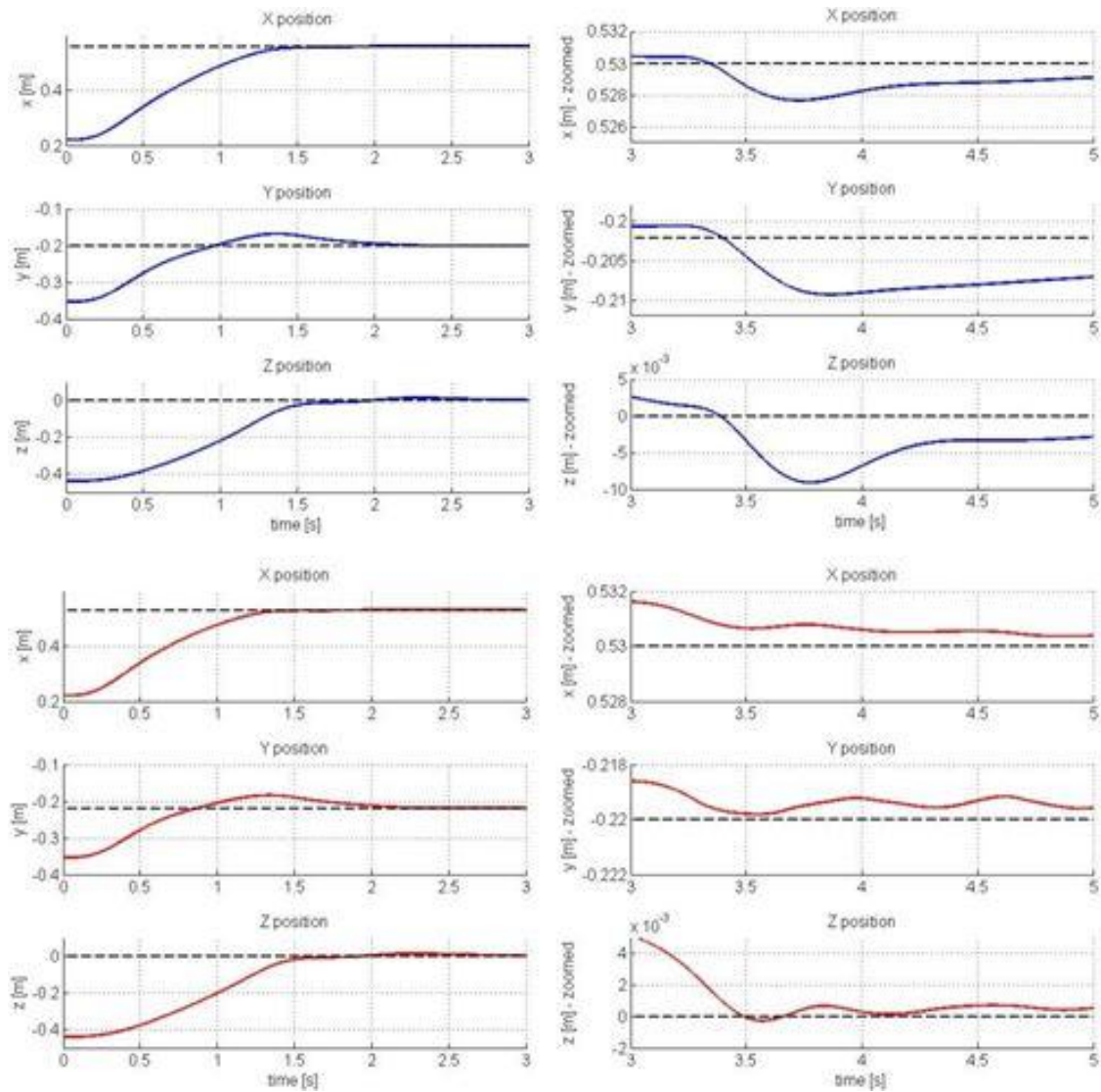


Figure 4.8. Pointing motion of the anthropomorphic arm in Cartesian coordinates. Two types of control approaches were applied to drive the hand tip from the arbitrarily selected initial position  $S_0$  (0.22, -0.35, -0.43) within the initial sphere  $X_s$  to the final point  $F_0$  (0.53, -0.22, 0) within the final sphere  $X_f$ . During the first phase of motion, only feedforward control was applied for 3s, resulting in position  $\hat{F}_0$  within the final sphere  $X_f$ . After 3s  $\div$  5s, FB control was added. These two periods are divided among the left and right side of the figure, respectively, to clearly demonstrate the contributions of FF and FB control. The first control approach combined the nearest-neighbor approach for FF (top left) with the addition of the nearest-neighbor approach for FB (top right). The results are shown in blue. The second control approach combined the neural network approach for FF (bottom left) and the fuzzy theory with kinematic coefficient estimation for FB (bottom right). The results are shown in red.

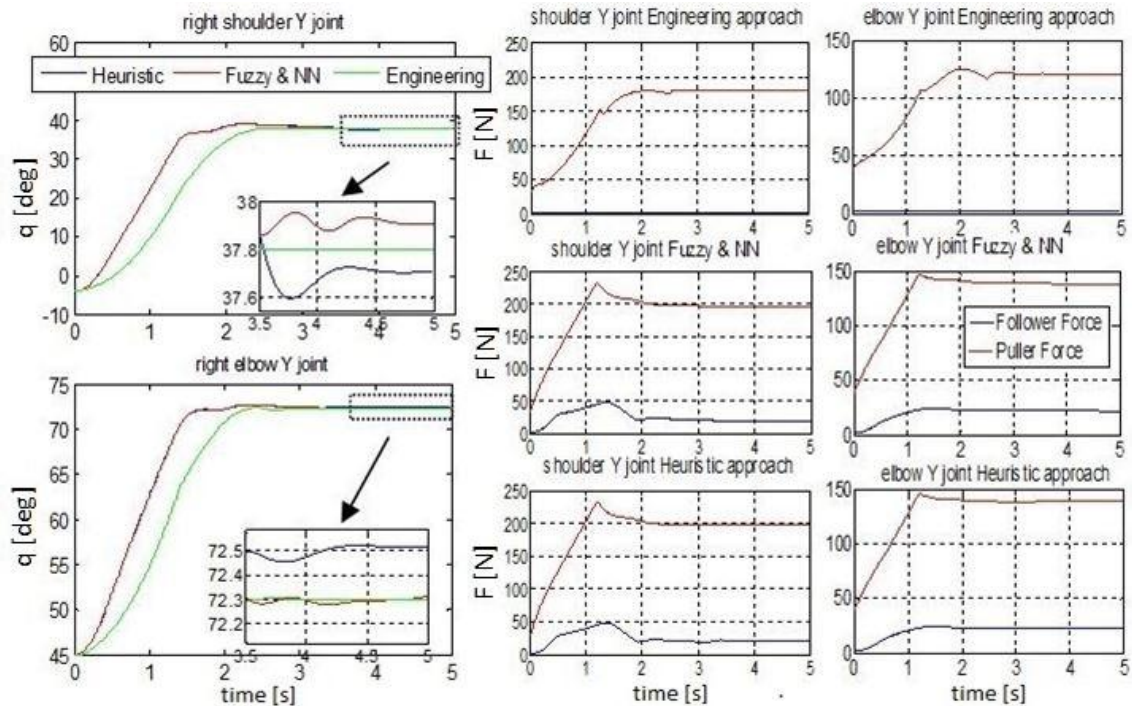


Figure 4.9. Joint coordinates (shoulder and elbow rotation, joints 3 and 4 of the arm model depicted in Figure 4.1, right) in the vertical plane during the pointing motion presented in Figure 4.8. The joint coordinates are depicted for both control methods that rely on cognition and for the engineering puller-follower control method. The figure proves that while the arm was controlled either by the puller-follower method or cognitive methods, both joints positions ended at the same value (left); Force distribution between the agonist and antagonist if the robot arm is controlled by (respectively, top-down): the puller-follower (engineering approach), neural networks and fuzzy control with kinematic coefficient estimation (Fuzzy & NN), and the nearest-neighbor method (heuristic approach). The main feature of the puller-follower control approach is highlighted; antagonistic forces were controlled at a low level and, consequently, the agonist forces were lower than in the other two cases (right).

## 4.6 Conclusions

Human-like compliant robots are certainly the future of service robotics. Since our daily ambience is fully adapted to humans, the greatest challenge in robotics is how to build a robot capable of maneuverability and safe interaction in such an environment. As a result, the design of anthropomorphic robots is a growing trend in engineering. However, such complex mechanical structures, with a high level of compliance, are

very demanding from a control point of view. Many of them have tendons crossing several joints and/or multi-DoF joints that are almost impossible to model. Even if possible, such models are too complex for use in model-based control techniques and require large computing resources. Consistent with the technology that mimics biological patterns, the thesis presented several control approaches that imitate the human learning process and apply it to robot control. The nearest-neighbor method and control approaches that involve neural networks and fuzzy logic with estimated kinematic coefficients do not require an exact model of the robot, but only a previously acquired set of input-to-output recordings of similar movements, considered as an experience base for interpolation of succeeding movements.

Although the previous subsection demonstrated noteworthy results in anthropomimetic robot arm control, the primary contribution is admittedly the high resolution of the experience base. The control methods elaborated in this section are mostly inapplicable for extrapolation, or, in other words, a pointing task would not be possible to accomplish if the initial position  $S_0$  or the final position  $F_0$  was located outside of the initial sphere  $X_s$  or final sphere  $X_f$ . As such, if the proposed cognitive control approaches were to be applied to a wider range of motions, the experience acquisition phase would be very time consuming and cumbersome. Even more so, we could not theoretically guarantee that they would be successful. Finally, the cognitive control methods presented in this section do not consider external disturbances or planned /unplanned interaction.

There are several enhancements to the suggested methods, which could be the focus of ongoing research activities. They mostly consider experience-base design and planning, user-shaped control signals for its creation, control signal parameters that could be varied in the exploitation phase, etc. In particular, any available information, such as any known robot analytics or intuitive expectations, can be used to acquire an experience base with much less data than with a previous exploration strategy, which would result in more accurate robot behavior. Such research has been preliminarily conducted by Stulp et al. at the Technical University of Munich in [251].

On the other hand, the control schemes can be applied to a variety of robots for which it would be almost impossible to produce dynamics and kinematics models, or they would be too complex and time consuming from a computational perspective. Namely, the inverse kinematic problem, which is unavoidable in complex redundant mechanical structures, could be avoided.

By elaborating cognitive approaches to anthropomorphic robot control, we only made a step forward on this topic of growing importance. No final solutions were offered, but some points of view and research direction were suggested, which are believed to be possible areas of complementary research towards bridging the limitations we face when we deal with the design of conventional control for anthropomorphic robots. For more comprehensive research on learning technologies and cognition-based control of anthropomorphic robot, one should refer to the work of A. Diamond at the University of Sussex, who is part of the group of Prof. O. Holland [128]. They primarily focus on certain conventional machine-learning techniques, and reinforcement learning in particular, which were for that reason avoided in the research associated with this thesis.

Finally, Subsection 4.5 pointed out the advantages and drawbacks of all developed methods, as well as their potential application. The results presented unequivocally lead to the conclusion that for effective control of such highly-complex mechanical systems, it is necessary to exploit all the benefits of the given methods. Therefore, once the final control scheme is set, it will represent a mixture of different control techniques – both engineering and cognitive. The symbiosis of the presented approaches will be a topic of the author's post-thesis research.

## **5 Control of a robot with antagonistically coupled compliant drives in contact tasks**

One of the major issues in the field of service robotics is robot control in contact tasks. On the one hand, it is important because numerous robotics applications comprise immediate interaction of the robot's end-effector and a workpiece (assembling, deburring, etc.). Therefore, the quality of task execution depends on controlled impedance between the robot and the processed object, rather than on pure robot positioning. On the other hand, control of robots in contact tasks is essential for safety. Robots as co-workers share work areas with humans and they, therefore, need to first of all prevent but also handle any collisions. To that end, passive (intrinsic) compliance is needed to prevent high-intensity impact forces, whereas active (controlled) compliance is necessary to control contact forces at lower frequencies. Moreover, the achievable Cartesian stiffness by decoupled passive compliance is limited, even in the case of variable stiffness actuators. Accordingly, as suggested by Petit and Albu-Schäffer in [252], symbiosis of active and variable stiffness compliance, to increase the stiffness range, is desirable.

In this section we consider the control of a robot driven by antagonistic compliant actuators in contact tasks. Since each robot joint is equipped with antagonistically-paired drives comprising elastic elements, variable impedance decoupled per particular joint is achieved. Consequently, Cartesian impedance of the robot can be controlled by varying the particular joint stiffness and the robot's pose.

Numerous researchers have studied Cartesian impedance control in robotics, beginning with Hogan [253], and several research groups have studied the application of impedance/stiffness control to antagonistic actuators [254], [132]. However, they usually did not consider multi-joint systems and the implication of antagonistic drives with passive compliance to the robot's Cartesian impedance. There are two mainstreams

leading to Cartesian impedance control, if a robot is driven by variable stiffness actuators based on the antagonistic principle.

The first maps the desired Cartesian impedance into desired single-joint impedances based on the principle of virtual work. The joint impedances are then controlled in a decoupled manner for each particular robot joint. However, an arbitrarily selected Cartesian stiffness matrix cannot be fully mapped in a joint stiffness matrix because its structure is often diagonal, since non-diagonal elements in a joint stiffness matrix lead to a complex mechanical design. The benefits of passively-compliant uncoupled joints to the Cartesian stiffness, as well as mapping issues between the Cartesian stiffness matrix and the joint stiffness matrix, are elaborated by Albu-Schäffer et al. in [255]. As a result of two antagonistically-coupled (nonlinear) drives besides stiffness, simultaneous control of joint position is possible. Feedback from the desired stiffness and position of the joint can be linearized to decouple and simultaneously control joint position and its stiffness (Palli et al. [132]). Also, knowing drive kinematics, the desired joint stiffness and joint position can be further reflected to the desired tendon force in each particular tendon (Wimböck et al. [254]). Even more so, given that the drive and transmission dynamics are known, the desired motor positions of each particular motor can be estimated.

The second approach to the control of a robot's Cartesian impedance is based on Hogan's impedance control resulting in the desired joint torque. Then, the torque is distributed to the agonist and antagonist tendon torques/forces, followed by control of the torque/force portion in each tendon. Following the anthropomorphic robot perspective, the latter approach could more likely be characterized as bio-inspired. Namely, joint torques can be more easily estimated than joint stiffness and, therefore, in the latter approach one can study bio-inspired patterns of force distribution between agonist and antagonist muscles in contacts tasks for different levels of applied joint torques. Such bio-inspired force distribution patterns, often described as a co-contraction and reciprocal activation, could be tested as concepts for the agonist-antagonist torque share in antagonistic actuators.

In this section we opt for the latter approach to the control of the Cartesian stiffness of a robot with antagonistically-coupled compliant actuators. To that end, we first recall the widely-accepted impedance robot control in Subsection 5.1. Then, the background research on the torque share between agonist and antagonist muscles in humans is presented. After considering current findings in these bio-inspired patterns, a torque distribution scheme of antagonistic actuators for the control of an anthropomorphic robot with antagonistic actuators in contact tasks is proposed in Subsection 5.2. The proposed control approach, applied to a two-DoF robot, is validated through simulations in Subsection 5.3.

## 5.1 Impedance robot control

Impedance control is highlighted as the first step of the proposed approach to the control of an anthropomorphic robot with antagonistic actuators in contact tasks. In that way, the desired Cartesian impedance results in the desired joint torques of the robot.

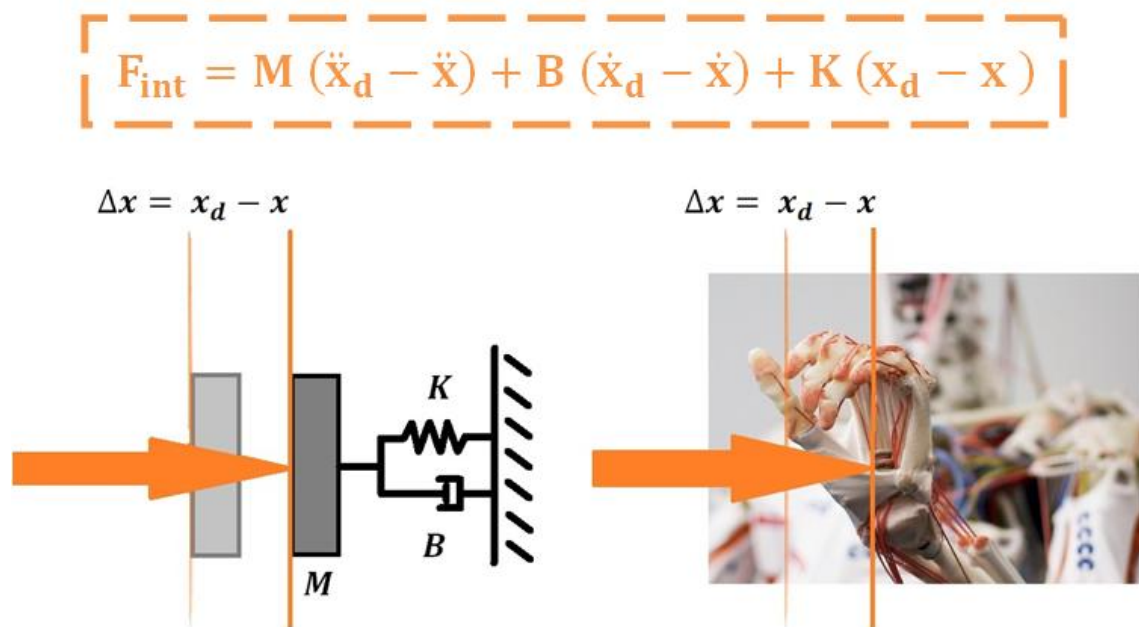


Figure 5.1. Impedance control principle. A robot controlled by an impedance controller behaves as a second order mass-spring-damper system in Cartesian space.

In summary, the idea of Cartesian impedance control introduced by Hogan [256] through his works on the theory, implementation and application, is to control the robot in such a way that its end-effector behaves as a mechanical impedance of predefined parameters – the second order mass-spring-damper system (Figure 5.1). Therefore, the impedance is described by an inertial mass  $\mathbf{M}_{6 \times 6}$  matrix, a viscous damping matrix  $\mathbf{B}_{6 \times 6}$  and a stiffness matrix  $\mathbf{K}_{6 \times 6}$ . These matrices are square matrices that show the mapping between the exerted interaction force  $\mathbf{F}_{int}$  and the position deviation  $\Delta \mathbf{x}$  resulting from this force in the Cartesian frame. In order to achieve decoupled impedance in each Cartesian direction (as it is often planned), these matrices have a diagonal form. Thus, each diagonal element of the inertial matrix –  $m_{ij} \in \mathbf{M}$ ,  $i = j$ , represents inertia on the  $i$ -th axis. The same principle applies to the diagonal elements of the damping matrix ( $b_{ij} \in \mathbf{B}$ ,  $i = j$ ) and the stiffness matrix ( $k_{ij} \in \mathbf{K}$ ,  $i = j$ ). The selection of these parameters is left to the user. However, there are some general rules of thumb:

- If a contact on the  $i$ -th axis is likely to occur, choose  $k_{ii}$  small.
- If a contact on the  $i$ -th axis is likely to occur, choose  $m_{ii}$  large,
- If a contact on the  $i$ -th axis is highly unlikely, choose  $k_{ii}$  large.
- If a contact in the  $i$ -th axis is highly unlikely, choose  $m_{ii}$  small.
- If good tracking on the  $i$ -th axis has priority over general safety in the application, choose  $k_{ii}$  large.
- If good tracking on the  $i$ -th axis has priority over general safety in the application, choose  $m_{ii}$  small.
- If overall safety on the  $i$ -th axis has priority over good tracking in the application, choose  $k_{ii}$  small.
- If overall safety on the  $i$ -th axis has priority over good tracking in the application, choose  $m_{ii}$  large.
- If transient behavior exhibits oscillations, choose  $b_{ii}$  large.

As shown in Figure 5.1 the idea of the controller is to implement a dynamic relation (5.1) between the manipulator's end-effector position and the exerted interaction force,

rather than just control these variables alone. A desired Cartesian position is denoted as  $\mathbf{x}_d$ .

$$\mathbf{F}_{\text{int}} = \mathbf{M} (\ddot{\mathbf{x}}_d - \ddot{\mathbf{x}}) + \mathbf{B} (\dot{\mathbf{x}}_d - \dot{\mathbf{x}}) + \mathbf{K} (\mathbf{x}_d - \mathbf{x}) \quad (5.1)$$

To recall the impedance controller initially introduced by Hogan [256], let us remind ourselves of the general model of robot dynamics transferred from joint position space  $\mathbf{q} = [q_1 \ q_2 \ \dots \ q_n]$ , ( $n$  – number of joints) to Cartesian space  $\mathbf{X} = [x \ y \ z \ \theta \ \psi \ \varphi]$ . These equations are given by (5.2) for joint space and (5.3) for Cartesian space:

$$\mathbf{H}(\mathbf{q})\ddot{\mathbf{q}} + \mathbf{C}(\mathbf{q}, \dot{\mathbf{q}})\dot{\mathbf{q}} + \mathbf{G}(\mathbf{q}) = \boldsymbol{\tau} + \mathbf{J}(\mathbf{q})^T \mathbf{F}_{\text{int}} \quad (5.2)$$

$$\boldsymbol{\Lambda}(\mathbf{q})\ddot{\mathbf{X}} + \boldsymbol{\Gamma}(\mathbf{q}, \dot{\mathbf{q}})\dot{\mathbf{X}} + \boldsymbol{\eta}(\mathbf{q}) = \mathbf{J}(\mathbf{q})^{-T} \boldsymbol{\tau} + \mathbf{F}_{\text{int}} \quad (5.3)$$

Here, the conventional joint space inertial matrix  $\mathbf{H}(\mathbf{q})$ , the matrix of Coriolis and centripetal effects  $\mathbf{C}(\mathbf{q}, \dot{\mathbf{q}})$ , and the gravity load matrix  $\mathbf{G}(\mathbf{q})$  are transformed to Cartesian space matrices of the same meaning:  $\boldsymbol{\Lambda}(\mathbf{q})$ ,  $\boldsymbol{\Gamma}(\mathbf{q}, \dot{\mathbf{q}})$ ,  $\boldsymbol{\eta}(\mathbf{q})$ . Entities (5.4) and (5.5) are used for kinematics mapping.  $\mathbf{J}(\mathbf{q})$  corresponds to a Jacobian matrix.

$$\dot{\mathbf{x}} = \mathbf{J}(\mathbf{q})\dot{\mathbf{q}} \Rightarrow \dot{\mathbf{q}} = \mathbf{J}^{-1}(\mathbf{q})\dot{\mathbf{x}} \quad (5.4)$$

$$\ddot{\mathbf{x}} = \mathbf{J}(\mathbf{q})\ddot{\mathbf{q}} + \dot{\mathbf{J}}(\mathbf{q})\dot{\mathbf{q}} \Rightarrow \ddot{\mathbf{q}} = \mathbf{J}^{-1}(\mathbf{q})[\ddot{\mathbf{x}} - \dot{\mathbf{J}}(\mathbf{q})\dot{\mathbf{q}}] \quad (5.5)$$

$$\boldsymbol{\Lambda}(\mathbf{q}) = \mathbf{J}(\mathbf{q})^{-T} \mathbf{H}(\mathbf{q}) \mathbf{J}^{-1}(\mathbf{q}) \quad (5.6)$$

$$\boldsymbol{\Gamma}(\mathbf{q}, \dot{\mathbf{q}}) = \mathbf{J}(\mathbf{q})^{-T} \mathbf{C}(\mathbf{q}, \dot{\mathbf{q}}) \mathbf{J}^{-1}(\mathbf{q}) - \boldsymbol{\Lambda}(\mathbf{q}) \dot{\mathbf{J}}(\mathbf{q}) \mathbf{J}^{-1}(\mathbf{q}) \quad (5.7)$$

$$\boldsymbol{\eta}(\mathbf{q}) = \mathbf{J}(\mathbf{q})^{-T} \mathbf{G}(\mathbf{q}) \quad (5.8)$$

Two basic impedance control laws can be distinguished: (5.9) and (5.10).

$$\boldsymbol{\tau} = \mathbf{J}(\mathbf{q})^T [\boldsymbol{\Lambda}(\mathbf{q})\mathbf{w}(t) + \boldsymbol{\Gamma}(\mathbf{q}, \dot{\mathbf{q}})\dot{\mathbf{X}} + \boldsymbol{\eta}(\mathbf{q}) - \mathbf{F}_{\text{int}}], \quad (5.9)$$

$$\text{where: } \mathbf{w}(t) = \ddot{\mathbf{x}}_d + \mathbf{M}^{-1} [\mathbf{B}(\dot{\mathbf{x}}_d - \dot{\mathbf{x}}) + \mathbf{K}(\mathbf{x}_d - \mathbf{x}) - \mathbf{F}_{\text{int}}]$$

$$\boldsymbol{\tau} = \mathbf{J}(\mathbf{q})^T [\boldsymbol{\Lambda}(\mathbf{q})\ddot{\mathbf{x}}_d + \mathbf{B}(\dot{\mathbf{x}}_d - \dot{\mathbf{x}}) + \mathbf{K}(\mathbf{x}_d - \mathbf{x}) + \boldsymbol{\Gamma}(\mathbf{q}, \dot{\mathbf{q}})\dot{\mathbf{X}} + \boldsymbol{\eta}(\mathbf{q})] \quad (5.10)$$

If the interaction force is measurable or known, then the interaction dynamics can be

designed arbitrarily (5.1). However, immediate measurement of the interaction force is rarely available; it is often estimated using measured joint torques/currents. Thus, if the interaction force is known, impedance control (5.9) is applied to compensate for gravity and Coriolis and centripetal forces. Finally, the desired impedance behavior of the robot's end-effector is defined by adopted matrix gains:  $\mathbf{M}$ ,  $\mathbf{B}$ ,  $\mathbf{K}$ .

The latter controller (5.10) is employed if the interaction force is not available. In such a case, a completely arbitrary selection of interaction dynamics is not possible. It is restricted to the desired stiffness and damping terms. The effective inertia of the robot is specified by the robot's pose according to (5.11).

$$\mathbf{M} = \mathbf{\Lambda}(\mathbf{q}) = \mathbf{J}(\mathbf{q})^{-T} \mathbf{H}(\mathbf{q}) \mathbf{J}^{-1}(\mathbf{q}) \quad (5.11)$$

The general framework for impedance control of flexible-joint robots is given by Albu-Schäffer et al. in [257]. They used the passivity feature of robots to derive controllers that ensured the desired impedance behavior. However, this theory should be extended to include tendon-driven robots, and specifically antagonistic actuators.

Wimböck et al. in [254] presented a general approach to impedance control for a variable-stiffness mechanism with nonlinear joint coupling. There, the authors consider the desired joint position and stiffness as references. They decoupled position control from stiffness control and calculated the desired positions of each tendon and corresponding motor in the outer control loop. However, the authors did not consider the pulling constraint of the tendons (always positive tendon forces). Instead, they assumed that enough pre-tension was provided to avoid tendon slackening.

Once again, impedance control of a single-axis tendon-driven joint was studied by Pali et al. in [132]. They considered feedback linearization for decoupling control of joint stiffness and joint position in antagonistically-coupled joints with non-linear elastic elements.

## 5.2 Bio-inspired force distribution between antagonistic drives

The most frequent and repetitive in-contact-tasks, such as walking or running, have been performed successfully by most advanced humanoids (for instance ASIMO or HRP-2LR). However, these robots are equipped with conventional, stiff electric drives, followed by a high reduction ratio in order to supply sufficient torques. Consequently, such drives are not back-drivable. As a result, they are not robust to external force/torque, not energy efficient and require carefully-designed motion planning and advanced force/torque control. Furthermore, even in a perfect scenario, their performance is far below that of humans. By contrast, humans complete such tasks with minimal effort and superior performance. The main reason of such superior behavior lies in simultaneous activities of antagonistic muscle groups, which shape their intrinsic compliance to match their natural dynamics. Therefore, besides a human-like robot design, robots need to mimic force distribution patterns and antagonistic group activities in order to achieve safe, stable, energy efficient, and smooth behavior. This is of the essence in contact tasks. To that end, the present subsection outlines basic research of force distribution among antagonistic muscle pairs in typical contact tasks.

As in the case of biological systems (unclear contribution of each particular muscle to the overall torque of a particular joint), it is very difficult to match tendon forces to joint torques of a tendon-driven anthropomorphic robot. This pairing usually depends on the joint position, tendon routing (which is often non-linear), and above all the presence of constraints. The main restriction is the pulling constraint (i.e. tendon force always positive), but the achievable tendon force range could also be a limiting factor. Regardless of antagonistic actuation or fully human-like tendon routing, these constraints have to be considered. In [163], Chalon et al. present some ideas for the optimization of tendon force distribution, in order to achieve the desired joint stiffness. Moreover, this paper is of special interest since it deals with antagonistically-paired tendons within the thumb of the DLR Hand Arm System. The authors suggest several cost functions, which are in general a combination of weighted position and stiffness

errors. However, as stated in the paper, the main issue is real-time optimization, regardless of the adopted optimization criterion. Note that the optimization target is only joint stiffness (i.e. “steady-state impedance”), and not impedance as an original comprehensive term. These initial results and the presented cascade impedance control could be enhanced once an efficient method for inverting the system of torque/stiffness equations under the tendon force constraints is designed. The authors’ effort in this direction was presented in [258].

However, in accordance with the scope of the thesis, we focus on antagonistic actuation. In this regard, two central activities of antagonistically-paired muscles in human motion control are pointed out [259], [260]: reciprocal activation and co-activation (or co-contraction). Reciprocal activation assumes that the net difference between the activities of the agonist and antagonist muscle groups result in a rise in the net joint torque. Co-activation is simultaneous activity of both antagonistically-paired muscle groups, leading to joint impedance modulation, while the net joint torque remains the same. Although co-activation enables more precise movements, its cost is higher energy consumption since simultaneously-activated opposing muscles do not generate mechanical work [261]. Although laboratory studies advocate that co-activation (joint stiffness) and reciprocal activation (net torque influencing a limb movement) could be controlled separately, there is evidence of closely related planning of reciprocal activation and co-activation [156], [262]. Atkeson and Hollerbach show in [263] that the same elbow movements performed at different velocities have very similar trajectory shapes. They attribute this fact to the prediction that if a movement is  $r$  times faster, then the muscle forces or the associated stiffness of the antagonistic muscles needs to be  $r^2$  times larger to achieve the same trajectory shape. A confirmation of the co-contraction-velocity relation is provided for the elbow and shoulder in [264], and for the knee in [211]. All the above mentioned experiments relating to the co-activation and reciprocal activation of antagonistic muscles are carried out by measuring the surface EMG as an activity measure of a particular agonist or antagonist muscle group.

Humphrey and Reed were pioneers in exploring different behavior patterns of antagonistic muscles in contact tasks. In [259] they explain the typical existence of two

partly independent motion control systems: one organized for reciprocal activation of agonist and antagonist muscles and the other for their co-activation (co-contraction). They conducted experiments on monkeys trained to control the position of the wrist in the presence of external perturbations. Based on the speed and frequency of the perturbations they observed: when slow perturbations were applied, the wrist position was controlled by the activity in the particular set of muscles whose action opposed the applied force; when the applied force alternated direction, there was reciprocal activation of the muscles, which acted about the joint; and when rapid perturbations were applied, the joint was stiffened by antagonistic co-contraction. Furthermore, a wide range of motor activities could be generated by a weighed combination of the previously-described control patterns.

Although co-contraction of antagonistic muscles influences joint stiffness, it is fair to point out that numerous researchers have shown that Cartesian end-effector stiffness depends predominantly on arm kinematics. Mussa-Ivaldi et al. in [265] experimentally verified that stiffness varies with joint configuration, so that the end point could be described by ellipsoids elongated in the distal direction. The existence of stiffness ellipsoids based on arm kinematics was later confirmed by Milner [266]. These authors claim that in the distal direction the major axis of the ellipsoids crosses the shoulder joint, whereas in the proximal direction the major axis is aligned with the forearm pointing direction. By carrying out experiments on different subjects, they conclude that stiffness between subjects is comparable in shape and orientation, but not in size (see Figure 5.2). Therefore, the role of the subject's ability to reach different levels of co-contraction could be the only source of these size inequalities. However, the contribution of a robot's kinematic configuration is not considered in the thesis, although previous studies demonstrated its dominant role over co-contraction in the overall Cartesian stiffness. The present research is restricted to co-contraction, to investigate the torque share between antagonistic actuators. The only research that suggests the joint torque share to the agonist and antagonist portions was presented by Chalon and d'Andrea-Novel [165]. There, the authors suggest a heuristic scheme to set equal torque offsets in both tendons and achieve the desired net torque by adding half of it to the agonist portion, while reducing the antagonist portion by the same amount.

Therefore, large pre-tension is needed to produce a large net torque, which makes this heuristic approach energy inefficient.

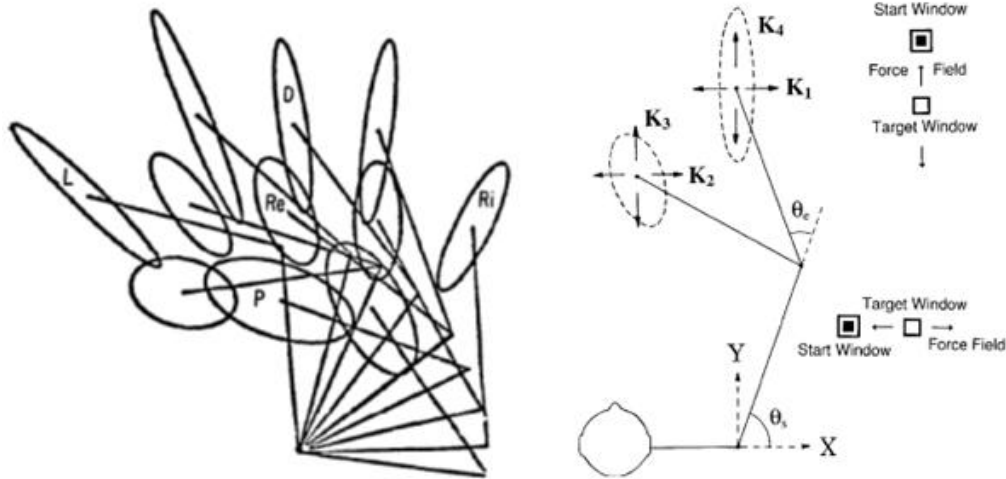


Figure 5.2. Cartesian stiffness ellipsoids related to the kinematics configuration of an arm. The shape and orientation indicate that the major ellipsoid axis crosses the shoulder joint. Results of Mussa-Ivaldi et al. from [265] - (left); and results of Milner from [266] - (right).

In summary, without going into greater detail of human physiology, there are several facts related to the level of antagonistic muscle co-activation, which are of particular importance for the co-contraction planning algorithm presented in this thesis:

- Co-contraction increases with an increase in reciprocal activation (rise of net joint torque).
- Co-contraction increases with an increase in the velocity of the joint (regardless of free or in-contact motion).
- Co-contraction increases if the performed tasks require high precision.

Following these biological patterns, the torque share algorithm (TSA) is proposed. The algorithm intends to divide the necessary joint torque into agonist and antagonist partitions. Since the net joint torque is a result of the difference between the agonist and antagonist torque portions, one of the two can be chosen arbitrarily. The selected tendon torque partition is identified with the selection of the tendon force (or the tendon

stiffness in the case of a non-linear force-length tendon characteristic). However, the selection of one of the tendon forces (or torque partitions), in combination with the known desired joint torque, defines the joint stiffness, or in light of the abovementioned theory – the level of co-contraction. Thus, supposing that the desired net joint torque is given (from Hogan’s impedance control theory, or other torque-based control algorithm), the selection of the force in the antagonistic tendon is introduced following bio-inspired co-contraction levels in human joints. A tendon is set as the antagonistic joint tendon if it opposes the required net joint torque in the initial configuration. A prescribed minimal level of the antagonistic tendon force  $F_{cc\_min}$  needs to be set first. In this manner, minimal co-contraction is preserved and slackening of the tendon prevented, while in the absence of other requirements good energy efficiency is achieved. A bio-inspired pattern of increasing co-contraction with the rise in reciprocal activation is achieved by identifying reciprocal activation with the desired net joint torque provided by the outer control loop. Therefore, the larger net joint torque required in the particular joint, the larger the desired antagonist force selected in the same joint. In a very similar manner, for a particular joint a higher value of the desired antagonistic tendon force should be selected if joint velocity increases. These bio-inspired laws in TSA are included by the coefficients  $k_\tau \left[ \frac{1}{Nm} \right] > 0$  and  $k_v \left[ \frac{s}{rad} \right] > 0$ . Requirements for high precision could also be incorporated in the desired antagonist force by additional scaling of expression (5.12) – scaling factor  $p \geq 1$ . Finally, for arbitrarily chosen parameters  $F_{cc\_min}$ ,  $k_\tau$ ,  $k_v$ , and  $p$ , TSA defines the force in the antagonist tendon of the  $i$ -th as in (5.12). Joint net torque and one of tendon forces determines the force in the other tendon according to (5.13).

$$F_{cc_i} = p_i F_{cc\_min_i} (1 + k_{\tau_i} |\tau_i|) (1 + k_{v_i} |\dot{q}_i|) \quad (5.12)$$

$$\tau_i = r_j (F_A - F_B) \quad (5.13)$$

Here,  $\tau_i$  determines the desired net torque in the  $i$ -th joint provided by the impedance control algorithm in the outer control loop (5.9) or (5.10), and  $\dot{q}_i$  is the estimated velocity of the  $i$ -th joint. Equation (5.12) is a basic relation that combines the abovementioned co-contraction dependencies. However, further elaboration on these

dependencies, as well as their weighted coefficients ( $k_\tau, k_v$ ), is needed. For instance, a study carried out at the Department of Psychology, McGill University [267], showed that co-contraction was low in the intervals near the peak velocity and increased near a maximum in the region where the deceleration phase of the movement started. Such a pattern would result in an exponential rise of co-contraction with increasing velocity. Figure 5.3 is a graphical representation of the desired antagonistic force in the TSA according to the basic adopted relation (5.12).

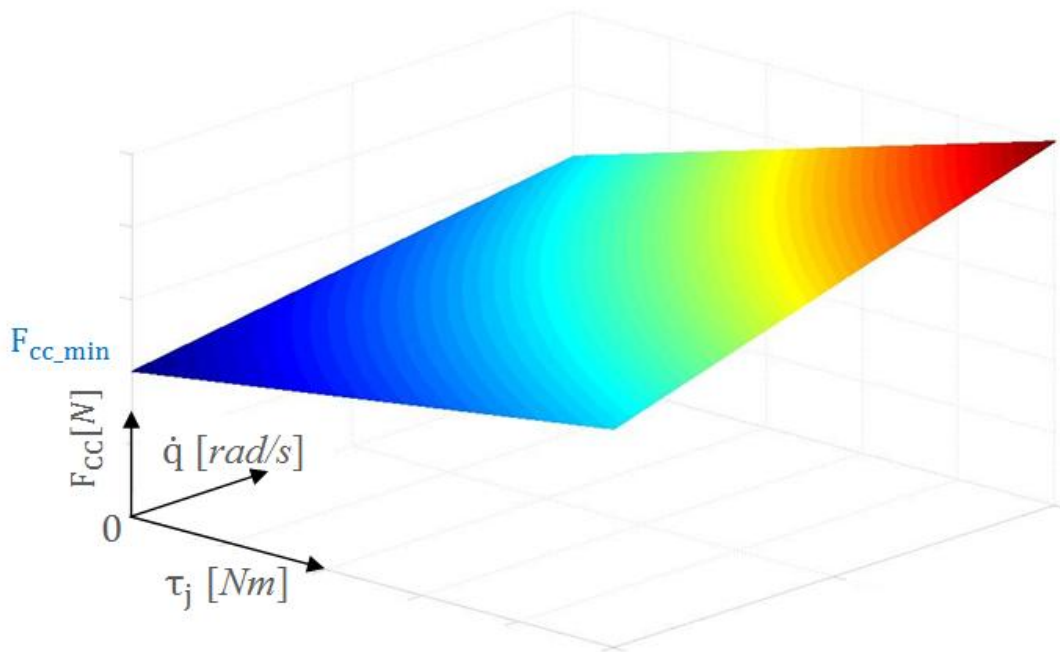


*Figure 5.3. Desired force in the antagonist tendon of the  $i$ -th joint, estimated using a bio-inspired torque share algorithm. Reference tension force rises with increase in desired net joint torque (corresponding to biological reciprocal activation) and increase in joint velocity.*

Similarly to the puller-follower approach presented in Subsection 3.3, the agonist and antagonist roles between tendons need to be exchanged. As already mentioned, we call it “switching”; it occurs if the agonist tendon force drops down to the level of the antagonist tendon force of the same joint (i.e. when the desired net torque changes its sign). If the tendons exchange their roles due to a change in direction of the desired joint net torque provided by the outer control loop, and the other tendon takes over the antagonistic role, the new desired antagonist force is again kept at least at the prescribed

minimal level.

The TSA algorithm does not consider a maximal tendon force, i.e. saturation of the actuator. Moreover, an agonist tendon force that requires an upper limit could be required directly from the increase in the desired antagonist tendon force according to (5.12). Inclusion of actuator saturation will be introduced as a constraint and elaborated in future research.

### **5.3 Impedance control of robots with antagonistically-coupled compliant joints**

The combination of active (controlled) and passive (mechanical) stiffness is exploited to achieve inherently safe robot behavior. In fact, we want to use mechanical stiffness to protect the robot from exerting large impact forces (high frequency disturbances), whereas the desired Cartesian impedance behavior is adjusted by the controller at lower frequencies. Furthermore, intrinsic compliance can provide a reduction in sampling frequency of the controller, and therefore more complex active control schemes can be applied. On the other hand, very stiff robot behavior and highly accurate fast motion are disabled due to mechanical properties (i.e. intrinsic compliance in joints).

Comprehensive insight into the introduced control algorithm is provided in Figure 5.4. As explained in the introductory paragraphs of this section, the approach presented in the thesis comprises estimation of the desired force/motor positions in each particular tendon in two steps. The first step is the application of the Cartesian impedance controller (5.9) or (5.10) in the outer control loop, which supplies the desired joint torque as a desired intermediate input for the inner control loop. Afterwards, the overall joint torque is divided in a bio-inspired manner using TAS in its agonist and antagonist partitions for each joint. A pulling constraint is prevented by using switching, similar to that explained in Subsection 3.3. Namely, if the agonist force decreases, switching occurs once the agonist force reaches the antagonist tendon force. To avoid cluttering between two modes (fast switching of one tendon between agonist and antagonist roles),

a dead-zone for the reference antagonist force is applied. Finally, motor positions are controlled using elementary PD controllers. In addition to PD feedback position control, a feedforward motor torque is commanded. The feedforward exploits statics compensating for the desired tendon forces in accordance with Equations (3.4) through (3.11).

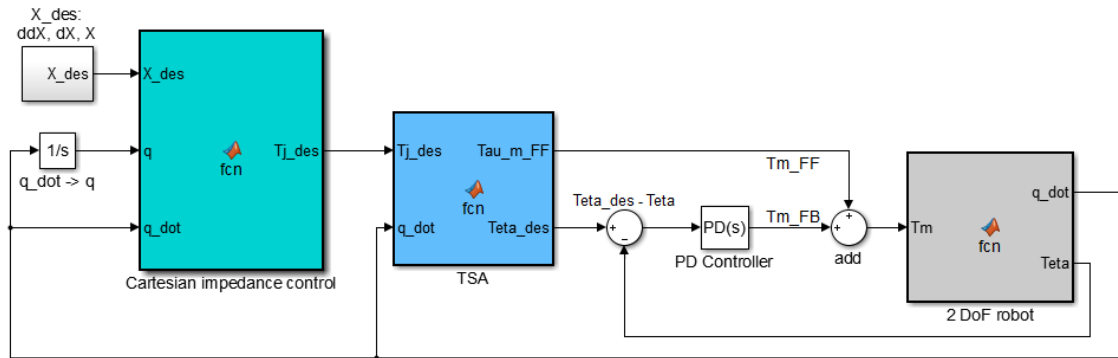


Figure 5.4. Bio-inspired algorithm for control of a robot with antagonistic actuators in contact tasks. The outer control loop is Hogan's Cartesian impedance control algorithm (in cyan), which provides the desired joint torques as inputs to the inner control loop. The inner control loop comprises a torque share algorithm (TSA), which divides the desired net joint torque, in a bio-inspired manner, into its agonist and antagonist partitions for each robot joint. Using inverse dynamics of the drives, TSA provides feedforward for motor torques as control inputs and the desired motor positions for the desired Cartesian behavior of the robot. Finally, the last control loop contains PD position controllers, which compensate for motor position errors.

In order to demonstrate the approach to the control of a robot driven by antagonistically-paired compliant drives, a simulation experiment was undertaken to demonstrate robot behavior in contact tasks. The simulation experiment exploited the same model of the two-DoF planar robot ( $x0z$  plane), driven by antagonistic compliant actuators (model given by (2.41)). The circular structure (see Subsection 2.3.1.1) with quadratic elastic elements in the tendons was used to model both robot joints. The parameters used in the simulation are given in Table 5.1. The initial robot's pose in accordance with Figure 2.14 corresponds to shoulder and elbow positions  $q_1 = \frac{\pi}{4}$ ,  $q_2 = \frac{\pi}{4}$ , respectively. Consequently, the initial Cartesian position [m] is  $\mathbf{X} = [x \ z]' = [0.5121 \ -0.2121]$ .

Table 5.1. Parameters used for simulations in Section 5.

Label	Numerical value	Units	Description
$l_u$	0.3	[m]	Upper arm length
$m_u$	3	[kg]	Upper arm mass
$I_u$	0.0225	[kg · m <sup>2</sup> ]	Upper arm moment of inertia tensor
$l_f$	0.3	[m]	Forearm length
$m_f$	3	[kg]	Forearm mass
$I_f$	0.0225	[kg · m <sup>2</sup> ]	Forearm moment of inertia
$l_r$	0.15	[m]	Circular joint parameters (stand for both joints)
$\alpha$	$\pi/2$	[rad]	
$k_2$	100	[N/m <sup>2</sup> ]	Quadratic spring coeff.
$k_1$	0	[N/m]	
$k_0$	0	[N]	
$I_{rot}$	0.001	[kg · m <sup>2</sup> ]	Motor parameters
$B_{rot}$	0.001	[Nms/rad]	
$r$	0.05	[m]	
$M$	$\begin{bmatrix} 1 & 0 \\ 0 & 1 \end{bmatrix}$	[kg]	Cartesian impedance control parameters
$K$	$\begin{bmatrix} 100 & 0 \\ 0 & 100 \end{bmatrix}$	[N/m]	
$B$	$\begin{bmatrix} 4 & 0 \\ 0 & 4 \end{bmatrix}$	[Ns/m]	
$F_{cc}$	10	[N]	TSA parameters
$p$	1	[–]	
$k_\tau$	0.1	[1/Nm]	
$k_v$	0.2	[s/rad]	

The simulation demonstrates the presented control algorithm for the antagonistically-driven robot in contact tasks, in static conditions and the horizontal plane. An external force of 10N is imposed to the robot in the  $x$  direction at  $t_{Fx} = 1s$ , and another external force of a trapezoid profile and 5N intensity starts acting at  $t_{Fz} = 4s$  in the  $z$  direction. The resulting Cartesian impedance behavior is achieved in a decoupled manner (decoupled impedance behavior in  $x$  and  $z$  directions), according to the diagonal form of  $M$ ,  $K$ , and  $B$  controller parameters, although such behavior requires effort of all four motors (two shoulder motors and two elbow motors). Figure 5.5 demonstrates deviations in Cartesian coordinates for imposed contact forces. In accordance with the

static force-deviation relation (stiffness) parameter of the impedance controller  $k_x = k_z = 100 \frac{N}{m}$ , the desired Cartesian  $x$  position deviates for  $\Delta x = x_{des} - x = 0.5121m - 0.4121m = 0.1m = \frac{10 N}{100 N/m} = \frac{F_{int_x}}{k_x}$ . The impedance dynamic is also defined and controlled in accordance with the selected control parameters. Therefore, the period of damped position oscillations in the  $x$  direction is exactly  $T = 0.628 s = \frac{2\pi}{\omega} = \frac{2\pi}{\sqrt{k_x/m_x}}$ . Here the controller given by (5.9) is used, so the Cartesian impedance dynamic can fully be shaped. If the contact force is not known, impedance dynamics will not be completely arbitrarily shaped, as explained in Subsection 5.1.

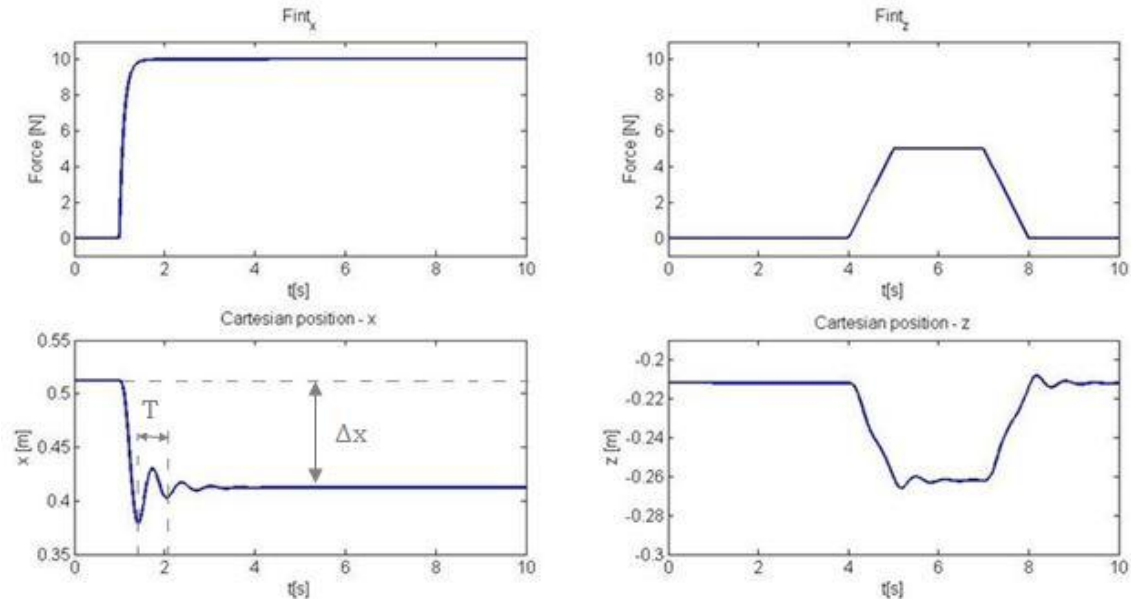


Figure 5.5. External contact force  $F_{int}$  causes a deviation in the Cartesian end-effector position according to impedance relation (5.1) and controller parameters. External force in  $x$  direction (top left); External force in  $z$  direction (top right); Cartesian position in  $x$  direction (in accordance with prescribed impedance Cartesian behavior and imposed force in  $x$  direction) - (bottom left); Cartesian position in  $z$  direction (in accordance with prescribed impedance Cartesian behavior and imposed force in  $z$  direction) - (bottom right).

The results of Cartesian impedance control were achieved by simultaneous activity of the antagonistically-paired drives in each robot joint, in accordance with the previously introduced bio-inspired TSA. Thus, the desired antagonistic force selection and the required net joint torque determine the agonist tendon force, which is commanded

independently in each joint. The desired antagonistic force is kept at a predefined low level, which changes due to a high desired joint torque or a high joint velocity as indicated in (5.12). An exchange of roles between A and B tendons occurs in order to ensure the desired net joint torque in an energy efficient manner, while preventing tendon slackening. The resulting tendon forces and their roles depicted in modes are shown in Figure 5.6. Mode 1 declares tendon A as the agonist, whereas mode 0 means that the agonist role is taken over by tendon B.

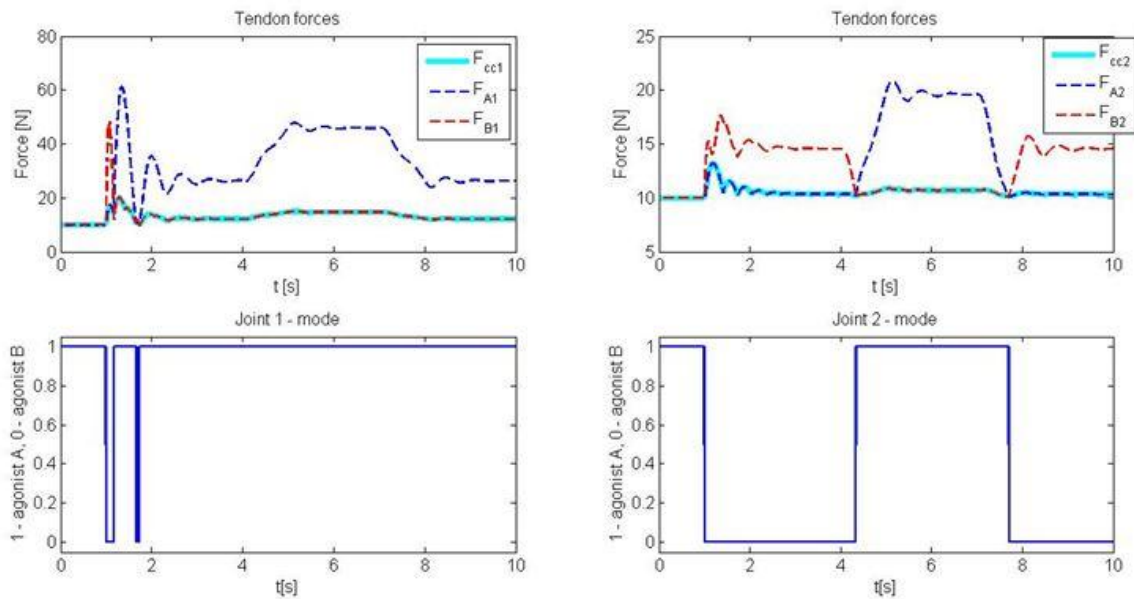


Figure 5.6. Result of bio-inspired TSA distribution of net joint torque into its agonist and antagonist portions. Antagonistic tendon forces in the first joint – shoulder (top left); Antagonistic tendon forces in the second joint – elbow (top right); Change of mode in the first joint – tendons A and B switch roles to achieve the desired net joint torque, while preserving energy efficiency and preventing slackening of shoulder tendons (bottom left); Change of mode in the second joint – tendons A and B switch roles to achieve the desired net joint torque, while preserving energy efficiency and preventing slackening of elbow tendons (bottom right).

Finally, the Cartesian impedance controller in the outer control loop followed by TSA defines the required positions of each individual motor. Identical rotation directions of the antagonistically-coupled electric drives means higher pre-tension in the joint, whereas their difference contributes to a higher net joint torque, resulting in joint shifts but also compensating for external disturbances. The motor and joint positions, as a

result of the Cartesian impedance control and selected TSA, are depicted in Figure 5.7.

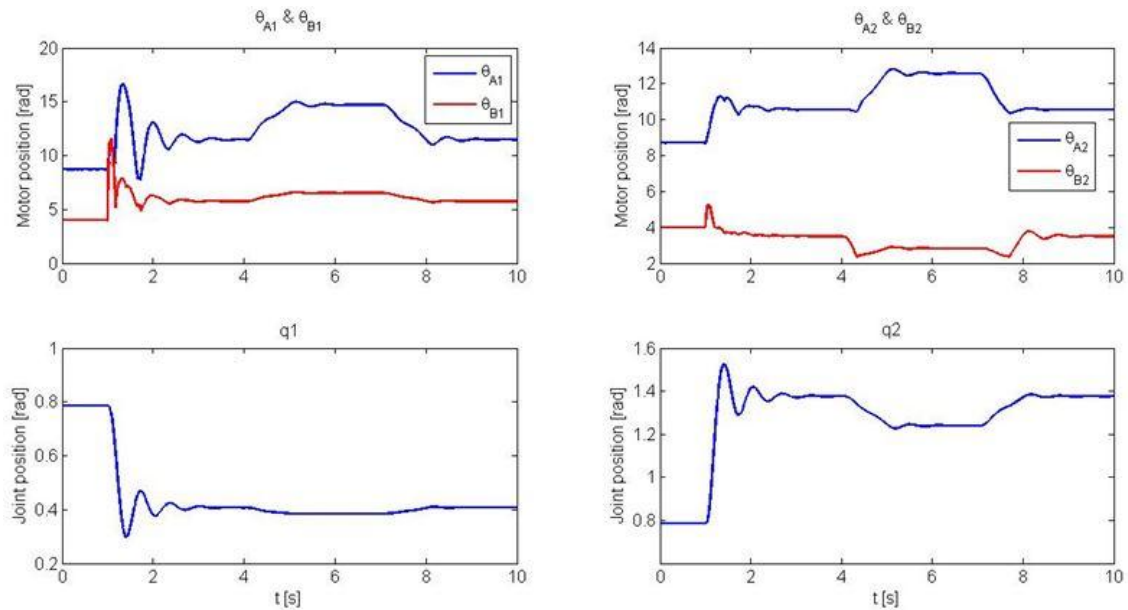


Figure 5.7. Positions of two antagonistically-coupled motors in joint 1 – shoulder (top left); Positions of two antagonistically-coupled motors in joint 1 – elbow (top right); Resulting shoulder position –  $q_1$  (bottom left); and Resulting elbow position –  $q_2$  (bottom right).

In summary, we opted for the impedance control approach that results in the desired joint torques, followed by bio-inspired force distribution between agonist and antagonist tendons, rather than mapping from Cartesian impedance space to the joint impedance space and simultaneous joint stiffness and position control, for several reasons. First, in accordance with the anthropomorphic robot perspective, the selected approach could be characterized and implemented as a bio-inspired concept. Also, the term ‘joint impedance’ is not yet a well-defined quantity and, as such, joint stiffness estimation is a challenging task in motor control. Otherwise, joint torques in humans and antagonistic muscle forces can be successfully estimated and their different levels are conveniently related to agonist and antagonist activities described in the literature as a co-contraction and reciprocal activation. Next, in the case of a fully-anthropomorphic robot design, if the Cartesian stiffness matrix in a joint space were to be considered, non-diagonal elements would appear. This could be a bottleneck for the mechanical design and particularly for the control of those terms. Although very demanding, tendon force-to-

joint torque mapping seems like an easier task. One more argument that governed the proposed approach is scalability, i.e. a larger external force causes a larger Cartesian position deviation due to commanded Cartesian compliance. This can be handled more efficiently than mapping between Cartesian stiffness and joint stiffness, which vary significantly for a larger position deviation.

The author's future work on the topic will include TSA reshaping and examination of the influence of different torque levels of succeeding joints in the kinematic chain on the co-contraction level (reference antagonist force), as well as of the contribution of the velocity of other joints in the kinematic chain to particular joint co-contraction. Finally, the robot's kinematic configuration and its contribution to the necessary co-contraction level in each of the joint needs to be explored.

## **6 Findings, conclusions & directions of ongoing research**

An inevitable glimpse into our future is a home robot of fully anthropomorphic shape, capable of performing a full range of human-like activities. Actuation systems of future robots will, therefore, fully resemble musculoskeletal human structures, to enable robots to climb stairs, turn knobs or door handles, etc. Copying the human shape, but also its structure, leads to anthropomimetic robots. This scenario is definitely more likely than one in which humans would change an ergonomically-shaped environment, fully designed to meet our needs and not the robot's.

By the time advances in technology, novel materials, computer hardware, sensors and actuation systems enable fully-functional anthropomimetic robots, roboticists will have enhanced their predecessors. These predecessors are compliant robots capable of safe human-robot interaction, and especially robots with variable stiffness actuation and, ultimately their subgroup – robots with antagonistically-coupled compliant drives.

Anthropomimetic robots have been built as engineering copies of human bodies, which should also be able to achieve a significant level of human performance. In order to facilitate this process, we first need to fully understand motor control in humans, and trade-off between desired levels of robot similarity to human appearance, performance, and reliability. Research groups have opposing views of the directions towards the final goal – construction of a fully-functional artificial human. On the one hand, projects like Kenshiro [54], ECCEROBOT [8], or Myrobotics [268] (University of Tokyo, Japan; University of Sussex, UK; University of Zurich, Switzerland; Technical University of Munich, Germany; The Robot Studio, France; and the University of Belgrade, Serbia) advocate straightforward resemblance of human anatomy, whereas performance, functionality and level of control of such robots are questionable or at least challenging.

On the other hand, projects such as the biped Lucy [269], STIFF [270], PHRIENDS [16], or VIATORS [271] (DLR Institute of Robotics and Mechatronics, Germany; Italian Institute of Technology, Italy; University of Pisa, Italy; La Sapienza University in Rome, Italy; Vrije University Brussels, Belgium; University of Twente, Netherlands; Imperial College London, UK) focus on human-like performance and emulation of the functionality of humans, while human anatomy and appearance of the robots are of secondary importance. Former approaches have already exhibited an amazing level of human likeness and captured the hearts of visitors introduced to the Kenshiro, Eccerobot or Myrobot. The latter approaches have already showcased a significant level of human performance and maneuverability, while demonstrating a high level of safety in interaction due to variable stiffness actuation. Tomorrow's fully-functional anthropomorphic robot will be created once the level of technology enables these complementary research directions to converge.

A detailed review was undertaken to present novel trends and technologies that lead to inherently safe anthropomorphic robots. The review covers state-of-the-art trends in robot actuation: active and passive compliant actuators, variable stiffness actuators, and, finally, antagonistically-coupled compliant actuators. Antagonistic actuators are of particular importance for this work since they achieve variable stiffness in a bio-inspired manner. Thus, since the main movers of the human body are actually antagonistically-driven muscles as a paragon for antagonistic robotic joints, some behavior patterns could be extracted from biology and applied to the design and control of antagonistic robot joints. Furthermore, antagonistic joints are not only a technology on its own, but a prerequisite for complex anthropomorphic structures: multi-axes robot joints (e.g. a shoulder replica) or multi-articular artificial muscles (e.g. a replica of biceps brachii). The detailed review of antagonistic robot joints is a general contribution of this thesis.

The first scientific contribution of the thesis is an analytical model of anthropomorphic robot dynamics. Stepanenko's approach to robot modeling was exploited in this regard, since it has demonstrated superior performance in simulating robot dynamics [123]. An anthropomorphic robot configuration driven by antagonistically coupled compliant drives was adopted in the present research (since antagonistic muscles are considered to

be the primary movers of the human body). The presented analytical model is of a form that could easily be implemented in simulation algorithms. It supports both free-motion and contact/interaction tasks. For demonstration purposes, the model was implemented in Matlab (with some routines in C++) and two case studies that emulate typical real-world scenarios of a robot working and interacting in our everyday environment were elaborated. Although some applications [1] to a physical robot and a simulation-based study [2] have already been undertaken, there is still a wide range for prospective model utilization:

- simulation and analysis of biomechanical systems/subsystems,
- study of the possibilities of moving from biological concepts to bio-inspired robotics,
- anthropomorphic robot system design,
- simulation of anthropomorphic robots in interaction tasks,
- development of model-based advanced control techniques for anthropomorphic robots, and
- testing of anthropomorphic control approaches with additional possibilities of control in interaction tasks, etc.

In particular, one rapidly growing industry that could benefit from the analytical model is the gaming and computer animation industry. With precipitous advances in computer hardware, animations do not need to be based on physical approximations of engines, but could simulate full models of character dynamics in real time with distinct realistic movements. This would open a new era in computer games and a completely new perception of them. A very famous work with already more than five hundred citations, which advocates and envisages advanced dynamics as an essential step towards a new level of computers animation, has been presented by Popovic et al. from Carnegie Mellon University in [272].

In summary, the results and contributions of the present research in the field of anthropomorphic robot modeling have generally been addressed in a number of author's publications: [2], [3], [106], [107], [273], [274], [275].

The second scientific contribution of this thesis concerns control of the anthropomorphic robot driven by antagonistic compliant drives using the multivariable, non-linear and robust control theories. The thesis first provided an outline of the background work on antagonistic joint control and feedback linearization in compliant robot control. Then it presented a biologically-inspired and energy efficient puller-follower approach for simultaneous control of joint position and force in one of the two tendons, as outlined in [4]. The puller-follower approach was upgraded to include simultaneous control of joint position and joint stiffness. This algorithm based on feedback linearization for decoupling and handling with non-linearities is first demonstrated on a single-axis robot joint and then adapted to a multi-joint robot. To that end, joint control was modified for model-based gravity compensation and estimation of effective joint inertia. Dynamic coupling in multi-joint systems was handled by introducing the  $H_\infty$  loop shaping robust control theory. The control methods developed for antagonistically-driven compliant joints are not only applicable to anthropomorphic mechanism based on antagonism. Complex anthropomorphic structures, such as spherical joints (shoulder, hip, or any other multi-axes joints) cannot be controlled using conventional drives, but with tendon driven and probably antagonistically-paired and compliant actuators. In such cases the puller-follower could be a sound foundation. The main findings of the present research in the field of anthropomorphic robot control, developed from engineering techniques for multivariable, non-linear and robust control, are summarized in following author's articles: [5], [11], [56], [106], [154], [161].

In addition to control methods that rely on conventional engineering techniques, several cognitive approaches to control of antagonistically-coupled compliant drives in robotics were also developed. In accordance with the bio-inspired background and fully human-like design of the anthropomorphic robot, the focus was on human-like control as well – control based on experience, learning and heuristics. To that end, the nearest-neighbor algorithm was developed for feedforward and feedback control of the anthropomorphic robot [213], neural network feedforward control using radial-basis networks [243], and feedback control based on on-line estimation of kinematic coefficients and fuzzy rules [214]. Although cognitive algorithms were not of primary importance in this thesis, they constitute a step forward towards control of a fully-anthropomorphic robot, since

engineering-based control algorithms reach their limits if multi-articular muscles or multi-axes joints are considered. On the other hand, cognitive methods outlined in the thesis can be applied to such systems without restriction. A complete overview of both engineering and cognitive methods developed in this thesis is provided in [5].

The author's point of view and initial research on control of intrinsically-compliant robots with antagonistically-driven joints in contact tasks [169], [276] are outlined in the thesis as well. The approach comprises Cartesian impedance control as a outer control loop followed by bio-inspired torque share algorithm. This algorithm defines agonist and antagonist torque partitions and calculates desired tendon forces by copying biological patterns of antagonistically coupled muscles in contact tasks. As a topic of rapidly growing interest, since the majority of contemporary and future robotic applications require handling of external objects and interaction with the environment, it will definitively be the subject of follow-up research. The results presented here with regard to this topic are collinear with future work and constitute a mixture of state-of-the-art conventional and widely adopted impedance control techniques and bio-inspired patterns of biological antagonistic structures.

Based on the extensive work on modeling, and especially control, of anthropomimetic robots with antagonistically-driven compliant joints reported in this thesis, the author is fully aware of its current status and potential, but also limitations. Consequently, it is safe to say that future service robots will not be controlled using analytical models and conventional control methods, or relying on the imitation of humans or experience-based learning, separately and solely. A combination of all these approaches will be followed and employed to deal with numerous and diverse tasks, which will be required from robots. However, since antagonistic muscle pairs are prime movers in humans, the puller-follower analytical approach to the control of antagonistic drives is expected to belong to the foundation of the ultimately-employed analytical control skills of robots. In addition, robots will imitate humans, assimilate behavior patterns by observing, learn from repetition and, therefore, resemble the behavior of humans. Such a robot of distinguished human shape and functionality could hardly do better than a human evolved through centuries. As a result, human motor-control patterns are the subject of

research in robotics, biomechanics, biology, etc. Accordingly, an attempt was made to exploit EMG patterns of human antagonistic muscles and transfer them to the antagonistically-driven robot, to enable accurate, energy-efficient but also safe robot performance. Finally, as each human being masters their skills while growing up, an essential feature in robot control would be experience-based learning or learning by trial-and-error. This learning process is unavoidable for acquiring and mastering new tasks and challenges. Consequently, a part of this thesis targeted experience acquisition in robot learning and exploitation based on cognitive and heuristic approaches. What was addressed here but is a target of ongoing research is the symbiosis of all the listed approaches, as elements towards the final control scheme of future anthropomimetic robots. So far, Stulp et al. in [251] have provided a preliminary empirical evaluation and demonstration that combines all the mentioned approaches to robot control, to enable the conventional rigid robot B21 to act more accurately and efficiently in an everyday human environment.

Patterns observed and learned from models of antagonistically driven mechanisms, their control in contact and non-contact tasks, and resulting muscle synergies could be applied in the field of functional electro simulations (FES) [211]. FES is perceived as a promising research field in the rehabilitation industry, where FES is recognized as a prospective tool for the feedback control.

Ultimately, the work on this thesis led to an unequivocal conclusion. Although a fully-anthropomimetic robot design would theoretically result in an “artificial human” and, therefore, a robot of superior performance in an everyday human-shaped environment, some compromises have to be made. Humans are not designed according to engineering principles, so the job of creating an artificial human should be left to biologist and geneticists. On the other hand, while creating a service humanoid of tomorrow by replicating human functionality and maneuverability, we as engineers should be aware of the rule [277]: *the mechanical structure, drives and control features of biological systems do not follow engineering principles, but they are not far and do not substantially violate any of them.*

## 7 Bibliography

- [1] Morena engineering, [Online]. Available: <http://www.morenaict.com:8080/>. [Accessed 6 December 2015].
- [2] V. Antoska, K. Jovanovic, V. Petrovic, N. Bascarevic, M. Stankoviski, "Balance analysis of the mobile anthropomorphic robot under disturbances – ZMP approach," *International Journal of Advanced Robotic Systems*, vol. 10, no. 206, pp. 1-10, 2013.
- [3] K. Jovanovic, V. Potkonjak, O. Holland, "Dynamic modelling of an anthropomorphic robot in contact tasks," *Advanced Robotics*, vol. 28, no. 11, pp. 793-806, 2014.
- [4] B. Svetozarevic, "Control of electrical agonist-antagonist drives with and without elastic effects in robotic systems (in Serbian)," Master thesis, School of Electrical Engineering, University of Belgrade, Belgrade, Serbia, 2010.
- [5] V. Potkonjak, K. Jovanovic, P. Milosavljevic, "Chapter 20: How to Control Anthropomorphic Robot - Engineering and Cognitive Approach," in *New trends in Medical and Service Robotics*, Switzerland, Springer International Publishing, 2014, pp. 299-313.
- [6] J. Liu, H. Hu, "Novel mechatronics design for a robotic fish," in *IEEE/RSJ International Conference on Intelligent Robots and Systems (IROS 2005)*, Edmonton, Canada, 2-6 August 2005.
- [7] C. Laschi, M. Cianchetti, B. Mazzolai, L. Margheri, M. Follador, P. Dario, "Soft robot arm inspired by the octopus," *Advanced Robotics*, vol. 26, no. 7, pp. 709-727, 2012.
- [8] "Embodied Cognition in a Compliantly Engineered Robot - ECCEROBOT," Seventh framework programme of the EU, [Online]. Available: <http://eccerobot.org/>. [Accessed 13 12 2015].
- [9] H. Dong, N. Mavridis, "Muscle force distribution for adaptive control of a

- humanoid robot arm with redundant bi-articular and mono-articular muscle mechanism," *Artificial Life and Robotics*, vol. 18, no. 1, pp. 41-51, 2013.
- [10] H. Marques, M. Jäntschi, S. Wittmeier, C. Alessandro, M. Lungarella, R. Knight, O. Holland, "ECCE1: the first of a series of anthropomimetic musculoskeletal upper torsos," in *IEEE-RAS International Conference on Humanoid Robotics (Humanoids 2010)*, Nashville, TN, US, 6-8 December, 2010.
- [11] S. Wittmeier, C. Alessandro, N. Bascarevic, K. Dalamagkidis, A. Diamond, M. Jäntschi, K. Jovanovic, R. Knight, H. G. Marques, P. Milosavljevic, B. Svetozarevic, V. Potkonjak, R. Pfeifer, A. Knoll, O. Holland, "Toward anthropomimetic robotics: development, simulation, and control of a musculoskeletal torso," *Artificial Life*, vol. 19, no. 1, pp. 171-193, 2013.
- [12] G. A. Pratt, M. M. Williamson, "Series elastic actuators," in *IEEE/RSJ International Conference on Intelligent Robots and Systems (IROS 1995)*, Pittsburgh, PA, USA, 5-9 Aug 1995.
- [13] M. Zinn, B. Roth, O. Khatib, K. J. Salisbury, "A new actuation approach for human friendly robot design," *International Journal of Robotics Research*, vol. 23, no. 4-5, pp. 379-398, 2004.
- [14] S. Haddadin, A. Albu-Schäffer, G. Hirzinger, "Safe Physical Human-Robot Interaction: Measurements, Analysis and New Insights," in *Robotics Research*, Springer Berlin Heidelberg, 2011, pp. 395-407.
- [15] S. Haddadin, S. Haddadin, A. Khoury, T. Rokahr, S. Parusel, R. Burgkart, A. Bicchi, A. Albu-Schäffer, "On making robots understand safety: embedding injury knowledge into control," *The International Journal of Robotics Research*, vol. 31, no. 13, pp. 1578-1602, 2012.
- [16] "Physical Human-Robot Interaction: Dependability and Safety - PHRIENDS," Sixth framework programme of the EU, [Online]. Available: <http://www.phriends.eu/>. [Accessed 13 12 2015].
- [17] "Safe and Autonomous Physical Human-Aware robot Interaction - SAPHARI," Seventh framework programme of the EU, [Online]. Available: <http://www.saphari.eu/>. [Accessed 13 12 2015].
- [18] D. Shin, I. Sardellitti, Y. L. Park, O. Khatib, M. Cutkosky, "Design and control of

- a bio-inspired human-friendly robot," *The International Journal of Robotics Research*, vol. 29, no. 5, pp. 571-584, 2010.
- [19] E. Cheung, V. J. Lumelsky, "Proximity sensing in robot manipulator motion planning: system and implementation issues," *IEEE Transactions on Robotics and Automation*, vol. 5, no. 6, pp. 740-751, 1989.
- [20] T. Sugaiwa, H. Iwata, S. Sugano, "Shock absorbing skin design for human-symbiotic robot at the worst case collision," in *IEEE-RAS International Conference on Humanoid Robots (Humanoids 2008)*, Daejeon, South Korea, 1-3 December 2008.
- [21] Y. Yamada, T. Morizono, Y. Umetani, H. Takahashi, "Highly soft viscoelastic robot skin with a contact object-location-sensing capability," *IEEE Transactions on Industrial Electronics*, vol. 52, no. 4, pp. 960-968, 2005.
- [22] S. Haddadin, "Towards safe robots: approaching Asimov's 1st law," PhD thesis, RWTH Aachen, Fakultät für Elektrotechnik und Informationstechnik, Aachen, Germany, 2011.
- [23] J. Hollerbach, I. Hunter, J. Ballantyne, "A comparative analysis of actuator technologies for robotics," in *Robotics Review 2*, Cambridge, MA, USA, MIT Press, 1991, pp. 299-342.
- [24] L. De Michieli, F. Nori, A. Pini Prato, G. Sandini, "Study on humanoid robot systems: an energy approach," in *IEEE-RAS International Conference on Humanoid Robots (Humanoids 2008)*, Daejeon, Korea, 1-3 December 2008.
- [25] M. Laffranchi, N.G. Tsagarakis, F. Cannella, D.G. Caldwell, "Antagonistic and series elastic actuators: a comparative analysis on the energy consumption," in *IEEE/RSJ International Conference on Intelligent Robots and Systems (IROS 2009)*, St. Louis, MO, USA, 11-15 October 2009.
- [26] B. Vanderborght, B. Verrelst, R. Van Ham, M. Van Damme, D. Lefeber, B. M. Y. Duran, P. Beyl, "Exploiting natural dynamics to reduce energy consumption by controlling the compliance of soft actuators," *International Journal of Robotics Research*, vol. 25, no. 4, p. 343-358, 2006.
- [27] S. Haddadin, N. Mansfeld, A. Albu-Schäffer, "Rigid vs. elastic actuation: requirements & performance," in *IEEE/RSJ International Conference on*

*Intelligent Robots and Systems (IROS 2012)*, Vilamoura, Algarve, Portugal, 7-12 October 2012.

- [28] W. Wang, R. Loh, E. Gu, "Passive compliance versus active compliance in robot-based automated assembly systems," *Industrial Robot*, vol. 25, no. 1, pp. 48-57, 1998.
- [29] A. Albu-Schäffer, O. Eiberger, M. Grebenstein, S. Haddadin, C. Ott, T. Wimböck, "Soft robotics: From torque feedback controlled lightweight robots to intrinsically compliant systems," *IEEE Robotics and Automation Magazine* 15, 20-30, 2008, vol. 15, no. 3, pp. 20-30, 2008.
- [30] O. Khatib, B. Roth, "New robot mechanisms for new robot capabilities," in *IEEE/RSJ International Conference on Intelligent Robots and Systems (IROS 1991)*, Osaka, Japan, 3-5 November 1991.
- [31] A. Bicchi, J. K. Salisbury, D. Brock, "Contact sensing from force measurements," *The International Journal of Robotics Research*, vol. 12, no. 3, pp. 249-262, 1993.
- [32] L. Zollo, B. Siciliano, C. Laschi, G. Teti, P. Dario, "An experimental study on compliance control for a redundant personal robot arm," *Robotics and Autonomous Systems*, vol. 44, no. 2, pp. 101-129, 2003.
- [33] A. Albu-Schäffer, S. Haddadin, Ch. Ott, A. Stemmer, T. Wimböck, G. Hirzinger, "The DLR lightweight robot: design and control concepts for robots in human environments," *Industrial Robot: An International Journal*, vol. 34, no. 5, pp. 376-385, 2007.
- [34] D.E. Whitney, J.L. Nevins, "What is the remote centre compliance and what can it do?," in *International Symposium and Exposition on Industrial Robots (ISIR 1979)*, Washington, DC, USA, 13-15 March 1979.
- [35] A. Bicchi, G. Tonietti, "Fast and soft arm tactics: Dealing with the safety-performance trade-off in robot arms design and control," *IEEE Robotics and Automation Magazine*, vol. 11, no. 2, p. 22-33, 2004.
- [36] R. Van Ham, T.G. Sugar, B. Vanderborght, K.W. Hollander, D. Lefeber, "Compliant actuator designs: Review of actuators with passive adjustable compliance/controllable stiffness for robotic applications," *IEEE Robotics & Automation Magazine*, vol. 16, no. 3, pp. 81-94, 2009.

- [37] K. W. Hollander, R. Ilg, T. G. Sugar, D. Herring, "An efficient robotic tendon for gait assistance," *Journal of Biomechanical Engineering*, vol. 128, no. 5, pp. 788-791, 2006.
- [38] S. K. Au, J. Weber, H. Herr, "Powered ankle-foot prosthesis improves walking metabolic economy," *IEEE Transactions on Robotics*, vol. 25, no. 1, pp. 51-66, 2009.
- [39] T. Morita, S. Sugano, "Design and development of a new robot joint using a mechanical impedance adjuster," in *IEEE International Conference on Robotics and Automation (ICRA 1995)*, Nagoya, Japan, 21-27 May 1995.
- [40] K. Hollander, T. Sugar, D. Herring, "Adjustable robotic tendon using a "jack spring"," in *International Conference on Rehabilitation Robotics (ICORR 2005)*, Chicago, IL, USA, 28 June-1 July 2005.
- [41] R. Van Ham, M. Van Damme, B. Verrelst, B. Vanderborght, D. Lefeber, "MACCEPA, the mechanically adjustable compliance and controllable equilibrium position actuator: A 3DOF joint with 2 independent compliances," *International Applied Mechanics*, vol. 43, no. 4, pp. 467-474, 2007.
- [42] S. Wolf, G. Hirzinger, "A new variable stiffness design: Matching requirements of the next robot generation," in *IEEE International Conference on Robotics and Automation (ICRA 2008)*, Pasadena, CA, USA, 19-23 May 2008.
- [43] B. Vanderborght, A. Albu-Schaeffer, A. Bicchi, E. Burdet, D.G. Caldwell, R. Carloni, M. Catalano, O. Eiberger, W. Friedl, G. Ganesh, M. Garabini, M. Grebenstein, G. Grioli, S. Haddadin, H. Hoppner, A. Jafari, M. Laffranchi, D. Lefeber, F. Petit, et al., "Variable impedance actuators: A review," *Robotics and Autonomous Systems*, vol. 61, no. 12, pp. 1601-1614, 2013.
- [44] B. Vanderborght, R. Van Ham, D. Lefeber, T. G. Sugar, K. W. Hollander, "Comparison of mechanical design and energy consumption of adaptable, passive-compliant actuators," *The International Journal of Robotics Research*, vol. 28, no. 1, pp. 90-103, 2009.
- [45] D. P. Popovic, M. Popovic, M. Jankovic, *Biomedicinska merenja i instrumentacija* (in Serbian), Beograd: Akademska misao, 2010.
- [46] M. Catalano, G. Grioli, M. Garabini, F. Bonomo, M. Mancini, N. Tsagarakis, A.

- Bicchi, "VSA-CubeBot: a modular variable stiffness platform for multiple degrees of freedom robots," in *IEEE International Conference on Robotics and Automation (ICRA 2011)*, Shanghai, China, 9-13 May 2011.
- [47] G. Grioli, S. Wolf, M. Garabini, M. G. Catalano, E. Burdet, D. G. Caldwell, R. Carloni, W. Friedl, M. Grebenstein, M. Laffranchi, D. Lefeber, S. Stramigioli, N. G. Tsagarakis, V. M. Damme, B. Vanderborght, A. Albu-Schaeffer, A. Bicchi, "Variable stiffness actuators: the user's point of view," *International Journal of Robotics Research*, vol. 34, no. 6, pp. 727-743, 2015.
- [48] T. Fukuda, R. Michelini, V. Potkonjak, S. Tzafestas, K. Valavanis, M. Vukobratovic, "How far away is "artificial man" - are we ready to take the first step...," *IEEE Robotics and Automation Magazine*, March 2001, pp. 66-73, 2001, vol. 8, no. 1, pp. 66-73, 2001.
- [49] Y. Sakagami, R. Watanabe, C. Aoyama, S. Matsunaga, N. Higaki, K. Fujimura, "The intelligent ASIMO: system overview and integration," in *IEEE/RSJ International Conference on Intelligent Robots and Systems (IROS 2002)*, Lausanne, Switzerland, 30 September - 4 October 2002.
- [50] D. Lee, S. J. Yi, S. McGill, Y. Zhang, S. Behnke, M. Missura, H. Schulz, D. Hong, J. Han, M. Hopkins, "RoboCup 2011 Humanoid League Winners," in *RoboCup 2011: Robot Soccer World Cup XV*, Springer Berlin Heidelberg, 2012, pp. 37-50.
- [51] Dennis Hong, "CHARLI Robot Gangnam Style," Youtube, [Online]. Available: <https://www.youtube.com/watch?v=kmeJvkN4ntI>. [Accessed 15 12 2015].
- [52] O. Holland, R. Knight,, "The anthropomimetic principle," in *The Symposium on Biologically Inspired Robotics - Adaptation in Artificial and Biological Systems (AISB 06)*, Bristol, England, 3-4 April 2006.
- [53] M. Jäntschi, S. Wittmeier, A. Knoll, "Distributed control for an anthropomimetic robot," in *IEEE/RSJ International Conference on Intelligent Robots and Systems (IROS 2010)*, Taipei, Taiwan, China, 18-22 October 2010.
- [54] "Jouhou System Kougaku Laboratory - JSK," University of Tokyo, [Online]. Available: <http://www.jsk.t.u-tokyo.ac.jp/>. [Accessed 16 12 2015].
- [55] A. Diamond, R. Knight, D. Devereux, O. Holland, "Anthropomimetic robots: concept, construction and modelling," *International Journal of Advanced Robotic*

*Systems*, vol. 9, no. 209, pp. 1-14, 2012.

- [56] V. Potkonjak, B. Svetozarevic, K. Jovanovic, O. Holland, "The puller-follower control of compliant and noncompliant antagonistic tendon drives in robotic system," *International Journal of Advanced Robotics Systems*, vol. 8, no. 5, pp. 143-155, 2012.
- [57] M. Inaba, I. Mizuuchi, R. Tajima, T. Yoshikai, D. Sato, K. Nagashima, H. Inoue, "Building Spined Muscle-Tendon Humanoid," in *Robotics Research*, Springer Berlin Heidelberg, 2003, pp. 113-127.
- [58] I. Mizuuchi, T. Yoshikai, Y. Sodeyama, Y. Nakanishi, A. Miyadera, T. Yamamoto, T. Niemela, M. Hayashi, J. Urata, Y. Namiki, T. Nishino, M. Inaba, "Development of musculoskeletal humanoid Kotaro," in *IEEE International Conference on Robotics and Automation (ICRA 2006)*, Orlando, FL, USA, 15-19 May 2006.
- [59] I. Mizuuchi, Y. Nakanishi, Y. Sodeyama, Y. Namiki, T. Nishino, N. Muramatsu, J. Urata, K. Hongo, T. Yoshikai, M. Inaba, "An advanced musculoskeletal humanoid Kojiro," in *IEEE-RAS International Conference on Humanoid Robots (Humanoids 2007)*, Pittsburgh, PA, USA, 29 November-1 December 2007.
- [60] Y. Nakanishi, T. Izawa, M. Osada, N. Ito, S. Ohta, J. Urata, M. Inaba, "Development of musculoskeletal humanoid Kenzoh with mechanical compliance changeable tendons by nonlinear spring unit," in *IEEE International Conference on Robotics and Biomimetics (ROBIO 2011)*, Karon Beach, Phuket, Thailand, 7-11 December 2011.
- [61] Y. Asano, H. Miyoguchi, T. Kozuki, Y. Motegi, M. Osada, J. Urata, Y. Nakanishi, K. Okada, M. Inaba, "Lower thigh design of detailed musculoskeletal humanoid – Kenshiro," in *IEEE-RSJ International Conference on Intelligent Robots and Systems (IROS 2012)*, Vilamoura, Algarve, Portugal, 7-12 Oct. 2012.
- [62] Y. Nakanishi, S. Ohta, T. Shirai, Y. Asano, T. Kozuki, Y. Kakehashi, H. Mizoguchi, T. Kurotobi, Y. Motegi, K. Sasabuchi, J. Urata, K. Okada, I. Mizuuchi, M. Inaba, "Design approach of biologically-inspired musculoskeletal humanoids," *International Journal of Advanced Robotics Systems*, vol. 10, no. 216, pp. 1-13, 2013.

- [63] H. G. Marques, R. Newcombe, O. Holland, "Controlling an anthropomorphic robot: a preliminary investigation," in *Advances in Artificial Life (ECAL 2007)*, Lisbon, Portugal, 10-14 September 2007.
- [64] P. L. Gribble, L. I. Mullin, N. Cothros, A. Matter, "Role of cocontraction in arm movement accuracy," *Journal of Neurophysiology*, vol. 89, no. 5, pp. 2396-2405, 2003.
- [65] N. Tsujiuchi, T. Koizumi, S. Nishino, H. Komatsubara, T. Kudawara, M. Hirano, "Development of pneumatic robot hand and construction of master-slave system," *Journal of System Design and Dynamics*, vol. 2, no. 6, pp. 1306-1315, 2008.
- [66] V. Potkonjak, "Distributed positioning for redundant robotic systems," *Robotica*, vol. 8, no. 1, pp. 61-67, 1990.
- [67] V. Potkonjak, S. Tzafestas, D. Kostic, G. Djordjevic., "Human-like behavior of robot arms: general considerations and the handwriting task, Part I: mathematical description of human-like motion: distributed positioning and virtual fatigue," *Robotics and Computer-Integrated Manufacturing*, vol. 17, no. 4, p. 305–315, 2001.
- [68] X. Xiong, F. Wörgötter, P. Manoonpong , "Virtual agonist-antagonist mechanisms produce biological muscle-like functions: An application for robot joint control," *Industrial Robot: An International Journal*, vol. 41, no. 4, pp. 340 - 346, 2014.
- [69] S. Klug, T. Lens, O. Von Stryk, B. Mohl, A. Karguth, "Biologically inspired robot manipulator for new applications in automation engineering," in *Robotik*, Munich, Germany, 11-12 Jun 2008.
- [70] S. C. Jacobsen, H. Ko, E. K. Iversen, C. C. Davis, "Control strategies for tendon-driven manipulators," *IEEE Control Systems Magazine*, vol. 10, no. 2, pp. 23-28, 1990.
- [71] P. C. Chou, B. Hannaford, "Study of human forearm posture maintenance with a physiologically based robotic arm and spinal level neural controller," *Biological Cybernetics*, vol. 76, no. 4, pp. 285-298, 1997.
- [72] A. M. Gordon, A. F. Huxley, F. J. Julian, "The variation in isometric tension with sarcomere length in vertebrate muscle fibers," *The Journal of Physiology*, vol. 84, no. 1, pp. 170-192, 1966.

- [73] A. V. Hill, "The heat of shortening and dynamic constraints of muscle," *Royal Society of London - Proceedings B Biological Sciences*, vol. 126, no. 843, pp. 136-195, 1938.
- [74] K. Koganezawa, Y. Watanabe, N. Shimizu, "Stiffness and angle control of antagonistically driven joint," *Advanced Robotics*, vol. 12, no. 7-8, pp. 771-789, 1997.
- [75] J. Yamaguchi, A. Takanishi, "Design of biped walking robots having antagonistic driven joints using nonlinear spring mechanism," in *IEEE/RSJ International Conference on Intelligent Robots and Systems (IROS 1997)*, Grenoble, France, 7-11 September 1997.
- [76] C. English, D. Russell, "Implementation of variable joint stiffness through antagonistic actuation using rolamite springs," *Mechanism and Machine Theory*, vol. 34, no. 1, pp. 27-40, 1999.
- [77] S. A. Migliore, E. A. Brown, S. P. DeWeerth, "Biologically inspired joint stiffness control," in *IEEE International Conference on Robotics and Automation (ICRA 2005)*, Barcelona, Spain, 18-22 April 2005.
- [78] K. Koganezawa, "Mechanical stiffness control for antagonistically driven joints," in *IEEE/RSJ International Conference on Intelligent Robots and Systems (IROS 2005)*, Edmonton, Canada, 2-6 August 2005.
- [79] K. Koganezawa, T. Nakazawa, T. Inaba, "Antagonistic control of multi-DOF joint by using the actuator with non-linear elasticity," in *IEEE International Conference on Robotics and Automation (ICRA 2006)*, Orlando, FL, USA, 15-19 May 2006.
- [80] J. Hurst, J. Chestnutt, A. Rizzi, "An actuator with physically variable stiffness for highly dynamic legged locomotion," in *IEEE International Conference on Robotics and Automation (ICRA 2004)*, New Orleans, LA, USA, 26 April-1 May 2004.
- [81] G. Tonietti, R. Schiavi, A. Bicchi, "Design and control of a variable stiffness actuator for safe and fast physical human/robot interaction," in *IEEE International Conference on Robotics and Automation (ICRA 2005)*, Barcelona, Spain, 18-22 April 2005.
- [82] R. Schiavi, G. Grioli, S. Sen, A. Bicchi, "VSA-II: a novel prototype of variable

- stiffness actuator for safe and performing robots interacting with humans," in *IEEE International Conference on Robotics and Automation (ICRA 2008)*, Pasadena, CA, USA, 19-23 May 2008.
- [83] M. Grebenstein, A. Albu-Schäffer, T. Bahls, M. Chalon, O. Eiberger, W. Friedl, R. Gruber, S. Haddadin, U. Hagn, R. Haslinger, H. Höppner, S. Jörg, M. Nickl, A. Nothhelfer, F. Petit, J. Reill, N. Seitz, T. Wimböck, S. Wolf, T. Wüsthoff, G. Hirzinger, "The DLR hand arm system," in *IEEE International Conference on Robotics and Automation (ICRA 2011)*, Shanghai, China, 9-13 May 2011.
- [84] M. Grebenstein, M. Chalon, G. Hirzinger, R. Siegwart, "Antagonistically driven finger design for the anthropomorphic DLR hand arm system," in *IEEE-RAS International Conference on Humanoid Robots (Humanoids 2010)*, Nashville, TN, USA, 6-8 December 2010.
- [85] W. Friedl, M. Chalon, J. Reinecke, M. Grebenstein, "FAS A flexible Antagonistic spring element for a high performance over actuated hand," in *IEEE/RSJ International Conference on Intelligent Robots and Systems (IROS 2011)*, San Francisco, CA, USA, 25-30 September 2011.
- [86] F. Petit, M. Chalon, W. Friedl, M. Grebenstein, A. Albu-Schäffer, G. Hirzinger, "Bidirectional antagonistic variable stiffness actuation: analysis, design & implementation," in *IEEE International Conference on Robotics and Automation (ICRA 2010)*, Anchorage, Alaska, USA, 3-8 May 2010.
- [87] "QB MOVE The lowcost VSA (Variable Stiffness Actuator)," qb robotics, [Online]. Available: <http://www.qbrobotics.com/>. [Accessed 7 December 2015].
- [88] R. Filippini, S. Sen, A. Bicchi, "Toward soft robots you can depend on: A study of antagonistic actuation," *IEEE Robotics & Automation Magazine*, vol. 15, no. 3, pp. 31-41, 2008.
- [89] S. C. Jacobsen, E. K. Iversen, D. Knutti, R. Johnson, K. Biggers, "Design of the Utah/M.I.T. dextrous hand," in *IEEE International Conference on Robotics and Automation (ICRA 1986)*, San Francisco, CA, USA, 7-10 April 1986.
- [90] E. Cattin, S. Roccella, N. Vitiello, I. Sardellitti, P. Artemiadis, P. Vacalebri, F. Vecchi, M. Chiarrar Carroza, K. Kyriakopoulos, P. Dario, "Design and development of a novel robotic platform for neuro-robotics applications: the

- NEURobotics ARM (NEURARM)," *Advanced Robotics*, vol. 22, no. 1, p. 3–37, 2008.
- [91] B. Tondu, P. Lopez, "Modeling and control of McKibben artificial muscle robot actuators," *IEEE Control Systems Magazine*, vol. 20, no. 2, pp. 15-38, 2000.
- [92] F. Daerden, D. Lefeber, "Pneumatic artificial muscles: actuators for robotics and automation," *European Journal of Mechanical and Environmental Engineering*, vol. 47, no. 1, pp. 11-21, 2002.
- [93] G. C. Klute, J. M. Czerniecki, B. Hannaford, "McKibben artificial muscles: pneumatic actuators with biomechanical intelligence," in *IEEE/ASME International Conference on Advanced Intelligent Mechatronics*, Atlanta, GA, USA, 19-23 September 1999.
- [94] J. Yamaguchi, D. Nishino, A. Takanishi, "Realization of dynamic biped walking varying joint stiffness using antagonistic driven joints," in *IEEE International Conference on Robotics and Automation (ICRA 1998)*, Leuven, Belgium, 16-20 May 1998.
- [95] B. Tondu, S. Ippolito, J. Guiochet, A. Daidie , "A seven-degrees-of-freedom robotarm driven by pneumatic artificial muscles for humanoid robots," *The International Journal of Robotics Research*, vol. 24, no. 4, pp. 257-274, 2005.
- [96] I. Boblan, J. Maschuw, D. Engelhardt, A. Schulz, H. Schwenk, R. Bannasch, I. Rechenberg, "A human-like robot hand and arm with fluidic muscles: modelling of a muscle driven joint with an antagonistic setup," in *International Symposium on Adaptive Motion in Animals and Machines*, Ilmenau, Germany, 25-30 September 2005.
- [97] N. G. Tsagarakis, D. G. Caldwell , "Development and control of a 'soft-actuated' exoskeleton for use in physiotherapy and training," *Autonomous Robots*, vol. 15, no. 1, pp. 21-33, 2003.
- [98] B. Verrelst, R. Van Ham, B. Vanderborght, F. Daerden, D. Lefeber, "The pneumatic biped "LUCY" actuated with pleated pneumatic artificial muscles," *Autonomous Robots*, vol. 18, no. 2, pp. 201-213, 2005.
- [99] F. Röthling, R. Haschke, J. Steil, H. Ritter, "Platform portable anthropomorphic grasping with the Bielefeld 20-DOF Shadow and 9-DOF TUM Hand," in

*IEEE/RSJ International Conference on Intelligent Robots and Systems (IROS 2007)*, San Diego, CA, USA, 29 October-2 November 2007.

- [100] B. Vanderborght, R. Van Ham, B. Verrelst, M. Van Damme, D. Lefeber, "Overview of the Lucy project: dynamic stabilization of a biped powered by pneumatic artificial muscles," *Advanced Robotics*, vol. 22, no. 10, pp. 1027-1051, 2008.
- [101] Y. Honda, F. Miyazaki, A. Nishikawa, "Angle control of pneumatically-driven musculoskeletal model using antagonistic muscle ratio and antagonistic muscle activity," in *IEEE International Conference on Robotics and Biomimetics (ROBIO 2010)*, Tianjin, China, 14-18 Decembar 2010.
- [102] K. Hosoda, T. Takuma, A. Nakamoto, S. Hayashi, "Biped robot design powered by antagonistic pneumatic actuators for multi-modal locomotion," *Robotics and Autonomous Systems*, vol. 56, no. 1, p. 46-53, 2008.
- [103] C. P. Chou, B. Hannaford, "Static and dynamic characteristics of McKibben pneumatic artificial muscles," in *IEEE International Conference on Robotics and Automation (ICRA 1994)*, San Diego, CA, USA, 8-13 May 1994.
- [104] K. Jovanovic, "Simulation model development of the humanoid robot with antagonistic drives in contact tasks (in Serbian)," Master thesis, School of Electrical Engineering, University of Belgrade, Belgrade, Serbia, 2010.
- [105] W. van Dijk, H. Van der Kooij,, "XPED2: a passive exoskeleton with artificial tendons," *IEEE Robotics & Automation Magazine*, vol. 21, no. 4, pp. 56-61, 2014.
- [106] V. Potkonjak, K. Jovanovic, B. Svetozarevic, O. Holland, D. Mikicic, "Modelling and control of a compliantly engineered anthropomimetic robot in contact tasks," in *ASME'2011 – 35th Mechanisms and Robotics Conference*, Washington, DC, USA, 28-31 August 2011.
- [107] N. Bascarevic, K. Jovanovic, P. Milosavljevic, V. Potkonjak, O. Holland, "Tip-over stability examination of a compliant anthropomimetic mobile robot," in *IEEE International Conference on Control Applications (CCA 2012)*, Dubrovnik, Croatia, 3-5 October 2012.
- [108] J. J. Uicker, "Dynamic force analysis of spatial linkages," *Journal of Applied Mechanics*, vol. 34, no. 2, pp. 418-424, 1967.

- [109] M. Vukobratovic, V. Potkonjak, "Contribution to computer construction of active chain models via Lagrangian form," *Journal of Applied Mechanics*, vol. 46, no. 1, pp. 181-185, 1979.
- [110] J. M. Hollerbach, "A recursive formulation of Lagrangian manipulator dynamics," *IEEE Transactions on Systems, Man and Cybernetics*, vol. 10, no. 11, pp. 730-736, 1980.
- [111] S. Dubowsky, E. Papadopoulos, "The kinematics, dynamics, and control of free-floating and free-flying space robotic systems," *IEEE Transactions on Robotics and Automation*, vol. 9, no. 5, p. 531-543, 1993.
- [112] L. Sentis, O. Khatib, "Control of free-floating humanoid robots through task prioritization," in *IEEE International Conference on Robotics and Automation (ICRA 2005)*, Barcelona, Spain, 18-22 April 2005.
- [113] R. Featherstone, "Chapter 6: Forward Dynamics—Inertia Matrix Methods," in *Rigid Body Dynamics Algorithms*, Boston, Springer US, 2008, pp. 101-118.
- [114] R. Featherstone, "Chapter 7: Forward Dynamics—Propagation Methods," in *Rigid Body Dynamics Algorithms*, Boston, Springer US, 2008, pp. 119-139.
- [115] W. Khalil, "Chapter 1: Dynamic Modeling of Robots Using Newton-Euler Formulation," in *Informatics in Control, Automation and Robotics*, Publisher Springer Berlin Heidelberg, 2011, pp. 3-20.
- [116] T. R. Kane, *Dynamics*, New York: Holt, Rinehart & Winston, 1968.
- [117] R. Huston, F. Kelly, "The development of equations of motion of single arm robots," *IEEE Transactions on Systems, Man, and Cybernetics*, vol. 12, no. 3, pp. 259-266, 1982.
- [118] V. Potkonjak, M. Vukobratovic, "Two new methods for computer forming of dynamic equations of active mechanisms," *Journal of Mechanisms and Machine Theory*, vol. 14, no. 3, pp. 189-200, 1979.
- [119] M. Vukobratovic, V. Potkonjak, "Chapter 2: Computer-Aided Methods for Setting and Solving Mathematical Models of Active Mechanisms in Robotics," in *Dynamics of Manipulation Robots: Theory and Application*, Heidelberg, Springer-Verlag Berlin, 1982, pp. 26-149.

- [120] M. Vukobratovic, N. Kircanski, "Computer-assisted generation of robot dynamic models in an analytical form," *Acta Applicandae Mathematicae*, vol. 3, no. 1, pp. 49-70, 1985.
- [121] M. Vukobratovic, V. Potkonjak, "Chapter 20: Robot Dynamics," in *Mechanical Systems Design Handbook: Modeling, Measurement, and Control*, CRC Press, 2001, pp. 487-522.
- [122] V. Potkonjak, S. Tzafestas, M. Vukobratovic, M. Petrovic, M. Jovanovic, "Human-and-humanoid postures under external disturbances: modeling, simulation, and robustness, part 1: modeling," *Journal of Intelligent & Robotic Systems*, vol. 63, no. 2, pp. 191-210, 2011.
- [123] M. Vukobratovic, Y. Stepanenko, "Mathematical models of general anthropomorphic systems," *Mathematical Biosciences*, vol. 17, no. 3, pp. 191-242, 1973.
- [124] E. Drumwright, J. Hsu, N. Koenig, D. Shell, "Extending Open Dynamics Engine for Robotics Simulation," in *Simulation, Modeling, and Programming for Autonomous Robots*, Springer Berlin Heidelberg, 2010, pp. 38-50.
- [125] A. M. Orner, Y. Ogura, H. Kondo, H. O. Lim, A. Takanishi, "Dynamic-based simulation for humanoid robot walking using walking support system," in *International Conference on Informatics in Control, Automation and Robotics (ICINCO 2008)*, Funchal, Portugal, 11-15 May 2008.
- [126] V. Tikhanoff, A. Cangelosi, P. Fitzpatrick, G. Metta, L. Natale, F. Nori, "An open-source simulator for cognitive robotics research: the prototype of the iCub humanoid robot simulator," in *Workshop on Performance Metrics for Intelligent Systems*, Washington, D.C., USA, 19-21 August 2008.
- [127] S. Wittmeier, M. Jäntsch, K. Dalamagkidis, A. Knoll, "Physics-based modeling of an anthropomimetic robot," in *IEEE-RSJ International Conference on Intelligent Robots and Systems (IROS 2011)*, San Francisco, CA, USA, 25-30 September 2011.
- [128] A. Diamond, "Bio-inspired approaches to the control and modelling of an anthropomimetic robot," PhD thesis, University of Sussex, Sussex, United Kingdom, 2013.

- [129] "OpenSim Community," Stanford University, [Online]. Available: <http://opensim.stanford.edu/work/index.html>. [Accessed 5 December 2015].
- [130] A. Seth, M. Sherman, J. Reinbolt, S. Delp, "OpenSim: A musculoskeletal modeling and simulation framework for in silico investigations and exchange," in *IUTAM Symposium on Human Body Dynamics: From Multibody Systems to Biomechanics*, Waterloo, ON, Canada, 5-8 Jun 2011.
- [131] J. Rasmussen, "AnyBody: CAE for the human body," in *ANSYS Conference & 25th CADFEM Users' Meeting*, Dresden, Germany, 21-23 November 2007.
- [132] G. Palli, C. Melchiorri, T. Wimböck, M. Grebenstein, G. Hirzinger, "Feedback linearization and simultaneous stiffness-position control of robots with antagonistic actuated joints," in *IEEE International Conference on Robotics and Automation (ICRA 2007)*, Rome, Italy, 10-14 April 2007.
- [133] V. Potkonjak, B. Svetozarevic, K. Jovanovic, O. Holland, "Control of compliant anthropomorphic robot joint," in *International Conference of Numerical Analysis and Applied Mathematics - ICNAAM 2010 (Symposium on Computational Geometric Methods in Multibody System Dynamics)*, Rhodes, Greece, 19-25 September 2010.
- [134] K. Radkhah, T. Lens, O. von Stryk, "Detailed dynamics modeling of BioBiped's monoarticular and biarticular tendon-driven actuation system," in *IEEE-RSJ International Conference on Intelligent Robots and Systems (IROS 2012)*, Vilamoura, Algarve, Portugal, 7-12 October 2012.
- [135] K. Bouyarmane, A. Kheddar, "On the dynamics modeling of free-floating-base articulated mechanisms and applications to humanoid whole-body dynamics and control," in *IEEE-RAS International Conference on Humanoid Robots (Humanoids 2012)*, Osaka, Japan, 29 November-1 December 2012.
- [136] T. Sugaiwa, G. Fujii, H. Iwata, S. Sugano, "A methodology for setting grasping force for picking up an object with unknown weight, friction, and stiffness," in *IEEE-RAS International Conference on Humanoid Robots (Humanoids 2010)*, Nashville, TN, USA, 6-8 December 2010.
- [137] J. Van Vliet, I. Sharf, O. Ma, "Experimental validation of contact dynamics simulation of constrained robotic tasks," *The International Journal of Robotics*

*Research*, vol. 19, no. 12, pp. 1203-1217, 2000.

- [138] A. De Luca, C. Manes, "Modeling of robots in contact with a dynamic Environment," *IEEE Transactions on Robotics and Automation*, vol. 10, no. 4, pp. 542-548, 1994.
- [139] S. Lee, C. Cho, M. Choi, M. Kim, J. Kim, "A dynamic model of humanoid robots using the analytical method," *International Journal of Precision Engineering and Manufacturing*, vol. 11, no. 1, pp. 67-75, 2010.
- [140] T. Wimböck, C. Ott, G. Hirzinger, "Immersion and invariance control for an antagonistic joint with nonlinear mechanical stiffness," in *IEEE Conference on Decision and Control (CDC 2010)*, Atlanta, GA, USA, 15-17 December 2010.
- [141] V. Potkonjak, M. Vukobratovic, K. Babkovic, B. Borovac, "Simulation model of general human and humanoid motion," *Multibody System Dynamics*, vol. 17, no. 1, pp. 71-96, 2007.
- [142] M. Vukobratovic, V. Potkonjak, V. Matijevic, "Chapter 2: Free Motion of a Rigid-Body Robot Arm," in *Dynamics of Robots with Contact Tasks*, Dordrecht, Kluwer Academic Publishers, 2003, pp. 11-48.
- [143] A. Diamond, O. Holland, H. Margues, "The role of the predicted present in artificial and natural cognitive systems," in *Second Annual Meeting of the BICA Society - Biologically Inspired Cognitive Architectures 2011*, Washington, D.C., USA, 5-6 November 2011.
- [144] M. Vukobratovic, V. Potkonjak, V. Matijevic, "Chapter 3: Rigid-Body Contact of a Robot with its Environment," in *Dynamics of Robots with Contact Tasks*, Dordrecht, Kluwer Academic Publishers, 2003, pp. 49-78.
- [145] T. Yoshikawa, T. Sugie, M. Tanaka, "Dynamic hybrid position/force control of robot manipulators-controller design and experiment," *IEEE Journal of Robotics and Automation*, vol. 4, no. 6, pp. 699-705, 1988.
- [146] D. Devereux, B. Mitra, O. Holland, A. Diamond, "Using the Microsoft Kinect to model the environment of an anthropomimetic robot," in *IASTED International Conference on Robotics (Robo 2011)*, Pittsburgh, PA, USA, 7-9 November 2011.
- [147] M. Vukobratovic, D. Juricic, "Contribution to the synthesis of biped gait," *IEEE*

*Transactions on Biomedical Engineering*, vol. 16, no. 1, pp. 1-6, 1969.

- [148] M. Vukobratovic, B. Borovac, V. Potkonjak, "ZMP: a review of some basic misunderstandings," *International Journal of Humanoid Robotics*, vol. 3, no. 2, p. 153–175, 2006.
- [149] Y. Li, Z. Wu, H. Zhong, "Control and simulation on the waist mechanism of a humanoid robot based on dynamic model," in *Chinese Control and Decision Conference (CCDC 2008)*, Yantai, China, 2-4 July 2008.
- [150] F. Gravez, O. Bruneau, F. Ben Ouezdou, "Analytical and automatic modeling of digital humanoids," *International Journal of Humanoid Robotics*, vol. 2, no. 3, p. 337–359, 2005.
- [151] "Maxon motors catalog," Maxon motors, [Online]. Available: <http://www.maxonmotor.com/maxon/view/catalog/>. [Accessed 27 November 2015].
- [152] Y. Li, D. Tan, Z. Wu, H. Zhong, "Dynamic stability analyses based on ZMP of a wheel-based humanoid robot," in *IEEE International Conference on Robotics and Biomimetics (ROBIO 2006)*, Kunming, China, 17-20 December 2006.
- [153] J. Wang, Y. Li, C. Qiu, "Analysis of dynamic stability constraints for a mobile humanoid robot," in *IEEE International Conference on Robotics and Biomimetics (ROBIO 08)*, Bangkok, Thailand, 22-25 February 2009.
- [154] V. Potkonjak, B. Svetozarevic, K. Jovanovic, O. Holland, "Biologically-inspired control of a compliant anthropomimetic robot," in *The 15th IASTED International Conference on Robotics and Applications*, Cambridge, Massachusetts, USA, 1-3 November 2010.
- [155] M. Fuchs, C. Borst, P. Giordano, A. Baumann, E. Kraemer, J. Langwald, R. Gruber, N. Seitz, G. Plank, K. Kunze, R. Burger, F. Schmidt, T. Wimböck, Gerd Hirzinger, "Rollin' Justin - Design considerations and realization of a mobile platform for a humanoid upper body," in *IEEE International Conference on Robotics and Automation (ICRA 2009)*, Kobe, Japan, 12-17 May 2009.
- [156] C. J. De Luca, B. Mambrito, "Voluntary control of motor units in human antagonist muscles: coactivation and reciprocal activation," *Journal of Neurophysiology*, vol. 58, no. 3, pp. 525-542, 1987.

- [157] R. Bortoletto, M. Sartori, F. He, E. Pagello, "Modeling and simulating compliant movements in a musculoskeletal bipedal robot," in *Lecture Notes in Computer Science: Simulation, Modeling, and Programming for Autonomous Robots*, vol. 7628, Tsukuba, Japan, Springer Berlin Heidelberg, 2012, pp. 237-250.
- [158] S. Oh, V. Salvucci, Y. Hori, "Development of simplified statics of robot manipulator and optimized muscle torque distribution based on the statics," in *IEEE American Control Conference (ACC 2011)*, San Francisco, CA, USA, 2011.
- [159] V. Potkonjak, B. Svetozarevic, K. Jovanovic, O. Holland, "The puller-follower control of compliant and noncompliant antagonistic tendon drives in robotic system," *International Journal of Advanced Robotics Systems*, vol. 8, no. 5, pp. 143-155, 2011.
- [160] B. Svetozarevic, K. Jovanovic, "Control of compliant anthropomorphic robot joint," *Serbian Journal of Electrical Engineering*, vol. 8, no. 1, pp. 85-93, 2011.
- [161] V. Potkonjak, K. Jovanovic, P. Milosavljevic, N. Bascarevic, O. Holland, "The puller-follower control concept for the multi-joint robot with antagonistically coupled compliant drives," in *The 2nd IASTED International Conference on Robotics (Robo 2011)*, Pittsburgh, USA, 7-9 November 2011.
- [162] S. C. Jacobsen, H. Ko, E. K. Iversen, C. C. Davis, "Antagonistic control of a tendon driven manipulator," in *IEEE International Conference on Robotics and Automation (ICRA 1989)*, Scottsdale, AZ, USA, 14-19 May 1989.
- [163] M. Chalon, W. Friedl, J. Reinecke, T. Wimböck, A. Albu-Schäffer, "Impedance control of a non-linearly coupled tendon driven thumb," in *IEEE/RSJ International Conference on Intelligent Robots and Systems*, San Francisco, CA, USA, 25-30 September 2011.
- [164] A. Astolfi, R. Ortega, "Immersion and invariance: a new tool for stabilization and adaptive control of nonlinear systems," *IEEE Transactions on Automatic Control*, vol. 48, no. 4, pp. 590-606, 2003.
- [165] M. Chalon, B. d'Andrea-Novell, "Backstepping experimentally applied to an antagonistically driven finger with flexible tendons," in *Preprints of the 19th World Congress The International Federation of Automatic Control*, Cape Town, South Africa, 24-29 August 2014.

- [166] Y. Zhang, B. Fidan, P. Ioannou, "Backstepping control of linear time varying systems with known and unknown parameters," *IEEE Transactions on Automatic Control*, vol. 48, no. 11, pp. 1908-1925, 2003.
- [167] M. Mancini, G. Grioli, M. Catalano, M. Garabini, F. Bonomo, A. Bicchi, "Passive impedance control of a multi-DOF VSA-CubeBot manipulator," in *IEEE International Conference on Robotics and Automation (ICRA 2012)*, Saint Paul, Minnesota, USA, 14-18 May 2012.
- [168] L. Balletti, A. Rocchi, F. Belo, M. Catalano, M. Garabini, G. Grioli, A. Bicchi, "Towards variable impedance assembly: the VSA peg-in-hole," in *IEEE International Conference on Humanoid Robots (Humanoids 2012)*, Osaka, Japan, 29 November - 1 December 2012.
- [169] K. Jovanovic, P. Milosavljevic, V. Potkonjak, "Control design for pick-and-place task using robot with intrinsic compliance - QB robot," in *2nd International Conference on Electrical, Electronic and Computing Engineering - IcETRAN 2015*, Silver Lake, Serbia, 8-11 June 2015.
- [170] D.G. Caldwell, G. A. Medrano-Cerda, M. Goodwin, "Braided pneumatic muscle actuator control of a multi-jointed manipulator," in *IEEE International Conference on Systems, Man and Cybernetics*, Le Touquet, France, 17-20 Oct 1993.
- [171] D.G. Caldwell, G. A. Medrano-Cerda, M. Goodwin, "Control of pneumatic muscle actuators," *IEEE Control Systems Magazine*, vol. 15, no. 1, p. 40-48, 1995.
- [172] N. Vitiello, T. Lenzi, S. De Rossi, S. Roccella, M. Chiara Carrozza, "A sensorless torque control for antagonistic driven compliant joints," *Mechatronics*, vol. 20, no. 3, p. 355-367, 2010.
- [173] A. Bicchi, S. L. Rizzini, G. Tonietti, "Compliant design for intrinsic safety: general issues and preliminary design," in *IEEE/RSJ International Conference on Intelligent Robots and Systems (IROS 2001)*, Maui, HI, USA, 29 October - 03 November 2001.
- [174] G. Tonietti, A. Bicchi, "Adaptive simultaneous position and stiffness control for a soft robot arm," in *IEEE/RSJ International Conference on Intelligent Robots and*

*Systems (IROS 2002)*, Lausanne, Switzerland, 30 September - 4 October 2002.

- [175] T. Hesselroth, K. Sarkar, P. P. van der Smagt, K. Schulten, "Neural network control of a pneumatic robot arm," *IEEE Transactions on Systems, Man and Cybernetics*, vol. 24, no. 1, pp. 28-38, 1994.
- [176] P. Carbonell, Z. P. Jiang, D. W. Repperger, "A fuzzy backstepping controller for a pneumatic muscle actuator system," in *IEEE International Symposium on Intelligent Control (ISIC '01)*, Mexico City, Mexico, 5-7 September 2001.
- [177] S. W. Chan, J. H. Lilly, D. W. Repperger, J. E. Berlin., "Fuzzy PD+I learning control for a pneumatic muscle," in *the 12th IEEE International Conference on Fuzzy Systems (FUZZ '03)*, St Louis, MO, USA, 25-28 May 2003,.
- [178] J. H. Lilly, "Adaptive tracking for pneumatic muscle actuators in bicep and tricep configurations," *IEEE Trans. Neural Systems and Rehabilitation Engineering*, vol. 11, no. 3, pp. 333-339, 2003.
- [179] A. Hildebrandt, O. Sawodny, R. Neumann, A. Hartmann, "A flatness based design for tracking control of pneumatic muscle actuators," in *IEEE International Conference on Control, Automation, Robotics and Vision (ICARCV 2002)*, Singapore, Singapore, 2-5 December 2002.
- [180] D. Jutras, P. Bigras, "Control of an actuator made of two antagonist McKibben muscles via LMI optimization," in *IEEE International Symposium on Industrial Electronics*, Montreal, Quebec, Canada, 9-12 July 2006.
- [181] I. Sardellitti, G. Palli, N. G. Tsagarakis, D. G. Caldwell, "Antagonistically actuated compliant joint: torque and stiffness control," in *IEEE/RSJ International Conference on Intelligent Robots and Systems (IROS 2010)*, Taipei, Taiwan, 18-22 October 2010.
- [182] Y. Honda, F. Miyazaki, A. Nishikawa, "Angle control of a pneumatically driven musculoskeletal model based on coordination of agonist-antagonist muscle," *Journal of Mechanics Engineering and Automation*, vol. 2, pp. 709-719, 2012.
- [183] Y. Ariga, H. Pham, M. Uemura, H. Hirai, F. Miyazaki, "Novel equilibrium-point control of agonist-antagonist system with pneumatic artificial muscles," in *IEEE International Conference on Robotics and Automation (ICRA 2012)*, Saint Paul, Minnesota, USA, 14-18 May 2012.

- [184] M. W. Spong, "Modeling and control of elastic joint robots," *Journal of Dynamic Systems, Measurement, and Control*, vol. 109, no. 4, pp. 310-318, 1987.
- [185] A. De Luca, "Dynamic control of robots with joint elasticity," in *IEEE International Conference on Robotics and Automation (ICRA 1988)*, Philadelphia, PA, USA, 24-29 April 1988.
- [186] S. Nicosia, P. Tomei, "On the feedback linearization of robots with elastic joints," in *IEEE Conference on Decision and Control (ICDC 1988)*, Austin, TX, USA, 7-9 December 1988.
- [187] A. De Luca, P. Lucibello, "A general algorithm for dynamic feedback linearization of robots with elastic joints," in *IEEE International Conference on Robotics and Automation (ICRA 1998)*, Leuven, Belgium, 16-21 May 1998.
- [188] M. Vukobratovic, V. Matijevic, V. Potkonjak, "Control of robots with elastic joints interacting with dynamic environment," *Journal of Intelligent and Robotics Systems*, vol. 23, no. 1, p. 87-100, 1998.
- [189] A. De Luca, "Feedforward/feedback laws for the control of flexible robots," in *IEEE International Conference on Robotics and Automation (ICRA 2000)*, San Francisco, CA, USA, 24-28 April 2000.
- [190] G. Palli, C. Melchiorri, A. De Luca, "On the feedback linearization of robots with variable joint stiffness," in *IEEE International Conference on Robotics and Automation (ICRA 2008)*, Pasadena, CA, USA, 19-23 May 2008.
- [191] A. De Luca, R. Farina, P. Lucibello, "On the control of robots with visco-elastic joints," in *IEEE International Conference on Robotics and Automation (ICRA 2005)*, Barcelona, Spain, 18-22 April 2005.
- [192] K. Jovanovic, N. Miljkovic, V. Potkonjak, M. Popovic, "Electromyography signal patterns of antagonistically coupled human muscles for some typical movements," in *preparation*.
- [193] M. Tomic, C. Vassallo, C. Chevallereau, A. Rodic, V. Potkonjak, "Arm Motions of a Humanoid Inspired by Human Motion," in *New Trends in Medical and Service Robots*, Springer International Publishing, 2015, pp. 227-238.
- [194] D. Franklin, E. Burdet, R. Osu, M. Kawato, T. Milner, "Functional significance of

- stiffness in adaptation of multijoint arm movements to stable and unstable dynamics," *Experimental Brain Research*, vol. 151, no. 2, pp. 145-157, 2003.
- [195] B. Hannaford, L. Stark, "Roles of the elements of the triphasic control signal," *Experimental Neurology*, vol. 90, no. 3, p. 619 – 634, 1985.
- [196] J. Gordon, C. Ghez, "EMG patterns in antagonist muscles during isometric contraction in man: relations to response dynamics," *Experimental Brain Research*, vol. 55, no. 1, pp. 167-171, 1984.
- [197] S. Northrup, N. Sarkar, K. Kawamura, "Biologically-inspired control architecture for a humanoid robot," in *IEEE/RSJ International Conference on Intelligent Robots and Systems (IROS 2001)*, Maui, HI, USA, 29 October - 3 November 2001.
- [198] M. Komiya, K. Kawashima, K. Tadano, T. Kagawa, "Control design for antagonistic drive with pneumatic actuators," in *8th JFPS International Symposium on Fluid Power*, Okinawa, Japan, 25-28 October 2011.
- [199] H. K. Khalil, "Chapter 13: State Feedback Stabilization," in *Nonlinear Systems, 3rd Edition*, Upper Saddle River, New Jersey, USA, Prentice Hall, 2002, pp. 197-227.
- [200] D. McFarlane, K. Glover, "A loop-shaping design procedure using H infinity synthesis," *IEEE Transactions on Automatic Control*, vol. 37, no. 6, p. 759 –769, 1992.
- [201] D. Shin, X. Yeh, O. Khatib, "Variable radius pulley design methodology for pneumatic artificial muscle-based antagonistic actuation systems," in *IEEE/RSJ International Conference on Intelligent Robots and Systems (IROS 2011)*, San Francisco, CA, USA, 25-30 September 2011.
- [202] F. Flacco, A. De Luca, I. Sardellitti, N. Tsagarakis, "Robust estimation of variable stiffness in flexible joints," in *IEEE Int. Conf. on Intelligent Robots and Systems (IROS 2011)*, San Francisco, CA, USA, 25-30 September 2011.
- [203] T. Menard, G. Grioli, A. Bicchi, "A stiffness estimator for agonistic–antagonistic variable-stiffness-actuator devices," *IEEE Transactions on Robotics*, vol. 30, no. 5, pp. 1269-1278, 2014.

- [204] D. Kistemaker, A. Van Soest, M. Bobbert, "A model of open-loop control of equilibrium position and stiffness of the human elbow joint," *Biological Cybernetics*, vol. 96, no. 3, pp. 341-350, 2007.
- [205] N. Lan, P. Cargo, "Optimal control of antagonistic muscle stiffness during voluntary movements," *Biological Cybernetics*, vol. 71, no. 2, pp. 123-135, 1994.
- [206] N. Vitiello, T. Lenzi, J. McIntyre, S. Roccella, E. Cattin, "Characterization of the NEURARM bio-inspired joint position and stiffness open loop controller," in *IEEE/RAS-EMBS International Conference on Biomedical Robotics and Biomechatronics*, Scottsdale, AZ, USA, 19-22 October 2008.
- [207] P. Axelsson, A. Helmersson, M. Norrlöf, " $H_{\infty}$  controller design methods applied to one joint of a flexible industrial manipulator," in *19th World Congress of the International Federation of Automatic Control (IFAC 2014)*, Cape Town, South Africa, 24-29 August 2014.
- [208] D. C. McFarlane, K. Glover, "Robust stabilization of normalized coprime factor plant descriptions with  $H_{\infty}$  bounded uncertainty," *IEEE Transactions on Automatic Control*, , vol. 34, no. 8, pp. 821-830, 1989.
- [209] S. Skogestad, I. Postlethwaite, "Chapter 8: robust stability and performance analysis," in *Multivariable Feedback Control, 2nd edition*, Chichester, John Wiley & Sons, 2005, pp. 309-370.
- [210] S. Ikemoto, Y. Kimoto, K. Hosoda, "Shoulder complex linkage mechanism for humanlike musculoskeletal robot arms," *Bioinspiration & Biomimetics*, vol. 10, no. 6, pp. 1-13, 2015.
- [211] C. L. Lynch, D. Sayenko, M. R. Popovic, "Co-contraction of antagonist muscles during knee extension against gravity: insights for functional electrical stimulation control design," in *International Conference on the IEEE Engineering in Medicine and Biology Society*, San Diego, CA, USA, 28 August- 1 September 2012.
- [212] D. W. Robinson, "Design and analysis of series elasticity in closed-loop actuator force control," PhD thesis, MIT, Department of Mechanical Engineering, Boston, USA, 1994.
- [213] P. Milosavljevic, K. Jovanovic, N. Bascarevic, V. Potkonjak, O. Holland,

- "Heuristic machine-learning approach to the control of an anthropomimetic robot arm," in *10th IFAC Symposium on Robot Control (SYROCO 2012)*, Dubrovnik, Croatia, 5-7 September 2012.
- [214] V. Potkonjak, N. Bascarevic, P. Milosavljevic, K. Jovanovic, O. Holland, "Experience-based fuzzy control of an anthropomimetic robot," in *International Joint Conference on Computational Intelligence (CFP IJCCI 2012)*, Barcelona, Spain, 5-7 October 2012.
- [215] E. Burdet, G. Ganesh, C. Yang, A. Albu-Schäffer, "Interaction force, impedance and trajectory adaptation: by humans, for robots, experimental robotics," in *Experimental Robotics*, Springer Berlin Heidelberg, 2014, pp. 331-345.
- [216] D. Kee, G. Wyeth, J. Roberts, "Biologically inspired joint control for a humanoid robot," in *IEEE/RAS International Conference on Humanoid Robots (Humanoids 2004)*, Santa Monica, CA, USA, 10-12 November 2004.
- [217] D. Wolpert, Z. Ghahramani, M. Jordan, "An internal model for sensorimotor integration," *Science*, vol. 269, no. 5232, p. 1880–1882, 1995.
- [218] D. Wolpert, R. Miall, M. Kawato, "Internal models in the cerebellum," *Trends in Cognitive Sciences*, vol. 2, no. 9, p. 338–347, 1998.
- [219] D. Wolpert, M. Kawato, "Multiple paired forward and inverse models for motor control," *Neural Networks*, vol. 11, no. 7-8, p. 1317–1329, 1998.
- [220] R. E. Kalman, "A new approach to linear filtering and prediction problems," *Transaction of the ASME—Journal of Basic Engineering*, vol. 82, no. 1, pp. 35-45, 1960.
- [221] B. Mehta, S. Schaal, "Forward models in visuomotor control," *Journal of Neurophysiology*, vol. 88, no. 2, pp. 942-953, 2002.
- [222] T. Shibata, S. Schaal, "Biomimetic gaze stabilization based on feedback-error-learning with nonparametric regression networks," *Neural Networks*, vol. 14, no. 2, p. 201–216, 2001.
- [223] E. Todorov, "Optimality principles in sensorimotor control," *Nature Neuroscience*, vol. 7, no. 9, p. 907–915, 2004.
- [224] A. Diamond, O. Holland, "Reaching control of a full-torso, modelled

musculoskeletal robot using muscle synergies emergent under reinforcement learning," *Bioinspiration & Biomimetics*, vol. 9, no. 1, pp. 1-16, 2014.

- [225] A. Feldman, "Functional tuning of the nervous system with control of movement or maintenance of a steady posture," *Biophysics*, vol. 11, pp. 565-578, 1966.
- [226] A. Feldman, D. Ostry, M. Levin, P. Gribble, A. Mitnitsk, "Recent tests of the equilibrium-point hypothesis ( $\lambda$  model)," *Biophysics*, vol. 2, no. 3, pp. 189-205, 1998.
- [227] X. Gu, D. Ballard, "Robot movement planning and control based on equilibrium point hypothesis," in *IEEE Conference on Robotics, Automation and Mechatronics, 2006*, Bangkok, Thailand, 1-3 June 2006.
- [228] M. Rakovic, B. Borovac, M. Nikolic, S. Savic, "Realization of Biped Walking in Unstructured Environment using Motion Primitives," *IEEE Transactions on Robotics*, vol. 30, no. 6, pp. 1318 - 1332, 2014.
- [229] M. Chhabra, A. Jacobs, "Learning to combine motor primitives via greedy additive regression," *The Journal of Machine Learning Research*, vol. 9, pp. 1535-1558, 2008.
- [230] L. P. Kaelbling, M. Littman, A. Moore , "Reinforcement Learning: A Survey," *Journal of Artificial Intelligence Research*, vol. 4, pp. 237-285, 1996.
- [231] A. Moore, C. Atkeson, "The partigame algorithm for variable resolution reinforcement learning in multidimensional state-spaces," *Machine Learning*, vol. 21, no. 3, p. 711-718, 1995.
- [232] J. Peters, S. Vijayakumar, S. Schaal, "Reinforcement learning for humanoid robotics," in *IEEE-RAS International Conference on Humanoid Robots (Humanoids 2003)*, Karlsruhe, Germany, 29-30 September 2003.
- [233] A. W. E. O. J. P. J Kober, "Reinforcement learning to adjust robot movements to new situations," *Autonomous Robots*, vol. 33, no. 4, pp. 361-379, 2012.
- [234] R. Shadmehr, "Learning virtual equilibrium trajectories for control of a robot arm," *Neural Computation*, vol. 2, no. 4, pp. 436-446, 1990.
- [235] S. Huh, G. Tonietti, A. Bicchi, "Neural network based robust adaptive control for a variable stiffness actuator," in *Mediterranean Conference on Control and*

*Automation*, Ajaccio, France, 25-27 June 2008.

- [236] Dj.Mitrovic, S. Klanke, S. Vijayakumar, "Learning impedance control of antagonistic systems based on stochastic optimization principles," *The International Journal of Robotics Research*, vol. 30, no. 5, p. 556–573, 2010.
- [237] Y. Ichijo, T. Murao, H. Kawai, M. Fujita, "Passivity-based iterative learning control for 2dof robot manipulators with antagonistic bi-articular muscles," in *IEEE Multi-Conference on Systems and Control*, Antibes, France, 8-10 October 2014.
- [238] H. Kawai, T. Murao, R. Sato, M. Fujita, "Passivity-based control for 2dof robot manipulators with antagonistic bi-articular muscles," in *IEEE Multi-Conference on Systems and Control*, Denver, CO, USA, 26-30 September 2011.
- [239] M. Desmurget, S. Grafton, "Forward modeling allows feedback control for fast reaching movements," *Trends in Cognitive Sciences*, vol. 4, no. 11, p. 423–431, 2000.
- [240] A. Tal'nov, S. Serenko, S. Strafun, A. Kostyukov, "Analysis of the electromyographic activity of human elbow joint muscles during slow linear flexion movements in isotorque conditions," *Neuroscience*, vol. 90, pp. 1123-1136, 1999.
- [241] A. Smith, "Does the cerebellum learn strategies for the optimal time-varying control of joint stiffness," *Behavioral and Brain Sciences*, vol. 19, pp. 399-410, 1996.
- [242] P. Milosavljevic, K. Jovanovic, N.Bascarevic, V. Potkonjak, O. Holland, "Heuristic machine-learning approach to the control of an anthropomorphic robot arm," in *10th IFAC Symposium on Robot Control (SYROCO 2012)*, Dubrovnik, Croatia, 5-7 September 2012.
- [243] P. Milosavljevic, N.Bascarevic, K. Jovanovic, G. Kvascev, "Neural networks in feedforward control of a robot arm driven by antagonistically coupled drives," in *Symposium on Neural Network Applications in Electrical Engineering*, Belgrade, Serbia, 20-23 September 2012.
- [244] J. Wang, Q. Hu, D. Jiang, "A Lagrangian network for kinematic control of redundant robot manipulators," *IEEE Transactions on Neural Networks*, vol. 10,

no. 5, p. 1123–1132, 1999.

- [245] T. Nanayakkara, K. Watanabe, K. Kiguchi, K. Izumi, "Fuzzy self-adaptive radial basis function neural network-based control of a seven-link redundant industrial manipulator," *Advanced Robotics*, vol. 15, no. 1, pp. 17--43, 2001.
- [246] C. Wu, C. Huang, "Back-propagation neural networks for identification and control of a direct drive robot," *Journal of Intelligent and Robotics Systems*, vol. 16, no. 1, p. 45–64, 1996.
- [247] L. Behera, M. Gopal, S. Chaudhury, "On adaptive trajectory tracking of a robot manipulator using inversion of its neural emulator," *IEEE Transactions on Neural Networks*, vol. 7, no. 6, pp. 1401-1414, 1996.
- [248] M. Jäntsch, S. Wittmeier, K. Dalamagkidis, G. Herrmann, A. Knoll, "Adaptive neural network dynamic surface control: an evaluation on the musculoskeletal robot anthrob," in *IEEE International Conference on Robotics and Automation (ICRA 2015)*, Seattle, WA, USA, 26-30 May 2015.
- [249] J. H. Park, S. H. Huh, S. H. Kim, S. J. Seo, G. T. Park, "Direct adaptive controller for nonaffine nonlinear systems using self-structuring neural networks," *IEEE Transaction on Neural Networks*, vol. 16, no. 2, pp. 414-422, 2005.
- [250] L. A. Zadeh, "Fuzzy sets," *Information and Control*, vol. 8, no. 3, pp. 338-353, 1965.
- [251] F. Stulp, A. Fedrizzi, F. Zacharias, M. Tenorth, J. Bandouch, M. Beetz, "Combining analysis, imitation, and experience-based learning to acquire a concept of reachability in robot mobile manipulation," in *IEEE-RAS International Conference on Humanoid Robots (Humanoids 2009)*, Paris, France, 7-10 December 2009.
- [252] F. Petit, A. Albu-Schäffer, "Cartesian impedance control for a variable stiffness robot arm," in *IEEE/RSJ International Conference on Intelligent Robots and Systems (IROS 2011)*, San Francisco, CA, USA, 25-30 September 2011.
- [253] N. Hogan, "Impedance control: an approach to manipulation," in *American Control Conference*, San Diego, CA, USA, 6-8 June 1984.
- [254] T. Wimböck, C. Ott, A. Albu-Schäffer, A. Kugi, G. Hitzinger, "Impedance control

for variable stiffness mechanisms with nonlinear joint coupling," in *IEEE/RSJ International Conference on Intelligent Robots and Systems (IROS 2008)*, Nice, France, 22-26 September 2008.

- [255] A. Albu-Schäffer, M. Fischer, G. Schreiber, F. Schoeppe, G. Hirzinger, "Soft robotics: what Cartesian stiffness can obtain with passively compliant, uncoupled joints?," in *IEEE/RSJ International Conference on Intelligent Robots and Systems (IROS 2004)*, Sendai, Japan, 28 September-2 October 2004.
- [256] N. Hogan, "Impedance control: An approach to manipulation, Part I - Theory, Part II - Implementation, Part III - Applications," *ASME Journal of Dynamic Systems, Measurement and Control*, vol. 107, no. 1, pp. 1-24, 1985.
- [257] A. Albu-Schäffer, Ch. Ott, G. Hirzinger, "A unified passivity based control framework for position, torque and impedance control of flexible joint robots," *International Journal of Robotics Research*, vol. 26, no. 1, pp. 23-39, 2007.
- [258] M. Chalon, T. Wimböck, M. Grebenstein, G. Hirzinger, "Torque and workspace analysis for flexible tendon driven mechanisms," in *IEEE International Conference on Robotics and Automation (ICRA 2010)*, Anchorage, AK, USA, 3-7 May 2010.
- [259] D. R. Humphrey, D. J. Reed, "Separate cortical systems for control of joint movement and joint stiffness: reciprocal activation and coactivation of antagonist muscles," *Motor Control Mechanisms in Health and Disease*, vol. 39, no. 1, pp. 347-372, 1983.
- [260] Y. Yamazaki, T. Ohkuwa, H. Itoh, M. Suzuki, "Reciprocal activation and coactivation in antagonistic muscles during rapid goal-directed movements," *Brain Research Bulletin*, vol. 34, no. 6, pp. 587-593, 1994.
- [261] N. Hogan, "Adaptive control of mechanical impedance by coactivation of antagonist muscles," *Transactions on Automatic Control*, vol. 29, no. 8, pp. 681-690, 1984.
- [262] R. E. Kearney, I. W. Hunter, "System identification of human joint dynamics," *Critical Reviews in Biomedical Engineering*, vol. 18, no. 1, pp. 55-87, 1990.
- [263] C. Atkeson, J. Hollerbach, "Kinematics features of unrestrained vertical arm movements," *The Journal of Neuroscience*, vol. 5, no. 9, pp. 2318-2330, 1985.

- [264] M. Suzuki, D. M. Shiller, P. L. Gribble, D. J. Ostry, "Relationship between cocontraction, movement kinematics and phasic muscle activity in single-joint arm movement," *Experimental Brain Research*, vol. 140, no. 2, pp. 171-181, 2001.
- [265] F. A. Mussa-Ivaldi, N. Hogan, E. Bizzi, "Neural, mechanical, and geometric factors subserving arm posture in humans," *Journal of Neuroscience*, vol. 5, no. 10, pp. 2732-2743, 1985.
- [266] T. Milner, "Contribution of geometry and joint stiffness to mechanical stability of the human arm," *Experimental Brain Research*, vol. 143, no. 4, pp. 515-519, 2002.
- [267] M. Darainy, D. J. Ostry, "Muscle cocontraction following dynamics learning," *Experimental Brain research*, vol. 190, no. 2, pp. 153-162, 2008.
- [268] "Myrobotics," [Online]. Available: <http://www.myrobotics.eu/>. [Accessed 30 November 2015].
- [269] "Bipedal Walking Robot Lucy," Vrije Universiteit Brussel, [Online]. Available: <http://lucy.vub.ac.be/>. [Accessed 25 December 2015].
- [270] "Enhancing biomorphic agility through variable stiffness - STIFF," Seventh framework programme of the EU, [Online]. Available: <http://www.stiff-project.org/>. [Accessed 30 November 2015].
- [271] "Variable impedance actuation systems embodying advanced interaction behaviours - VIATORS," Seventh framework programme of the EU, [Online]. Available: <http://www.viactors.eu/>. [Accessed 30 November 2015].
- [272] Z. Popovic, A. Witkin, "Physically based motion transformation," in *26th Annual Conference on Computer Graphics (SIGGRAPH 99)*, Los Angeles, CA, USA, 8-13 August 1999.
- [273] K. Jovanovic, J. Vranic, N. Miljkovic, "Hill's and Huxley's muscle models - tools for simulations in biomechanics," *Serbian Journal of Electrical Engineering*, vol. 12, no. 1, pp. 53-67, 2015.
- [274] V. Potkonjak, B. Svetozarevic, K. Jovanovic, O. Holland, "Anthropomimetic robot with passive compliance - contact dynamics and control," in *IEEE 19th*

*Mediterranean Conference on Control and Automation (MED 2011)*, Corfu, Greece, 20-23 Jun 2011.

- [275] K. Jovanovic, B. Svetozarevic, "Humanoid robot model with antagonistic drives," in *The 54th ETRAN Conference*, Donji Milanovac, Serbia, 7-11 Jun, 2010.
- [276] B. Lukic, K. Jovanovic, "Influence of mechanical characteristics of a compliant robot on Cartesian impedance control design," in *The 2nd IcETLAN Conference*, Silver Lake, Serbia, 8-11 Jun 2015.
- [277] V. Potkonjak, M. Popovic, M. Lazarevic, J. Sinanovic, "Redundancy problem in writing: from human to anthropomorphic robot arm," *IEEE Transactions on SMC, Part B: Cybernetics*, vol. 28, no. 6, pp. 790-805, 1998.

## Author's biography

Kosta Jovanović was born in Čačak, Serbia, on July 17, 1986. He attended Milica Pavlović Elementary School and Čačak High School, which he both completed as the top student in his class in 2001 and 2005, respectively. He enrolled in the undergraduate program at the University of Belgrade's School of Electrical Engineering in 2005. He graduated with a grade point average of 9.96 (out of 10), on top of his class (Signals & Systems Department). He completed his Master's studies in 2010 and immediately enrolled in the PhD program of the Control Systems & Signal Processing Department. His research interests lie in robotics and control systems, with a focus on compliant actuators and bio-inspired robots.

Kosta Jovanović has been a teaching assistant at the Signals & Systems Department (for several courses in Mechatronics and Robotics) since March 2010. He completed his four-month internship at the company SMS Siemag in 2009, a two-month research stay at the Robotics & Embedded Systems Department of TUM Munich in 2010, and a six-month research stay at DLR Institute for Robotics and Mechatronics, Wessling in 2014, all in Germany. His scientific achievements are closely tied to his involvement in the EU-funded project Eccerobot under the 7<sup>th</sup> Framework Programme, and the project Ambient Intelligent Service Robots of Anthropomorphic Characteristics funded by Serbian Ministry of Education, Science and Technological Development.

Kosta Jovanović has received several awards for his achievements in the field of robotics, including: Saphari NMMI Winter School on Robotics: Variable Stiffness Actuators, Sapienza University of Rome, Italy, 2015; Young Researcher Best Paper Award, Section ROI, IcETRAN Conference, 2014; SUPERSTE award for the best Serbian young scientist in the field of natural and technical sciences, 2013; DAAD grant for a research stay, 2013; Belgrade Award for organizing the event-of-the-year (Days of the Future: Robotics), City of Belgrade, 2012; Nikola Tesla Junior Achievement Award, 2011; and Belgrade University Award for the best student's scientific work in the field of technical & technological sciences, 2011.

## Selected publications:

1. V. Potkonjak, **K. Jovanovic**, P. Milosavljevic, Chapter 20: “How to control an anthropomimetic robot: engineering and cognitive approach”, *New trends in Medical and Service Robotics*, pp 299-313, 2014. (M14)

DOI: 10.1007/978-3-319-05431-5

2. **K. Jovanovic**, V. Potkonjak, O. Holland, “Dynamic modelling of an anthropomimetic robot in contact tasks”, *Advanced Robotics*, Vol 28(11), pp 793-806, 2014. (M23)

DOI: 10.1080/01691864.2014.896748

3. V. Antoska, **K. Jovanovic**, V. Petrovic, N. Bascarevic, M. Stankovski, “Balance analysis of the mobile anthropomimetic robot under disturbances – ZMP approach”, *International Journal of Advanced Robotic Systems*, Vol 10(206), pp 1-10, 2013. (M23)

DOI: 10.5772/56238

4. S. Wittmeier, C. Alessandro, N. Bascarevic, K. Dalamagkidis, A. Diamond, M. Jantsch, **K. Jovanovic**, R. Knight, H. G. Marques, P. Milosavljevic, B. Svetozarevic, V. Potkonjak, R. Pfeifer, A. Knoll, O. Holland, “Towards anthropomimetic robotics”, *Artificial Life*, Vol 19(1), pp 171-193, 2013. (M21)

DOI: 10.1162/ARTL\_a\_00088

5. V. Potkonjak, B. Svetozarevic, **K. Jovanovic**, O. Holland, “The puller-follower control of compliant and noncompliant antagonistic tendon drives in robotic system”, *International Journal of Advanced Robotic Systems, (InTech)*, Volume 8, pp 143-155, 2012. (M23)

DOI: 10.5772/10690

6. V. Potkonjak, M. Vukobratovic, **K. Jovanovic**, M. Medenica, “Virtual mechatronic/robotic laboratory - A step further in distance learning”, *Computers & Education*, Vol 55, pp 465-475, 2010. (M21)

DOI: 10.1016/j.compedu.2010.02.010

Прилог 1.

## Изјава о ауторству

Потписани Коста М. Јовановић

број индекса 2010/5017

### Изјављујем

да је докторска дисертација под насловом

**Modeling and control of the anthropomimetic robot with antagonistic joints in contact and non-contact tasks**

(српски: "Моделирање и управљање антропомиметичког робота са антагонистичким погонима у контактним и бескотактним задацима")

- резултат сопственог истраживачког рада,
- да предложена дисертација у целини ни у деловима није била предложена за добијање било које дипломе према студијским програмима других високошколских установа,
- да су резултати коректно наведени и
- да нисам кршио/ла ауторска права и користио интелектуалну својину других лица.

Потпис докторанда

У Београду, 25.12.2015. год.

К. Јовановић

Прилог 2.

## Изјава о истоветности штампане и електронске верзије докторског рада

Име и презиме аутора Коста М. Јовановић

Број индекса 2010/5017

Студијски програм Управљање системима и обрада сигнала

Наслов рада

**Modeling and control of the anthropomimetic robot with antagonistic joints in contact and non-contact tasks**

**(српски: "Моделирање и управљање антропомиметичког робота са антагонистичким погонима у контактним и бескотактним задацима")**

Ментор проф. др Вељко Поткоњак

Потписани Коста М. Јовановић

Изјављујем да је штампана верзија мог докторског рада истоветна електронској верзији коју сам предао/ла за објављивање на порталу **Дигиталног репозиторијума Универзитета у Београду**.

Дозвољавам да се објаве моји лични подаци везани за добијање академског звања доктора наука, као што су име и презиме, година и место рођења и датум одбране рада.

Ови лични подаци могу се објавити на мрежним страницама дигиталне библиотеке, у електронском каталогу и у публикацијама Универзитета у Београду.

Потпис докторанда

У Београду, 25.12.2015. год.

K. Jovanović

Прилог 3.

## Изјава о коришћењу

Овлашћујем Универзитетску библиотеку „Светозар Марковић“ да у Дигитални репозиторијум Универзитета у Београду унесе моју докторску дисертацију под насловом:

**Modeling and control of the anthropomorphic robot with antagonistic joints in contact and non-contact tasks**

(српски: "Моделирање и управљање антропомиметичког робота са антагонистичким погонима у контактним и бескотактним задацима")

која је моје ауторско дело.

Дисертацију са свим прилозима предао/ла сам у електронском формату погодном за трајно архивирање.

Моју докторску дисертацију похрањену у Дигитални репозиторијум Универзитета у Београду могу да користе сви који поштују одредбе садржане у одабраном типу лиценце Креативне заједнице (Creative Commons) за коју сам се одлучио/ла.

1. Ауторство
2. Ауторство - некомерцијално
3. Ауторство – некомерцијално – без прераде
4. Ауторство – некомерцијално – делити под истим условима
5. Ауторство – без прераде
6. Ауторство – делити под истим условима

(Молимо да заокружите само једну од шест понуђених лиценци, кратак опис лиценци дат је на полеђини листа).

Потпис докторанда

У Београду, 25.12.2015. год.

К. Јовановић